THE UNIVERSITY OF CHICAGO

ACCEPTORLESS CATALYTIC DEHYDROGENATIVE ELECTROCYCLIZATION

A DISSERTATION SUBMITTED TO

THE FACULTY OF THE DIVISION OF THE PHYSICAL SCIENCES

IN CANDIDACY FOR THE DEGREE OF

DOCTOR OF PHILOSOPHY

DEPARTMENT OF CHEMISTRY

BY

TATSUHIRO TSUKAMOTO

CHICAGO, ILLINOIS

AUGUST 2020

TABLE OF CONTENTS

List of figures vii

List of schemes viii

List of tables xii

Acknowledgement xiii

List of Abbreviations xvi

1. Introduction p. 1

1.1 Bottom-up synthesis of nanographenes p. 1

1.2 Cyclodehydrogenation in nanographene synthesis p. 5

1.2.1 The Scholl/Mallory reactions p. 5

1.2.2 Recently developed conditions p. 9

1.3 Redox-neutral cyclization to triphenylenes p. 11

1.4 Cobaloxime-type acceptorless dehydrogenation catalysts p. 20

1.5 Cobaloxime catalysis in acceptorless dehydrogenative transformations p. 22

1.6 The author's work p. 31

1.7 References p. 32

2**. Acceptorless catalytic dehydrogenative cyclization of *o*-teraryls** p. 36

2.1 Introduction p. 36

2.2 Results & discussion p. 38

2.2.1 Optimization process p. 38

2.2.2 Substrate scope p. 41

2.2.3 Mechanistic study p. 44

2.3 Conclusion p. 47

2.4 Experimental sections p. 48

2.5 References p. 85

2.6 Scanned ^{1}H and ^{13}C NMR spectra p. 94

3. Acceptorless catalytic dehydrogenative cyclization of protonated arylpyridinium salts p. 151

3.1 Introduction p. 151

3.2 Results&discussion p. 155

3.2.1 Optimization process p. 155

3.2.2 Substrate scope p. 158

3.3 Conclusion p. 162

3.4 Experimental sections p. 163

3.5 NMR spectra p. 177

3.6 References p. 188

4. Dehydrogenative Alkyne Diannulation (DAD) p. 190

4.1 Introduction p. 190

4.2 Results&discussion p. 193

4.3 Conclusion p. 195

4.4 Experimental sections p. 196

4.5 ^{1}H and ^{13}C NMR spectra p. 201

4.6 References p. 203

A LIST OF FIGURES

Fig. 2.1. Proposed Catalytic Cycle p. 47

Fig. S1 Top view of the reaction set up for the catalytic dehydrogenative electrocyclization

p. 60, 176, 199

Fig. S2 Side view of the reaction set up for the catalytic dehydrogenative electrocyclization

p. 60, 176, 199

Fig. S3 alternative mechanism A p. 83

Fig. S4 alternative mechanism B p. 84

Fig. 3.1 Azonia aromatic heterocycles (AZAHs) p. 151

Fig. 4.1 Dibenzo[*g,p*]chrysene p. 190

A LIST OF SCHEMES

Scheme 1.1 Suzuki-Miyaura polymerization/Scholl reaction sequence in *N*=9 aGNR synthesis p. 3

Scheme 1.2 Yamamoto polymerization/Scholl reaction sequence in *N*=18 aGNR synthesis p. 4

Scheme 1.3 Sonogashira polymerization/Scholl reaction sequence in *N*=13 aGNR synthesis p. 5

Scheme 1.4 The Scholl reaction p. 6

Scheme 1.5 Representative side reactions in the Scholl reaction p. 7

Scheme 1.6 The Mallory reaction p. 9

Scheme 1.7 Shindo's condition p. 10

Scheme 1.8 Hilt's DDQ-mediated electrocatalytic condition p. 11

Scheme 1.9 Pd-catalyzed deacetonative coupling reaction p. 12

Scheme 1.10 Pd-catalyzed deacetonative coupling reaction p. 13

Scheme 1.11 Rh-catalyzed [2+2+2] cyclization of diynes and internal/terminal alkynes p. 14

Scheme 1.12 HOMe-eliminative photocyclization of stilbenes p. 15

Scheme 1.13 HCl-eliminative photocyclization of stilbene p. 16

Scheme 1.14 HCl-eliminative photocyclization for the synthesis of ullazine heterocycles p. 17

Scheme 1.15 Silicon-catalyzed HF-eliminative cyclization for the synthesis of carbon materials p. 19

Scheme 1.16 Al_2O_3-mediated HF-eliminative photocyclization for the synthesis of carbon materials p. 20

Scheme 1.17 cobaloxime-catalyzed proton reduction under PCET mechanism p. 21

Scheme 1.18 Direct desaturation of alkanes under tungstate/cobaloxime dual catalysis p. 22

Scheme 1.19 Acceptorless dehydrogenative amination/hydroxylation reactions under photoredox/cobaloxime catalysis (selectivity = yield/conversion) p. 24

Scheme 1.20 Reaction mechanism of Acceptorless dehydrogenative amination/hydroxylation reactions p. 25

Scheme 1.21 Acceptorless dehydrogenative indole synthesis under photoredox/cobaloxime catalysis

p. 26

Scheme 1.22 Acceptorless dehydrogenative aromatic lactone synthesis under photoredox/cobaloxime catalysis

p. 28

Scheme 1.23 Acceptorless dehydrogenativeimine/alkene [4+2] cycloaddition under photoredox/cobaloxime catalysis

p. 28

Scheme 1.24 Acceptorless dehydrogenative styrene/alkyne [4+2] cycloaddition under photoredox/cobaloxime catalysis

p. 30

Scheme 2.1 Cyclodehydrogenation of *o*-teraryls p. 38

Scheme 2.2 Preliminary Mechanistic Explorations p. 45

Scheme S1 reaction under dark conditions p. 78

Scheme 3.1 Synthetic approaches to azonia aromatic heterocycles (AZAHs) p. 153

Scheme 3.2 This work p. 155

Scheme 3.3. Initial studies p. 156

Scheme 3.4 C–H zipping strategy p. 158

Scheme 3.5 Substrate scope under C–H zipping p. 159

Scheme 3.6 Diazonia synthesis under C–H zipping p. 160

Scheme 3.7 Synthesis of the hexacyclic azonia nanographene p. 161

Scheme 3.8 Challenging examples p. 162

Scheme 4.1. Sb^{V}-mediated oxidative cyclization p. 191

Scheme 4.2. Strategy to dibenzo[*g.p*]chrysene: CDE (left, unsuccessful) and DAD (right, this work) p. 192

Scheme 4.3. DAD catalysis and its potential application p. 192

Scheme 4.4. Design of the DAD catalysis p. 193

A LIST OF TABLES

Table 2.1 Optimization study p. 40

Table 2.2 Substrate Scope p. 43

Table S1 Consumption of the starting material p. 77

Table 3.1. Optimization of reaction conditions p. 157

Table 4.1 Lewis acid screening p. 194

Table 4.2 Solvent screening p. 195

ACKNOWLEDGEMENT

I am extremely grateful to The University of Chicago for providing me with a rich research environment to learn and grow as an independent researcher.

I'd like to express my highest gratitude to my Ph.D. advisor, Prof. Guangbin Dong, for his constant support and patience throughout my Ph.D. journey. I first met Guangbin in 2014 when he delivered a lecture in Japan. His broad interest in organic chemistry has allowed me a lot of freedom in my research projects and valuable feedback when I needed it. His guidance allowed me to think professionally, independently, and freely, even when my Ph.D. journey had many detours.

I'd like to thank Profs. Rawal and Rowan for their academic advice and support as my dissertation committee members. Their assistance made my dissertation special.

In 2013, I applied for the Ph.D. course at the University of Chicago, and that's when I first contacted Prof. Rawal. Although I couldn't join his group, I still remember the moment when I had the chance to meet him in person. I respect Prof. Rawal because he is a humble person who is leading organic synthesis for long time. He is my role model, and I look up to him as an inspiration

for my future career as a professor.

I'm also grateful to Prof. Keisuke Suzuki for teaching me the joy, beauty, and importance of organic chemistry. His *"積み木 (tsumiki)"*concept in synthetic chemistry has always been one of my research disciplines when designing and creating molecules.

At The University of Tokyo, Prof. Shū Kobayashi taught me the importance of synthetic methodology for industrial and sustainable society. Prof. Kobayashi has always been open to discussing new approaches to human health/sustainable society through synthetic chemistry, which made me learn a wide perspective on chemical science in general.

I'd like to thank all the lab members in the Dong lab, who shared a wonderful time with me, including but not limited to; Dr. Brent Billett, Dr. Chengpeng Wang, Jiaxin Xie, Dr. Ki-Young Yoon, Alexander Rago, Shusuke Ochi, Andrew Ng, Carlo Berti, Yibin Xue, Dr. Mike Young, Dr. John Thompson, Dr. Rachel Whittaker, Dr. Zhi Ren, Danny Thach, Dr. Zhe Dong, Dr. Zhongxing Huang, Dr. Penghao Chen, Dr. Yan Xu, Dr. Jianchun Wang, Likun Jin, Dr. Lin Deng, Dr. Marshall Brennan, Renhe Li, Yun Zhou, Dr. Jun Zhu, Dr. Hairong Lyu, Dr. Ming Chen, Dr. Ying Xia, Dr.

Sihua Hou, Dr. Zhao Wu, Dr. Xiaoyang Chen, Dr. Xukai Zhou, Dr. Saiyong Pan, Dr. Hee Nam Lim, Shinyoung Choi, Dr. Ziqiang Rong, Dr. Rong Zeng, Lei Zhang, Dr. Xuan Zhou, Dr. Dong Xing, Feipeng Liu, Pengfei Zhang, Dr. Gan Li, and Zixi Zhu.

I'm also grateful to have Prof. Aaron Dinner and Dr. Bahareh Lampert in the Department of Chemistry for their helpful advice on my thesis.

Finally, I'd like to express my deepest gratitude to my parents, who have supported me throughout my life and allowed me to pursue my dreams. Studying in the US was only possible with their help.

Tatsuhiro Tsukamoto

July 2020

LIST OF ABBREVIATIONS

Ac	Acetyl
AFM	Atomic force microscopy
aGNR	Armchair graphene nanoribbon
Ar	Aryl
Bn	Benzyl
Boc	*tert-Butoxycarbonyl*
Bu	Butyl
Bz	Benzoyl
COD	1,5-Cyclooctadienyl
CV	Cyclic voltammetry
Cy	Cyclohexyl

δ	Chemical shift
DCE	1,2-Dichloroethane
DCM	Dichloromethane
DDQ	2,3-Dichloro-5,6-dicyano-1,4-benzoquinone
DLS	Dynamic light scattering
DMF	*N,N*-Dimethylformamide
dppf	1,1'-bis(Diphenylphosphino)ferrocene
Et	Ethyl
equiv	Equivalent
GNR	Graphene nanoribbon
TfOH	Trifluoromethanesulfonic acid
UV	Ultraviolet

1. Introduction

1.1 Bottom-up synthesis of nanographenes

Graphenes are carbon-based two-dimensional chemical entities that have conjugated carbon–carbon (C–C) π system. Owing to their unique structures, they exhibit extraordinary physicochemical properties such as flexibility and high charge-carrier mobility, which could be valuable future electronics. This has led numerous researchers from different background to explore graphenes.[1] However, its lack of the bandgap makes it unavailable for application in field-effect transistors (FETs).[2] Compared to graphenes, structurally confined units of graphenes, e.g. graphene nanoribbons (GNRs), have a bandgap that is precisely controlled by its size (width and length), carbon scaffolds, and edge structures.[3] The "top-down" approach to GNRs relies on deconstructive methods such as hydrothermal or lithographic scission of graphenes, which cannot precisely control the size and structure of GNRs.[4] In contrast, the "bottom-up" approach functionalizes small aromatic compounds that can construct GNRs with defined structures and properties. Due to its precision and modularity, "bottom-up"

synthesis of GNRs has been widely studied.

The “bottom-up” approach to nanographenes including GNRs consists of two major sequences; 1) polymerization and 2) cyclodehydrogenation. The recent progress on the polymerization methodologies, especially transition-metal-catalyzed C–C bond-forming reactions, have enabled the efficient synthesis of precursors for structurally defined GNRs. For example, in 2008, Müllen and his co-workers have reported the synthesis of *N*=9 aGNR; the key intermediate was synthesized through Suzuki–Miyaura polymerization, followed by the $FeCl_3$-mediated Scholl cyclodehydrogenation to access the GNR that possessed 2.2 eV bandgap (Scheme 1.1).[5] In addition, nickel-catalyzed Yamamoto polymerization (Scheme 1.2),[6] palladium-catalyzed Sonogashira polymerization and decarbonylative benzannulation (Scheme 1.3)[7,8,9] etc. have been shown to be efficient for GNR synthesis. All these approaches need the Scholl reaction to construct target nanographenes (*vide infra*).

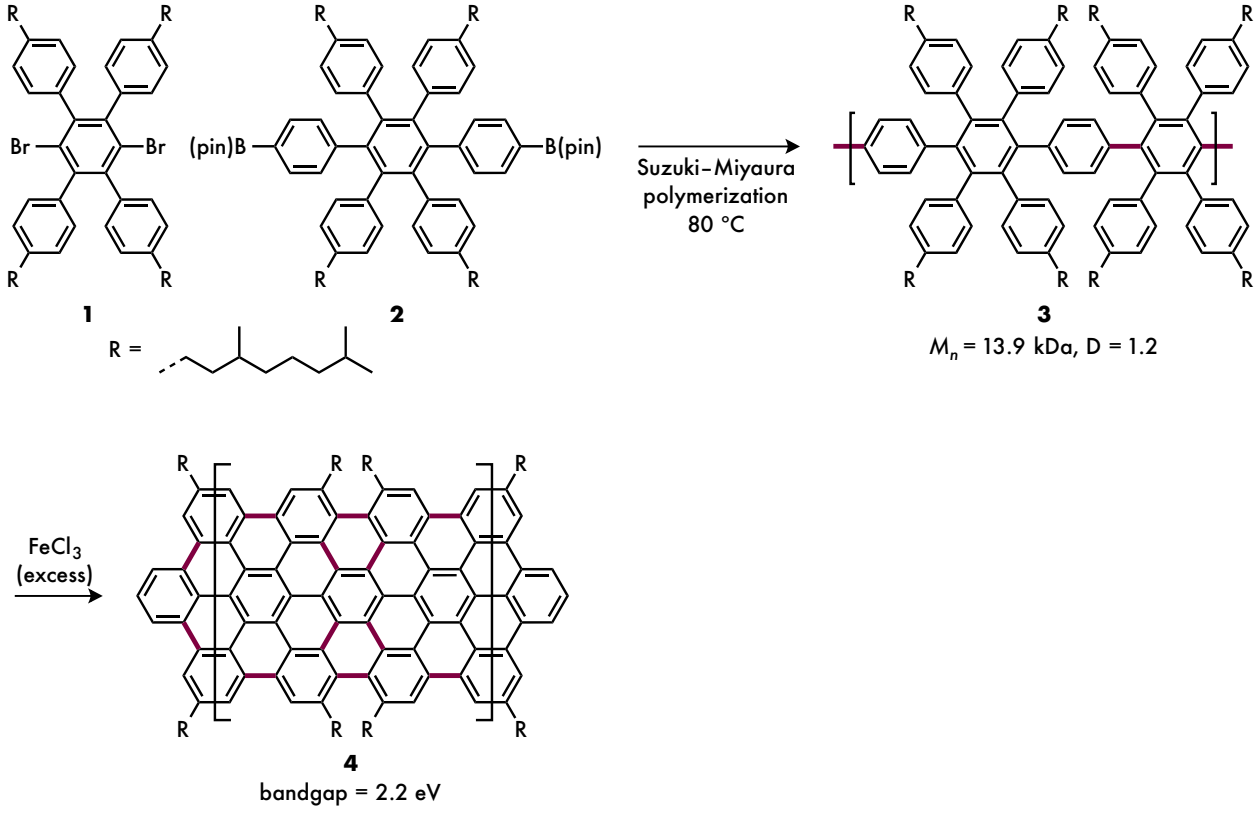

Scheme 1.1 Suzuki-Miyaura polymerization/Scholl reaction sequence in *N*=9 aGNR synthesis

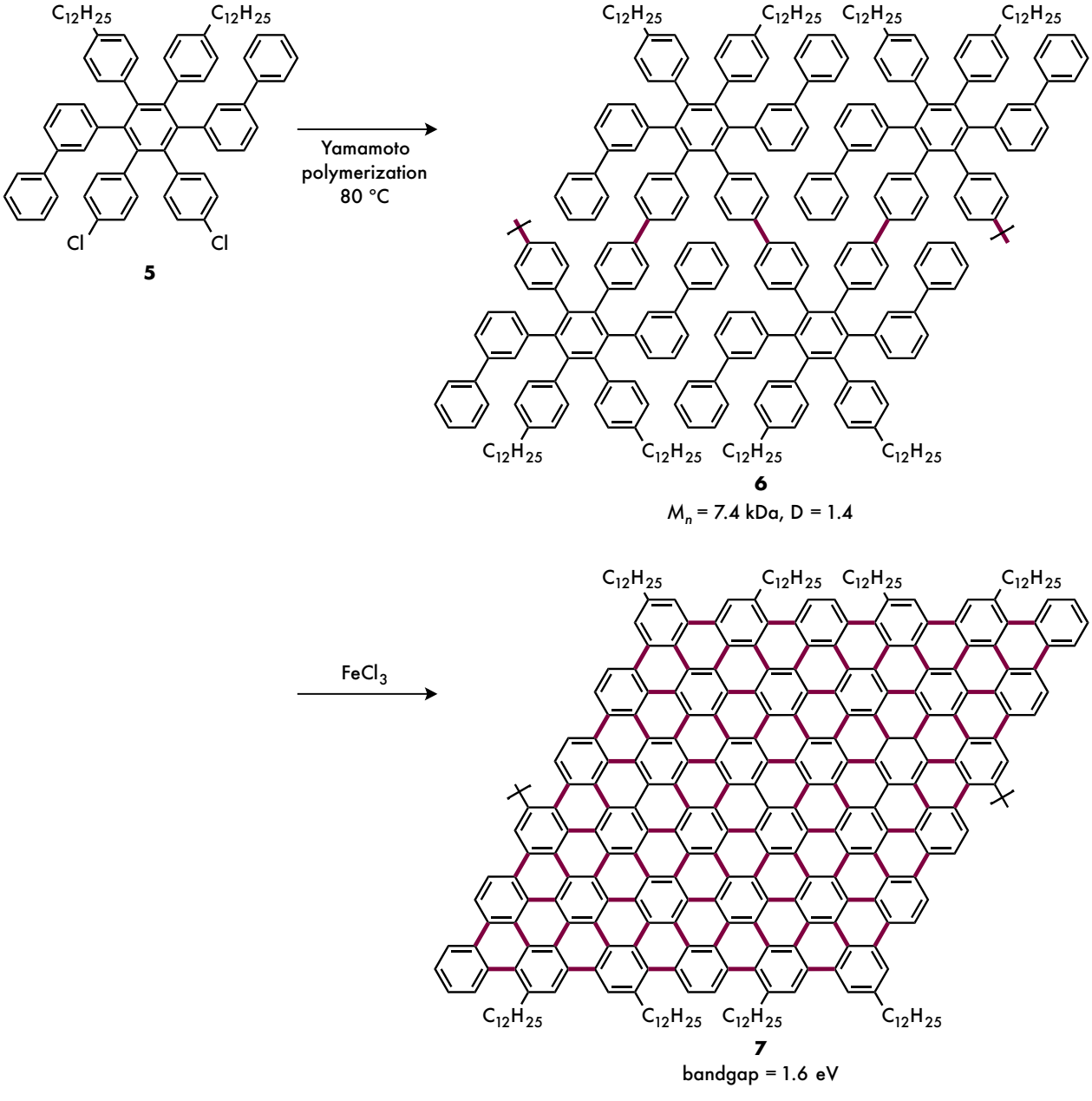

Scheme 1.2 Yamamoto polymerization/Scholl reaction sequence in *N*=18 aGNR synthesis

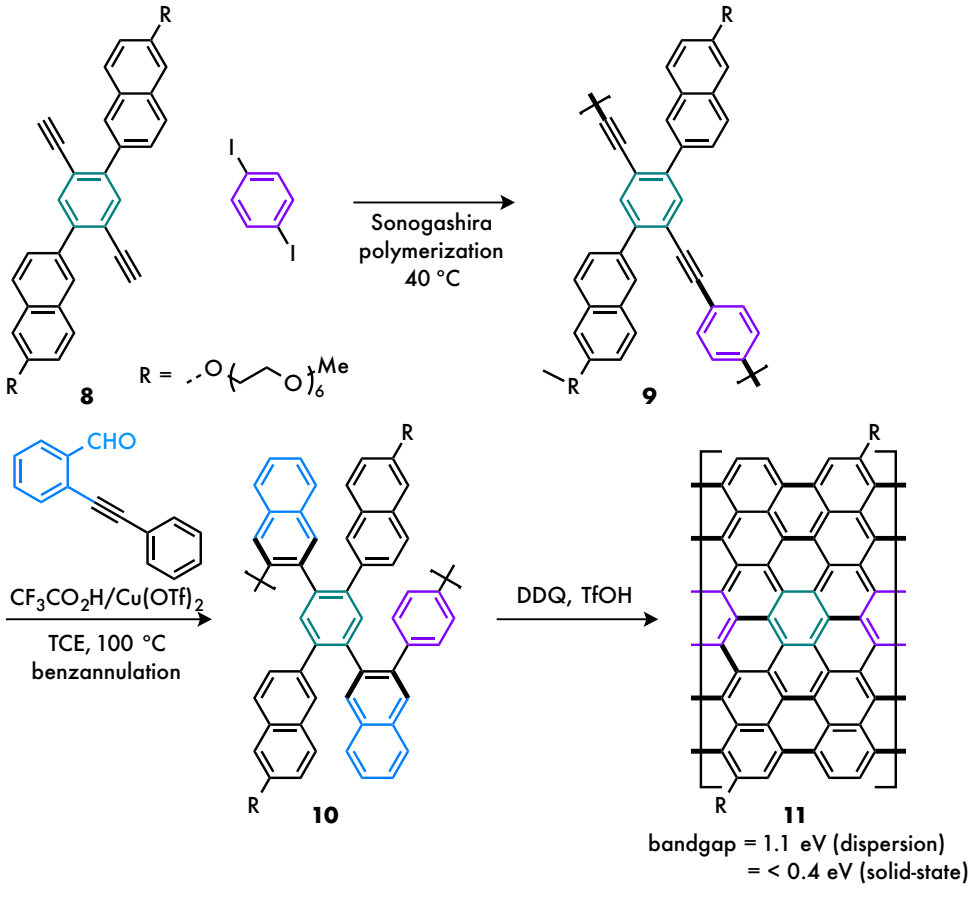

Scheme 1.3 Sonogashira polymerization/Scholl reaction sequence in *N*=13 aGNR synthesis

1.2 Cyclodehydrogenation in nanographene synthesis

1.2.1 The Scholl reaction

One of the most common and important steps in the GNR synthesis is cyclodehydrogenation, which allows the direct molecular engineering of simple polyarenes to GNRs. Among the cyclodehydrogenation protocols, the Scholl reaction is the most reliable method in GNR synthesis (Scheme 1.4). Selected examples of application of the Scholl reaction in GNR synthesis were described in Scheme 1.1-1.3.

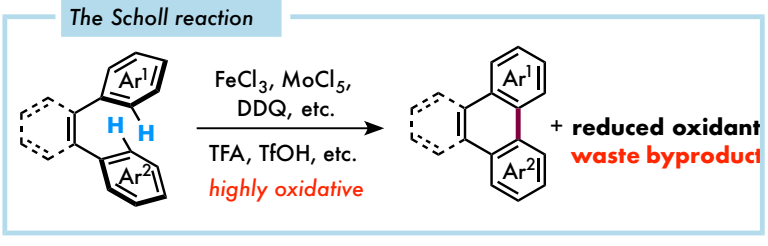

Scheme 1.4 The Scholl reaction

Despite the high impact of the Scholl reaction in GNR synthesis, it requires stoichiometric amount of strong oxidant and/or acid to generate active cationic intermediates due to the inertness of aromatic sp^2 C–H bonds. As such, the reaction is severely acidic and stoichiometric amount of byproduct is formed as a waste, which has been a problem in environment and atom economy. Due to the severe acidic/oxidative conditions, the Scholl reaction is not compatible to acid-sensitive functional groups and even simple arenes, which eventually can be the bottleneck in the "bottom-up" approach to the

target GNRs. Scheme 1.5 summarizes the failed examples of the Scholl reactions in nanographene synthesis; 1,2-aryl shift of multi-aryl benzenes are one of the significant side reactions in the Scholl condition, where the resultant products are no longer the originally desired (see compounds **12**, **19**)[10,11,12]. Undesired polymerization/decomposition of *o*-terphenyl derivatives **22** took place when the generated cationic intermediates have active reaction sites.[13] Chlorination of aromatic sp^2 C–H bonds[14,15] were reported when multi-aryl polymer was subjected to $FeCl_3$ conditions.

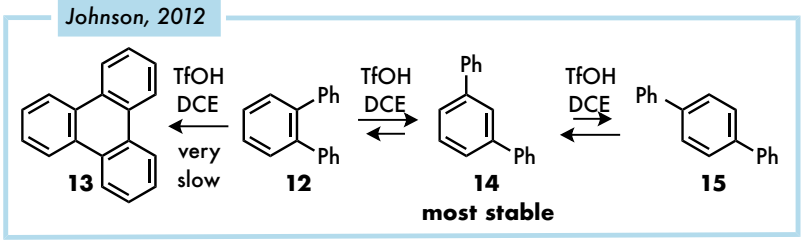

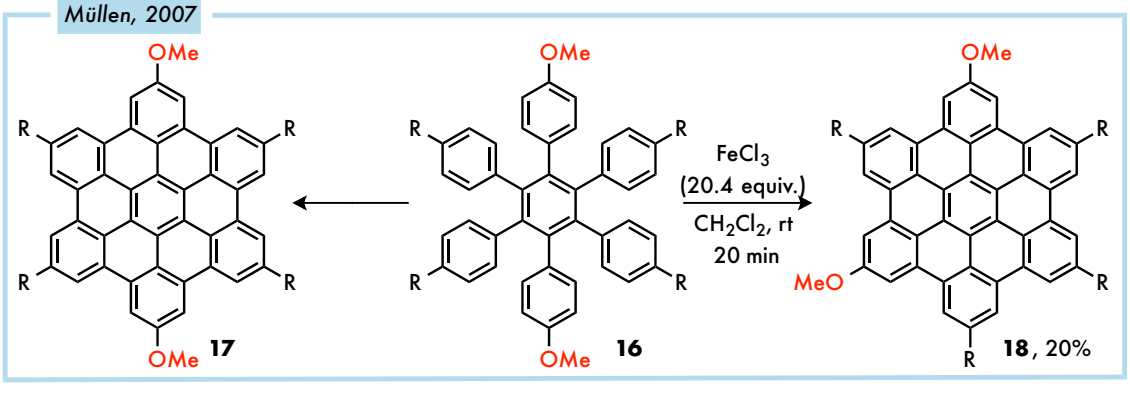

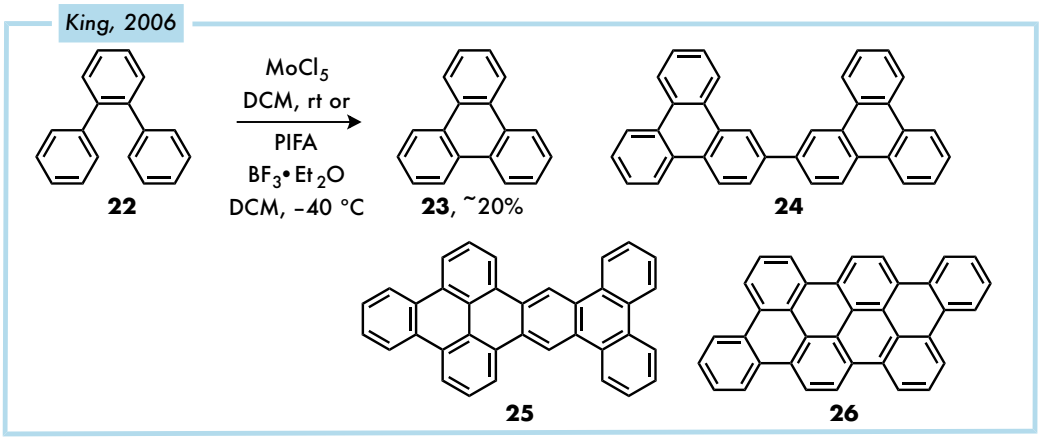

Scheme 1.5 Representative side reactions in the Scholl reaction

Cyclodehydrogenation, except for the Scholl reaction, can be done in the presence of light and an oxidant; the Mallory reaction has been also widely used for cyclodehydrogenation of stilbene delivatives (Scheme 1.6). In the Mallory reaction, starting material undergoes photoexcitation and 6π electrocyclization under UV light irradiation; concomitantly, iodine is homolytically cleaved to produce iodo radical, which abstracts the hydrogen atom from the tetracyclic intermediate. The second hydrogen atom abstraction takes place to afford product and hydrogen iodide as an acidic byproduct. This methodology, however, requires stoichiometric amount of iodine, and hydrogen iodide needs to get neutralized by base. Although the improved condition by Katz *et al*. enabled the use of catalytic

amount of iodine for the cyclodehydrogenation, the atmospheric oxygen gas in the reaction system (under UV light irradiation) can decompose the aromatic species (starting material, intermediate, or product) by [4+2] cycloaddition reactions.

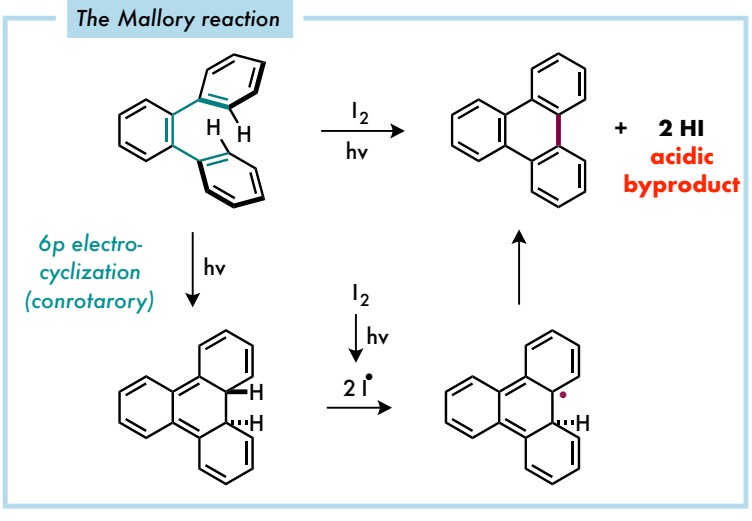

Scheme 1.6 The Mallory reaction

1.2.2 Recently developed conditions

In 2016, Shindo and his co-workers reported the cyclodehydrogenation of *o*-teraryls under Pd/Al_2O_3 catalysis in the presence of molecular oxygen (Scheme 1.7). This protocol affords products from electron-rich substrates, but still requires highly acidic media such as the stoichiometric amount of TfOH as well as solvent amount of HFIP. Hence, electron-deficient substrates were found inert and

some electron-rich arenes underwent complex side reactions in their reaction conditions.

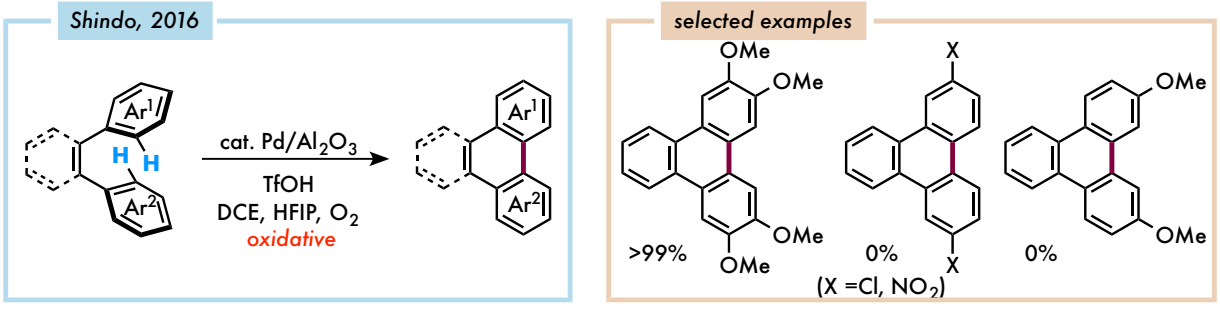

Scheme 1.7 Shindo's condition

In 2017, Hilt and his-coworkers discovered the DDQ-mediated cyclodehydrogenation under electrolysis (Scheme 1.8). According to the proposed mechanism, catalytic amount of DDQ is regenerated on anode and the proton is reduced on cathode. Despite its wide substrate scope, 10% of the reaction solvent is strongly acidic TfOH (pKa = 0.23).

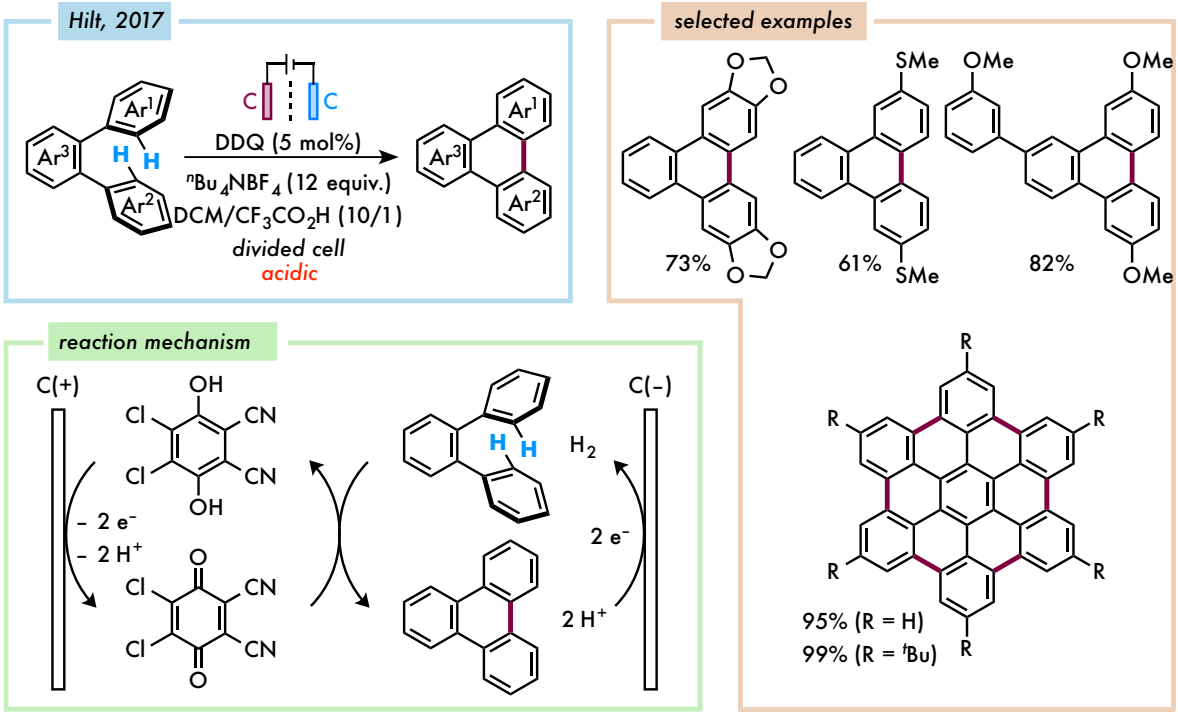

Scheme 1.8 Hilt's DDQ-mediated electrocatalytic condition

1.3 Redox-neutral cyclization to triphenylenes

In addition to the aforementioned oxidative transformations, redox-neutral intermolecular construction of triphenylene moiety has been reported through transition-metal catalysis. In 2015, Nishihara and his coworkers developed the palladium-catalyzed deacetonative cross-coupling reaction of 2-iodobiphenyls and *o*-bromobenzylalcohols (Scheme 1.9).[16] Substrate scope shows that both electron-rich/poor substrates are compatible to give desired products in moderate to good yield.

Proposed mechanism suggests that deacetonative cross-coupling reaction takes place first, then followed by C–Br oxidative addition/C–H activation/reductive elimination.

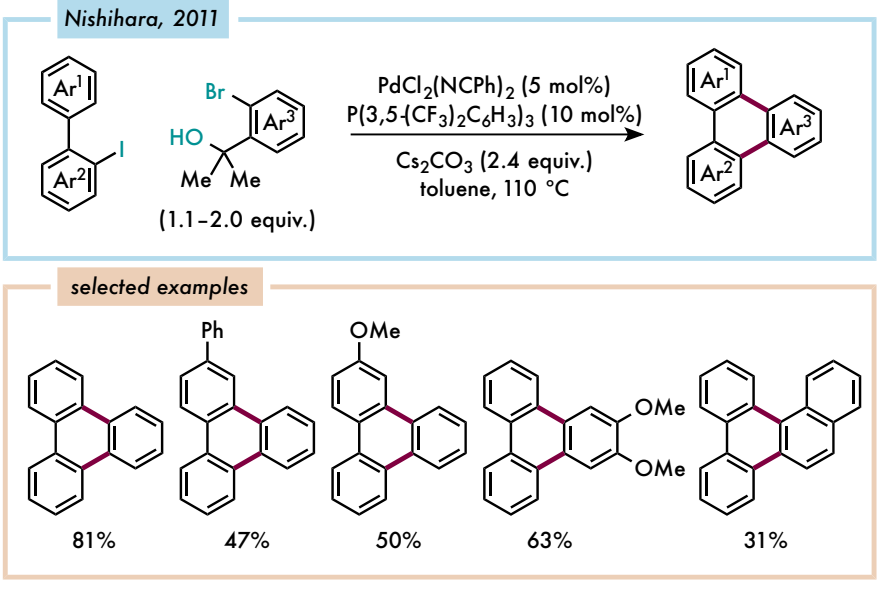

Scheme 1.9 Pd-catalyzed deacetonative coupling reaction

Later, Li and Xu reported palladium-catalyzed cross-coupling reaction of 2,2'-dibromobiphenyls and arylboronic acids to make triphenylenes through sequential Suzuki–Miyaura cross-coupling/C–H activation process (Scheme 1.10).

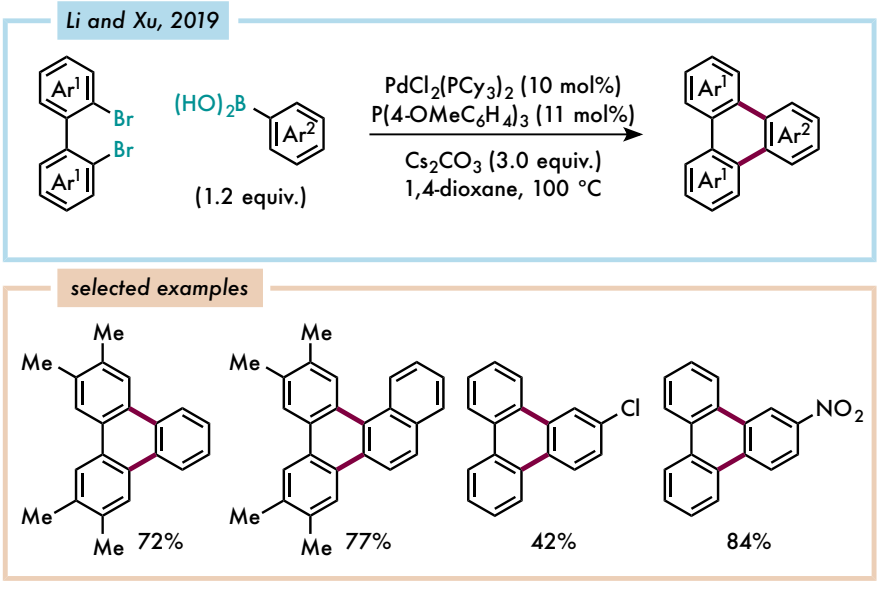

Scheme 1.10 Pd-catalyzed deacetonative coupling reaction

Tanaka and his coworkers demonstrated the rhodium-catalyzed [2+2+2] cyclization of various diynes and internal/terminal alkynes to afford triphenylenes. With this methodology, multi-functionalized products can be obtained in high yield, and double cyclization afforded triphenylene-based long ladder molecules that exhibited high fluorescence quantum yields in chloroform (Scheme 1.11).

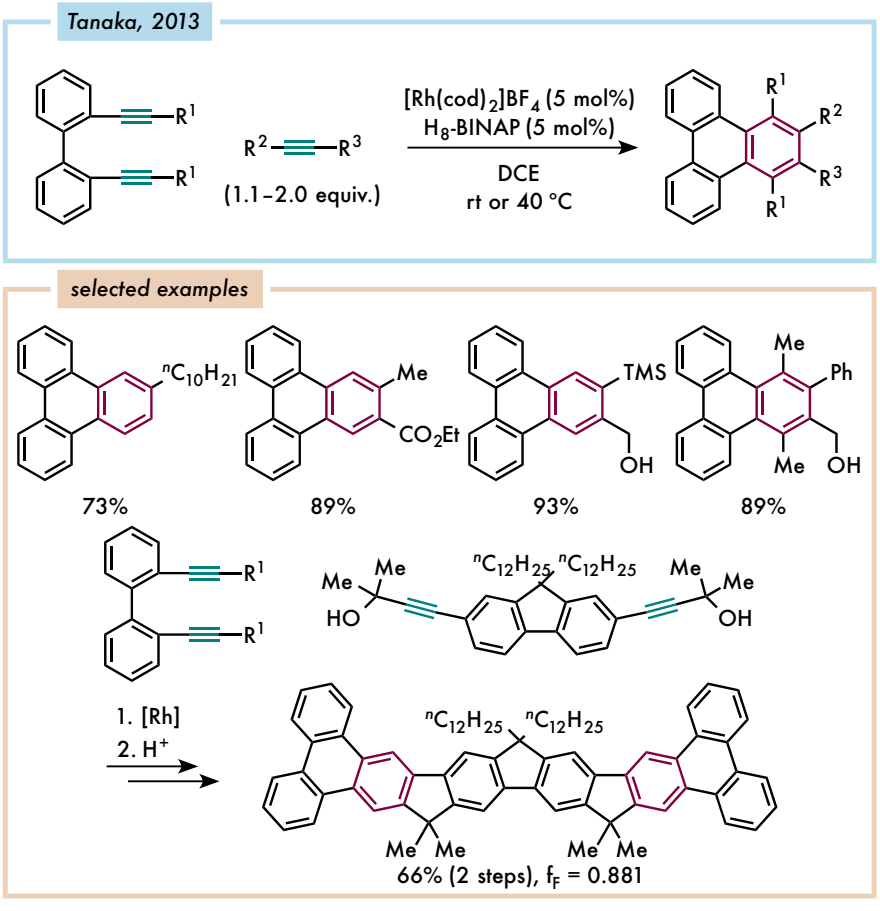

Scheme 1.11 Rh-catalyzed [2+2+2] cyclization of diynes and internal/terminal alkynes

In addition to the transition-metal catalysis, eliminative photocyclization reactions also enable the redeox-neutral construction of triphenylene motifs. Sargent *et al*. reported the eliminative photocyclization of methoxy-substituted stilbenes under the medium mercury lamp irradiation, and phenanthrene products were obtained in moderate to good yield (Scheme 1.12).

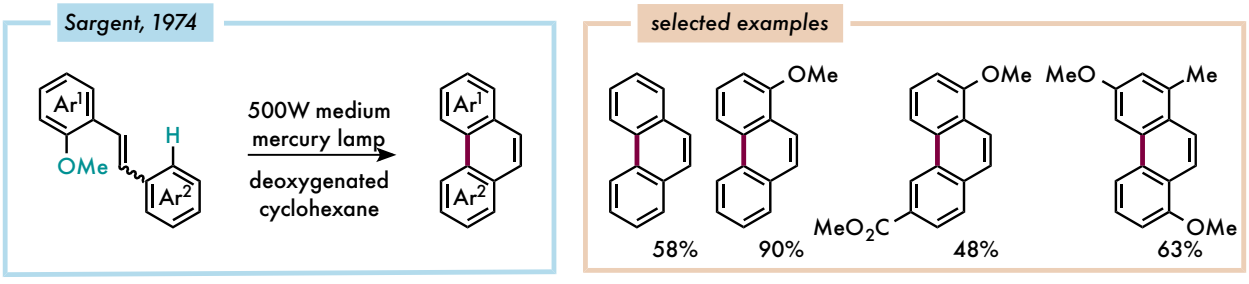

Scheme 1.12 HOMe-eliminative photocyclization of stilbenes

Eliminative cyclization of H–X (X = halogens) have been extensively studied and found its utility in GNR synthesis; HCl-eliminative photocyclization of **27** to **28** was first reported by Morin, and it showed great regioselectivity in C–C bond formation.[17] The proposed reaction mechanism starts with 6π electrocyclization, followed by base-mediated elimination of HCl (Scheme 1.13).

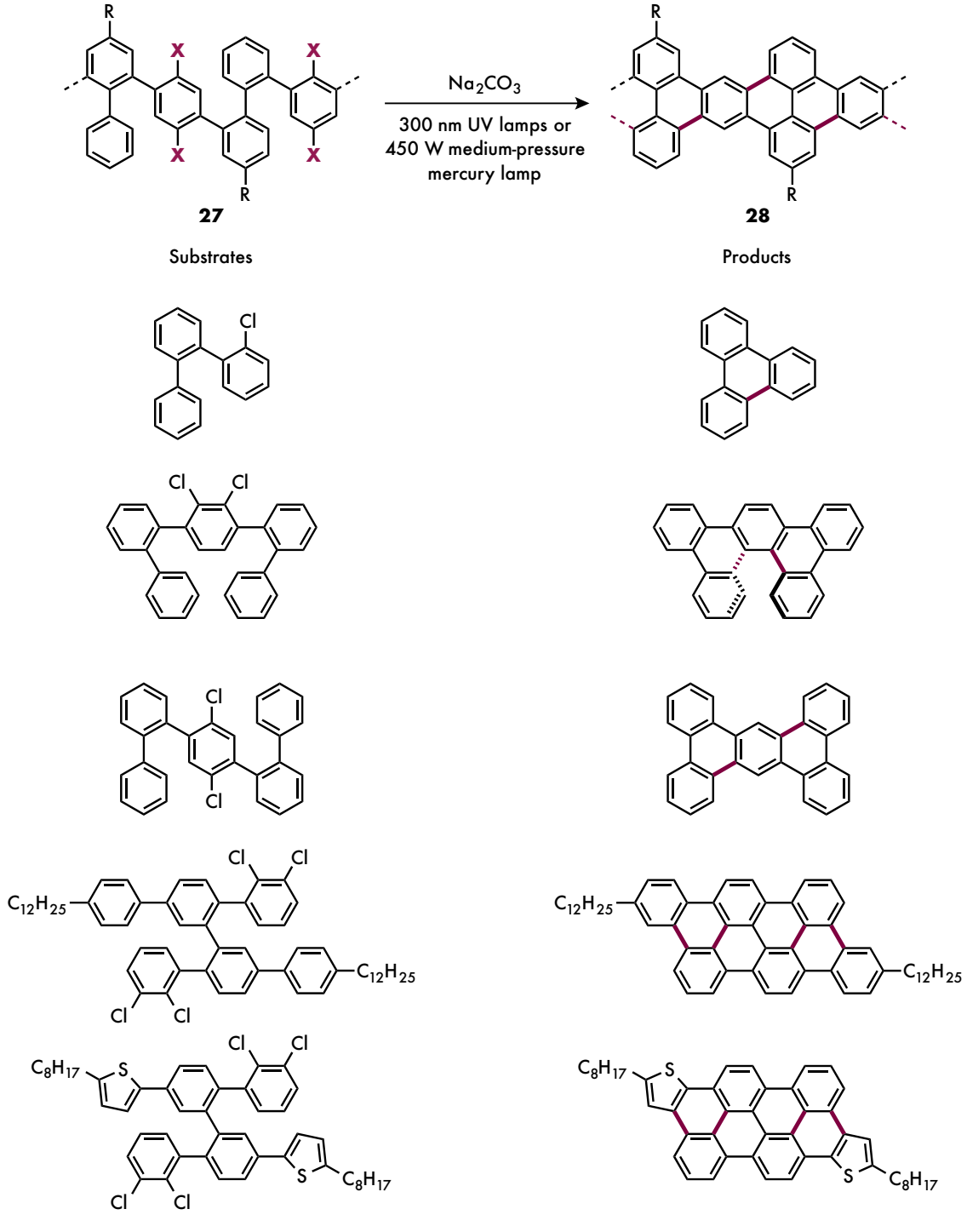

Scheme 1.13 HCl-eliminative photocyclization of stilbene

Later, the same group reported the synthesis of ullazine derivatives through HCl-eliminative photocyclization, with which pyridine and thiophene moieties were successfully introduced into the hexacyclic π-system (Scheme 1.14).[18] In this work, thiophene products were further transformed into donor-acceptor polymers that showed far-red to NIR absorption.

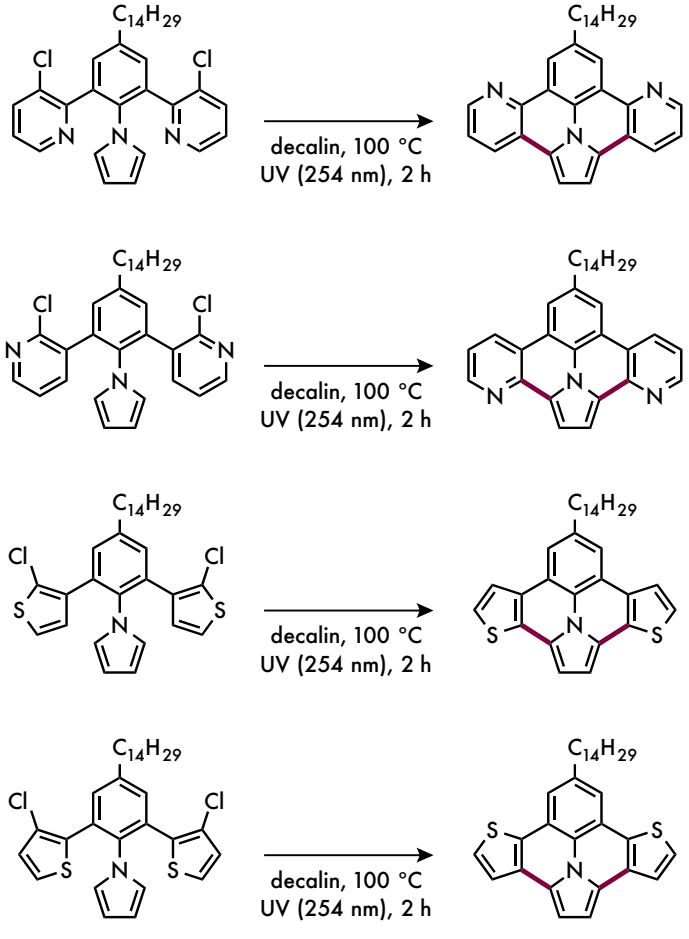

Scheme 1.14 HCl-eliminative photocyclization for the synthesis of ullazine heterocycles

In 2011, the Siegel group has reported HF-eliminative cyclization of aryl fluorides **29** through silyl cation-catalyzed C–F bond activation (Scheme 1.15).[19] Driving force in this transformation is the formation of strong Si–F bond that is stronger than C(sp^2)–F by about 120 kJ/mol. A molar equivalent of proton is generated during the reaction, and $Me_2Si(Mes)_2$ works as a base to neutralize the reaction system. Their reaction conditions were suitable for the formation of five- and six-membered ring systems, affording moderate to high yield of the desired products.

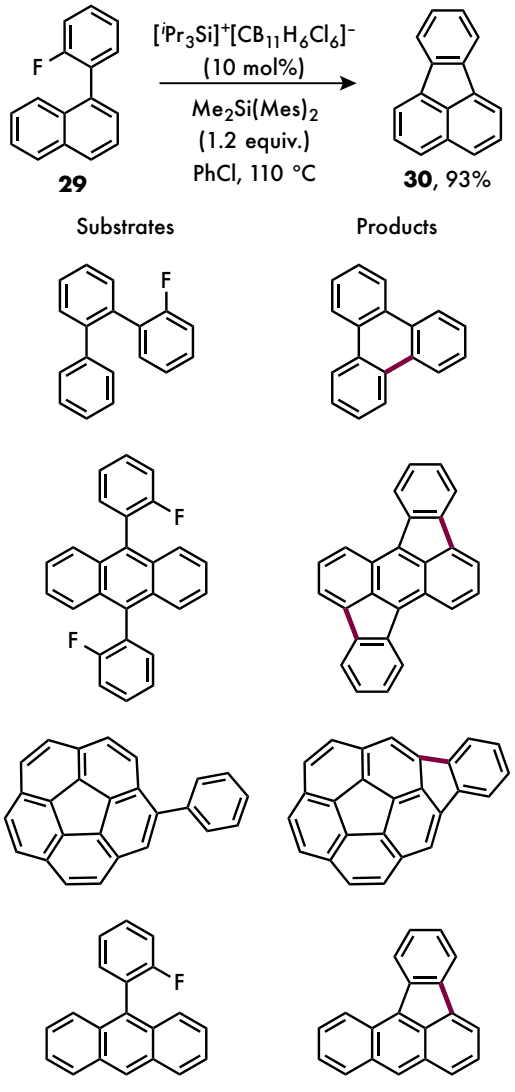

Scheme 1.15 Silicon-catalyzed HF-eliminative cyclization for the synthesis of carbon materials

In 2012, Amsharov and his coworkers reported the bucky-bowl synthesis by regiospecific cove-region closure by HF elimination (Scheme 1.16).[20] Numbers of substrates were found reactive on γ-Al_2O_3 at

150–200 ºC. The HF-eliminative reaction is proposed to undergo dyotropic rearrangement where two sigma bonds migrate simultaneously through a six-electron transition state.

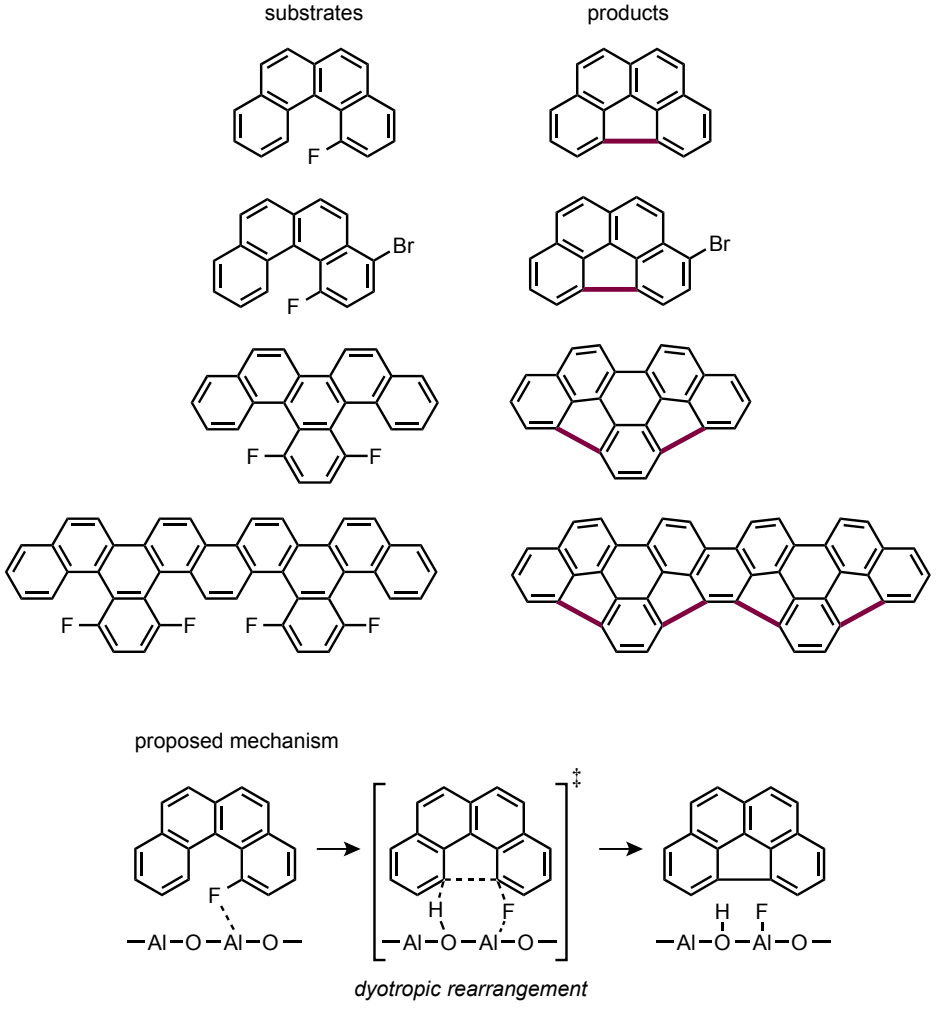

Scheme 1.16 Al_2O_3-mediated HF-eliminative photocyclization for the synthesis of carbon materials

1.4 Cobaloxime-type acceptorless dehydrogenation catalysts

In the research field of water splitting, it is known that certain metalloxime (cobaloxime/nickeloxime) species can work as a water-splitting catalyst that reduces two protons to the molecular hydrogen through **PCET (*Proton-Coupled Electron Transfer*)** mechanism when combined with either photocatalysis or electrolysis. For example, under visible light irradiation, photocatalyst-tethered **31** undergoes excitation to its excited state through MLCT (Metal-to-Ligand Charge Transfer), which can work as single electron reductant to Co^{II} species **32** to produce Co^{I} intermediate **33**. Under sufficiently acidic media the Co^{I} intermediate can be protonated to generate Co^{III}–H complex **34**, which can undergo hydrogen gas release in bimolecular fashion to regenerate Co^{II} catalyst **35**. In the presence of reductant **35** can be reduced to **31**. In case of electrolysis, cathode can provide an electron to Co^{II} species to produce Co^{I} intermediate; the rest of the cobaloxime-catalyzed mechanism is similar to photocatalysis condition.

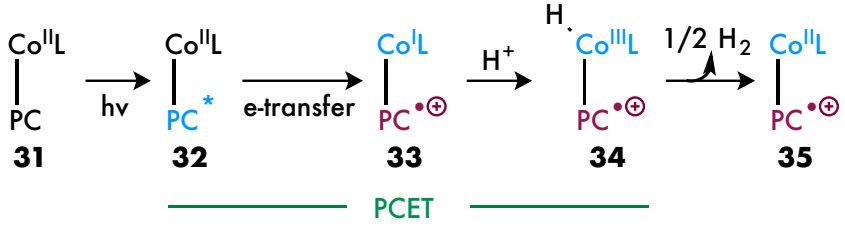

Scheme 1.17 cobaloxime-catalyzed proton reduction under PCET mechanism

1.5 Cobaloxime catalysis in acceptorless dehydrogenative organic transformations

Recently, synthetic effort towards the merger of photoredox catalysis and cobaloxime catalysis has enabled the dehydrogenative cross-coupling reactions of various organic molecules.

In 2015, the Sorensen group reported the tungstate/cobaloxime cooperative catalysis that enabled the direct desaturation of simple alkanes **36** through stepwise HAT (Scheme 1.18).[21] This work, the dehydrogenation of unactivated alkanes, is important in industrial and biological systems, but the substrate scope is quite limited and yields are low.

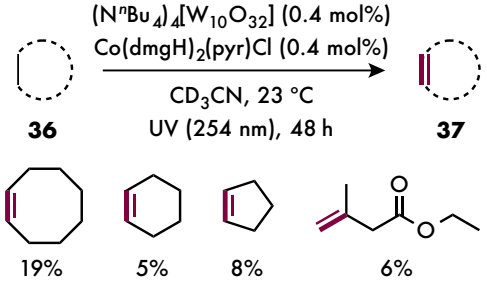

Scheme 1.18 Direct desaturation of alkanes under tungstate/cobaloxime dual catalysis

In 2016, Wu, Tang, and their coworkers have reported the first example of cooperative photoredox/cobaloxime catalysis in organic synthesis; simple benzene and alcohols or amines are cross-coupled in a dehydrogenative manner to produce phenol and aniline derivatives that are valuable feedstocks in synthesis of pharmaceutical and materials (Scheme 1.19).[22] They claimed their approach *"hydrogen-evolution cross-couplings"*, as it avoids the use of stoichiometric amount of oxidants and produces hydrogen gas as a sole byproduct. Amination of benzene was first investigated with Boc–NH_2 as the reagent. The reaction condition were optimized by irradiating the solution of benzene, amination reagent **38** (2 equiv), $QuCN^+ClO_4^-$ (5 mol%), and $Co(dmgBF_2)_2(CH_3CN)_2$ (3 mol%) in dry and degassed acetonitrile with a light of wavelength >300 nm at room temperature. The yields of both Boc-protected aniline **39** and hydrogen gas based on the consumption of benzene were nearly quantitative. Control experiments revealed that all the photocatalyst, cobaloxime catalyst, and light irradiation were necessary for the amination to occur. As well as Boc–NH_2, "NH_2" nucleophiles ($Co(NH_3)_6Cl_3$ and NH_3) can be used to afford aniline up to around 40% yield.

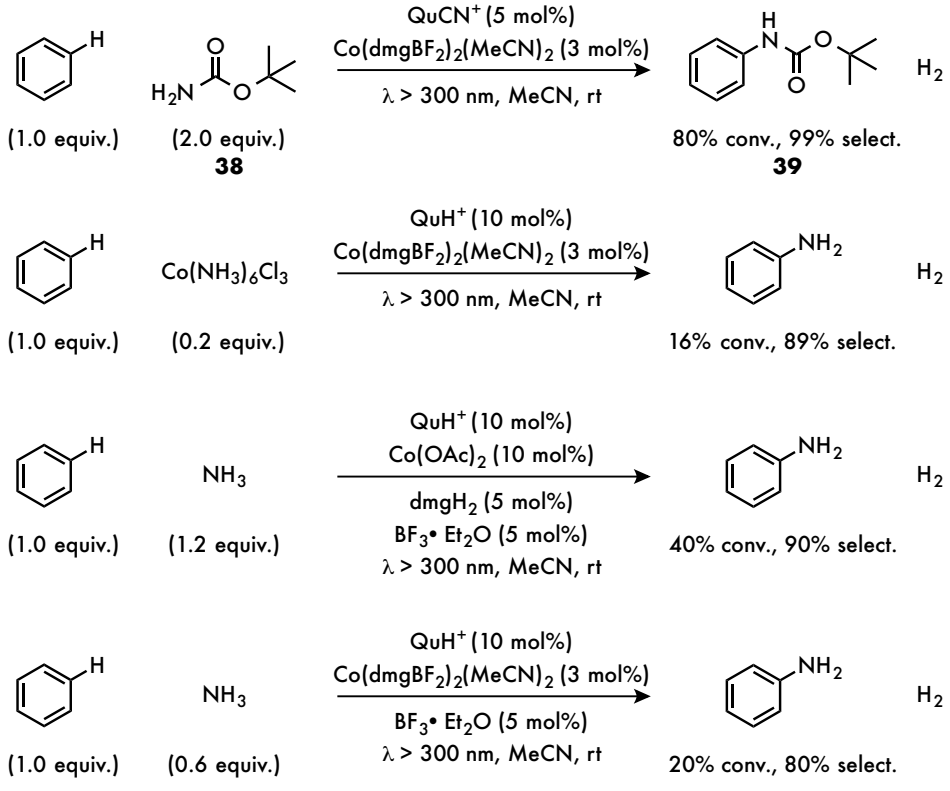

Scheme 1.19 Acceptorless dehydrogenative amination/hydroxylation reactions under photoredox/cobaloxime catalysis (selectivity = yield/conversion)

Mechanistically, the reaction starts with the excitation of acridinium-based photocatalyst (PC^+) to produce PC^{+}* (QuH+ and QuCN's E_{red} = 2.46 and 2.72 V vs. SCE at excited state, respectively), which can oxidize benzene (E_{ox} = 2.48 V vs. SCE in acetonitrile) to form aryl radical species **41** (Scheme 1.20). The radical intermediate is electrophilic enough to couple with anionic oxygen or nitrogen

nucleophile. Concomitantly, the $PC^{\bullet}$ can reduce the Co^{III} species to form Co^{II} intermediate and regenerate the photocatalyst PC^{+}. Single electron oxidation of the carbon-centered radical intermediate **42** by Co^{II} intermediate takes place to regenerate Co^{I} and cationic intermediate **43**, which is followed by deprotonation to afford amination/hydroxylation product **44**.

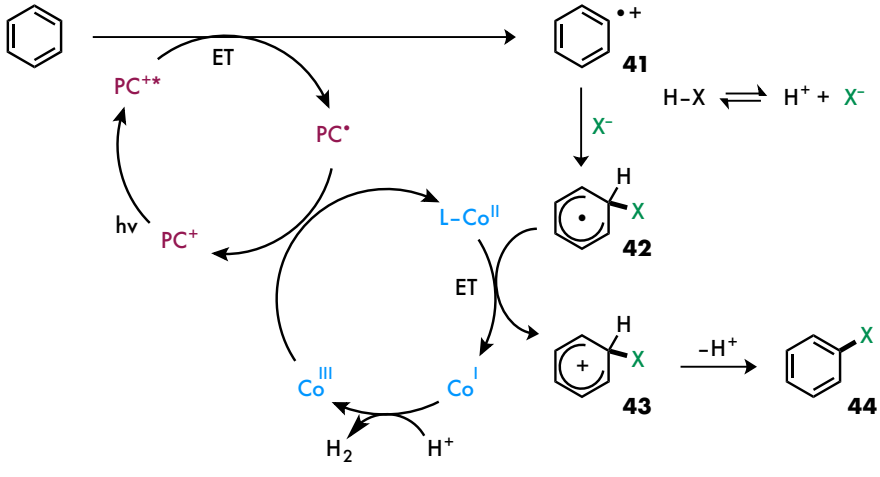

Scheme 1.20 Reaction mechanism of Acceptorless dehydrogenative amination/hydroxylation reactions

After this report, numbers of examples of photoredox/cobaloxime catalysis in C–C, C–N, C–O, and C–S bond formations have been reported. Herein, the C–C bond formation reactions though the photoredox/cobaloxime catalysis are summarized; in 2016, Wu reported the first example of

hydrogen-evolution C–C bond formation of **45**, which gives indole **46** under visible light irradiation (Scheme 1.21).[23] During the mechanic study, they observed kinetic isotope effect (KIE) as high as 1.6 that suggested the late-determining step involved the C(sp^2)–H cleavage step. After the careful mechanistic study, they proposed that the iridium-based photocatalyst intermediate was responsible for oxidation of electron-rich **47** to occur, which triggered the deprotonation and cyclization.

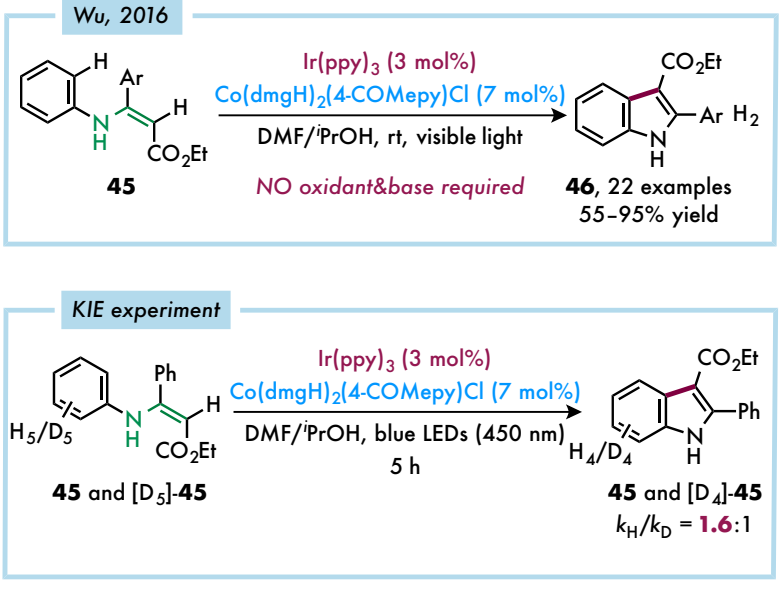

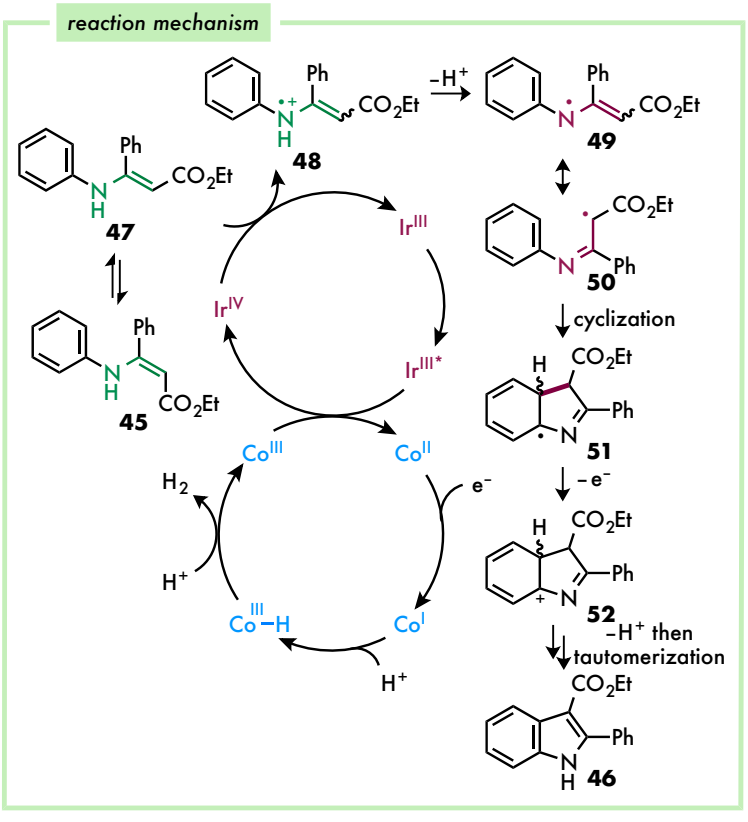

Scheme 1.21 Acceptorless dehydrogenative indole synthesis under photoredox/cobaloxime catalysis

Lei reported the hydrogen-evolution lactonization of 2-arylbenzoic acids via visible light photocatalysis (Scheme 1.22).[24] High functional group tolerance was shown in this work, and the reaction was scaled up to the gram scale that gave 85% yield of the product.

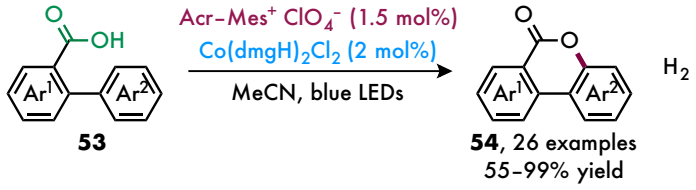

Scheme 1.22 Acceptorless dehydrogenative aromatic lactone synthesis under photoredox/cobaloxime catalysis

The same group also reported the oxidative [4+2] intermolecular annulations of aryl imines and alkenes (Scheme 1.23).[25] Highly diastereoselective cyclization was achieved.

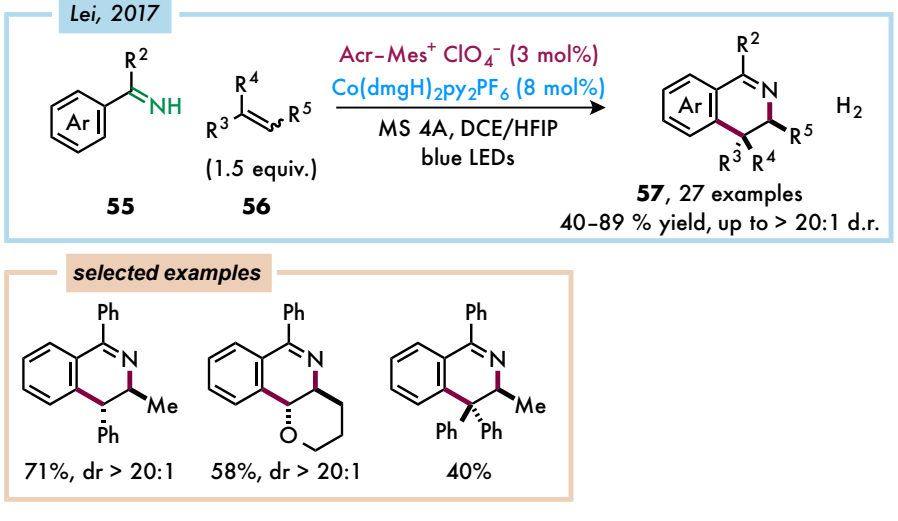

Scheme 1.23 Acceptorless dehydrogenativeimine/alkene [4+2] cycloaddition under photoredox/cobaloxime catalysis

More recently, Lei reported the oxidative [4+2] annulations of styrenes and alkynes under photoredox/cobaloxime catalysis (Scheme 1.24).[26] This reaction can be formally seen as oxidative Diels–Alder reaction under oxidant-free conditions, and is the powerful method for making aromatic motifs including heteroaromatics. Under the sunlight, the gram-scale reaction was successful without stirring the reaction mixture.

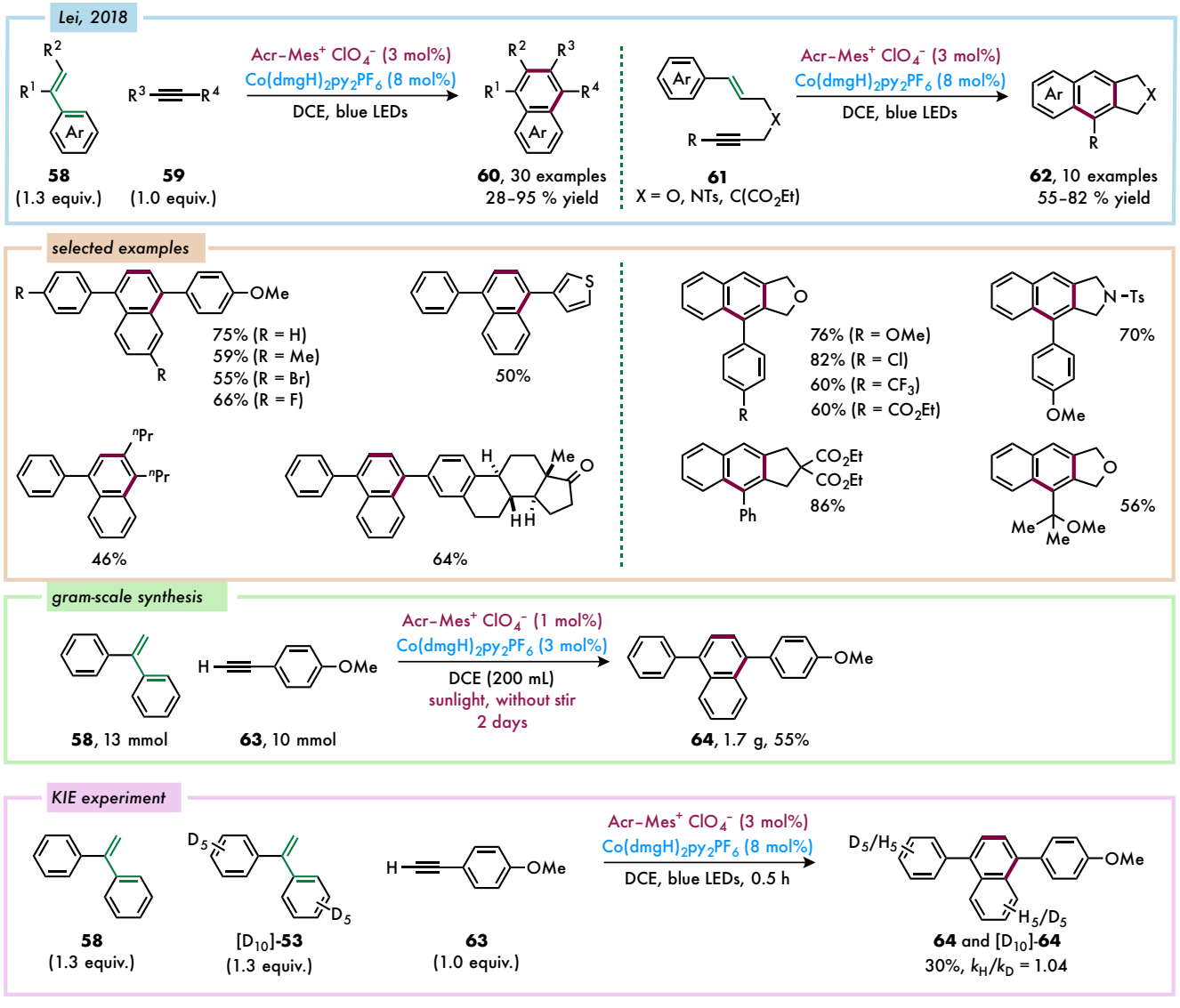

Scheme 1.24 Acceptorless dehydrogenative styrene/alkyne [4+2] cycloaddition under photoredox/cobaloxime catalysis

1.6 The author's work

My work in this thesis is mainly dedicated to the development of cabaloxime catalysis that allows acid/oxidant-free intramolecular cyclodehydrogenation of arenes. During the PhD work, I have independently come up with the idea on the projects and conducted experiments.

1.7 References

[1] (a) K. S. Novoselov, A. K. Geim, S. V. Morozov, D. Jiang, Y. Zhang, S. V. Dubonos, I. V. Grigorieva and A. A. Firsov, *Science* **2004**, *306*, 666. (b) A. K. Geim and K. S. Novoselov, *Nat. Mater.* **2007**, *6*, 183. (c) R. F. Service, *Science* **2009**, *324*, 875. (d) K. S. Novoselov, V. I. Falko, L. Colombo, P. R. Gellert, M. G. Schwab and K. Kim, *Nature* **2012**, *490*, 192.

[2] F. Schwierz, *Nat. Nanotechnol.* **2010**, *5*, 487.

[3] (a) R. Rieger and K. Müllen, *J. Phys. Org. Chem.* **2010**, *23*, 315. (8) M. Bacon, S. J. Bradley and T. Nann, Part. Part. Syst. Charact., **2014**, *31*, 415. (9) S. Kim, S. W. Hwang, M.-K. Kim, D. Y. Shin, D. H. Shin, C. O. Kim, S. B. Yang, J. H. Park, E. Hwang, S.-H. Choi, G. Ko, S. Sim, C. Sone, H. J. Choi, S. Bae and B. H. Hong, *ACS Nano* **2012**, *6*, 8203.

[4] (a) J. Wu, W. Pisula and K. Müllen, *Chem. Rev.* **2007**, *107*, 718. (b) K. Müllen, *ACS Nano* **2014**, *8*, 6531.

[5] X. Yang, X. Dou, A. Rouhanipour, Linjie Zhi, Hans Joachim Räder, and Klaus Müllen. *J. Am. Chem. Soc.* **2008**, *130*, 4216.

[6] M. E. Gemayel et. al. *Nanoscale* **2014**, *6*, 6301.

[7] J. Gao *et. al. ACS Nano* **2016**, *10*, 4847.

[8] Naoki Asao *et al*. *J. Am. Chem. Soc*. **2003**, *125*, 10921.

[9] Hasan Arslan *et al*. *Angew. Chem. Int. Ed*. **2012**, *51*, 12051.

[10] A. Ajaz, E. C. McLaughlin, S. L. Skraba, R. Thamatam, R. P. Johnson. *J. Org. Chem.* **2012**, *77*, 9487−9495.

[11] X. Dou, X. Yang, G. J. Bodwell, M. Wagner, V. Enkelmann, K. Müllen. *Org. Lett.* **2007**, *9*, 2485.

[12] J. Liu, A. Narita, S. Osella, W. Zhang, D. Schollmeyer, D. Beljonne, X. Feng, K. Mullen. *J. Am. Chem. Soc.* **2016**, *138*, 2602−2608.

[13] B. T. King, J. Kroulík, C. R. Robertson, P. Rempala, C. L. Hilton, J. D. Korinek, L. M. Gortari. *J. Org. Chem.* **2007**, *72*, 2279-2288.

[14] X.-Y. Cao, H. Zi, W. Zhang, H. Lu, J. Pei. *J. Org. Chem.* **2005**, *70*, 3645–3653.

[15] F. Dötz, J. Diedrich Brand, S. Ito, L. Gherghel, K. Müllen. *J. Am. Chem. Soc.* **2000**, *122*, 7707-7717

[16] M. Iwasaki, Y. Araki, S. Iino, Y. Nishihara. *J. Org. Chem.* **2015**, *80*, 9247−9263.

[17] M. Daigle, A. Picard-Lafond, E. Soligo, J.-F. Morin. *Angew. Chem. Int. Ed.* **2016**, *55*, 2042 –2047.

[18] D. Miao, C. Aumaitre, J.-F. Morin. *J. Mater. Chem.* **2019**, *7*, 3015.

[19] O. Allemann, S. Duttwyler, P. Romanato, K. K. Baldridge, J. S. Siegel. *Science* **2011**, *332*, 574-577.

[20] (a) K. Yu. Amsharov, M. A. Kabdulov, M. Jansen. *Angew. Chem. Int. Ed.* **2012**, *51*, 4594 –4597; (b) K.Yu. Amsharov, P. Merz, *J. Org. Chem.* **2012**, *77*, 5445−5448.

[21] J. G. West, D. Huang, E. J. Sorensen. *Nat. Commun* **2015**, *6*, 10093.

[22] Y.-W. Zheng, B. Chen, P. Ye, K. Feng, W. Wang, Q.-Y. Meng, L.-Z. Wu, C.-H. Tung. *J. Am. Chem. Soc.* **2016**, *138*, 10080−10083.

[23] C.-J. Wu, Q.-Y. Meng, T. Lei, J.-J. Zhong, W.-Q. Liu, L.-M. Zhao, Z.-J. Li, B. Chen, C.-H. Tung, L.-Z. Wu. *ACS Catal*. **2016**, *6*, 4635−4639.

[24] A. Shao, J. Zhan, N. Li, C.-W. Chiang, A. Lei. *J. Org. Chem.* **2018**, *83*, 3582−3589.

[25] X. Hu, G. Zhang, F. Bu, A. Lei. *Angew. Chem. Int. Ed.* **2018**, *57*, 1286–1290.

[26] G. Zhang, Y. Lin, X. Luo, X. Hu, C. Chen, AE. Lei, *Nat. Commun* **2018**, *9*, 1225.

2. Acceptorless catalytic dehydrogenative cyclization of *o*-teraryls

(Contents of this chapter were published in *Angew. Chem. Int. Ed.* 10.1002/anie.202004719)

2.1 Introduction

Cyclodehydrogenation reactions, also known as the Scholl-type reactions, have found broad utilities in synthesis of various bioactive or functional molecules (Scheme 1A).[1] In particular, the aromatization reaction involving *o*-teraryls has emerged as an increasingly important method in preparing polyaromatic hydrocarbons (PAHs) that often exhibit interesting optical and electronic properties.[2] While extensively employed, the Scholl oxidation typically requires excess strong acids (e.g. $AlCl_3$, $FeCl_3$, $MoCl_5$, TfOH) and/or strong oxidants (e.g. DDQ), which consequently results in many waste byproducts. In addition, many functional groups could not be tolerated, and side reactions, such as 1,2-aryl shift, over-oxidation and substrate decomposition, are often observed under such conditions.[3] Regarding the scope of substrates, the Scholl oxidation generally prefers electron-neutral or moderately rich arenes;[3a,4] by contrast, electron-deficient arenes or highly electron-rich heterocycles are problematic.[1c] While the same

type cyclodehydrogenations of *o*-teraryls have also been realized with other approaches, including the use of heterogeneous catalysts,[4] electrochemical[5] or photochemical conditions (the Mallory−Katz reaction),[6] use of stoichiometric strong acids or oxidants is still needed. On the other hand, the triphenylene products could also be accessed via related and redox-neutral approaches, such as Pd-catalyzed cross couplings[7] and eliminative photocyclization reaction,[8] though the use of more functionalized substrates is required. Hence, it could be highly appealing to realize an efficient, general, mild and atom-economical cyclodehydrogenative reaction of *o*-teraryls.

Cobaloximes have been reported as versatile catalysts in many hydrogen-atom transfer (HAT) and water-splitting-type hydrogen evolution reactions.[9] Especially, the recent merge of photoredox catalysis with the cobaloxime HAT catalysis has led to a number of new hydrogen gas-releasing transformations.[10] However, its use in cyclodehydrogenation of simple arene substrates is still rare and limited to date.[10h,o] On the other hand, a direct coupling of an organic photochemical process, e.g. electrocyclization, (in the absence of photoredox catalysts) with the cobaloxime-catalyzed hydrogen evolution has not been reported, to the best of our knowledge.[11]

Given the attractive aspects of having hydrogen as a useful byproduct[12] and the demand for more chemoselective PAH synthesis, herein, we describe our discovery of a cobaloxime-catalyzed acceptorless dehydrogenative cyclization of *o*-teraryls under acid and oxidant-free conditions (Scheme 2.1B).

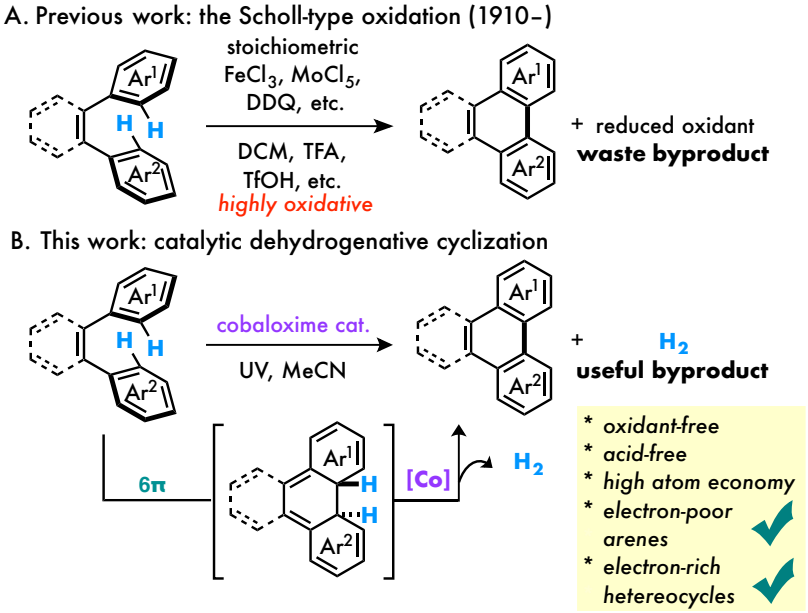

Scheme 2.1 Cyclodehydrogenation of *o*-teraryls

2.2 Results & discussion

2.2.1 Optimization process

We hypothesized that under photochemical conditions *o*-teraryls would first undergo established conrotatory 6π electrocyclization,[13] and the resulting highly reactive dihydrotriphenylene intermediate could then be dehydrogenated by the cobaloxime catalyst with H_2 evolution. To examine this hypothesis, *o*-terphenyl **1a** was chosen as the model substrate. After careful optimization of the reaction conditions, including catalysts, solvents, reaction time, concentration and setups (for details, see the Supporting Information), the desired triphenylene product **2a** was ultimately obtained in a quantitative yield, using $Co(dmg(BF_2))_2(OH_2)_2$ as the catalyst (**A**) irradiated by 254 nm light (Table 2.1, entry 1). A number of control experiments were carried out under the catalytic system. First, in the absence of either the cobalt catalyst or light, no desired product was obtained (entries 2 and 3). The wavelength of light was also important, as a longer wavelength (300 nm) or using the photoredox/cobaloxime dual catalytic system under blue LEDs[10] gave no desired product (entries 4 and 5). The Co catalyst is also unique; using the conventional Pd/C as the catalyst or Sorensen's dehydrogenative catalyst system[14] gave no conversion of o-terphenyl **1a** (entries 6 and 7). When only 3 mol% of the Co catalyst was used, 35% yield of triphenylene **2a** was observed (entry 8) and a *quantitative* yield could still be

obtained with a prolonged reaction time (entry 9). Finally, the solvent effect was studied (entries 10–12). Among all solvent screened, MeCN proved to be the most effective. While less polar solvents, such as toluene and CH_2Cl_2, gave almost no reactivity, MeOH can nevertheless deliver 23% yield of **2a**.

Table 2.1. Optimization study

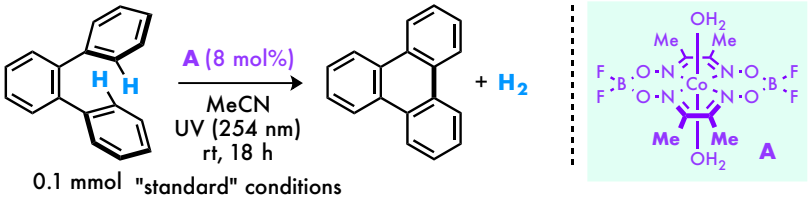

0.1 mmol "standard" conditions

entry	variation(s) from the "standard" conditions	yield(%)[a]
1	none	quant.
2	no **A**	< 5
3	no UV	< 5
4	UV (300 nm) instead	< 5
5	Acr–$Mes^+ClO_4^-$ (3 mol%), **A** (8 mol%) and blue LEDs instead of UV (254 nm)	< 5
6	Pd/C (5 mol%) instead of **A**	< 5
7	COPC (3 mol%) & tetra-*n*-butylammonium decatungstate (1 mol%), instead of **A**	< 5
8	**A** (3 mol%)	35
9	**A** (3 mol%), 48 h	quant.
10	MeOH instead of MeCN	23
11	PhMe instead of MeCN	< 5
12	CH_2Cl_2 instead of MeCN	< 5

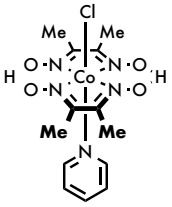

COPC

2.2.2 Substrate scope

With optimized conditions in hand, we studied the substrate scope. To our delight, various electron-neutral and rich substrates (**1a**–**1d**) gave excellent yields, which typically showed somewhat lower yields under the Scholl or oxidative conditions.[3a,4] Notably, the more electron-rich triphenylene **2e** was difficult to obtain due to severe side reactions under strongly acidic conditions;[3a,4] our acid-free reaction condition afforded **2e** in excellent yield. In addition, a number of *acid sensitive* functional groups, such as free benzylic alcohol (**2f**), MOM (**2f-MOM**) and TBS (**2f-TBS**) ethers, were tolerated. These moieties have not been shown compatible previously under the conventional Scholl oxidation conditions. Dimers or oligomers of starting materials were not observed in these cases. Substrates with electron-withdrawing groups such as –CN, $–CF_3$, and –Cl (**1g-1j**) were successfully transformed to the corresponding triphenylenes in good to excellent yields. These electron-deficient substrates usually show low to no reactivity under the cyclodehydrogenative conditions that require a direct single-electron oxidation or protonation process.[1c] Moreover, olefin-linked substrates also provided the desired cyclized products in moderate to high yields; bulkier olefins gave higher yields because the steric

hindrance could suppress the undesired [2+2] cycloaddition pathway. Given the high reactivity of olefins towards oxidants/electrophiles, e.g. in I_2-mediated Mallory reaction,[15] this oxidant-free protocol could be beneficial for this type of substrates. Furthermore, heterocyclic groups including electron-rich thiophenes (**2o**, **2r**) and electron-deficient pyridines (**2p**) and pyrimidine (**2q**), were well tolerated, affording heterocyclic polyaromatic motifs in excellent yields. Double cyclodehydrogenation proceeded smoothly to deliver the hexacyclic heteroaromatic product (**2s**), which was previously synthesized for the OLED study under oxidative conditions.[16]

Table 2.2 Substrate Scope

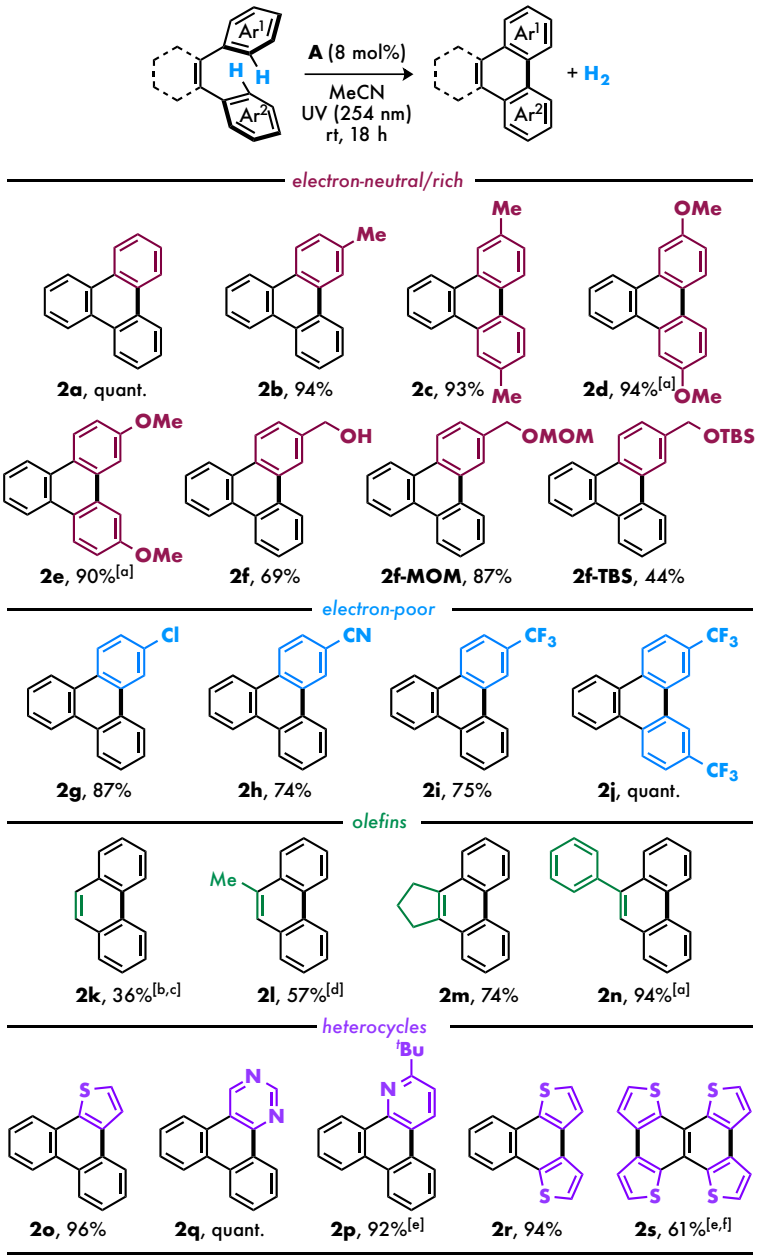

[a] MeCN (0.6 mL) was used. [b] MeCN (0.3 mL) was used. [c] (*Z*)-stilbene was used as a substrate. [d] (*E*)-□-methylstilbene was used as a substrate. [e] Reaction time = 36 h. [f] MeCN/dichloromethane (2/1, 0.5 mL) and 16 mol% of **A** were used.

2.2.3 Mechanistic study

Preliminary studies were then carried out to explore the reaction mechanism. First, hydrogen gas was detected through GC with thermal conductivity detector (TCD). Under the standard conditions, hydrogen gas was detected as 71% yield (Scheme 2.2A). This result suggests that the dehydrogenative C–C bond forming event primarily takes place through an acceptorless dehydrogenation process, instead of an oxidative manner. Second, a light on/off experiment revealed that the reaction efficiently took place under light irradiation and was suppressed under dark, which suggests that light is required to promote the reaction. (Scheme 2.2B). Effective cooling was found important for high yields, which ruled out a heat-mediated process. Lastly, the dehydrogenation step with the $Co(dmg(BF_2))_2(OH_2)_2$ catalyst was studied using 1,4-dihydronaphthalene as a simplified model compound. It was clear that dehydrogenation could take place in the presence of both the Co catalyst and the light (Scheme 2.2C). Only a very small amount of naphthalene was observed in the absence of Co or light; the trace product was probably formed due to aerobic oxidation during the workup. This result indicates that the dehydrogenation process likely involves photoexcitation of the substrate or the Co catalyst or

both.

A. detection of hydrogen gas

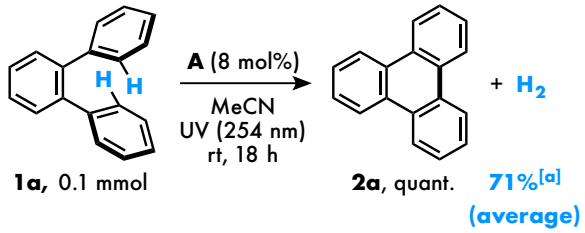

B.light on/off experiment

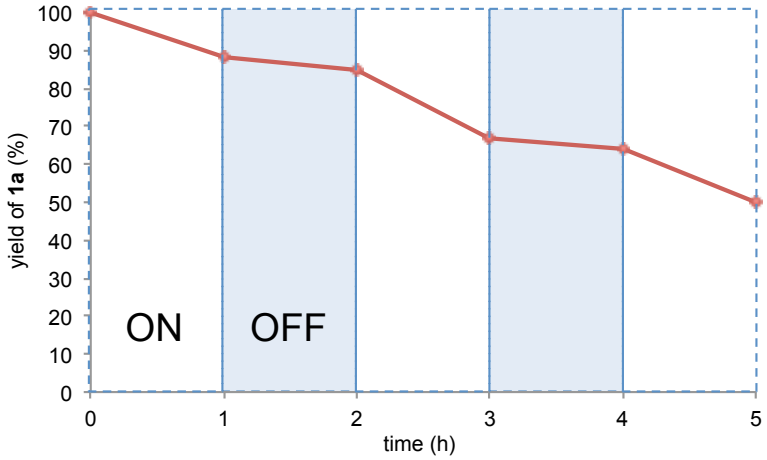

C. desaturation of 1,4-dihydronaphthalene

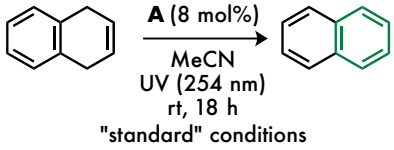

entry	variation(s) from the standard condition	yield(%)[b]
1	none	20
2	no light	3
3	no **A**	3

[a] Yields were determined by GC-TCD analysis. The average yield was calculated through three experiments. [b] Yields were determined by ^{1}H-NMR spectroscopy using 1,1,2,2-tetrachloroethane as an internal standard.

Scheme 2.2 Preliminary Mechanistic Explorations

While some mechanistic details of this reaction remain unclear and are the topic for further investigation, the above and previously reported data allow us to propose a hypothesis about the mechanism for the Co-catalyzed dehydrogenative cyclization of *o*-teraryls (Figure 2.1). The reaction starts with photo-excited conrotatory 6π electrocyclization to generate a transient *trans*-dihydro-triphenylene intermediate (**I**). Given that *o*-terphenyl exhibits a maximum UV absorption (λ_{max}) at 235 nm (in EtOH),[17] the observed wavelength dependence is consistent with the hypothesis of the 6π electrocyclization instead of single-electron oxidation of **1a** either by the photoredox catalyst or cobalt catalyst. Meanwhile, the photoexcited Co(II) catalyst ($[Co(dmg(BF_2))_2(MeCN)_2]^*$ = 1.91 V vs. SCE in DCE ($E^{II*/I} = E^{II/I} + E_{00}$))[18] would be able to accept an electron from the polyene intermediate (**I**) (less conjugated cyclohexadiene has an oxidation potential of 1.82 V vs. SCE in MeCN)[19] to give a highly delocalized radical cation intermediate (**II**), and the resulting anionic Co(I) would abstract an proton from **II**.[20] Alternatively, a single electron transfer from photoexcited **I*** to Co(II) followed by Co(I)-mediated deprotonation, or direct HAT between the Co(II) and $\mathbf{I}^*$ to give the same Co(III)-hydride. Cobaloxime hydrides would undergo homolytic cleavage of the Co−H bond for

H_2 evolution.[21] Thus, they can either dimerize, or abstract the hydrogen from the weakened C–H bond of radical intermediate **III** to regenerate the Co(II) catalyst and H_2, ultimately.

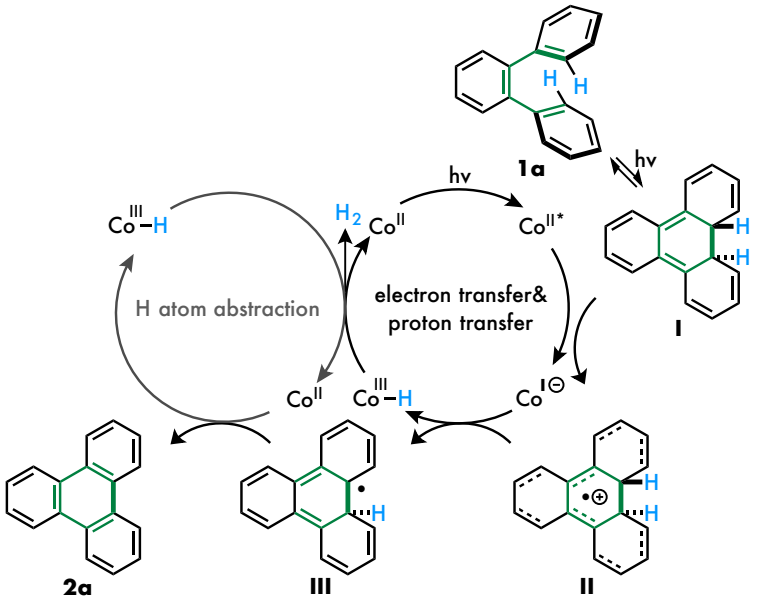

Figure 2.1 Proposed Catalytic Cycle

2.3 Conclusion

In conclusion, an efficient and general dehydrogenative cyclization of *o*-teraryls has been developed under photochemical conditions. The reaction is pH-neutral and oxidant-free, and operates at near room temperature. The tolerance of a broad range of substrates with various electronic properties and labile functional groups, as well as different heteroarenes, could make

this method attractive for preparing functional PAH-based materials.[22]

2.4 Experimental Sections

General information

All UV-mediated reactions were carried out in 20 mL Quartz test tubes under nitrogen atmosphere. Acetonitrile was purchased from Acros Organics. $Co(dmg(BF_2)_2)(OH_2)_2$ was prepared following the reported procedure[23]. 25W UVC lamps (λ = 254 nm, L x W x H = 8.5 x 2 x 2 inches) were purchased from coospider

(https://www.amazon.com/gp/product/B07KYVRVX7/ref=ppx_yo_dt_b_asin_title_o03_s00?ie=UTF8&psc=1), and used as light source. All commercially available substrates were used without further purification. Thin layer chromatography (TLC) analysis was run on silica gel plates purchased from EMD Chemical (silica gel 60, F254). Infrared spectra were recorded on a Nicolet iS5 FT-IR Spectrometer using neat thin film technique. High-resolution mass spectra (HRMS) were obtained on an Agilent 6224 TOF-MS spectrometer and are reported as m/z.

Amounts of H_2 generated in the photo-catalytic experiments were determined by gas chromatography (GC) using an SRI 8610C Gas Chromatograph with the nitrogen carrier gas and a TCD detector. Methane was used as internal standard for the measurement of the yield of H_2. UV–Vis spectra was measured with NanoDrop™ One^C. UV-Vis spectrometer. Nuclear magnetic resonance spectra (^{1}H NMR and ^{13}C NMR) were recorded with a Bruker Model DMX 400 (400 MHz, ^{1}H at 400 MHz, ^{13}C at 101 MHz). For $CDCl_3$ solutions, the chemical shifts were reported as parts per million (ppm) referenced to residual protium or carbon of the solvents: $CHCl_3$ δ H (7.26 ppm) and $CDCl_3$ δ C (77.00 ppm). For CD_2Cl_2 solutions, the chemical shifts were reported as parts per million (ppm) referenced to residual protium or carbon of the solvents: CH_2Cl_2 δ H (5.32 ppm) and CD_2Cl_2 δ C (53.80 ppm). Coupling constants were reported in Hertz (Hz). Data for ^{1}H NMR spectra were reported as following: chemical shift (δ, ppm), multiplicity (br = broad, s = singlet, d = doublet, t = triplet, q = quartet, dd = doublet of doublets, td = triplet of doublets, ddd = doublet of doublet of doublets, m = multiplet), coupling constant (Hz), and integration.

Synthesis and characterization of substrates

Compounds **1b**[24], **1d**[25], **1e**[3], **1h**[26], **1i**[27], **1j**[5], **1m**[28], **1o**[29], **1r**[30], **1s**[31] were synthesized according to the literature procedures. Compounds **1c**, **1f**, **1g**, **1p**, **1q** were prepared according to the following procedures. Compounds **1c** and **1f** are known.[3,10] The others are commercially available and used without further purification.

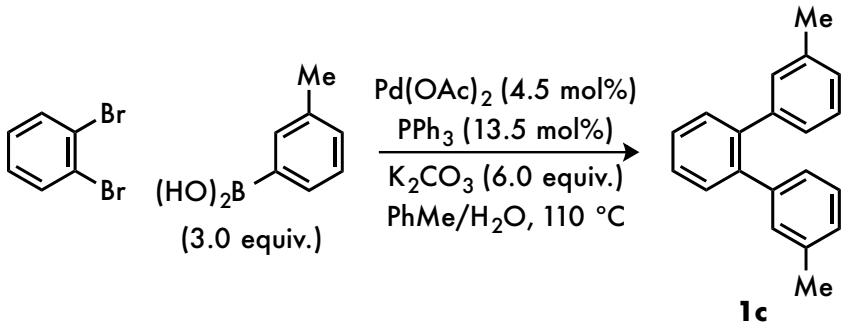

3,3''-dimethyl-1,1':2',1''-terphenyl (1c)[3]: A 40 mL vial was charged with 1,2-dibromobenzene (235.9 mg, 1.0 equiv.), 3-tolylboronic acid (408.0 mg, 3.0 equiv.), PPh_3 (35.4 mg, 13.5 mol%), K_2CO_3 (829.3 mg, 6.0 equiv.), PhMe (3 mL), and H_2O (2 mL). The mixture was bubbled with N_2 for 5 min and $Pd(OAc)_2$ (10.1 mg, 4.5 mol%) was added and the vial was sealed with the cap. The mixture was heated to 110 ºC and stirred overnight. The mixture was cooled to room temperature and diluted with ethyl acetate and extracted with ethyl acetate three times. The

combined organic layers were washed with brine, dried over $MgSO_4$, and concentrated. The residue was purified by column chromatography (hexane) to give product **1d** as a colorless oil (160.1 mg) in 62% yield. R_f = 0.4 (hexane). **^{1}H NMR** (400 MHz, $CDCl_3$) δ 7.49 – 7.43 (m, 4H), 7.15 – 6.94 (m, 8H), 2.32 (s, 6H). **^{13}C NMR** (101 MHz, $CDCl_3$) δ 141.5, 140.6, 137.3, 130.51, 130.47, 127.5, 127.3, 127.06, 127.03, 21.4.

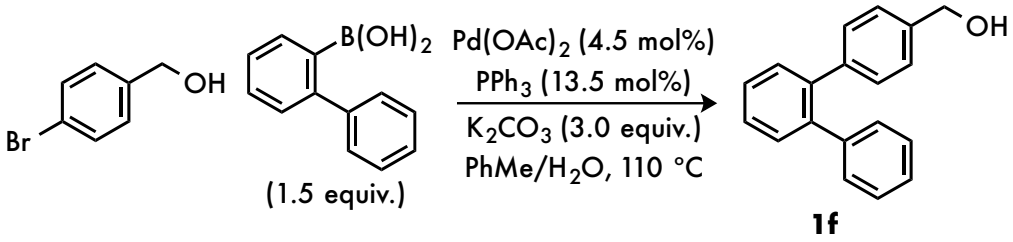

[1,1':2',1''-terphenyl]-4-ylmethanol (1f)[32]: A 40 mL vial was charged with 4-bromobenzyl alcohol (187.0 mg, 1.0 mmol, 1.0 equiv.), 2-biphenylboronic acid (297.0 mg, 1.5 equiv.), PPh_3 (35.4 mg, 13.5 mol%), K_2CO_3 (414.7 mg, 3.0 equiv.), PhMe (3 mL), and H_2O (2 mL). The mixture was bubbled with N_2 for 5 min and $Pd(OAc)_2$ (10.1 mg, 4.5 mol%) was added and the vial was sealed with the cap. The mixture was heated to 110 ºC and stirred overnight. The mixture was cooled to room temperature and diluted with ethyl acetate and extracted with ethyl

acetate three times. The combined organic layers were washed with brine, dried over $MgSO_4$, and concentrated. The residue was purified by column chromatography (hexane/ethyl acetate = 3/1) to give product **1g** as a white solid (221.3 mg) in 85% yield. R_f = 0.3 (hexane/ethyl acetate = 3/1). **^{1}H NMR** (400 MHz, $CDCl_3$) δ 7.44 – 7.41 (m, 4H), 7.25 – 7.13 (m, 9H), 4.66 (s, 2H), 1.67 (brs, 1H). **^{13}C NMR** (101 MHz, $CDCl_3$) δ 141.4, 140.9, 140.5, 140.1, 138.9, 130.64, 130.57, 130.0, 129.8, 127.9, 127.5, 126.54, 126.45.

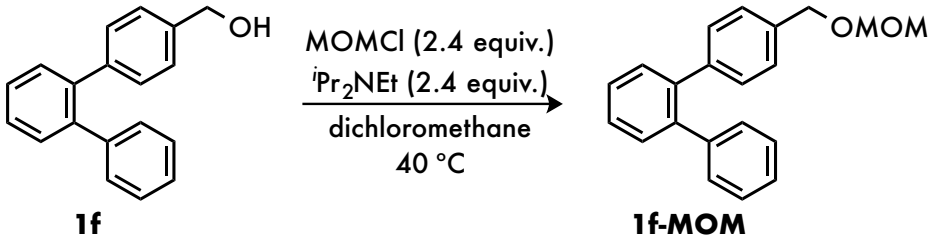

4-((methoxymethoxy)methyl)-1,1':2',1''-terphenyl (1f-MOM): A 20 mL vial was charged with **1f** (65.1 mg, 0.25 mmol, 1.0 equiv.), dichloromethane (2.5 mL), and ^{i}Pr$_2$NEt (77.7 mg, 2.4 equiv.), MOMCl (48.3 mg, 2.4 equiv.) was added into the mixture and the vial was sealed with the cap. The mixture was heated to 40 ºC and stirred overnight. The mixture was cooled to room temperature and diluted with ethyl acetate and extracted with ethyl acetate three times. The

combined organic layers were washed with brine, dried over $MgSO_4$, and concentrated. The residue was purified by column chromatography (hexane/ethyl acetate = 4/1) to give product **1f-MOM** as a colorless oil (177.2 mg) in 97% yield. R_f = 0.4 (hexane/ethyl acetate = 4/1). **^{1}H NMR** (400 MHz, $CDCl_3$) δ 7.42 (m, 4H; Ar–H), 7.22 – 7.14 (m, 9H; Ar–H), 4.70 (s, 2H; Ar–CH_2–O), 4.56 (s, 2H; O–CH_2–O), 3.40 (s, 3H; OCH_3). **^{13}C NMR** (101 MHz, $CDCl_3$) δ 141.5, 141.0, 140.6, 140.2, 136.0, 130.64, 130.61, 129.93, 129.86, 127.9, 127.48, 127.46, 126.5, 95.8, 69.1, 55.4. IR (KBr, cm^{-1}) 3057, 2931, 1475, 1400, 1148, 1047, 778. HRMS calcd $C_{21}H_{20}O_2$ $[M]^+$: 304.1463. Found: 304.1464.

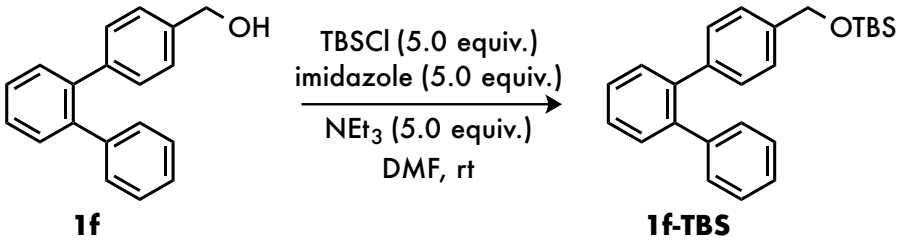

([1,1':2',1''-terphenyl]-4-ylmethoxy)(*tert*-butyl)dimethylsilane (1f-TBS): A 20 mL vial was charged with **1f** (65.1 mg, 0.25 mmol, 1.0 equiv.), DMF (2.0 mL), NEt_3 (126.5 mg, 5.0 equiv.), and imidazole (85.1 mg, 5.0 equiv.). TBSCl (188.4 mg, 5.0 equiv.) was added into the mixture

and the vial was sealed with the cap. The mixture was stirred for 2 h at room temperature. The mixture was diluted with ethyl acetate and extracted with ethyl acetate three times. The combined organic layers were washed with brine, dried over $MgSO_4$, and concentrated. The residue was purified by column chromatography (hexane/ethyl acetate = 10/1) to give product **1f-TBS** as a white solid (93.6 mg) in quantitative yield. R_f = 0.3 (hexane/ethyl acetate = 10/1). **^{1}H NMR** (400 MHz, $CDCl_3$) δ 7.43 (m, 4H; Ar–H), 7.24 – 7.11 (m, 9H; Ar–H), 4.72 (s, 2H; CH_2), 0.95 (s, 9H; 3*C–CH_3), 0.09 (s, 6H; 2*Si–CH_3). **^{13}C NMR** (101 MHz, $CDCl_3$) δ 141.5, 140.5, 140.4, 140.1, 139.6, 130.63, 130.59, 129.9, 129.7, 127.9, 127.43, 127.35, 126.4, 125.6, 64.8, 26.0, 18.4. -5.2. IR (KBr, cm^{-1}) 2955, 2856, 1473, 1256, 1209, 1090, 761. Melting point: 86 – 87 ºC. HRMS calcd $C_{25}H_{30}OSi$ $[M]^+$: 374.2066. Found: 374.2066.

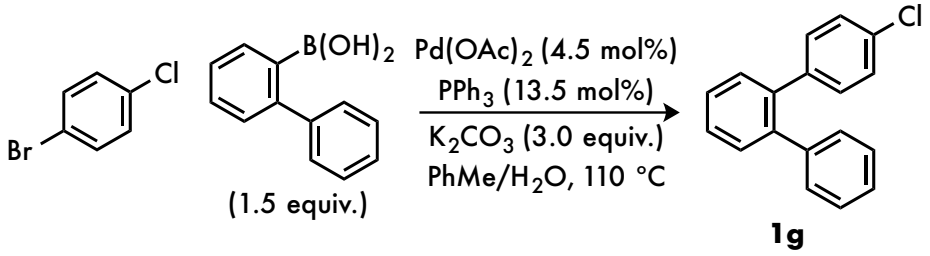

4-chloro-1,1':2',1''-terphenyl (1g): A 40 mL vial was charged with 1-bromo-2-chlorobenzene

(191.5 mg, 1.0 equiv.), 2-biphenylboronic acid (297.0 mg, 1.0 equiv.), PPh_3 (35.4 mg, 13.5 mol%), K_2CO_3 (414.7 mg, 3.0 equiv.), PhMe (3 mL), and H_2O (2 mL). The mixture was bubbled with N_2 for 5 min and $Pd(OAc)_2$ (10.1 mg, 4.5 mol%) was added and the vial was sealed with the cap. The mixture was heated to 110 ºC and stirred overnight. The mixture was cooled to room temperature and diluted with ethyl acetate and extracted with ethyl acetate three times. The combined organic layers were washed with brine, dried over $MgSO_4$, and concentrated. The residue was purified by column chromatography (hexane/ethyl acetate = 40/1) to give product **1h** as a white solid (243.6 mg) in 92% yield. R_f = 0.4 (hexane/ethyl acetate = 60/1). **^{1}H NMR** (400 MHz, $CDCl_3$) δ 7.43 – 7.40 (m, 4H; Ar–H), 7.26 – 7.08 (m, 9H; Ar–H). **^{13}C NMR** (101 MHz, CD_2Cl_2) δ 141.6, 140.9, 140.6, 139.6, 132.8, 131.6, 131.0, 130.7, 130.21, 130.19, 128.3, 128.2, 127.9, 127.0. IR (KBr, cm^{-1}) 3057, 2925, 1472, 1448, 1091, 831, 700. Melting point: 83 – 84 ºC. HRMS calcd $C_{18}H_{13}Cl$ $[M]^+$: 264.0706. Found: 264.0716.

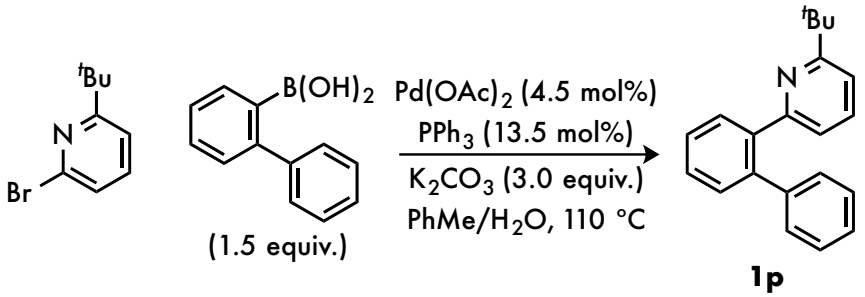

2-([1,1'-biphenyl]-2-yl)-6-(tert-butyl)pyridine (1p): A 40 mL vial was charged with 2-bromo-6-(*tert*-butyl)pyridine[33] (214.1 mg, 1.0 mmol, 1.0 equiv.), 2-biphenylboronic acid (297.0 mg, 1.5 equiv.), PPh_3 (35.4 mg, 13.5 mol%), K_2CO_3 (414.7 mg, 3.0 equiv.), PhMe (3 mL), and H_2O (2 mL). The mixture was bubbled with N_2 for 5 min and $Pd(OAc)_2$ (10.1 mg, 4.5 mol%) was added and the vial was sealed with the cap. The mixture was heated to 110 ºC and stirred overnight. The mixture was cooled to room temperature and diluted with ethyl acetate and extracted with ethyl acetate three times. The combined organic layers were washed with brine, dried over $MgSO_4$, and concentrated. The residue was purified by column chromatography (hexane/ethyl acetate = 20/1) to give product **1h** as a white solid (275.9 mg) in 96% yield. R_f = 0.5 (hexane/ethyl acetate = 20/1). **^{1}H NMR** (400 MHz, $CDCl_3$) δ 7.72 – 7.70 (m, 1H; Ar–H), 7.47 – 7.39 (m, 4H; Ar–H), 7.22 – 7.12 (m, 6H; Ar–H), 6.89 (d, J = 4.0 Hz, 1H; N–C(^{t}Bu)–C–**H**), 1.22 (s, 9H; 3*CH_3).**^{13}C NMR** (101 MHz, $CDCl_3$) δ 168.6, 157.7, 142.1, 141.0, 140.3, 135.5,

130.7, 130.5, 129.6, 128.1, 127.9, 127.4, 126.3, 121.5, 116.4, 37.4, 30.0. IR (KBr, cm^{-1}) 3445, 2957, 1572, 1447, 745, 700. Melting point: 70 – 71 ºC. HRMS calcd $C_{21}H_{21}N$ $[M]^+$: 287.1674. Found: 287.1679.

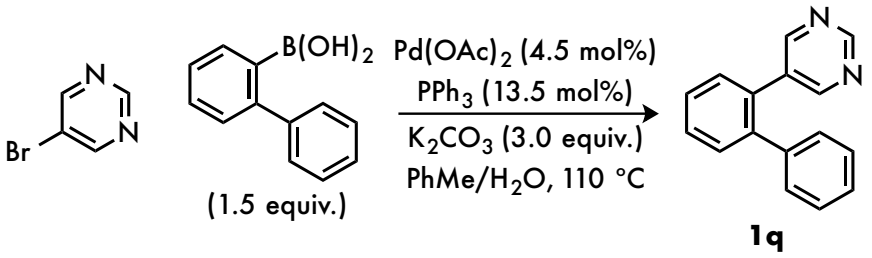

5-([1,1'-biphenyl]-2-yl)pyrimidine (1q): A 40 mL vial was charged with 5-bromopyrimidine (158.0 mg, 1.0 mmol, 1.0 equiv.), 2-biphenylboronic acid (297.0 mg, 1.0 equiv.), PPh_3 (35.4 mg, 13.5 mol%), K_2CO_3 (414.7 mg, 3.0 equiv.), PhMe (3 mL), and H_2O (2 mL). The mixture was bubbled with N_2 for 5 min and $Pd(OAc)_2$ (10.1 mg, 4.5 mol%) was added and the vial was sealed with the cap. The mixture was heated to 110 ºC and stirred overnight. The mixture was cooled to room temperature and diluted with ethyl acetate and extracted with ethyl acetate three times. The combined organic layers were washed with brine, dried over $MgSO_4$, and concentrated. The residue was purified by column chromatography (hexane/ethyl acetate = 2/1) to give product **1h**

as a white solid (227.9 mg) in 78% yield. R_f = 0.3 (hexane/ethyl acetate = 2/1). **^{1}H NMR** (400 MHz, CD_2Cl_2) δ 8.99 (s, 1H; N–C(**H**)–N), 8.47 (s, 2H; 2*C–C(**H**)–N), 7.54 – 7.43 (m, 4H; Ar–H), 7.30 – 7.27 (m, 3H; Ar–H), 7.15 – 7.12 (m, 2H; Ar–H). **^{13}C NMR** (101 MHz, CD_2Cl_2) δ 157.3, 156.9, 141.5, 140.6, 135.4, 133.6, 131.2, 130.6, 130.4, 129.4, 128.7, 128.4, 127.5. IR (KBr, cm^{-1}) 3039, 2926, 1551, 1479, 728, 632. Melting point: 108 – 109 ºC. HRMS calcd $C_{16}H_{12}N_2$ $[M]^+$: 232.1000. Found: 232.1000.

General experimental procedure for the catalytic dehydrogenative electrocyclization

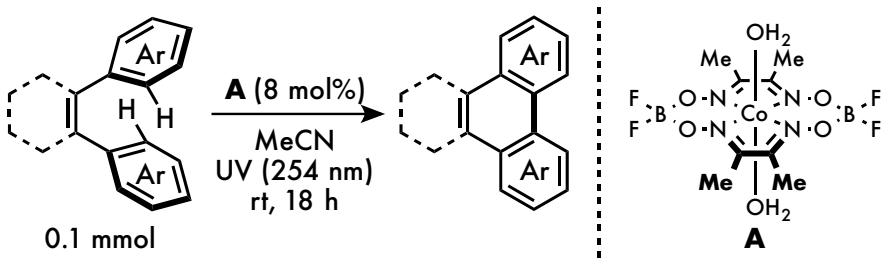

To a flame-dried 20 mL Quartz test tube with a stir bar was added *o*-terphenyl (23.0 mg, 0.0999 mmol) and $Co(dmg(BF_2))_2(OH_2)_2$ (**A**) (3.4 mg, 0.0079 mmol, 8 mol%). The test tube and the septum were transferred to the glove box. AcroSeal® MeCN (0.16 mL) was added to the test tube, before it was sealed with the septum and transferred out of the glove box. The septum was covered with aluminum foil, and the mixture was irradiated by 25 W UV lamps at room temperature under vigorous stirring for 18 hours (see fig. S1 and S2). After the completion of the reaction, the mixture was diluted with 2 mL of dichloromethane and passed through a plug of silica gel (1 cm). After removing solvents under vacuum, the residue was purified by flush column chromatography to give the desired product.

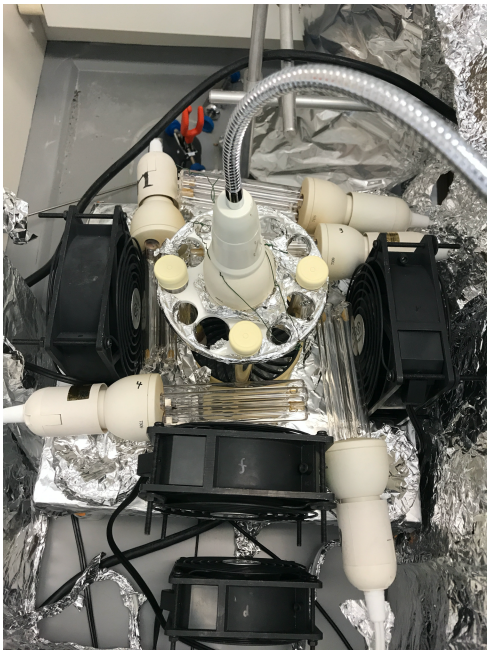

Fig. S1. Top view of the reaction set up for the catalytic dehydrogenative electrocyclization. Six 25 W UV lamps and five fans are used as shown. They are on the cardboard box that has a hole in the center. Side fans on the cardboard box are about 3–4 cm away from the edge of the center fan. CAUTION: cover the reaction setup with cardboard boxes and aluminum foil to avoid exposure to UV.

Fig. S2. Side view of the reaction set up for the catalytic dehydrogenative electrocyclization. Some 20 mL vials are put under the cardboard box to adjust the height and use the fan in the

center. CAUTION: cover the reaction setup with cardboard boxes and aluminum foil to avoid exposure to UV.

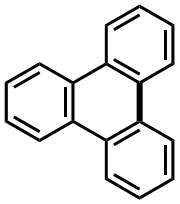

2a

triphenylene (2a)[34]: white solid (22.8 mg, quantitative yield). R_f = 0.4 (hexane). **^{1}H NMR** (400 MHz, $CDCl_3$) δ 8.69 – 8.64 (m, 6H), 7.69 – 7.65 (m, 6H). **^{13}C NMR** (101 MHz, $CDCl_3$) δ 129.7, 127.2, 123.3.

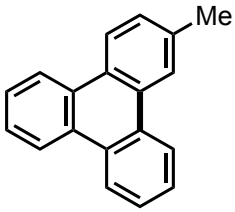

2b

2-methyltriphenylene (2b)[35]: white solid (22.8 mg, 94% yield). R_f = 0.4 (hexane). **^{1}H NMR** (400 MHz, $CDCl_3$) δ 8.67–8.41 (m, 5H), 8.55 (d, J = 8.0 Hz, 1H), 8.45 (s, 1H), 7.67–7.63 (m, 4H), 7.49 (m, 1H), 2.62 (s, 3H). **^{13}C NMR** (101 MHz, $CDCl_3$) δ 136.9, 129.9, 129.8, 129.7, 129.4, 128.7, 127.5, 127.15, 127.08, 127.06, 126.8, 123.31, 123.28, 123.24, 123.23, 123.1, 21.8.

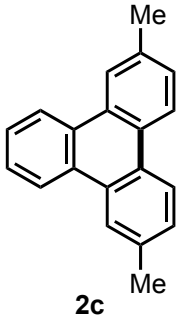

2c

2,7-dimethyltriphenylene (2c)[36]: white solid (23.8 mg, 93% yield). R_f = 0.4 (hexane).**^{1}H NMR** (400 MHz, CD_2Cl_2) δ 8.67–8.65 (m, 2H), 8.52–8.45 (m, 4H), 7.67–7.65 (m, 2H), 7.50 (dd, J = 4.0, 8.0 Hz, 2H), 2.61 (s, 6H). **^{13}C NMR** (101 MHz, CD_2Cl_2) δ 137.0, 130.1, 129.6, 129.1, 127.8, 127.4, 123.6, 123.3, 21.9.

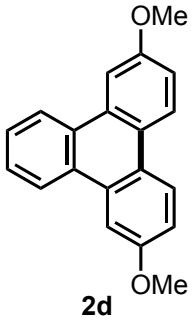

2d

2,7-dimethoxytriphenylene (2d)[3]: MeCN (0.6 mL) instead of MeCN (0.16 mL) was used in the general procedure. white solid (27.1 mg, 94% yield). R_f = 0.3 (hexane/ethyl acetate = 20/1). **^{1}H NMR** (400 MHz, CD_2Cl_2) δ 8.62–8.48 (m, 4H), 8.05 (d, J = 4.0 Hz, 2H), 7.69–7.66 (m, 2H), 7.29 – 7.26 (m, 2H), 4.02 (s, 6H). **^{13}C NMR** (101 MHz, CD_2Cl_2) δ 158.7, 130.4, 130.2, 127.5, 124.7, 124.2, 123.8, 116.3, 106.0, 55.8.

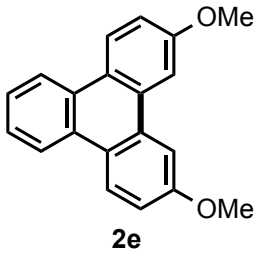

2e

2,11-dimethoxytriphenylene (2e)[37]: MeCN (0.6 mL) instead of MeCN (0.16 mL) was used in

the general procedure. white solid (25.9 mg, 90% yield). R_f = 0.3 (hexane/ethyl acetate = 20/1). **^{1}H NMR** (400 MHz, CD_2Cl_2) δ 8.59–8.53 (m, 4H), 7.99 (s, 2H), 7.59 (d, J = 4.0 Hz, 2H), 7.31–7.28 (m, 2H), 4.02 (s, 6H). **^{13}C NMR** (101 MHz, CD_2Cl_2) δ 159.3, 131.2, 129.2, 126.7, 125.4, 124.4, 123.1, 116.1, 106.4, 55.9.

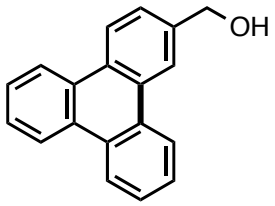

2f

triphenylen-2-ylmethanol (2f)[38]: white solid (17.8 mg, 69% yield). R_f = 0.3 (hexane/ethyl acetate = 2/1). **^{1}H NMR** (400 MHz, $CDCl_3$) δ 8.70 – 8.64 (m, 6H), 7.68 – 7.64 (m, 5H), 4.97 (d, J = 4.0 Hz, 2H), 1.84 (t, J = 4.0 Hz, 1H). **^{13}C NMR** (101 MHz, $CDCl_3$) δ 139.6, 129.90, 129.87, 129.7, 129.62, 129.59, 129.2, 127.32, 127.25, 127.22, 126.1, 123.7, 123.33, 123.31, 123.30, 121.5, 65.6.

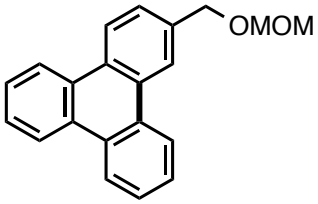

2f-MOM

2-((methoxymethoxy)methyl)triphenylene (2f-MOM): white solid (26.3 mg, 87% yield). R_f = 0.4 (hexane/ethyl acetate = 4/1). **^{1}H NMR** (400 MHz, $CDCl_3$) δ 8.70 – 8.64 (m, 6H; Ar–H), 7.68 – 7.66 (m, 5H; Ar–H), 4.87 (s, 2H; Ar–CH_2–O), 4.82 (s, 2H; O–CH_2–O), 3.49 (t, J = 4.0 Hz, 3H; OCH_3). **^{13}C NMR** (101 MHz, $CDCl_3$) δ 136.7, 129.9, 129.8, 129.7, 129.3, 127.3, 127.24, 127.21, 126.9, 123.6, 123.4, 123.34, 123.30, 122.5, 95.8, 69.4, 55.5. IR (KBr, cm^{-1}) 3079, 2926, 1439, 1261, 1148, 1034, 801. Melting point: 84– 85 ºC. HRMS calcd $C_{21}H_{18}O$ $[M]^+$: 302.1307. Found: 302.1308.

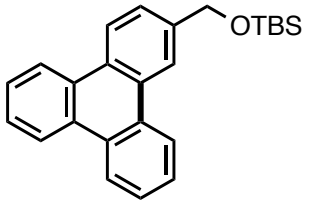

2f-TBS

***tert*-butyldimethyl(triphenylen-2-ylmethoxy)silane (2f-TBS)[39]**: white solid (16.4 mg, 44% yield). R_f = 0.25 (hexane/ethyl acetate = 10/1). **^{1}H NMR** (400 MHz, $CDCl_3$) δ 8.70 – 8.64 (m, 6H; Ar–H), 7.68 – 7.64 (m, 5H; Ar–H), 4.97 (d, J = 4.0 Hz, 2H; Ar–CH_2–O), 1.02 (s, 9H; 3*C–CH_3), 0.18 (s, 6H; 2*Si–CH_3). **^{13}C NMR** (101 MHz, $CDCl_3$) δ 140.3, 129.90, 129.87, 129.82, 129.7, 129.6, 128.7, 127.2, 127.1, 127.0, 125.4, 123.31, 123.29, 123.28, 123.27, 123.24, 120.5, 65.2, 26.0, 18.5, -5.1. IR (KBr, cm^{-1}) 2955, 2856, 1473, 1256, 1209, 1090, 761. Melting point: 88 – 89 ºC. HRMS calcd $C_{25}H_{28}OSi$ $[M]^+$: 372.1909. Found: 372.1911.

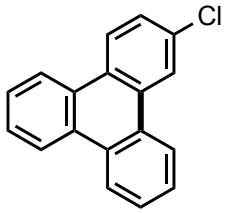

2g

2-chlorotriphenylene (2g)[40]: white solid (22.3 mg, 87% yield). R_f = 0.3 (hexane/ethyl acetate = 60/1). **^{1}H NMR** (400 MHz, $CDCl_3$) δ 8.64 – 8.52 (m, 6H), 7.68 – 7.57 (m, 5H). **^{13}C NMR** (101

MHz, $CDCl_3$) δ 133.3, 131.2, 130.1, 129.6, 129.1, 128.6, 128.2, 127.8, 127.5, 127.40, 127.38, 127.37, 124.9, 123.34, 123.32, 123.2, 123.0.

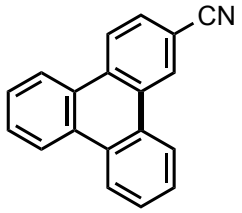

2h

triphenylene-2-carbonitrile (2h)[41]: white solid (18.7 mg, 74% yield). R_f = 0.3 (hexane/ethyl acetate = 2/1). **^{1}H NMR** (400 MHz, CD_2Cl_2) δ 8.96 (m, 1H), 8.74 – 8.64 (m, 6H), 7.88 – 7.71 (m, 4H). **^{13}C NMR** (101 MHz, CD_2Cl_2) δ 133.2, 131.1, 130.4, 130.2, 129.4, 129.3, 128.8, 128.7, 128.6, 128.2, 128.1, 124.7, 124.3, 123.9, 123.8, 123.6, 119.6, 111.0.

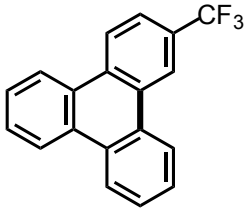

2i

2-(trifluoromethyl)triphenylene (2i)[42]: white solid (22.2 mg, 75% yield). R_f = 0.3 (hexane). **^{1}H**

NMR (400 MHz, $CDCl_3$) δ 8.90 (s, 1H), 8.75 – 8.65 (m, 5H), 7.87 – 7.84 (m, 1H), 7.75 – 7.68 (m, 4H). **^{13}C NMR** (101 MHz, $CDCl_3$) δ 132.2, 130.5, 130.1, 129.7, 129.1, 129.0, 128.7, 128.3, 128.1, 127.62, 127.55, 127.2, 125.9, 124.1, 123.7, 123.45, 123.43, 123.36, 123.28, 123.17 (q, $^3J_{C–F}$ = 3.3 Hz), 120.6 (q, $^3J_{C–F}$ = 4.0 Hz). **^{19}F NMR** (376 MHz, $CDCl_3$) δ -62.1.

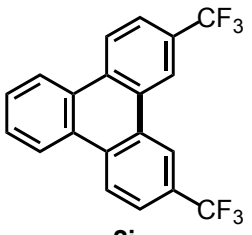

2j

2,11-bis(trifluoromethyl)triphenylene (2j)[43]: white solid (36.3 mg, quantitative yield). R_f = 0.3 (hexane). **^{1}H NMR** (400 MHz, $CDCl_3$) δ 8.77 – 8.60 (m, 6H), 7.89 – 7.86 (m, 2H), 7.76 – 7.73 (m, 2H). **^{13}C NMR** (101 MHz, $CDCl_3$) δ 132.5, 129.31 (q, $^3J_{C–F}$ = 32.0 Hz), 129.28, 128.8, 128.7, 124.3 (q, $^3J_{C–F}$ = 271.4 Hz), 124.2, 124.0 (q, $^3J_{C–F}$ = 4.0 Hz), 123.8, 120.5 (q, $^3J_{C–F}$ = 4.5 Hz). **^{19}F NMR** (376 MHz, $CDCl_3$) δ -62.1.

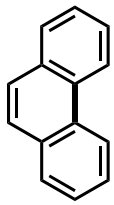

2k

phenanthrene (2k)[44]: Synthesized from (*Z*)-stilbene. MeCN (0.3 mL) instead of MeCN (0.16 mL) was used in the general procedure. White solid (6.4 mg, 36% yield). R_f = 0.3 (hexane). **^{1}H NMR** (400 MHz, $CDCl_3$) δ 8.71 (d, J = 8.0 Hz, 2H), 7.91 (dd, J = 4.0, 8.0 Hz, 2H), 7.76 (s, 2H), 7.69 – 7.59 (m, 4H). **^{13}C NMR** (101 MHz, $CDCl_3$) δ 132.0, 130.3, 128.6, 126.9, 126.55, 126.54, 122.6.

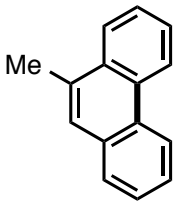

2l

9-methylphenanthrene (2l)[45]: Synthesized from (*E*)-□-Methylstilbene. White solid (11.1 mg, 57% yield). R_f = 0.3 (hexane).**^{1}H NMR** (400 MHz, $CDCl_3$) δ 8.76 – 8.66 (m, 2H), 8.09 – 8.07 (m, 1H), 7.84 – 7.82 (m, 1H), 7.71 – 7.56 (m, 4H), 2.76 (s, 3H). **^{13}C NMR** (101 MHz, $CDCl_3$) δ 132.5, 132.1, 132.0, 130.4, 129.7, 127.8, 126.7, 126.6, 126.5, 126.2, 125.8, 124.6, 123.0, 122.4,

20.0.

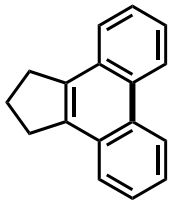

2m

2,3-dihydro-1*H*-cyclopenta[*l*]phenanthrene (2m) [46]: white solid (16.2 mg, 74% yield). Observing small amount of inseparable impurity in ^{1}H-NMR analysis, we determined the product purity as 94% using 1,3,5-trimethoxybenzene as an internal standard. R_f = 0.3 (hexane). **^{1}H NMR** (400 MHz, $CDCl_3$) δ 8.72 – 8.71 (m, 2H), 7.89 – 7.87 (m, 2H), 7.65 – 7.62 (m, 4H), 3.37 (t, J = 8.0 Hz, 10H), 2.37 (t, J = 8.0 Hz, 2H). **^{13}C NMR** (101 MHz, $CDCl_3$) δ 137.5, 130.1, 130.0, 126.5, 125.5, 124.9, 123.0, 32.2, 23.4.

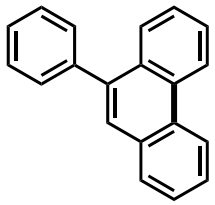

2n

9-phenylphenanthrene (2n)[47]: white solid (23.9 mg, 94% yield). R_f = 0.3 (hexane). **^{1}H NMR** (400 MHz, $CDCl_3$) δ 8.81 – 8.74 (m, 2H), 7.96 – 7.94 (m, 2H), 7.71 – 7.48 (m, 10H). **^{13}C NMR** (101 MHz, $CDCl_3$) δ 140.8, 138.8, 131.5, 131.1, 130.6, 130.0, 129.9, 128.6, 128.3, 127.5, 127.3, 126.9, 126.8, 126.6, 126.5, 126.4, 122.9, 122.5.

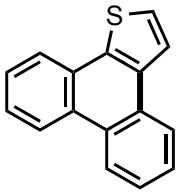

2o

phenanthro[9,10-*b*]thiophene (2o)[48]: white solid (22.5 mg, 96% yield). R_f = 0.25 (hexane). **^{1}H NMR** (400 MHz, $CDCl_3$) δ 8.72 – 8.68 (m, 2H), 8.34 – 8.32 (m, 1H), 8.17 – 8.15 (m, 1H), 7.98 – 7.56 (m, 5H). **^{13}C NMR** (101 MHz, $CDCl_3$) δ 136.6, 135.0, 129.0, 128.8, 128.6, 128.3, 127.2, 127.1, 126.3, 126.0, 124.9, 124.28, 124.26, 123.6, 123.5, 123.2.

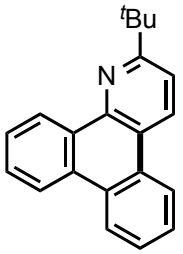

2-(*tert*-butyl)dibenzo[*f*,*h*]quinoline (2p): Reaction time was 36 h instead of 18 h. white solid (26.3 mg, 92% yield). R_f = 0.5 (hexane/ethyl acetate = 20/1)). **^{1}H NMR** (400 MHz, $CDCl_3$) δ 9.49 – 9.47 (m, 1H; Ar–H), 8.76 (d, J = 8.0 Hz, 1H; Ar–H), 8.67 – 8.52 (m, 3H; Ar–H), 7.77 – 7.64 (m, 5H; Ar–H), 1.59 (s, 9H; 3*C–CH_3). **^{13}C NMR** (100 MHz, $CDCl_3$) δ 168.1, 144.9, 131.5, 131.3, 130.9, 129.4, 129.0, 128.4, 127.22, 127.18, 127.13, 125.6, 123.3, 123.0, 122.4, 121.7, 118.3, 38.2, 30.4. IR (KBr, cm^{-1}) 3071, 2961, 2361, 1595, 1485, 1387, 758. Melting point: 73 – 74 ºC. HRMS calcd $C_{21}H_{19}N$ $[M+H]^+$: 285.1517. Found: 285.1523.

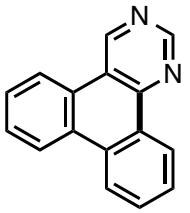

2q

dibenzo[*f*,*h*]quinazoline (2q): yellow solid (23.0 mg, quantitative yield). R_f = 0.3 (hexane/ethyl

acetate = 2/1)). **^{1}H NMR** (400 MHz, CD_2Cl_2) δ 9.93 (s, 1H; N–C(H)–N), 9.41 (s, 1H; C–C(H)–N), 9.24 (d, J = 8.0 Hz, 1H; Ar–H), 8.65 – 8.60 (m, 3H; Ar–H), 7.87 – 7.70 (m, 4H; Ar–H). **^{13}C NMR** (101 MHz, $CDCl_3$) δ 156.1, 153.4, 151.2, 133.0, 130.9, 129.8, 128.8, 128.7, 128.0, 127.8, 126.6, 125.6, 123.5, 122.7, 122.4, 121.2. IR (KBr, cm^{-1}) 3041, 2363, 1571, 1402, 751, 732. Melting point: 112 – 113 ºC. HRMS calcd $C_{16}H_{10}N_2$ $[M]^+$: 230.0844. Found: 230.0847.

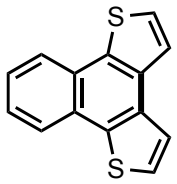

2r

naphtho[1,2-*b*:4,3-*b'*]dithiophene (2r) [49]: white solid (22.6 mg, 94% yield). R_f = 0.3 (hexane).**^{1}H NMR** (400 MHz, $CDCl_3$) δ 8.20 – 8.18 (m, 2H), 7.74 (d, J = 4.0 Hz, 2H), 7.59 – 7.56 (m, 4H). **^{13}C NMR** (101 MHz, $CDCl_3$) δ 135.5, 133.3, 126.9, 126.3, 125.4, 124.5, 123.0.

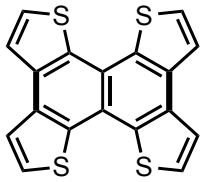

2s

1,1,2,2-tetra(thiophen-2-yl)ethene (2s)[50]: The reaction was performed in 0.025 mmol scale. MeCN/dichloromethane (2/1, 0.5 mL) was used as the reaction solvent. Reaction time was 36 h. Pale-yellow solid (5.4 mg, 61% yield). R_f = 0.2 (hexane/ethyl acetate = 20/1). **^{1}H NMR** (400 MHz, CD_2Cl_2) δ 8.11 (d, J = 6.0 Hz, 4H), 7.95 (d, J = 6.0 Hz , 4H). ^{13}C NMR of **2s** was not available due to its poor solubility in common deuterated solvents (see ref. 27).

Hydrogen gas detection experiment

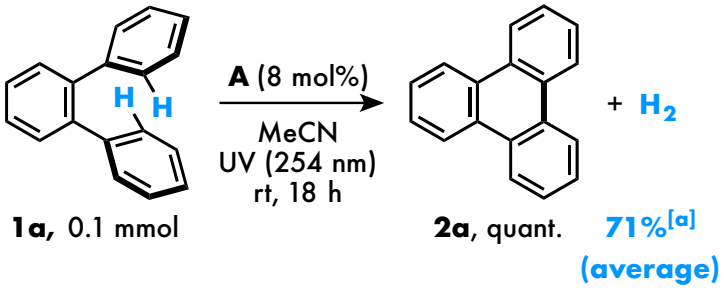

The reaction was performed according to the aforementioned procedure to prepare **2a**. After the reaction, the gas in the headspace of the test tube (50 □L) was analyzed by GC-TCD to determine the amount of hydrogen gas generated. Methane was used as an internal standard. In the three experiments, **2a** was obtained in quantitative yield with hydrogen gas in 68, 70, 75% yield, respectively (71% average).

Desaturation of 1,4-dihydronaphthalene

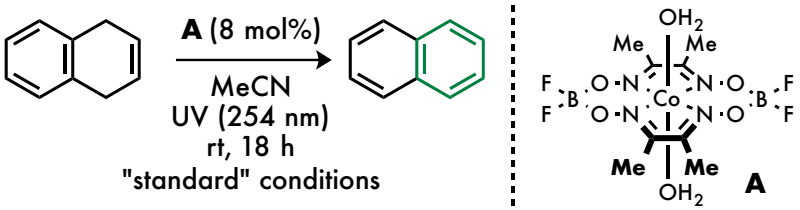

entry	variation(s) from the standard condition	yield(%)
1	none	20
2	no light	3
3	no **A**	3

The reactions were performed according to the aforementioned procedure to prepare **2a**, where 1,4-dihydronaphthalene was used as a starting material. Yields were determined by ^{1}H-NMR spectroscopy using 1,1,2,2-tetrachloroethane as an internal standard.

1. Light-on/off experiment

The reactions were performed according to the aforementioned procedure to prepare **2a**, where 1,3,5-trimethoxybenzene (1.7 mg, 0.1 equiv.) was added as an internal standard. The reaction was stirred under UV irradiation for 1 h at which point a reaction aliquot (0.03 mL) was taken, diluted with $CDCl_3$, and yield of *o*-terphenyl was analyzed by ^{1}H-NMR spectroscopy (**2a** has poor solubility in MeCN). The light was switched off and the mixture was stirred under dark for

1 h at which point a reaction aliquot (0.03 mL) was taken, diluted with $CDCl_3$, and yield of *o*-terphenyl was analyzed by ^{1}H-NMR spectroscopy. The light was switched on and the mixture was stirred under irradiation for 1 h at which point a reaction aliquot (0.03 mL) was taken, diluted with $CDCl_3$, and yield of *o*-terphenyl was analyzed by ^{1}H-NMR spectroscopy. The light was switched off and the mixture was stirred under dark for 1 h at which point a reaction aliquot (0.03 mL) was taken, diluted with $CDCl_3$, and yield of *o*-terphenyl was analyzed by ^{1}H-NMR spectroscopy. The light was switched on and the mixture was stirred under irradiation for 1 h at which point a reaction aliquot (0.03 mL) was taken, diluted with $CDCl_3$, and the yield of *o*-terphenyl was analyzed by ^{1}H-NMR spectroscopy.

Table S1 Consumption of the starting material (continued)

time (h)	yield (%)
1	88
2	85
3	67
4	64
5	50

Table S1 Consumption of the starting material

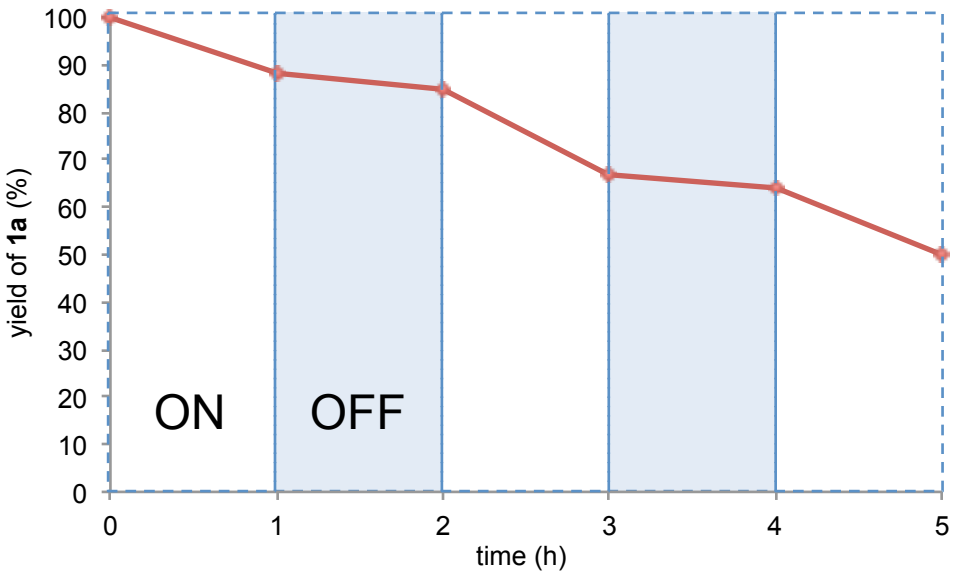

The control experiment at 100 ºC under dark was conducted; the starting material was fully recovered and the desired product was not detected in ^{1}H-NMR analysis (1,1,2,2-tetrachloroethane was used as an internal standard).

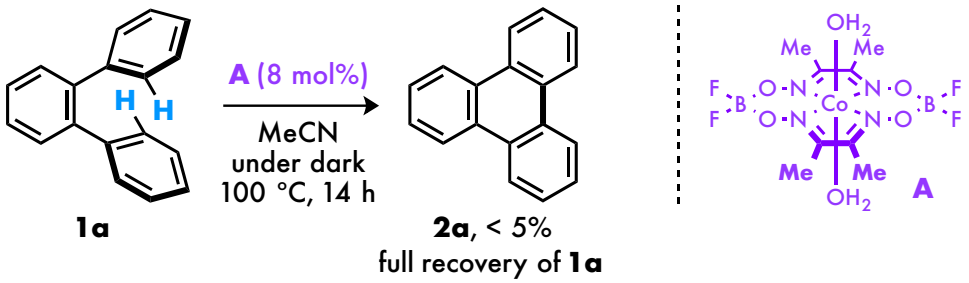

Scheme S1 reaction under dark conditions

Less successful substrates

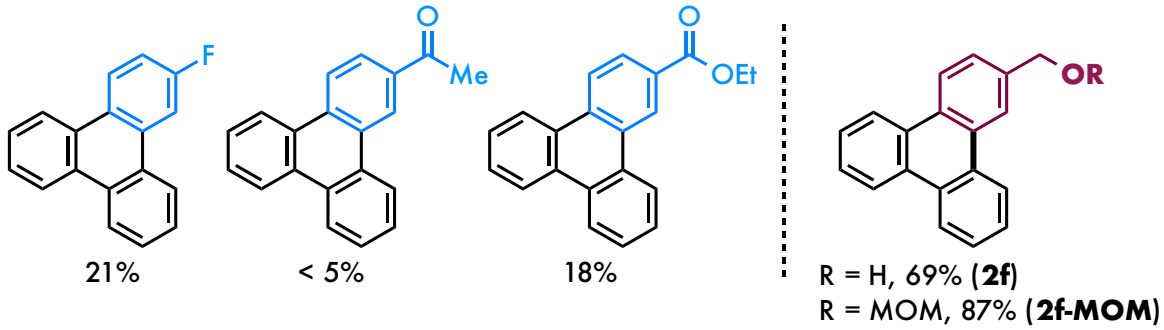

–F, –COR and –COOR substrates have also been attempted under the optimal reaction condition. Both the F and COOR-substituted substrates indeed provided the desired products albeit in lower conversions (21% and 18% yields, respectively). The ketone substrate gave almost no conversion. In all three cases, most of the starting materials remained in these reactions. We believe that the low reactivity with these substrates is NOT due to their electron deficiency, as $–CF_3$ and –CN groups are more electron withdrawing than -F, -COR, or - COOR based on their Hammett substituent constants.[29]

$–CF_3$ *meta* +0.43 *para* +0.54

–CN *meta* +0.56 *para* +0.55

–COMe *meta* +0.38 *para* +0.50

–COOEt *meta* +0.37 *para* +0.45

We reason that the low reactivity with carbonyl compounds is likely due to the competing absorption and excitation of the carbonyl moiety under irradiation at 254 nm. Given that the hydroxymethyl-substituted products can be obtained in good yields (69% for OH (**2f**) and 87% for OMOM (**2f-MOM**)), they could be easily converted to the corresponding carbonyl compounds through oxidation. The reduced reactivity of the –F substrate remains unclear and will be thoroughly studied when optimizing the catalytic system in the future.

Molecular extinction coefficient of 1a and A

According to their UV-Vis spectra, the molar extinction coefficient of catalyst **A** and substrate **1a**

in MeCN solution ($1.1*10^{-5}$ M and $1.4*10^{-5}$M, respectively) were measured as $1.2*10^{4}$ and $2.4*10^{4}$ $M^{-1}cm^{-1}$, respectively, at the excitation wavelength of 254 nm.

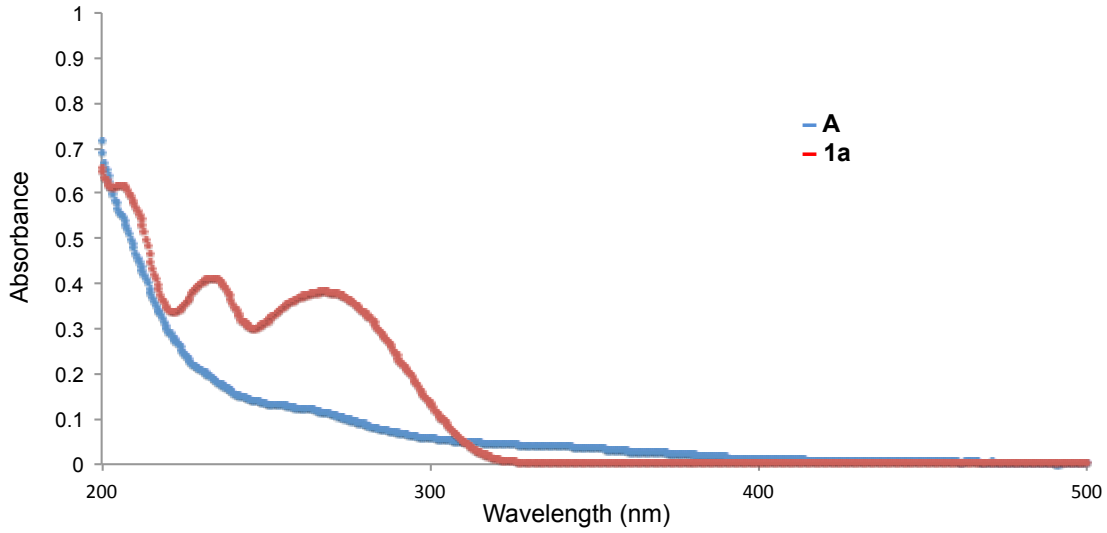

Alternative mechanisms

Two alternative mechanisms of the cobaloxime-catalyzed acceptorless cyclodehydrogenation are depicted here. In the alternative mechanism A (Fig S3), 6π-electrocyclization intermediate **I** would undergo excitation to form **I***, which then could transfer a single electron to the Co^{II} catalyst ($E_{1/2}(Co^{II}/Co^{I})$ = –0.55 V vs. SCE in MeCN)[30] to produce radical cation **II** and Co^{I} species. The rest of the mechanism is the same as the one described in Figure 1. According to the previous report, peak absorption wavelength of **I** is predicted to appear at 670 nm, which matches the experiment (TDDFT B3LYP, 6-31+g* was used for calculation).[31]

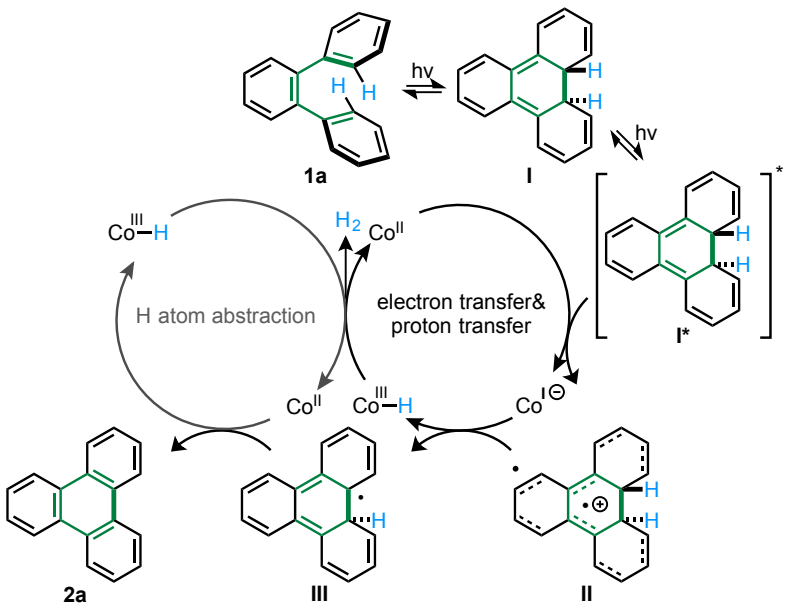

Fig S3. alternative mechanism A

Another possible mechanism B starts with light-mediated transformation of **1a** to **I***, which contains two much weakened C–H bonds (BDEs of sp^3-hybridized benzylic C–H bonds of excited aromatic hydrocarbons are about 30–55 kcal/mol, whereas BDE of **H–Co**(dmg$(BF_2)_2(OH_2)_2$ was calculated as 50.5 kcal/mol).[32,33] These C–H bonds could be homolytically cleaved by Co^{II} to produce **III** and Co^{III}–H intermediate, which then reacts in the same way as shown in Figure 1 (Fig S4).

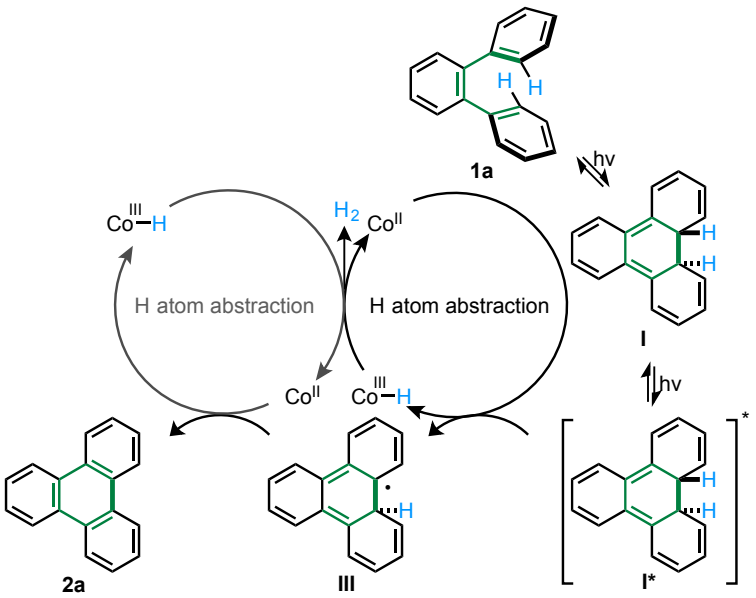

Fig S4. alternative mechanism B

On the other hand, a mechanism that involves electron transfer from **2a*** to Co^{II} is less likely due to that addition of 10 mol% of **2a** to the reaction (Table 1, entry 8) did not affect the yield of **2a**.

2.5 References

[1] a) J. Löwe. *Z. Chemie*, **1868**, *4*, 603; b) A. T. Balaban, C. D. Nenitzescu in *Friedel-Crafts and Related Reactions*, *vol. 2* (Eds: G. A. Olah), Wiley, New York, **1964**, pp. 979–1047. For reviews on Scholl reaction, see; c) M. Grzybowski, K. Skonieczny, H. Butenschoen, D. T. Gryko, *Angew. Chem. Int. Ed.*, **2013**, *52*, 9900.

[2] For recent reviews of synthesis of PAHs, see: a) D. Pérez, E. Guitián. *Chem. Soc. Rev.* **2004**, *33*, 274. (b) K. Y. Yoon, G. Dong. *Mater. Chem. Front*. **2020**, 4, 29. (c) A. Jolly, D. Miao, M. Daigle, J. F. Morin. *Angew. Chem. Int. Ed.* **2020**, *59*, 4624. (d) B. P. Mathew, M. R. Kuram. *Inorg. Chim. Acta.* **2019**, *490*, 112. (e) Y. Segawa, T. Maekawa, K. Itami. *Angew. Chem. Int. Ed*. **2015**, *54*, 66.

[3] a) B. T. King, J. Kroulík, C. R. Robertson, P. Rempala, C. L. Hilton, J. D. Korinek, L. M. Gortari. *J. Org. Chem.* **2007**, *72*, 2279; b) X. Dou, X. Yang, G. J. Bodwell, M. Wagner, V. Enkelmann, K. Müllen. *Org. Lett.* **2007**, *9*, 2485.

[4] S. Fujimoto, K. Matsumoto, M. Shindo. *Adv. Synth. Catal.* **2016**, *358*, 3057.

[5] P. Röse, S. Emge, C. A. König, G. Hilt. *Adv. Synth. Catal.* **2017**, *359*, 1359.

[6] a) L. Liu, B. Yang, T. J. Katz, M. K. Poindexter. *J. Org. Chem.* **1991**, *56*, 3769; b) K. B. Jørgensen, *Molecules* **2010**, *15*, 4334; c) F. B. Mallory, C. W. Mallory. *Org. React.* **1984**, *30*, 1.

[7] a) M. Shimizu, I. Nagao, Y. Tomioka, T. Kadowaki, T. Hiyama. *Tetrahedron* **2011**, *67*, 8014; b) J. Tu, G. Li, X. Zhao, F. Xu. *Tetrahedron Lett.* **2019**, *60*, 44; c) K. Murayama, Y. Sawada, K. Noguchi, K. Tanaka. *J. Org. Chem.* **2013**, *78*, 6202; d) T. T. Jayanth, C. H. Cheng, *Chem. Commun.* **2006**, *8*, 894; e) M. Iwasaki, Y. Araki, S. Iino, Y. Nishihara. *J. Org. Chem.* **2015**, *80*, 924.

[8] For H-OMe eliminative photocyclization, see; a) R. G. Giles, M. V. Sargent. *J. Chem. Soc., Perkin Trans. 1,* **1974**, 2447. For H-Cl eliminative photocyclization, see; b) M. Daigle, A. Picard-Lafond, E. Soligo, J. F. Morin. *Angew. Chem. Int. Ed.* **2016***, 55*, 2042. For H-F eliminative photocyclization, see: c) O. Allemann, S, Duttwyler, P. Romanato, K. K. Baldridge, J. S. Siegel. *Science*, **2011**, *332*, 574; d) K. Y. Amsharov, P. Merz. *J. Org. Chem,* **2012**, *77*, 5445.

[9] For recent reviews, see: a) J. L. Dempsey, B. S. Brunschwig, J. R. Winkler, H. B. Gray. *Acc. Chem. Res.* **2009**, *42*, 1995–2004; b) N. Kaeffer, M. Chavarot-Kerlidou, V. Artero. *Acc. Chem. Res.* **2015**, *48*, 1286.

[10] For selected examples, see: a) Y. W. Zheng, B. Chen, P. Ye, K. Feng, W. Wang, Q. Y. Meng, L. Z. Wu, C. H. Tung. *J. Am. Chem. Soc.* **2016**, *138*, 10080; b) Q. Yang, L. Zhang, C. Ye, S. Luo, L. Z. Wu, C. H. Tung. *Angew. Chem. Int. Ed.* **2017**, *56*, 3694; c) X. W. Gao, Q. Y. Meng, J. X. Li, J. J. Zhong, T. Lei, X. B. Li, C. H. Tung, L. Z. Wu. *ACS Catal.* **2015**, *5*, 2391; d) X. Hu, G. Zhang, F. Bu, A. Lei. *Angew. Chem. Int. Ed.* **2018**, *57*, 1286; e) F. Zhao, Q. Yang, J. Zhang, W. Shi, H. Hu, F. Liang, W. Wei, S. Zhou. *Org. Lett.* **2018**, *20*, 7753; f) H. Yi, L. Niu, C. Song, Y. Li, B. Dou, A. K. Singh, A. Lei. *Angew. Chem. Int. Ed.* **2017**, *56*, 1120; g) L. Niu, H. Yi, S. Wang, T. Liu, J.

Liu, A. Lei. *Nat. Commun.* **2017**, *8*, 14226. h) G. Zhang, Y. Lin, X. Luo, X. Hu, C. Chen, A. Lei. *Nat. Commun.* **2018**, *9*, 1225; i) G. Zhang, C. Liu, H. Yi, Q. Meng, C. Bian, H. Chen, J. X. Jian, L. Z. Wu, A. Lei, *J. Am. Chem. Soc*. **2015**, *137*, 9273; j) J. J. Zhong, Q. Y. Meng, B. Liu, X. B. Li, X. W. Gao, T. Lei, C. J. Wu, Z. J. Li, C. H. Tung, L. Z. Wu. *Org. Lett*. **2014**, *16*, 1988; k) G. Zhang, X. Hu, C. W. Chiang, H. Yi, P. Pei, A. K. Singh, A. Lei, *J. Am. Chem. Soc.* **2016**, *138*, 12037; l) C. J. Wu, Q. Y. Meng, T. Lei, J. J. Zhong, W. Q. Liu, L. M. Zhao, Z. J. Li, B. Chen, C. H. Tung, L. Z. Wu. *ACS Catal*. **2016**, *6*, 4635; m) M. Xiang, Q. Y. Meng, J. X. Li, Y. W. Zheng, C. Ye, Z. J. Li, B. Chen, C. H. Tung, L. Z. Wu. *Chem. Eur. J.* **2015**, *21*, 18080; n) K. H. He, F. F. Tan, C. Z. Zhou, G. J. Zhou, X. L. Yang, Y. Li. *Angew. Chem. Int. Ed.* **2017**, *56*, 3080; o) W. Cao, C. Wu, T. Lei, X. Yang, B. Chen, C. Tung, L. Wu, *Chin. J. Catal.* **2018**, *39*, 1194.

[11] For a catalyst-free direct photochemical annulation of special styrene-type substrates, see: J. Zhang, X. Zhang, T. Wang, X. Yao, P. Wang, P. Wang, S. Jing, Y. Liang, Z. Zhang. *J. Org. Chem.* **2017**, *82*, 12097-.

[12] a) G. E. Dobereiner, R. H. Crabtree. *Chem. Rev.* **2010**, *110*, 681; b) Momirlan, M.; Veziroglu, T. N. *Int. J. Hydrogen Energy* **2005**, *30*, 795; d) Sartbaeva, A.; Kuznetsov, V. L.; Wells, S. A.; Edwards, P. P. *Energy Environ. Sci.* **2008**, *1*, 79; e) Armaroli, N.; Balzani, V. *ChemSusChem* **2011**, *4*, 21; f) Gunanathan, G.; Milstein, D. *Science* **2013**, *341*, 1229712; g) A. C. Marr. *Catal. Sci. Technol*. **2012**, *2*, 279.

[13] T. J. Cuppen, W. H. Laarhoven. *J. Am. Chem. Soc.* **1972**, 94, 5914.

[14] J. G. West, D. Huang, E. J. Sorensen. *Nat. Commun*, **2015**, *6*, 10093.

[15] F. B. Mallory, C. S. Wood. *J. Org. Chem*. **1964**, *29*, 3374.

[16] A. Yamamoto, Y. Matsui, T. Asada, M. Kumeda, K. Takagi, Y. Suenaga, N. Nagae, E. Ohta, H. Sato, S. Koseki, H. Naito, H. Ikeda. *J. Org. Chem.* **2016**, *81*, 3168.

[17] T. Sato, S. Shimada, K. Hata. *Bull. Chem. Soc. Jpn.* **1971**, *44*, 2484.

[18] W. Q. Liu, T. Lei, S. Zhou, X. L. Yang, J. Li, B. Chen, J. Sivaguru, C. H. Tung, L. Z. Wu. *J. Am. Chem. Soc.* **2019**, *141*, 13941.

[19] N. P. Schepp and L. J. Johnston. *J. Am. Chem. Soc.* **1996**, *118*, 2872.

[20] pKa values of hydrocarbon radical cation are known to be very low (in DMSO, for example, toluene's pKa ($C–H^{\bullet+}$) = –23 and 9,10-dihydroanthracene's pKa ($C–H^{\bullet+}$) = –24). Thus, Co^{I}-mediated deprotonation from **II** (Figure 1) or 1,4-dihydronaphthalene radical cation (Scheme 2C) is feasible. BDE of hydrocarbon radical cation are known to be very low too. For references of pKa/BDE values of hydrocarbon radical cations: a) X. Zhang, F. G. Bordwell. *J. Org. Chem.* **1992**, *57*, 4163; b) X. S. Xue, P. Ji, B. Zhou, J. P. Cheng. *Chem. Rev.* **2017**, *117*, 8622.

[21] T. H. Chao, J. H. Espenson. *J. Am. Chem. Soc.* **1978**, *100*, 129.

[22] Using this method to prepare nanographenes was unfruitful under the current reaction conditions primarily due to the solubility issue of the substrate in MeCN.

[23] Bakac, A.; Brynildson, M. E.; Espenson, J. H., *Inorg. Chem.* **1986**, *25*, 4108.

[24] Mueller, Andreas; Amsharov, Konstantin Yu. *Eur. J. Org. Chem.* **2015**, *2015*, 3053.

[25] Röse, Philipp; Emge, Steffen; König, Christoph Alexander; Hilt, Gerhard. *Adv. Synth. Catal.* **2017**, *359*, 1359.

[26] Tang, Jie; Biafora, Agostino; Goossen, Lukas J. *Angew. Chem. Int. Ed.* **2015**, *54*, 13130.

[27] Koyanagi, Masashi; Eichenauer, Nils; Ihara, Hideki; Yamamoto, Takeshi; Suginome, Michinori, *Chem. Lett.* **2013**, *42*, 541.

[28] Somers, J. B. M.; Couture, A.; Lablache-Combier, A.; Laarhoven, W. H. *J. Am. Chem. Soc.* **1985**, *107*, 1387.

[29] Shibata, Yosei; Kono, Takahiro; Ohashi Noboru; Yoshida, Juji. *Thin Solid Films* **2015**, *583*, 163.

[30] Pelter, Andrew; Jenkins, Ieuan; Jones, D. Elfyn. *Tetrahedron 1997*, **53**, 10357.

[31] Yamamoto, Atsushi; Matsui, Yasunori; Asada, Toshio; Kumeda, Motoki; Takagi, Kenichiro; Suenaga, Yu; Nagae, Kunihiko; Ohta, Eisuke; Sato, Hiroyasu; Koseki, Shiro; Naito, Hiroyoshi; Ikeda, Hiroshi. *J. Org. Chem*. **2016**, *81*, 3168.

[32] Eseola, Abiodun Omokehinde; Geibig, Daniel; Görls, Helmar; Sun, Wen-Hua; Hao, Xiang; Woods, Joseph Anthony Orighomisan; Plass, Winfried. *J. Organomet. Chem*. **2014**, *754*, 3.

[33] Henrion, Guilhem; Chavas, Thomas E. J.; Le Goff, Xavier; Gagosz, Fabien. *Angew. Chem. Int. Ed.* **2013**, *52*, 6277.

[34] Daigle, Maxime; Picard-Lafond, Audrey; Soligo, Eliane; Morin, Jean-François. *Angew. Chem. Int. Ed.* **2016**, *55*, 2042.

[35] Liang, Zunjun; Yao, Jinzhong; Wang, Kai; Li, Haoran; Zhang, Yuhong, *Chem. Eur. J*. **2013**, *19*, 16825.

[36] Fujimoto, Shigenobu; Matsumoto, Kenji; Shindo, Mitsuru. *Adv. Synth. Catal.* **2016**, *358*, 3057.

[37] Nagao, Ikuhiro; Shimizu, Masaki; Hiyama, Tamejiro. *Angew. Chem. Int. Ed*. **2009**, *48*, 7573.

[38] Murayama, Koichi; Oike, Yasuaki; Furumi, Seiichi; Takeuchi, Masayuki; Noguchi, Keiichi; Tanaka, Ken. Eur. *J. Org. Chem.* **2015**, *2015* 1409.

[39] Murayama, Koichi; Oike, Yasuaki; Furumi, Seiichi; Takeuchi, Masayuki; Noguchi, Keiichi; Tanaka, Ken. Eur. *J. Org. Chem.* **2015**, *2015* 1409.

[40] Iwasaki, Masayuki; Araki, Yasuhiro; Iino, Shohei; Nishihara, Yasushi. *J. Org. Chem*. **2015**, *80*, 9247.

[41] Wu, Xunshen; Han, Jianwei; Wang, Limin. *J. Org. Chem.* **2018**, *83*, 49.

[42] Mao, Wenbin; Zhu, Chen. *J. Org. Chem.* **2017**, *82*, 9133.

[43] Zhang, Yanghui; Pan, Shulei; Jiang, Hang; Zhang, Yu; Chen, Dushen. *Org. Lett*. **2016**, *18,* 5192.

[44] Barbero, Nekane; Martin, Ruben. *Org. Lett*. **2012**, *14*, 796.

[45] Murai, Masahito; Hosokawa, Naoki; Roy, David; Takai, Kazuhiko. *Org. Lett.* **2014**, *16*, 4134.

[46] Wang, Yahui; Muratore, Michael E.; Rong, Zhouting; Echavarren, Antonio M. *Angew. Chem. Int. Ed.* **2014**, *53*, 14022.

[47] Budén, María E.; Guastavino, Javier F.; Rossi, Roberto A. *Org. Lett*. **2013**, *15*,1174.

[48] Yang, Yuzhong; Zhou, Bang; Zhu, Xiaoming; Deng, Guobo; Liang, Yun; Yang, Yuan. *Org. Lett.* **2018**, *20*, 5402.

[49] Shimizu, Masaki; Nagao, Ikuhiro; Tomioka, Yosuke; Kadowaki, Tsugumi; Hiyama, Tamejiro. *Tetrahedron* **2011**, *67*, 8014.

[50] S Yamamoto, Atsushi; Matsui, Yasunori; Asada, Toshio; Kumeda, Motoki; Takagi, Kenichiro; Suenaga, Yu; Nagae, Kunihiko; Ohta, Eisuke; Sato, Hiroyasu; Koseki, Shiro; Naito, Hiroyoshi; Ikeda, Hiroshi. *J. Org. Chem*. **2016**, *81*, 3168.

[29] C. Hansch, A. Leo, R. W. Taft. *Chem. Rev.* **1991**, *91*, 165–195.

[30] X. Hu, B. M. Cossairt, B. S. Brunschwig, N. S. Lewis, J. C. Peters. *Chem. Commun.* **2005**, 4723–4725.

[31] M. C. Smith, J. A. Snyder, B. C. Streifel, A. E. Bragg. *J. Phys. Chem. Lett.* **2013**, *4*, 1895-1900.

[32] X. S. Xue, P. Ji, B. Zhou, J. P. Cheng. *Chem. Rev*. **2017**, *117*, 8622−8648.

[33] J. G. West, D. Huang, E. J. Sorensen. *Nat. Commun,* **2015**, *6*, 10093.

2.6. Scanned ^{1}H and ^{13}C spectra

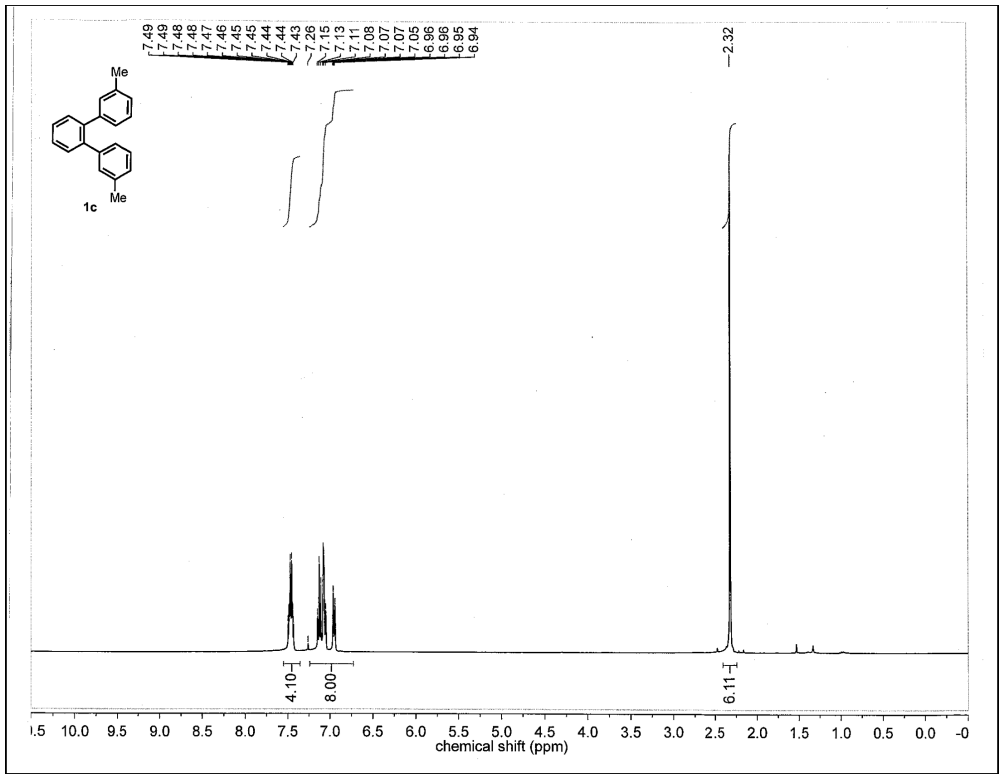

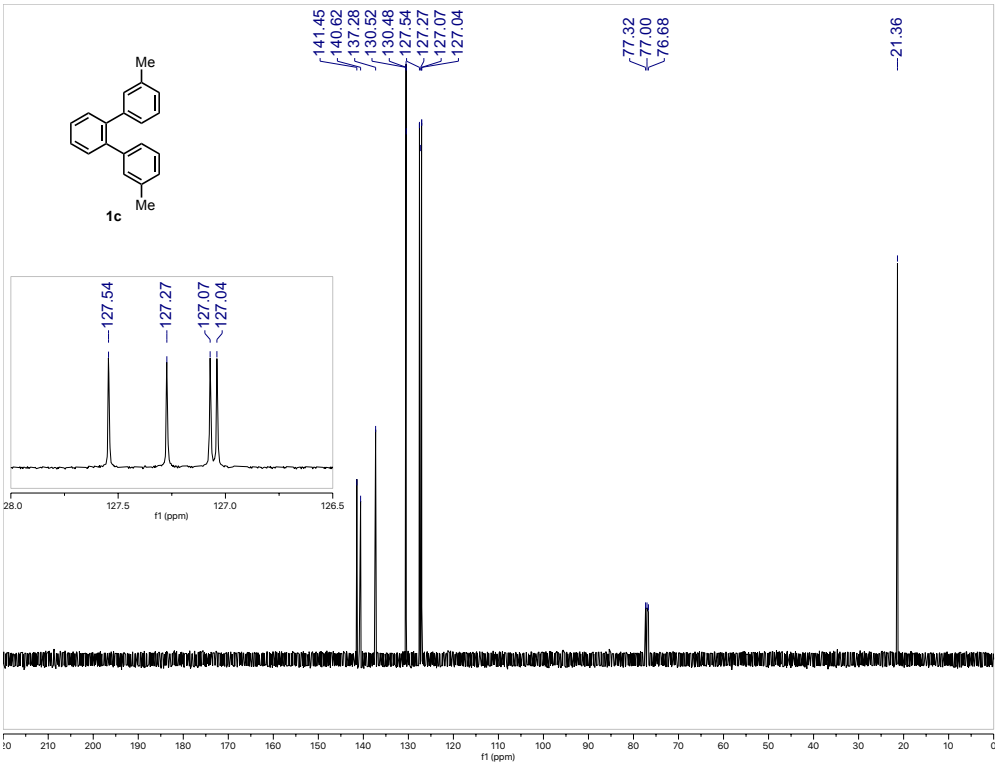
141.45
140.62
137.28
130.52
130.48
127.54
127.27
127.07
127.04
77.32
77.00
76.68
21.36
Me
Me
1c
127.54
127.27
127.07
127.04
28.0
127.5
127.0
126.5
f1 (ppm)
210
200
190
180
170
160
150
140
130
120
110
100
90
80
70
60
50
40
30
20
10
f1 (ppm)

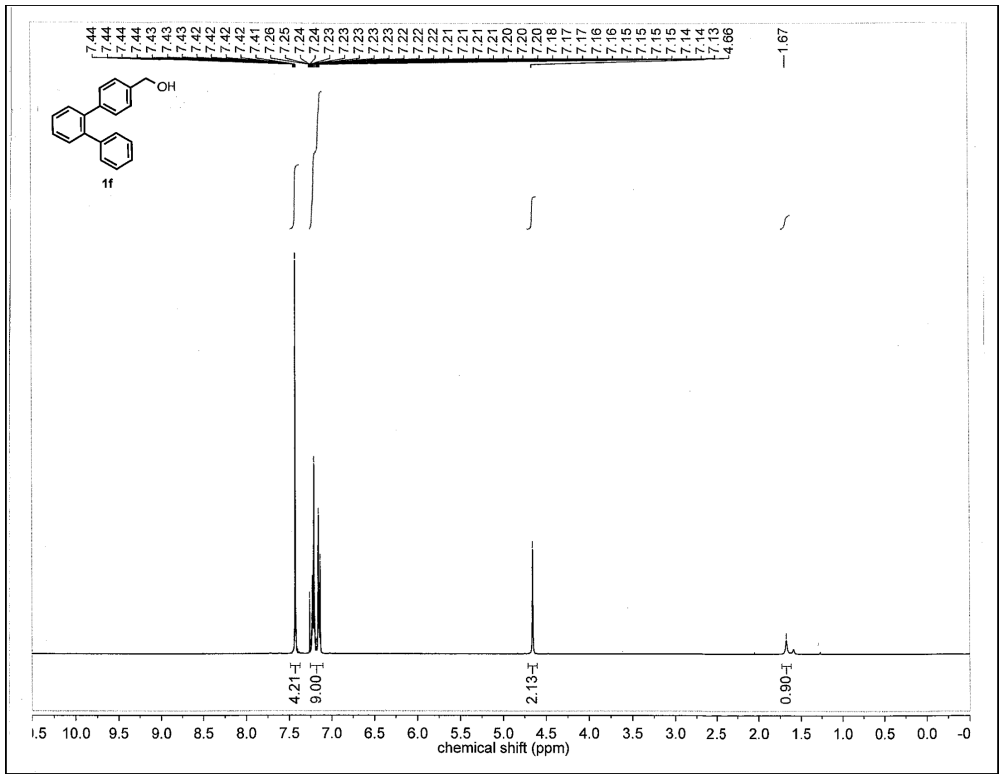
OH
1f
4.21
9.00
2.13
0.90
chemical shift (ppm)

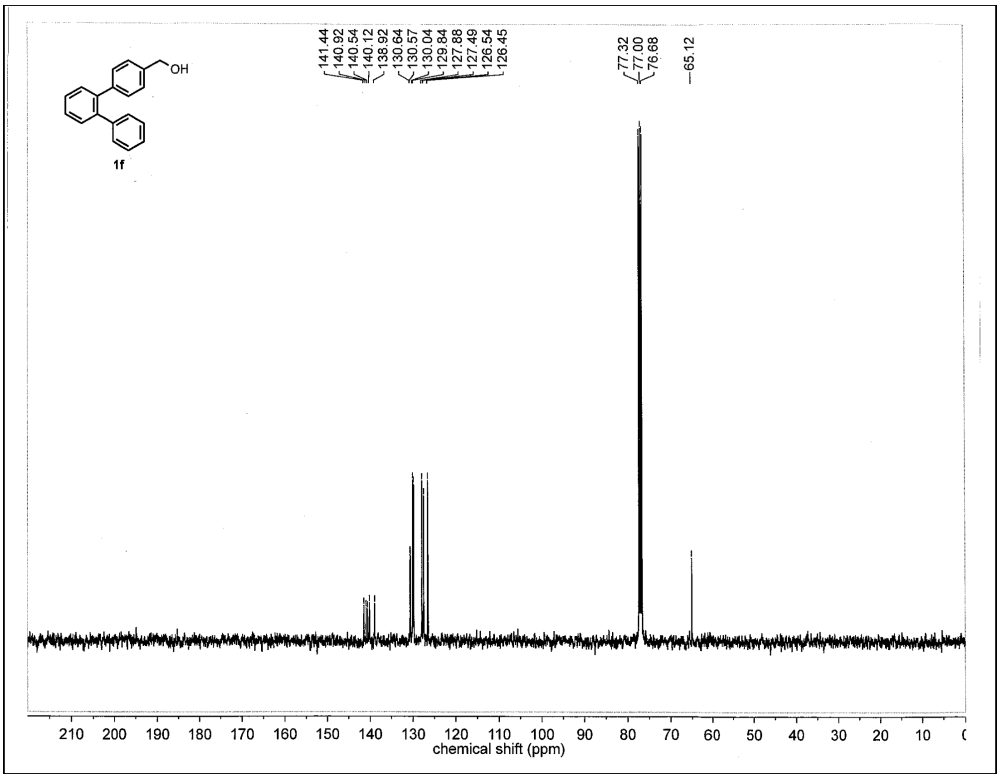
OH
1f
141.44
140.92
140.54
140.12
138.92
130.64
130.57
130.04
129.84
127.88
127.49
126.54
126.45
77.32
77.00
76.68
65.12
210 200 190 180 170 160 150 140 130 120 110 100 90 80 70 60 50 40 30 20 10
chemical shift (ppm)

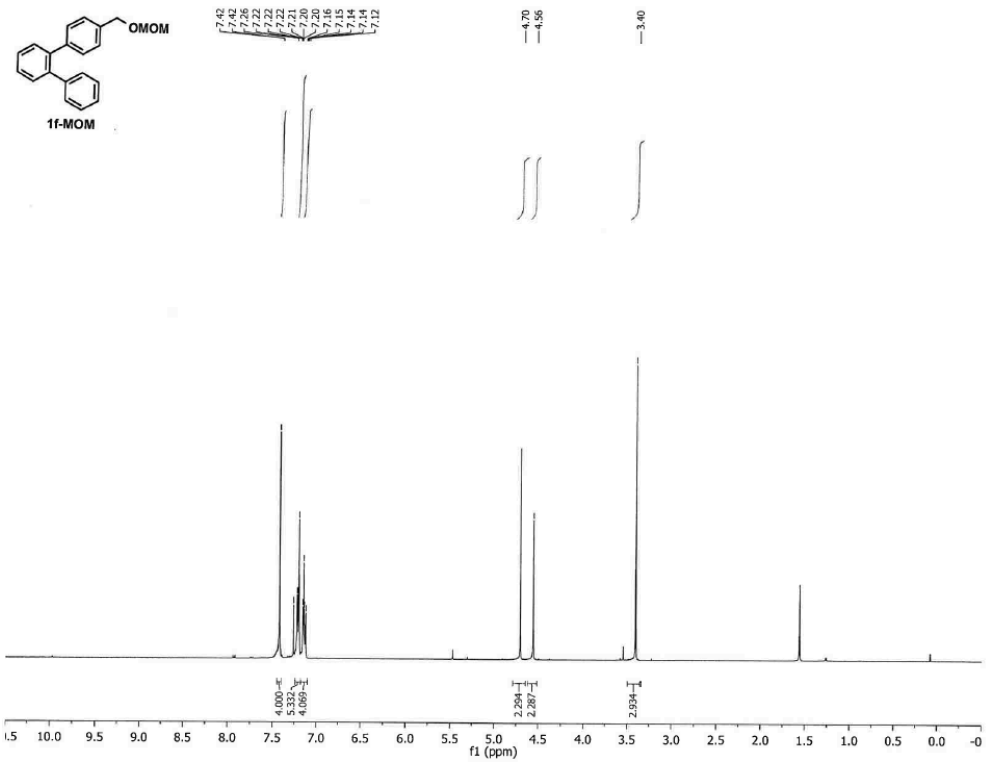
OMOM
1f-MOM
7.42
7.42
7.26
7.22
7.22
7.22
7.21
7.20
7.20
7.16
7.15
7.14
7.14
7.12
4.70
4.56
3.40
4.000
5.332
4.069
2.294
2.287
2.934
f1 (ppm)

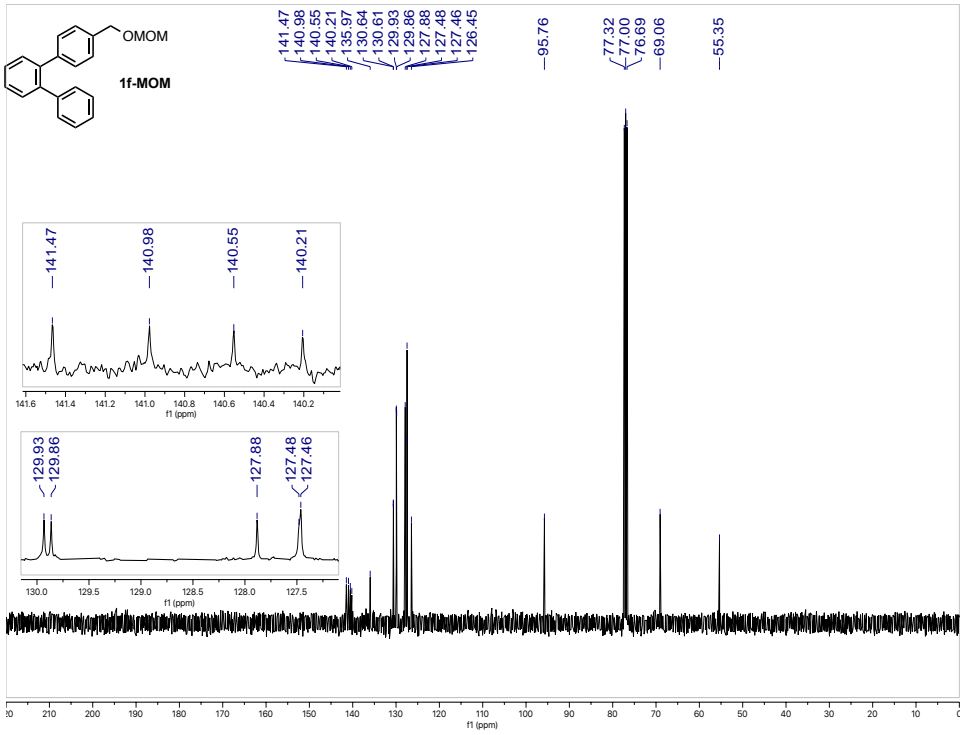
OMOM
1f-MOM
141.47
140.98
140.55
140.21
135.97
130.64
130.61
129.93
129.86
127.88
127.48
127.46
126.45
95.76
77.32
77.00
76.69
69.06
55.35
f1 (ppm)

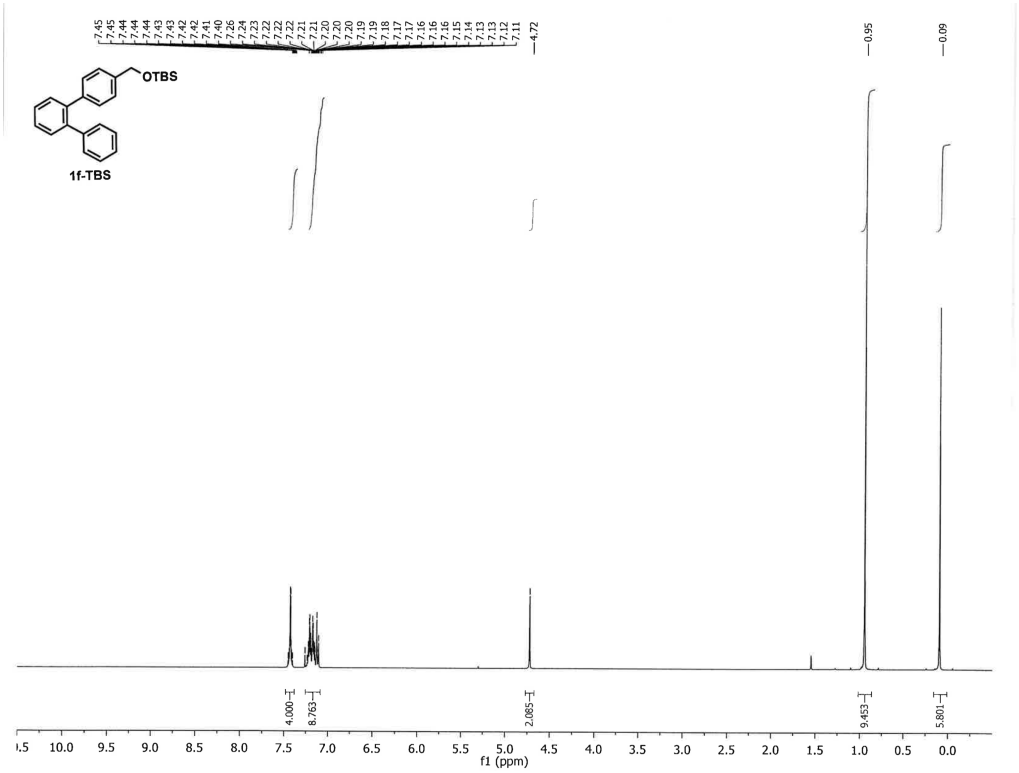
OTBS
1f-TBS
7.45
7.45
7.44
7.44
7.44
7.43
7.43
7.42
7.41
7.40
7.26
7.24
7.23
7.22
7.22
7.21
7.21
7.20
7.20
7.19
7.19
7.18
7.17
7.17
7.16
7.16
7.15
7.14
7.13
7.13
7.12
7.11
4.72
0.95
0.09
4.000
8.763
2.085
9.453
5.801
f1 (ppm)

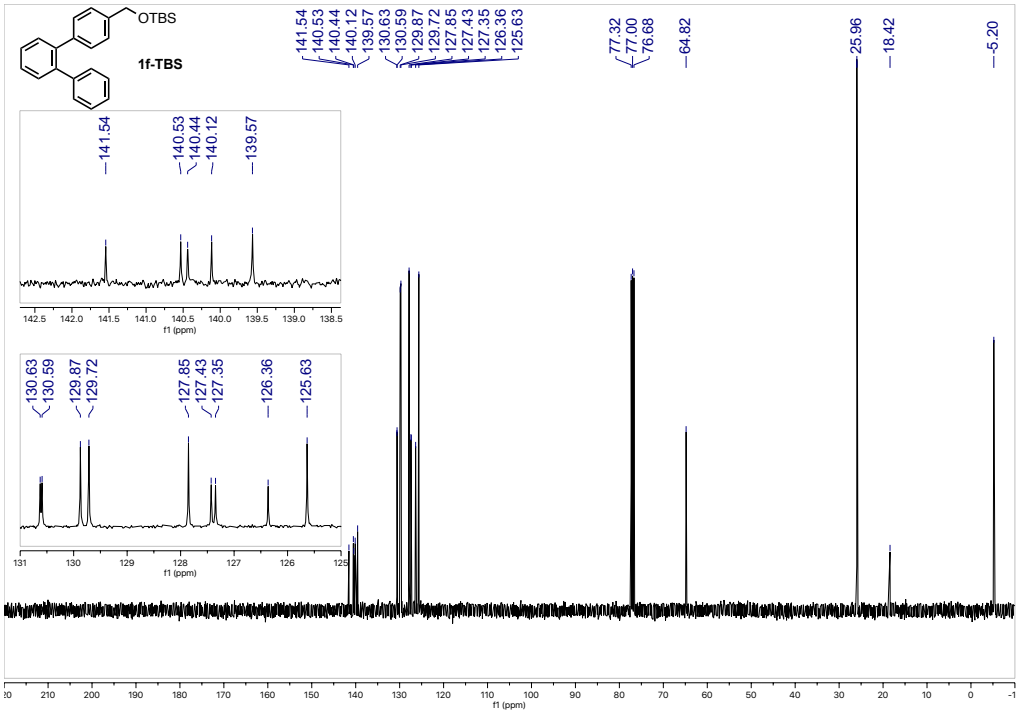
OTBS
1f-TBS
141.54
140.53
140.44
140.12
139.57
130.63
130.59
129.87
129.72
127.85
127.43
127.35
126.36
125.63
77.32
77.00
76.68
64.82
25.96
18.42
-5.20
f1 (ppm)

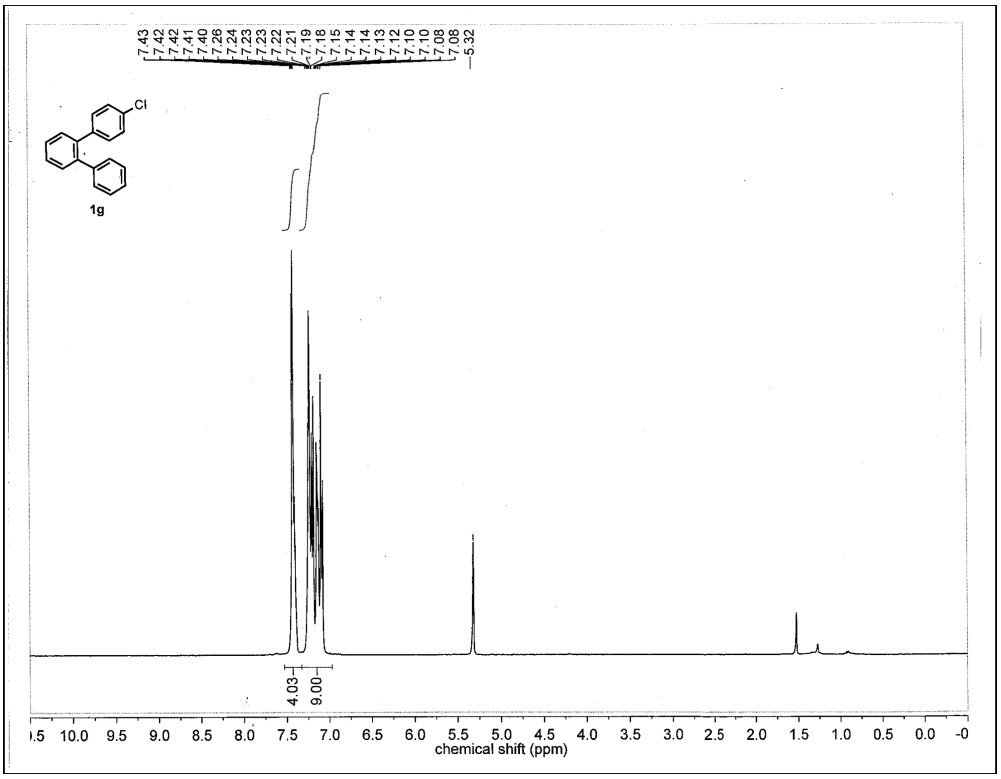
7.43
7.42
7.42
7.41
7.40
7.26
7.24
7.23
7.23
7.22
7.21
7.19
7.18
7.15
7.14
7.14
7.13
7.12
7.10
7.10
7.08
7.08
5.32
Cl
1g
4.03
9.00
10.0 9.5 9.0 8.5 8.0 7.5 7.0 6.5 6.0 5.5 5.0 4.5 4.0 3.5 3.0 2.5 2.0 1.5 1.0 0.5 0.0
chemical shift (ppm)

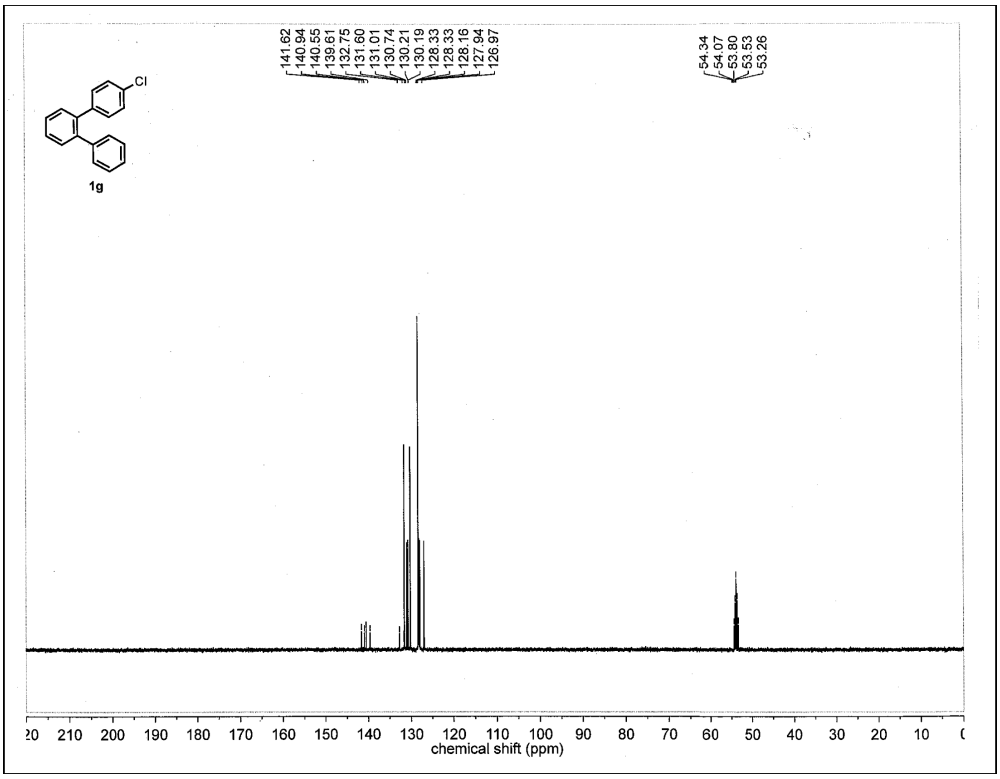
141.62
140.94
140.55
139.61
132.75
131.60
131.01
130.74
130.21
130.19
128.33
128.33
128.16
127.94
126.97
54.34
54.07
53.80
53.53
53.26
Cl
1g
chemical shift (ppm)

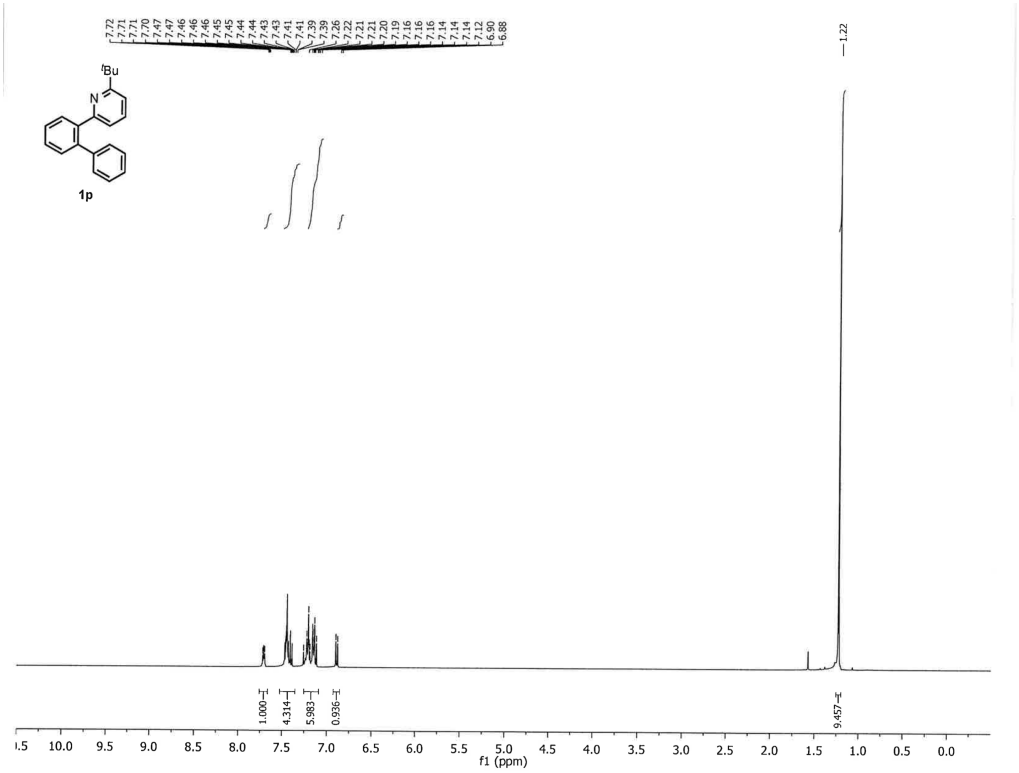
7.72
7.71
7.71
7.70
7.47
7.47
7.46
7.46
7.46
7.45
7.45
7.44
7.44
7.43
7.43
7.41
7.41
7.39
7.39
7.26
7.22
7.21
7.21
7.20
7.19
7.16
7.16
7.16
7.14
7.14
7.14
7.12
7.09
6.88
1.22
tBu
N
1p
1.000
4.314
5.983
0.936
9.457
10.0
9.5
9.0
8.5
8.0
7.5
7.0
6.5
6.0
5.5
5.0
4.5
4.0
3.5
3.0
2.5
2.0
1.5
1.0
0.5
0.0
f1 (ppm)

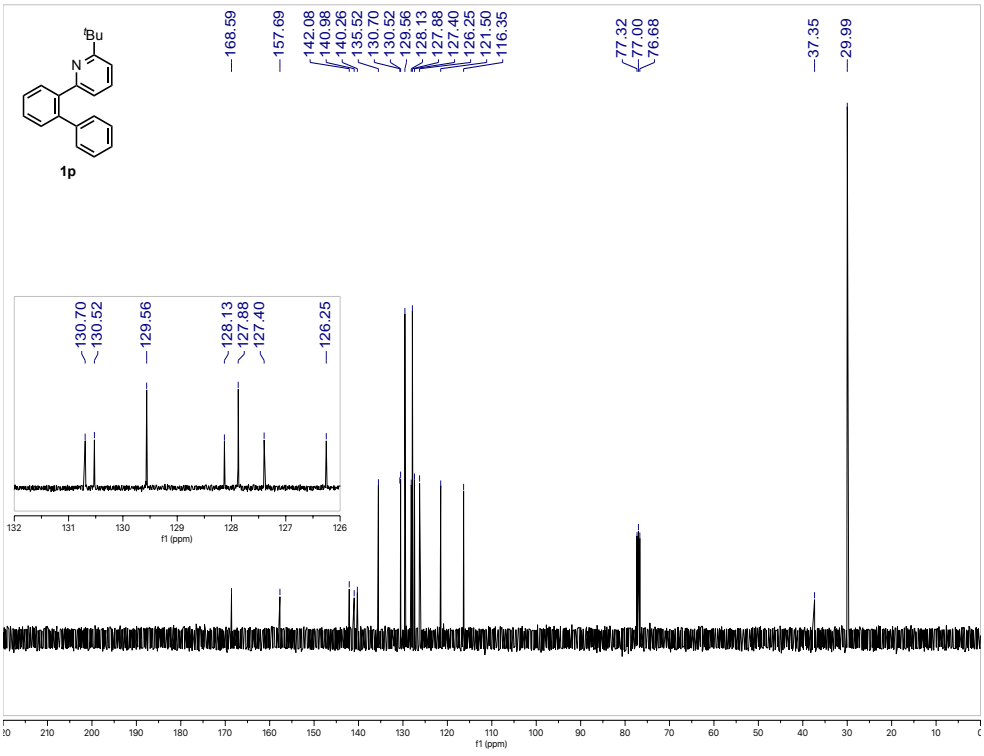
tBu
N
1p
168.59
157.69
142.08
140.98
140.26
135.52
130.70
130.52
129.56
128.13
127.88
127.40
126.25
121.50
116.35
77.32
77.00
76.68
37.35
29.99
f1 (ppm)

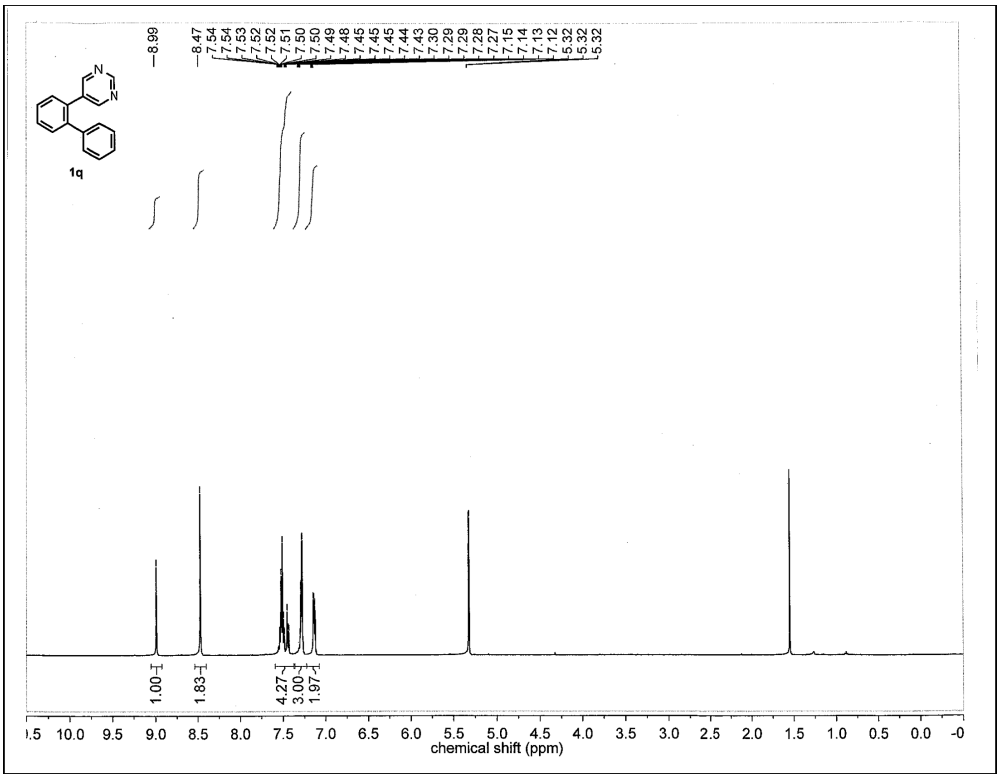
8.99
8.47
7.54
7.54
7.53
7.52
7.52
7.51
7.50
7.50
7.49
7.48
7.45
7.45
7.44
7.43
7.30
7.29
7.29
7.28
7.27
7.15
7.14
7.13
7.12
5.32
5.32
5.32
1q
1.00
1.83
4.27
3.00
1.97
chemical shift (ppm)

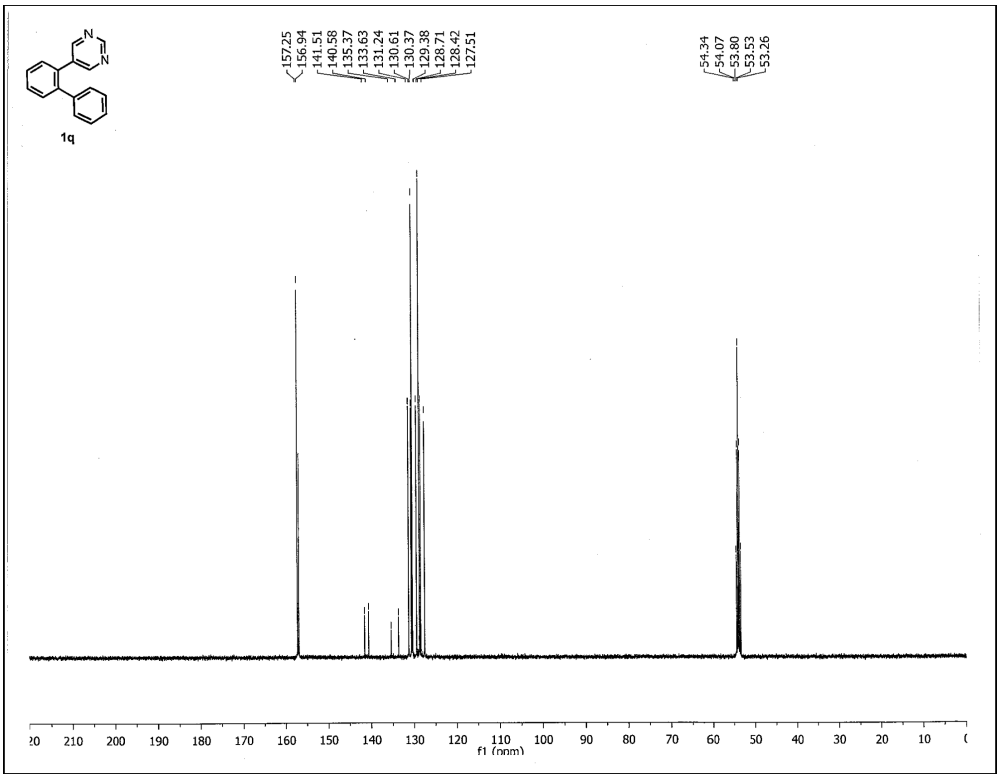
1q
157.25
156.94
141.51
140.58
135.37
133.63
131.24
130.61
130.37
129.38
128.71
128.42
127.51
54.34
54.07
53.80
53.53
53.26
f1 (ppm)

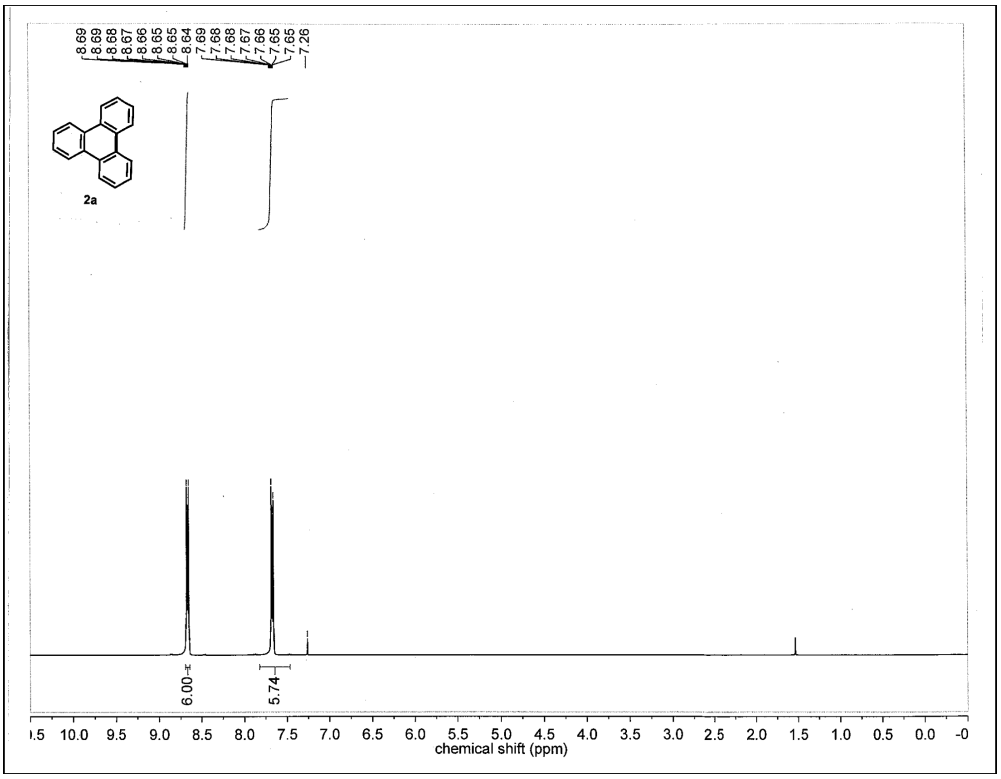
8.69
8.69
8.68
8.67
8.66
8.65
8.65
8.64
7.69
7.68
7.68
7.67
7.66
7.65
7.65
7.26
2a
6.00
5.74
chemical shift (ppm)

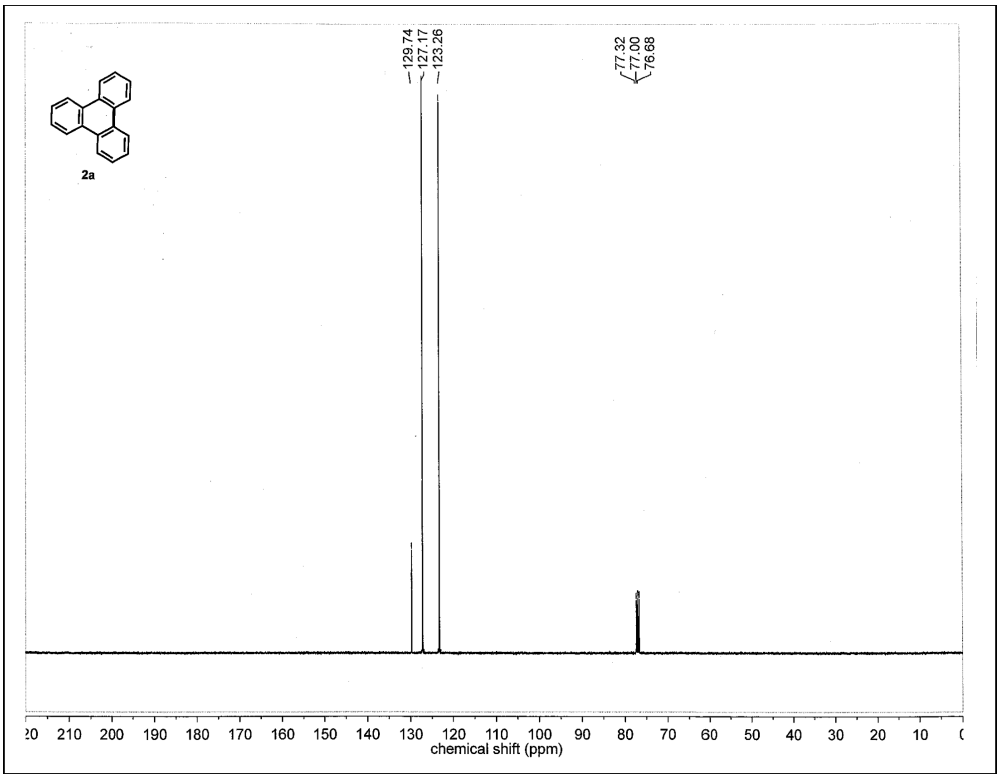
129.74
127.17
123.26
77.32
77.00
76.68
2a
chemical shift (ppm)

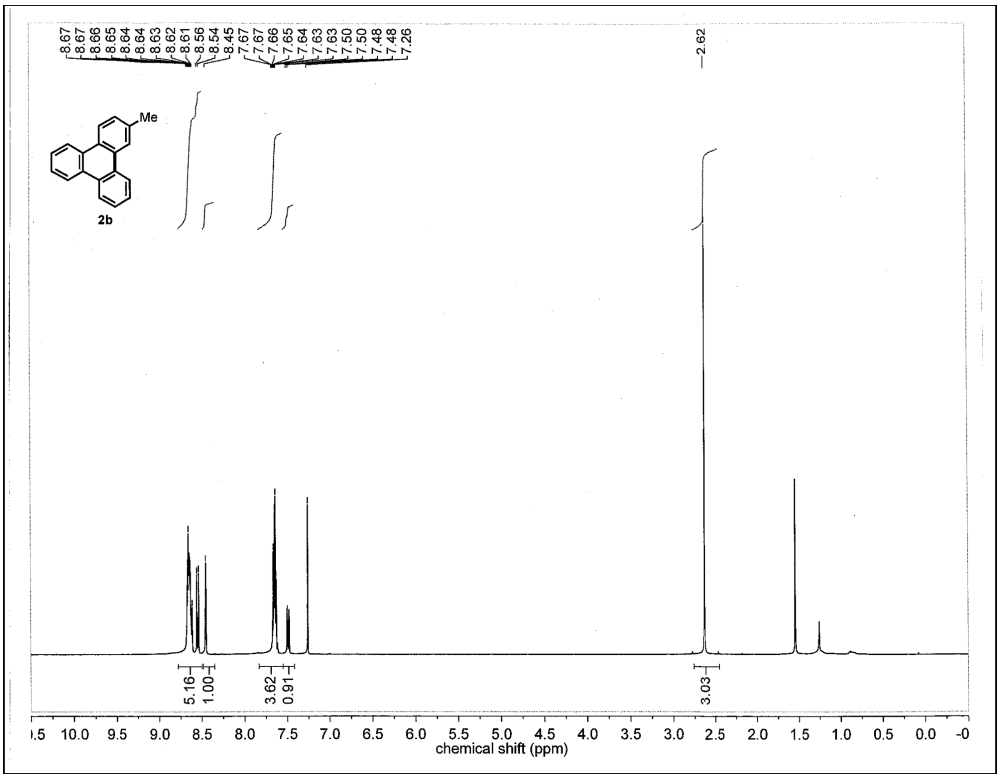
8.67
8.67
8.66
8.65
8.64
8.64
8.63
8.62
8.61
8.56
8.54
8.45
7.67
7.67
7.66
7.65
7.64
7.63
7.63
7.50
7.50
7.48
7.48
7.26
2.62
Me
2b
5.16
1.00
3.62
0.91
3.03
chemical shift (ppm)

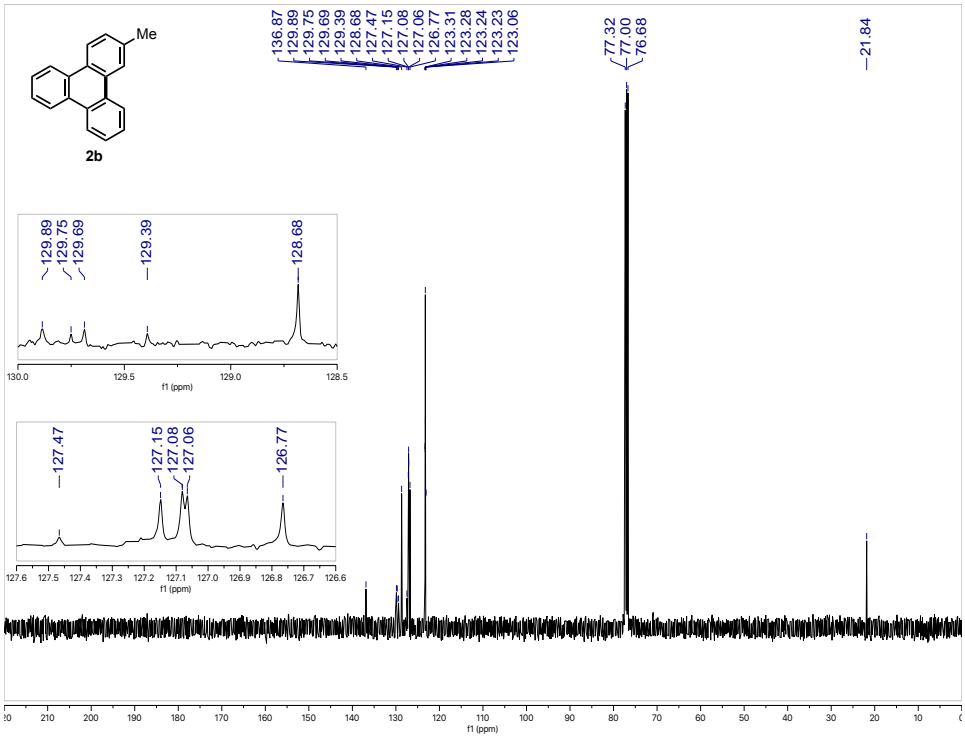
Me
2b
136.87
129.89
129.75
129.69
129.39
128.68
127.47
127.15
127.08
127.06
126.77
123.31
123.28
123.24
123.23
123.06
77.32
77.00
76.68
21.84
f1 (ppm)

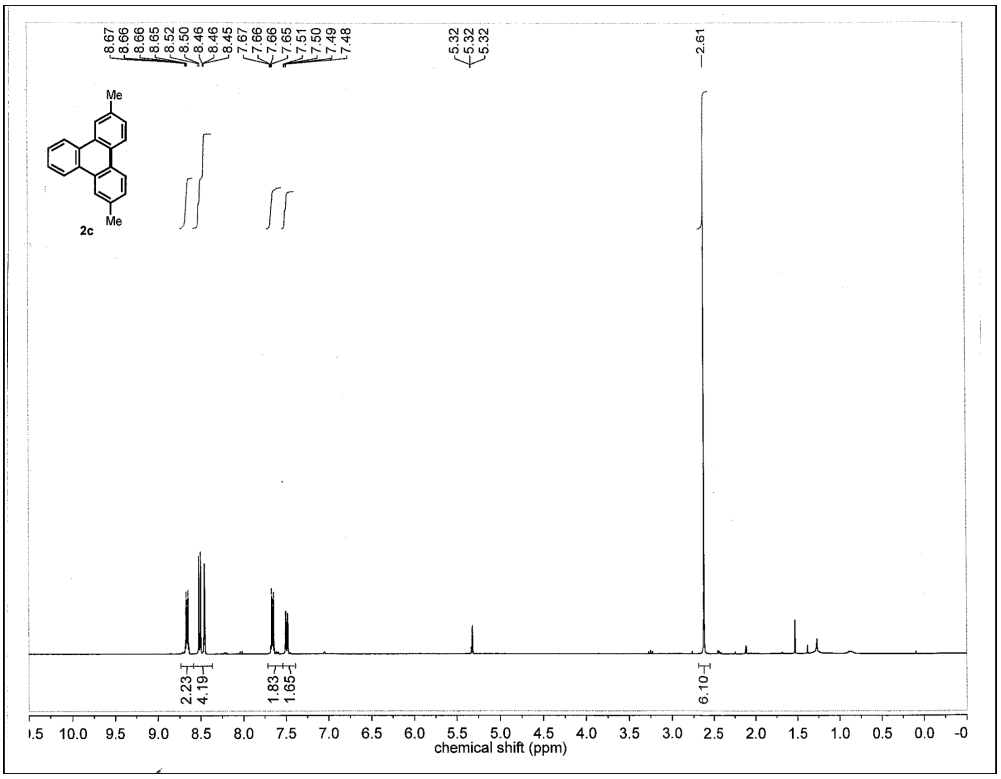
8.67
8.66
8.66
8.65
8.52
8.50
8.46
8.46
8.45
7.67
7.66
7.66
7.65
7.51
7.50
7.49
7.48
5.32
5.32
5.32
2.61
Me
Me
2c
2.23
4.19
1.83
1.65
6.10
chemical shift (ppm)

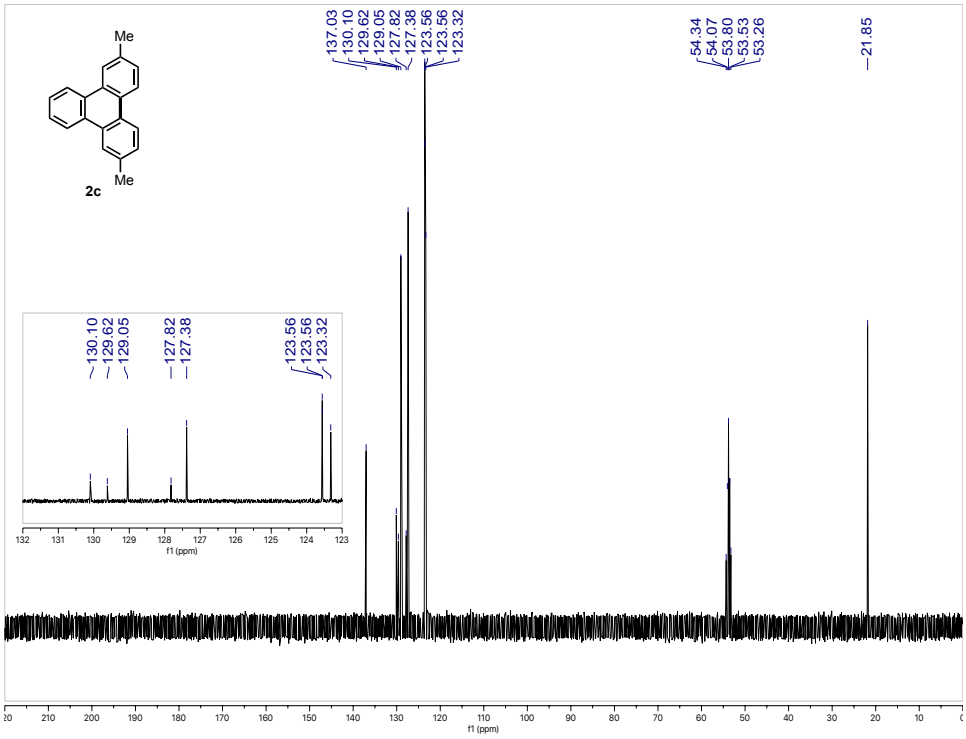
Me
Me
2c
137.03
130.10
129.62
129.05
127.82
127.38
123.56
123.56
123.32
54.34
54.07
53.80
53.53
53.26
21.85
f1 (ppm)

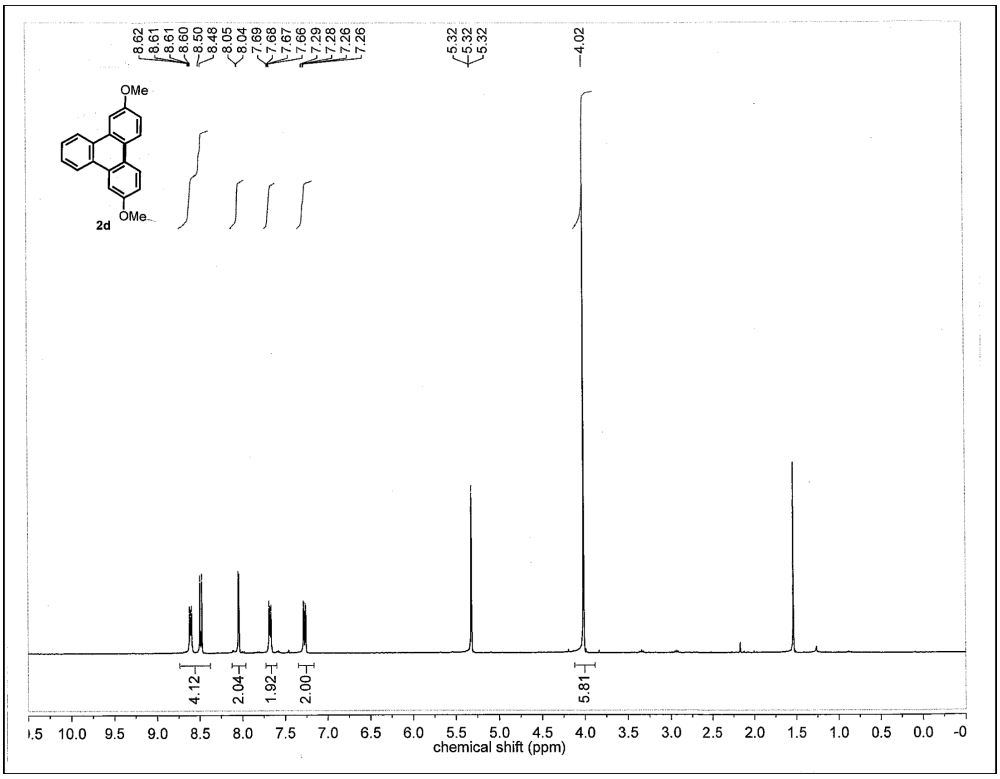
8.62
8.61
8.61
8.60
8.50
8.48
8.05
8.04
7.69
7.68
7.67
7.66
7.29
7.28
7.26
7.26
5.32
5.32
5.32
4.02
OMe
OMe
2d
4.12
2.04
1.92
2.00
5.81
chemical shift (ppm)

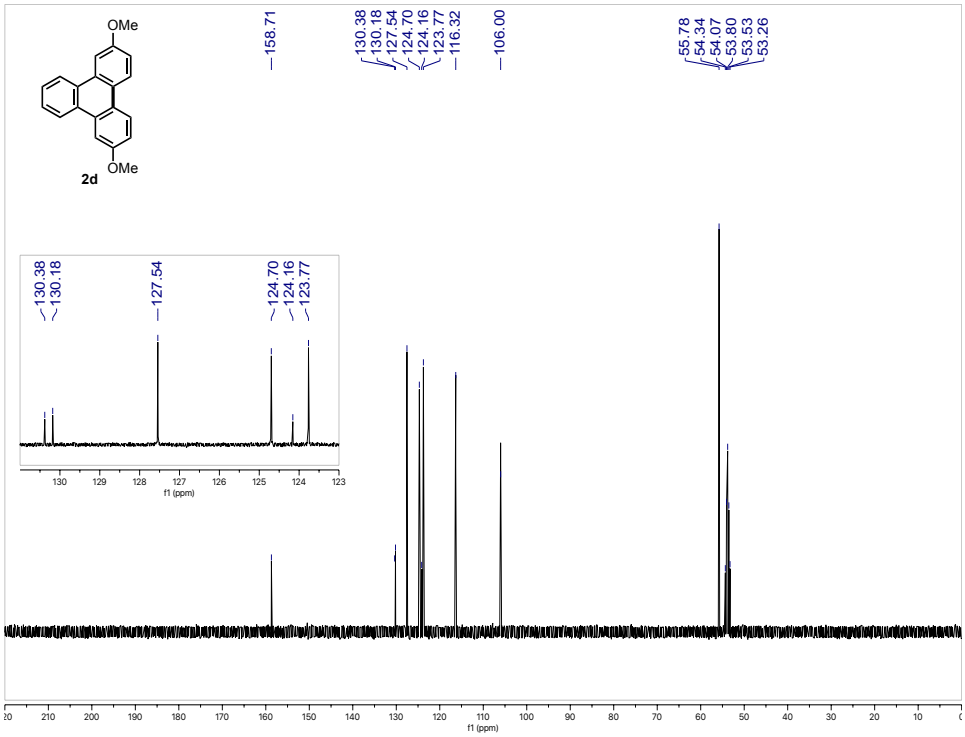
OMe
OMe
2d
158.71
130.38
130.18
127.54
124.70
124.16
123.77
116.32
106.00
55.78
54.34
54.07
53.80
53.53
53.26
f1 (ppm)

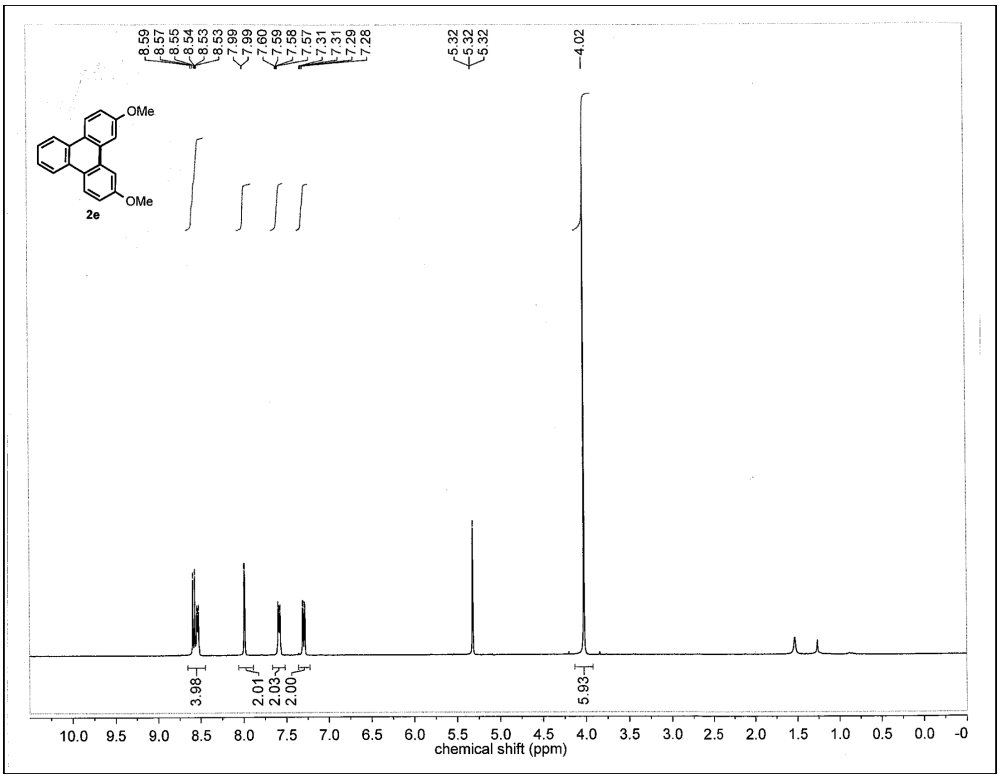
8.59
8.57
8.55
8.54
8.53
8.53
7.99
7.99
7.60
7.59
7.58
7.57
7.31
7.31
7.29
7.28
5.32
5.32
5.32
4.02
OMe
OMe
2e
3.98
2.01
2.03
2.00
5.93
10.0 9.5 9.0 8.5 8.0 7.5 7.0 6.5 6.0 5.5 5.0 4.5 4.0 3.5 3.0 2.5 2.0 1.5 1.0 0.5 0.0 -0
chemical shift (ppm)

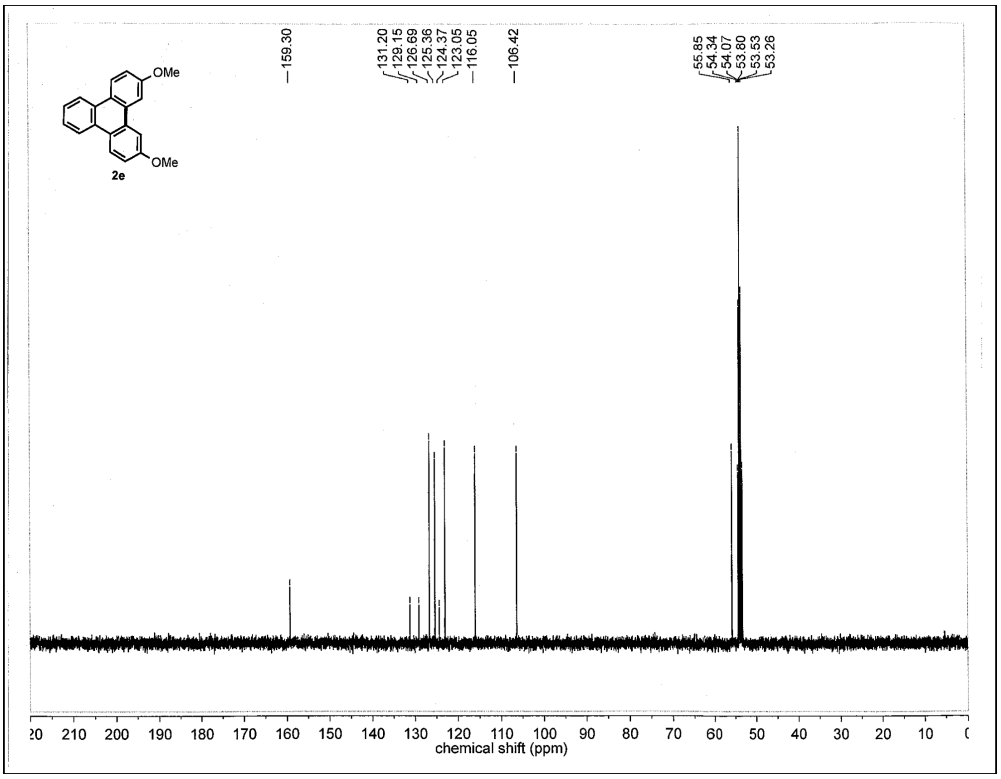
OMe
OMe
2e
159.30
131.20
129.15
126.69
125.36
124.37
123.05
116.05
106.42
55.85
54.34
54.07
53.80
53.53
53.26
chemical shift (ppm)

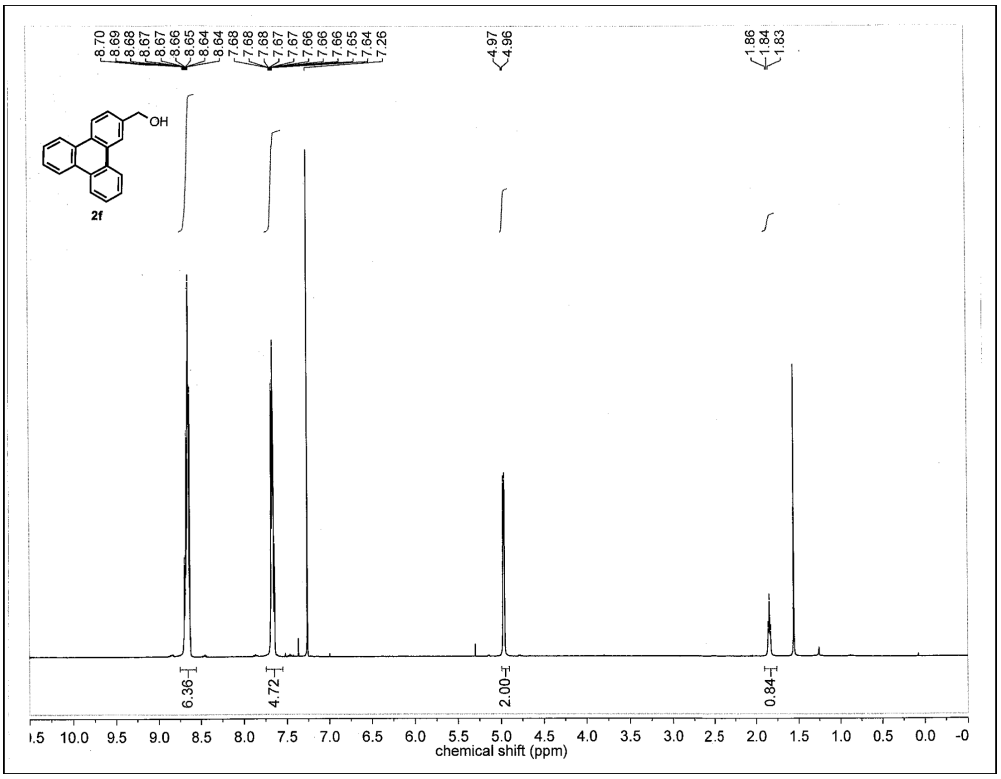
8.70
8.69
8.68
8.67
8.67
8.66
8.65
8.64
8.64
7.68
7.68
7.68
7.67
7.67
7.66
7.66
7.66
7.65
7.64
7.26
4.97
4.96
1.86
1.84
1.83
OH
2f
6.36
4.72
2.00
0.84
chemical shift (ppm)

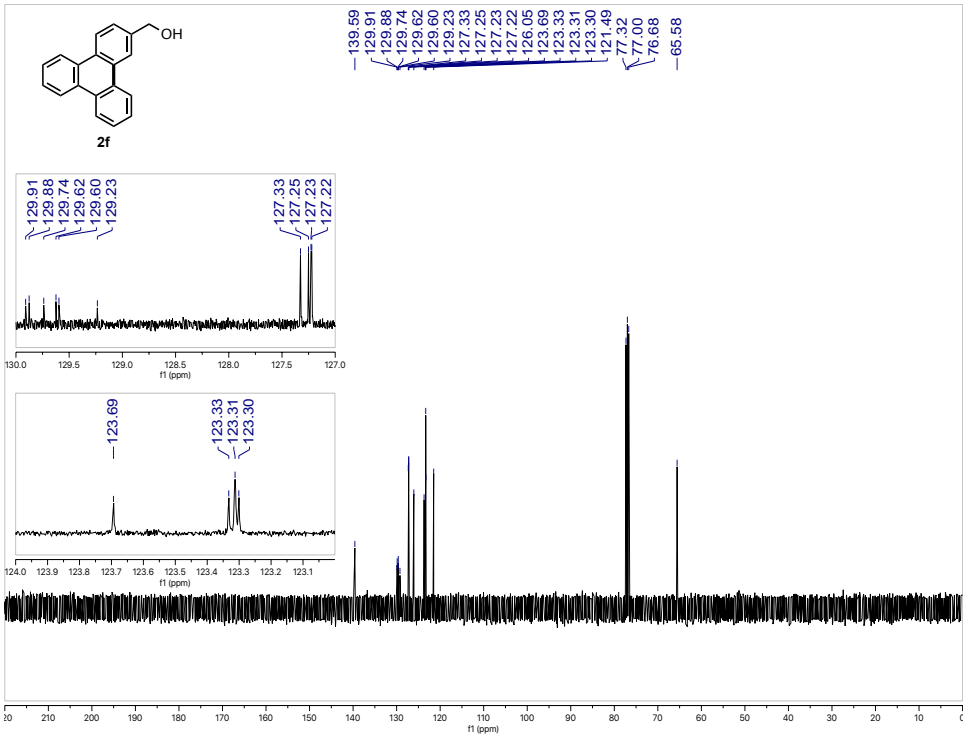
OH
2f
139.59
129.91
129.88
129.74
129.62
129.60
129.23
127.33
127.25
127.23
127.22
126.05
123.69
123.33
123.31
123.30
121.49
77.32
77.00
76.68
65.58
f1 (ppm)

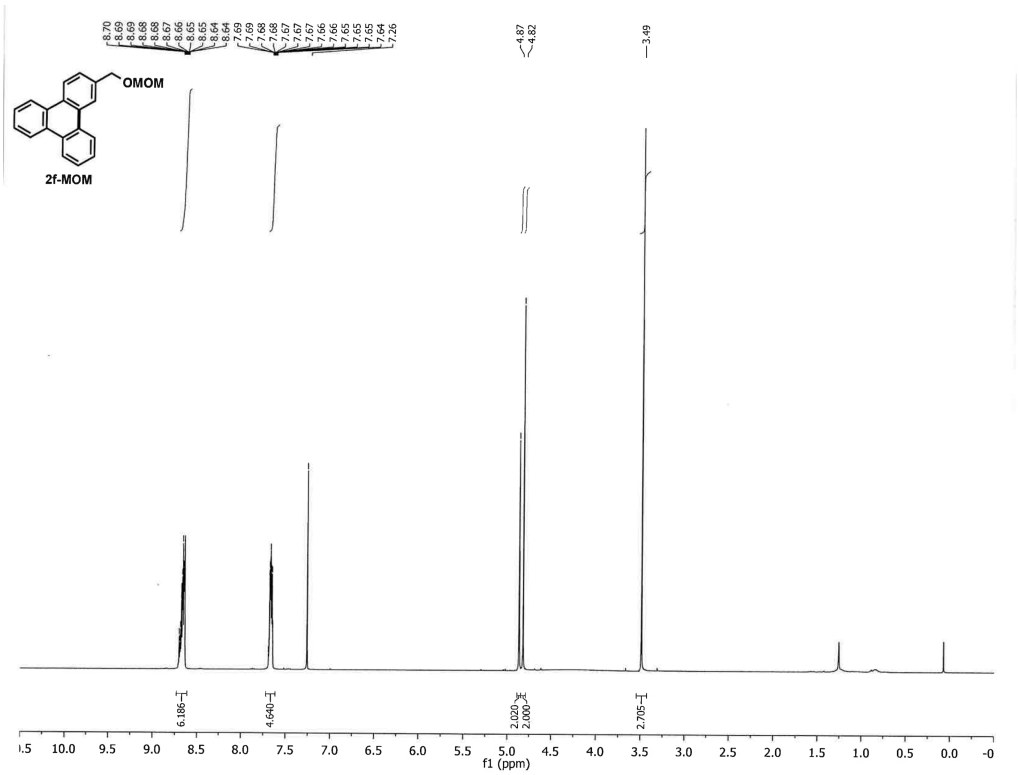
OMOM
2f-MOM
8.70
8.69
8.69
8.68
8.68
8.67
8.66
8.65
8.65
8.64
8.64
7.69
7.69
7.68
7.68
7.67
7.67
7.67
7.66
7.65
7.65
7.65
7.64
7.26
4.87
4.82
3.49
6.186
4.640
2.020
2.000
2.705
f1 (ppm)

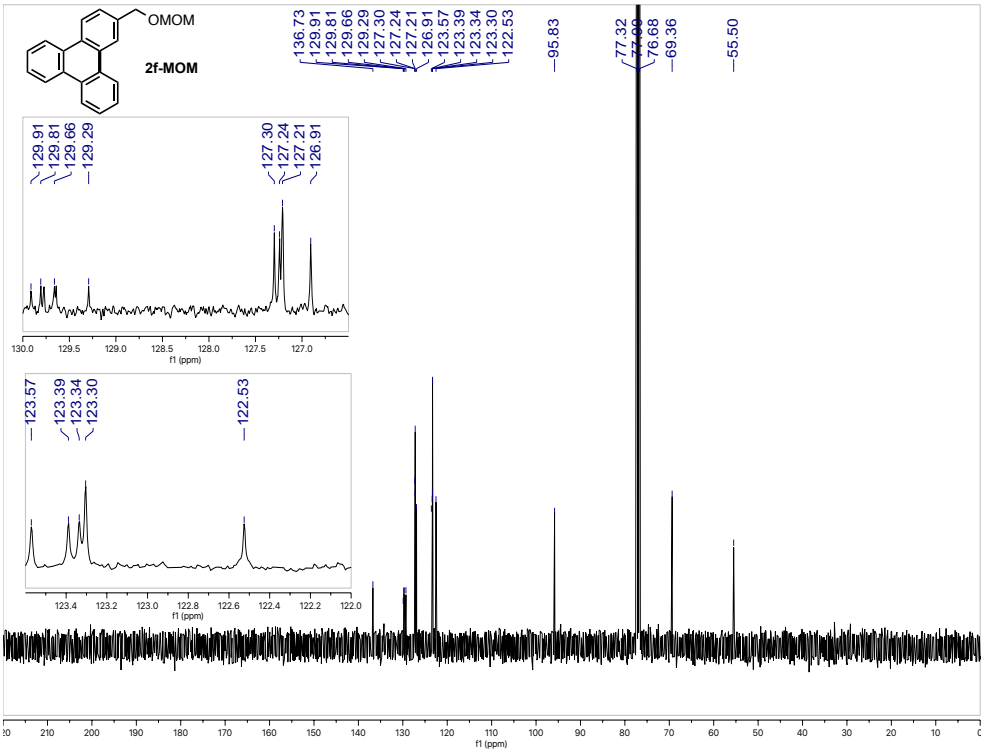
OMOM
2f-MOM
136.73
129.91
129.81
129.66
129.29
127.30
127.24
127.21
126.91
123.57
123.39
123.34
123.30
122.53
95.83
77.32
77.00
76.68
69.36
55.50
f1 (ppm)

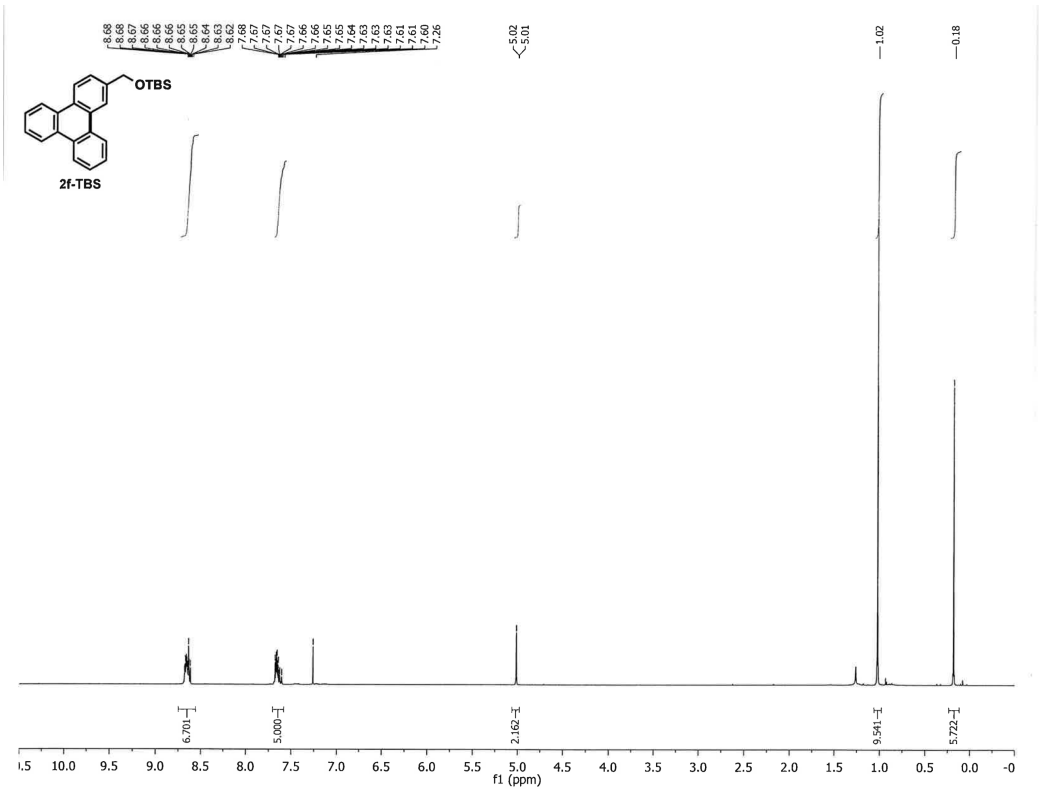
OTBS
2f-TBS
f1 (ppm)

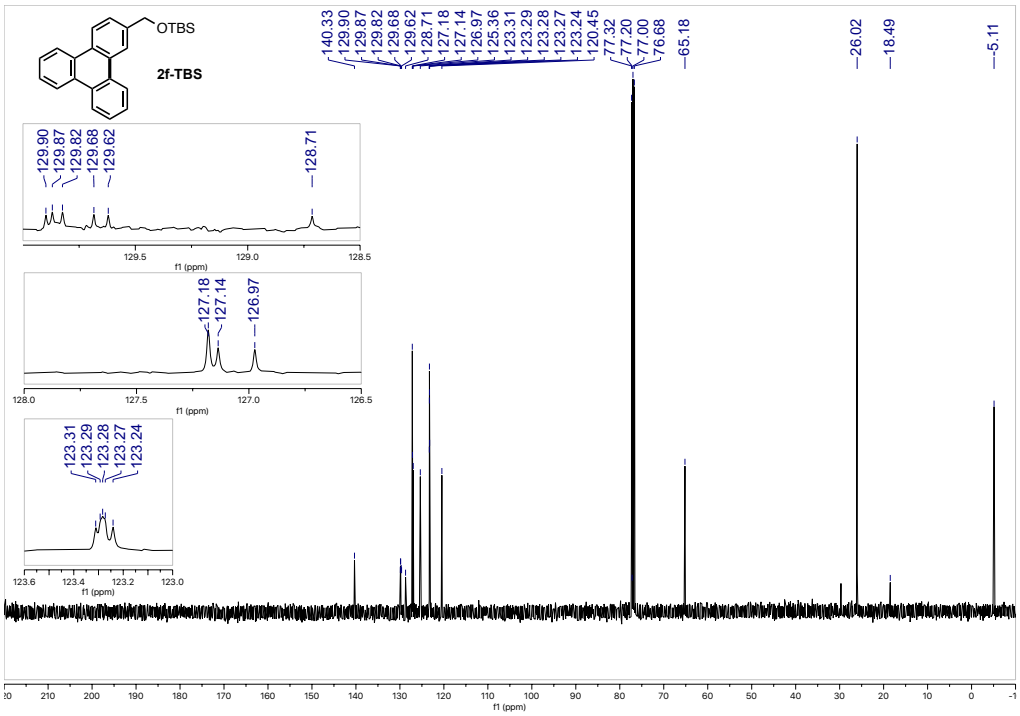
OTBS
2f-TBS
140.33
129.90
129.87
129.82
129.68
129.62
128.71
127.18
127.14
126.97
125.36
123.31
123.29
123.28
123.27
123.24
120.45
77.32
77.20
77.00
76.68
65.18
26.02
18.49
-5.11
f1 (ppm)

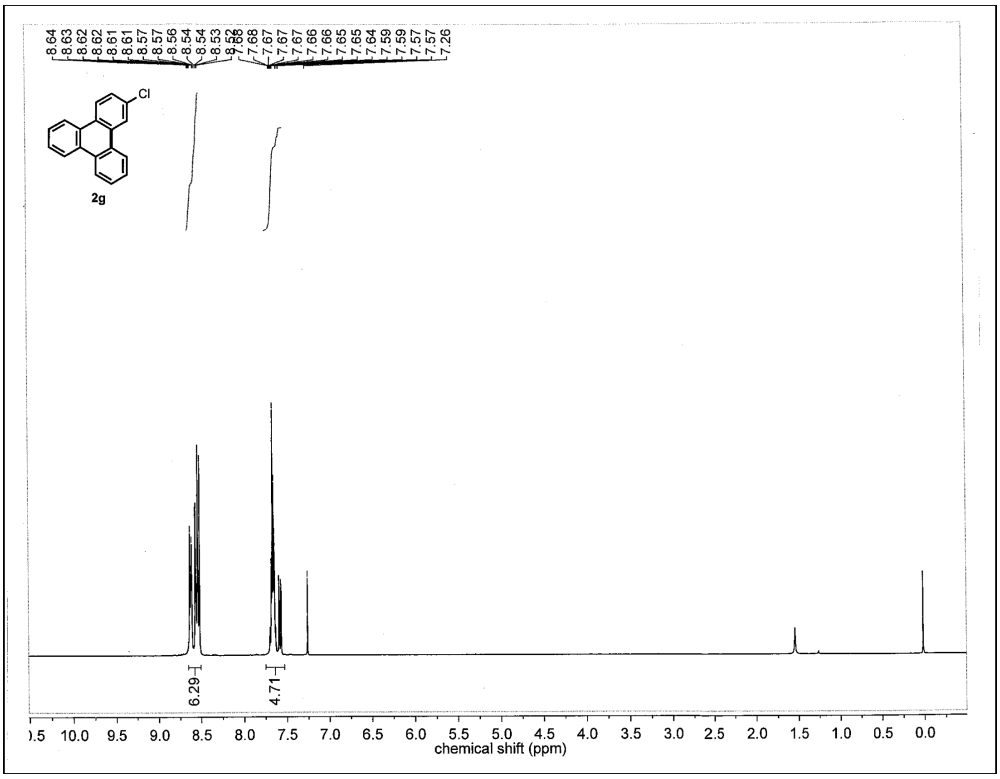
8.64
8.63
8.62
8.62
8.61
8.61
8.57
8.57
8.56
8.54
8.54
8.53
7.68
7.68
7.67
7.67
7.67
7.66
7.66
7.65
7.65
7.64
7.59
7.59
7.57
7.57
7.26
Cl
2g
6.29
4.71
chemical shift (ppm)

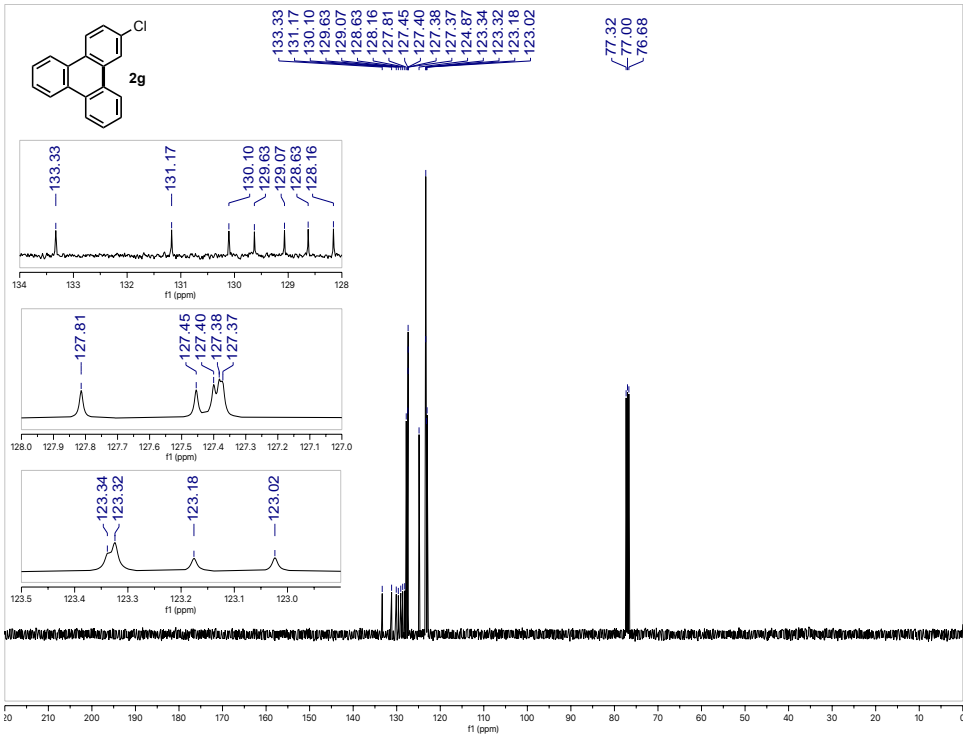
Cl
2g
133.33
131.17
130.10
129.63
129.07
128.63
128.16
127.81
127.45
127.40
127.38
127.37
124.87
123.34
123.32
123.18
123.02
77.32
77.00
76.68
f1 (ppm)

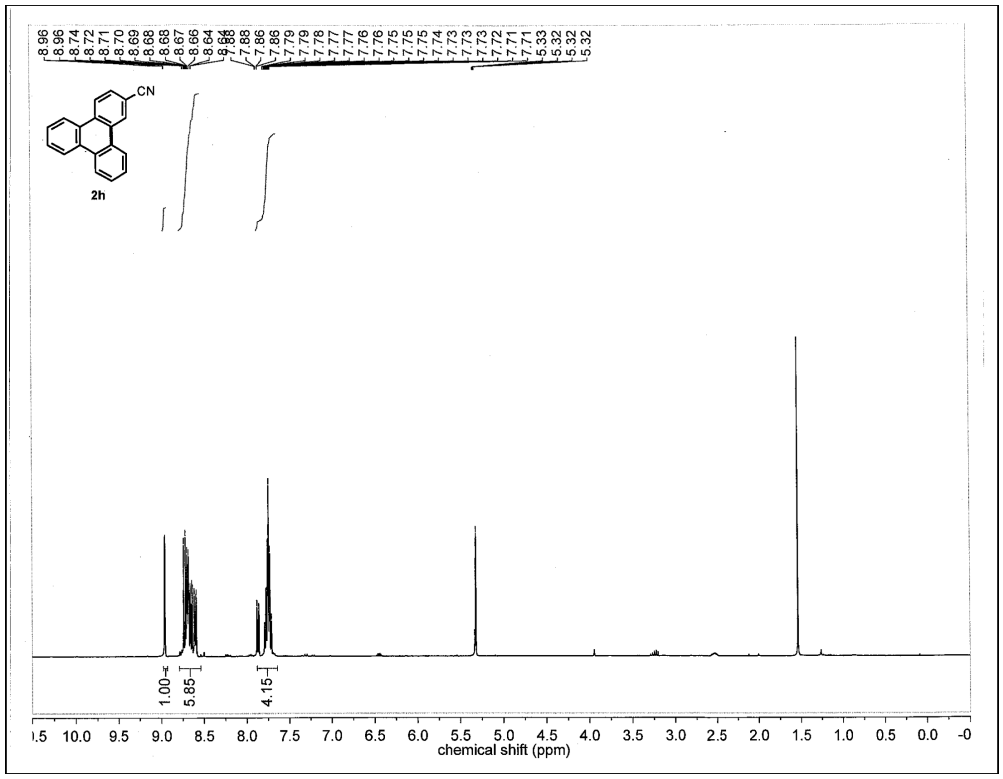
8.96
8.96
8.74
8.72
8.71
8.70
8.69
8.68
8.68
8.67
8.66
8.64
7.88
7.86
7.86
7.79
7.79
7.78
7.77
7.77
7.76
7.76
7.75
7.75
7.75
7.74
7.73
7.73
7.72
7.71
7.71
5.33
5.32
5.32
CN
2h
1.00
5.85
4.15
chemical shift (ppm)

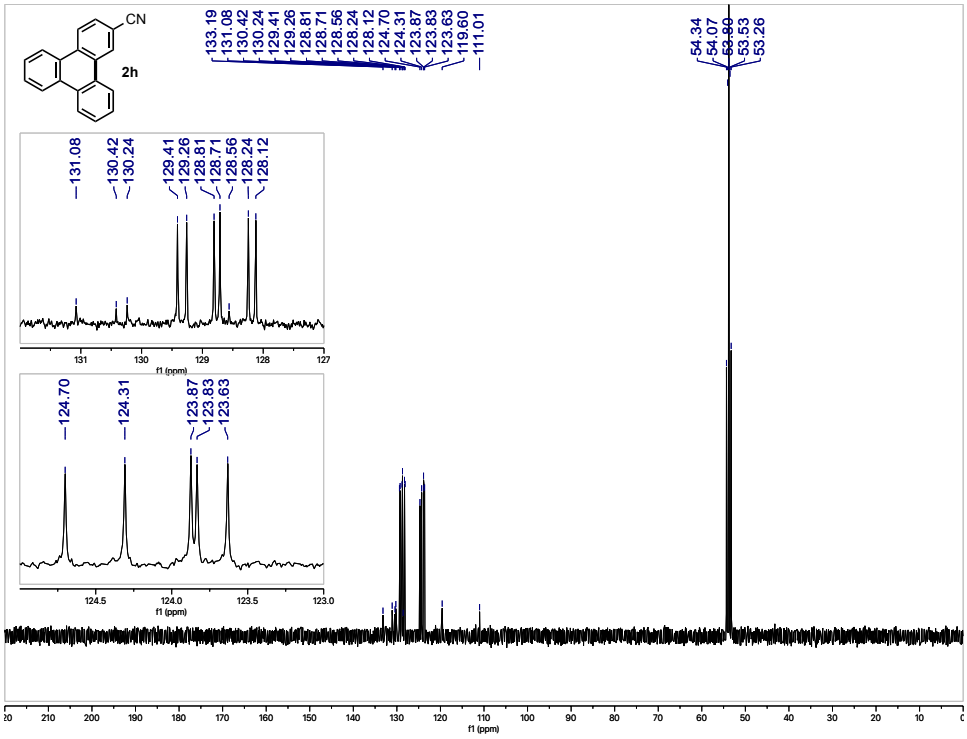
CN
2h
133.19
131.08
130.42
130.24
129.41
129.26
128.81
128.71
128.56
128.24
128.12
124.70
124.31
123.87
123.83
123.63
119.60
111.01
54.34
54.07
53.80
53.53
53.26
131.08
130.42
130.24
129.41
129.26
128.81
128.71
128.56
128.24
128.12
f1 (ppm)
124.70
124.31
123.87
123.83
123.63
f1 (ppm)
f1 (ppm)

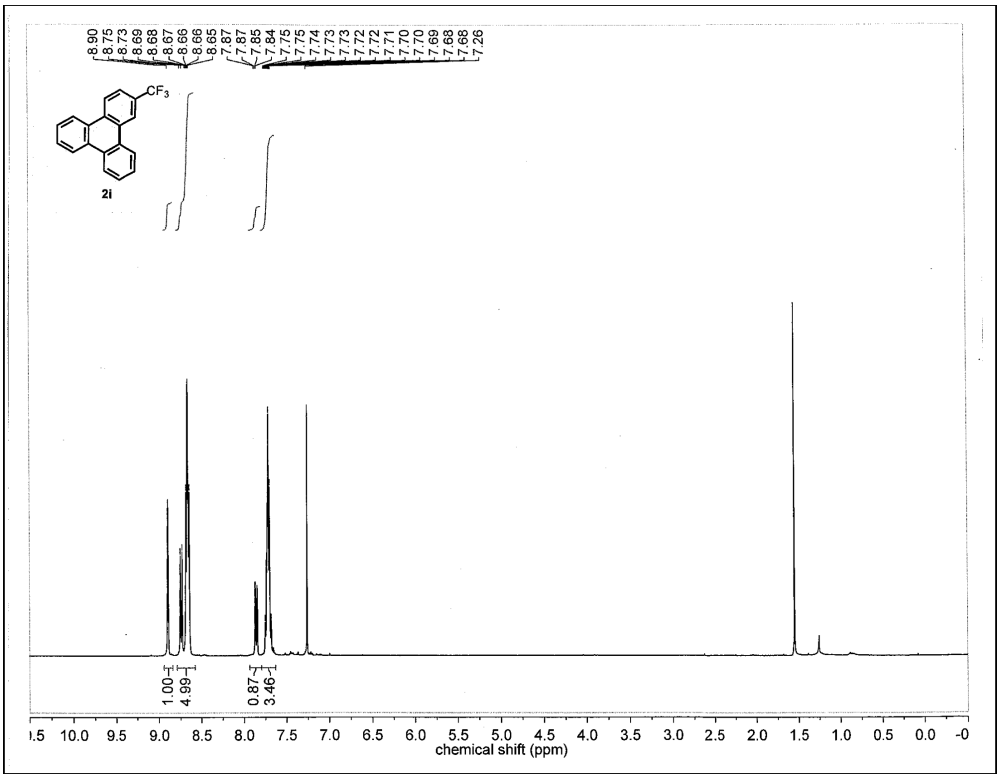
8.90
8.75
8.73
8.69
8.68
8.67
8.66
8.66
8.65
7.87
7.87
7.85
7.84
7.75
7.75
7.74
7.73
7.73
7.72
7.72
7.71
7.70
7.70
7.69
7.68
7.68
7.26
CF3
2i
1.00
4.99
0.87
3.46
chemical shift (ppm)

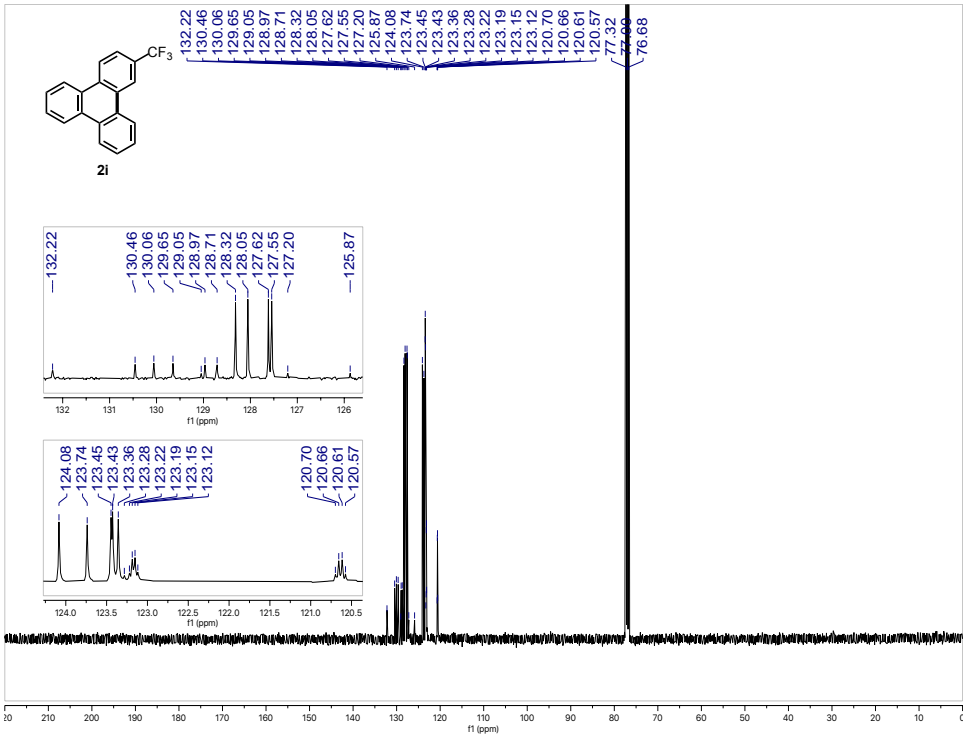
CF3
2i
132.22
130.46
130.06
129.65
129.05
128.97
128.71
128.32
128.05
127.62
127.55
127.20
125.87
124.08
123.74
123.45
123.43
123.36
123.28
123.22
123.19
123.15
123.12
120.70
120.66
120.61
120.57
77.32
77.00
76.68
f1 (ppm)

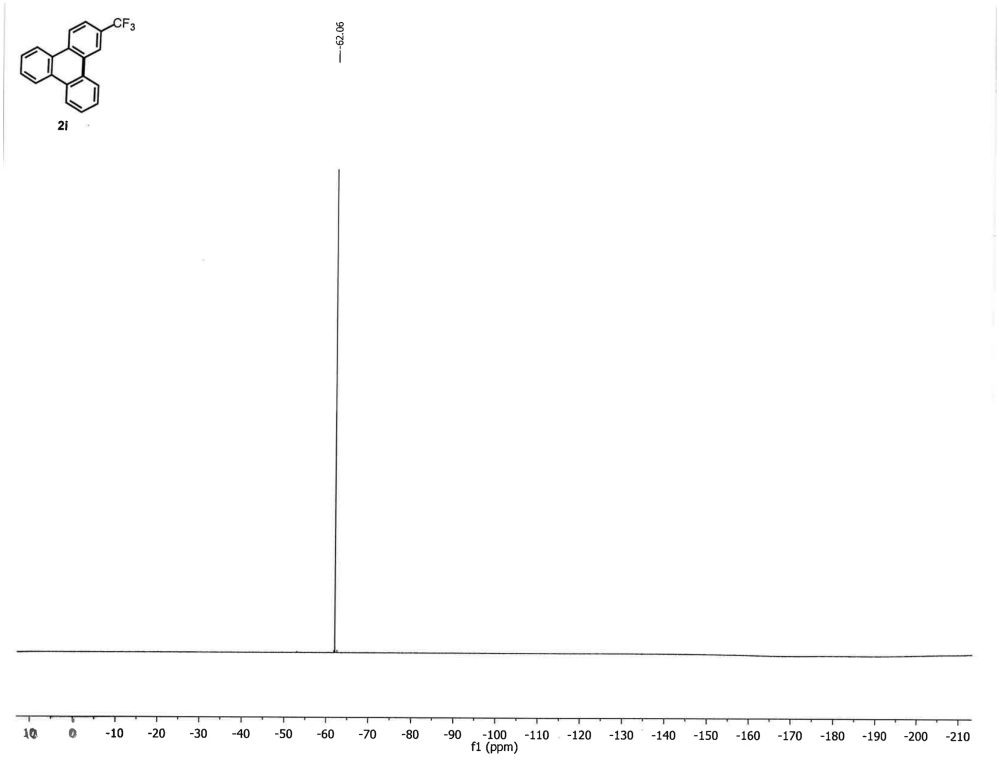
CF3
2l
-62.06
10
0
-10
-20
-30
-40
-50
-60
-70
-80
-90
-100
-110
-120
-130
-140
-150
-160
-170
-180
-190
-200
-210
f1 (ppm)

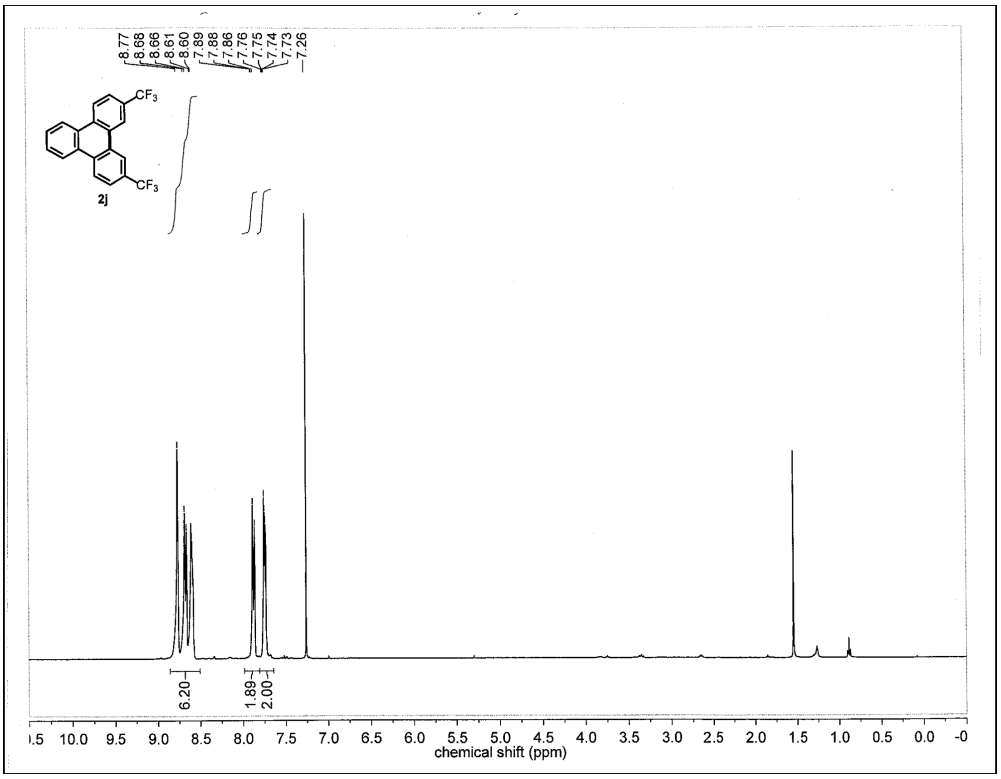
8.77
8.68
8.66
8.61
8.60
7.89
7.88
7.86
7.76
7.75
7.74
7.73
7.26
CF3
CF3
2j
6.20
1.89
2.00
chemical shift (ppm)

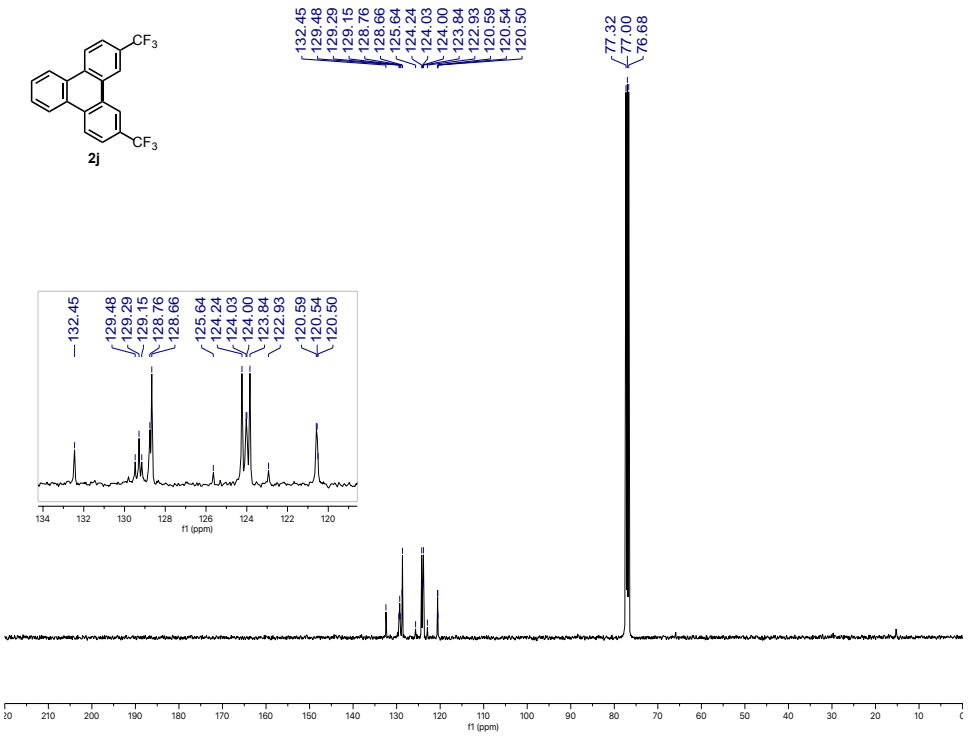
CF3
CF3
2j
132.45
129.48
129.29
129.15
128.76
128.66
125.64
124.24
124.03
124.00
123.84
122.93
120.59
120.54
120.50
77.32
77.00
76.68
f1 (ppm)

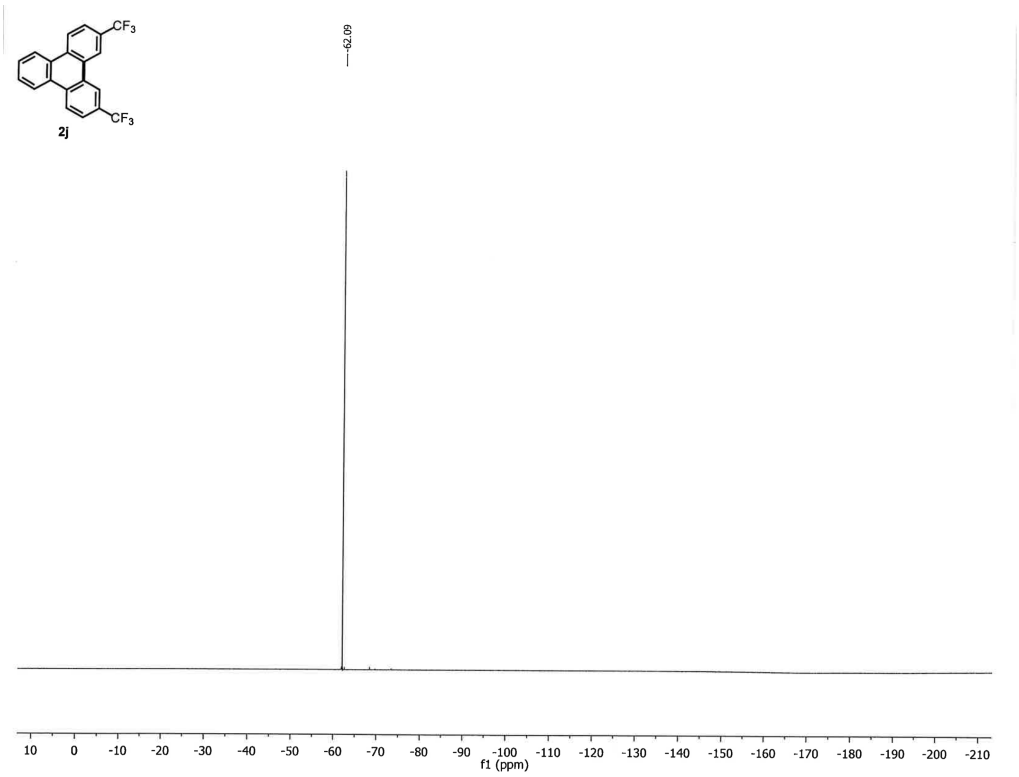
CF3
CF3
2j
-62.09
10
0
-10
-20
-30
-40
-50
-60
-70
-80
-90
-100
-110
-120
-130
-140
-150
-160
-170
-180
-190
-200
-210
f1 (ppm)

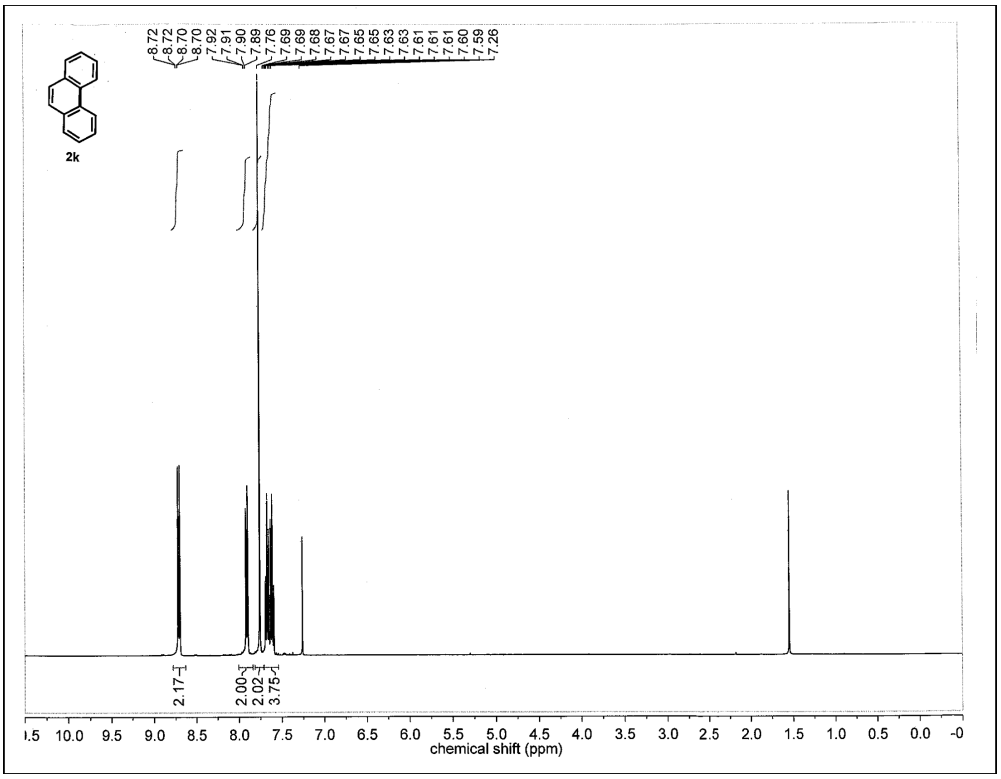
8.72
8.72
8.70
8.70
7.92
7.91
7.90
7.89
7.76
7.69
7.68
7.68
7.67
7.67
7.65
7.65
7.63
7.63
7.61
7.61
7.61
7.60
7.59
7.26
2k
2.17
2.00
2.02
3.75
chemical shift (ppm)

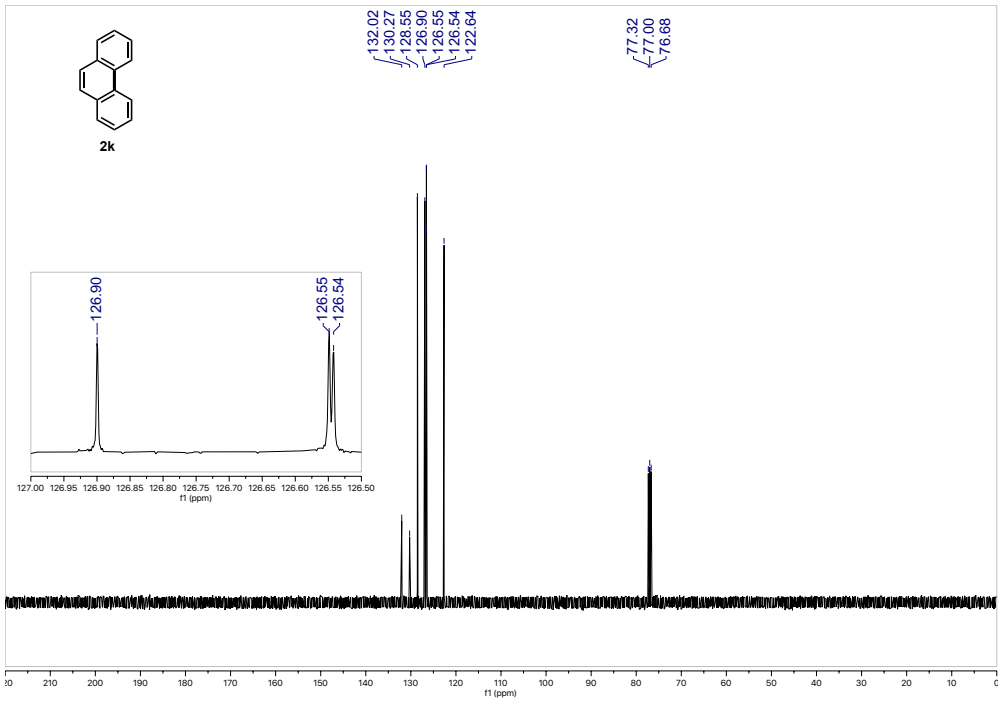
2k
132.02
130.27
128.55
126.90
126.55
126.54
122.64
77.32
77.00
76.68
126.90
126.55
126.54
127.00 126.95 126.90 126.85 126.80 126.75 126.70 126.65 126.60 126.55 126.50
f1 (ppm)
210 200 190 180 170 160 150 140 130 120 110 100 90 80 70 60 50 40 30 20 10
f1 (ppm)

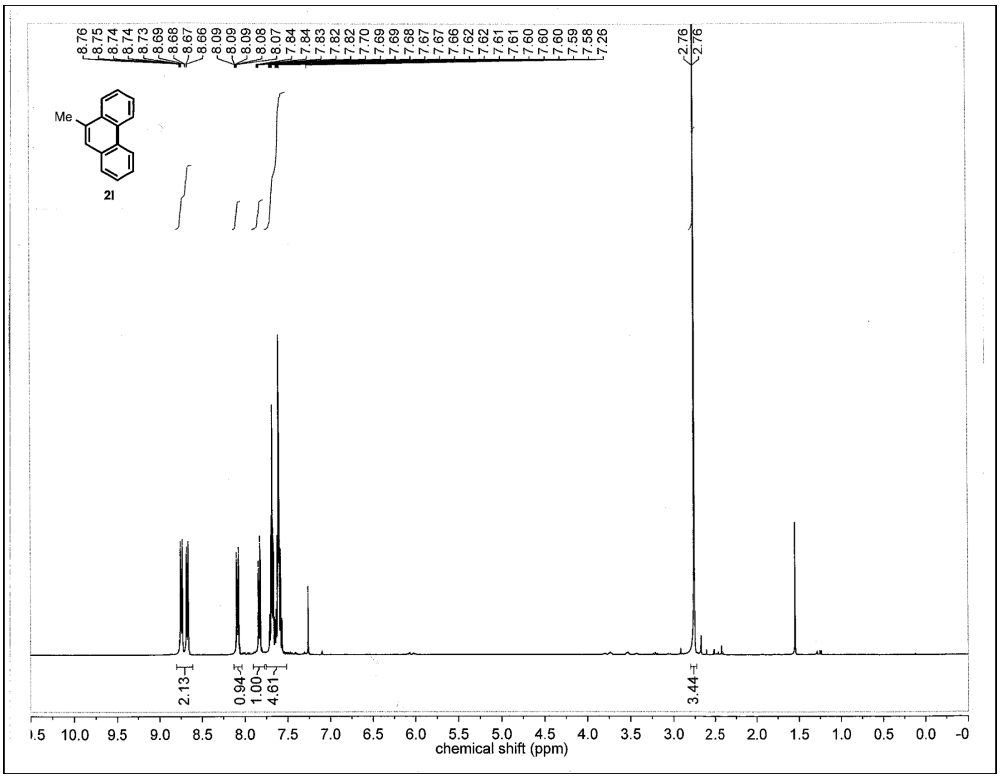
8.76
8.75
8.74
8.74
8.73
8.69
8.68
8.67
8.66
8.09
8.09
8.09
8.08
8.07
7.84
7.84
7.83
7.82
7.82
7.70
7.69
7.69
7.68
7.67
7.67
7.66
7.62
7.62
7.61
7.61
7.60
7.60
7.60
7.59
7.58
7.26
2.76
2.76
Me
2l
2.13
0.94
1.00
4.61
3.44
chemical shift (ppm)

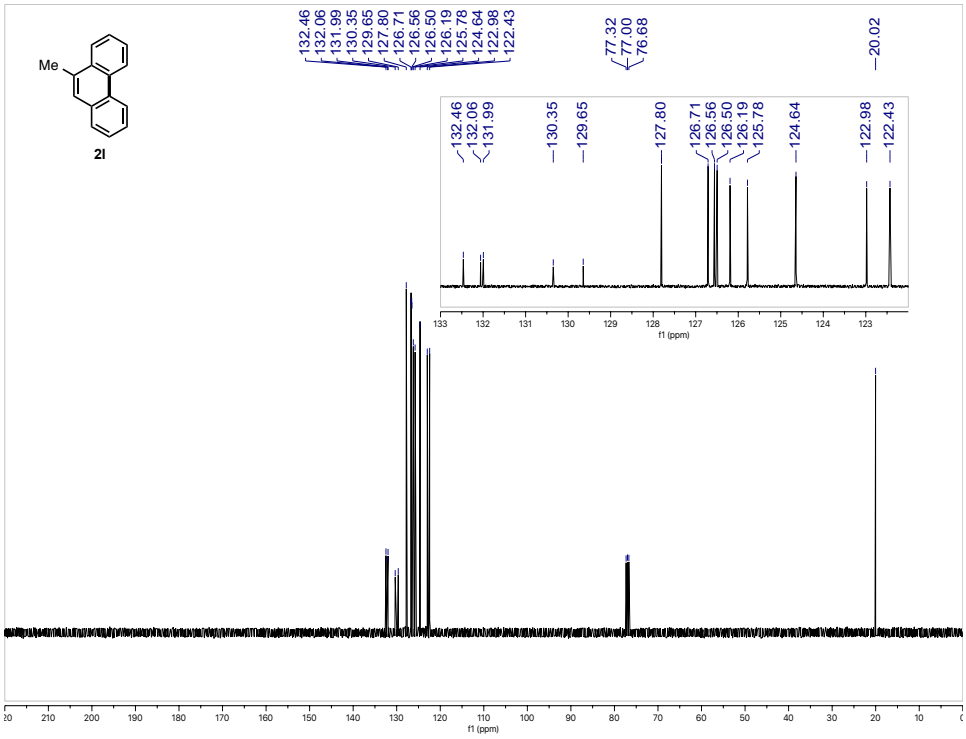
Me
2l
132.46
132.06
131.99
130.35
129.65
127.80
126.71
126.56
126.50
126.19
125.78
124.64
122.98
122.43
77.32
77.00
76.68
20.02
f1 (ppm)

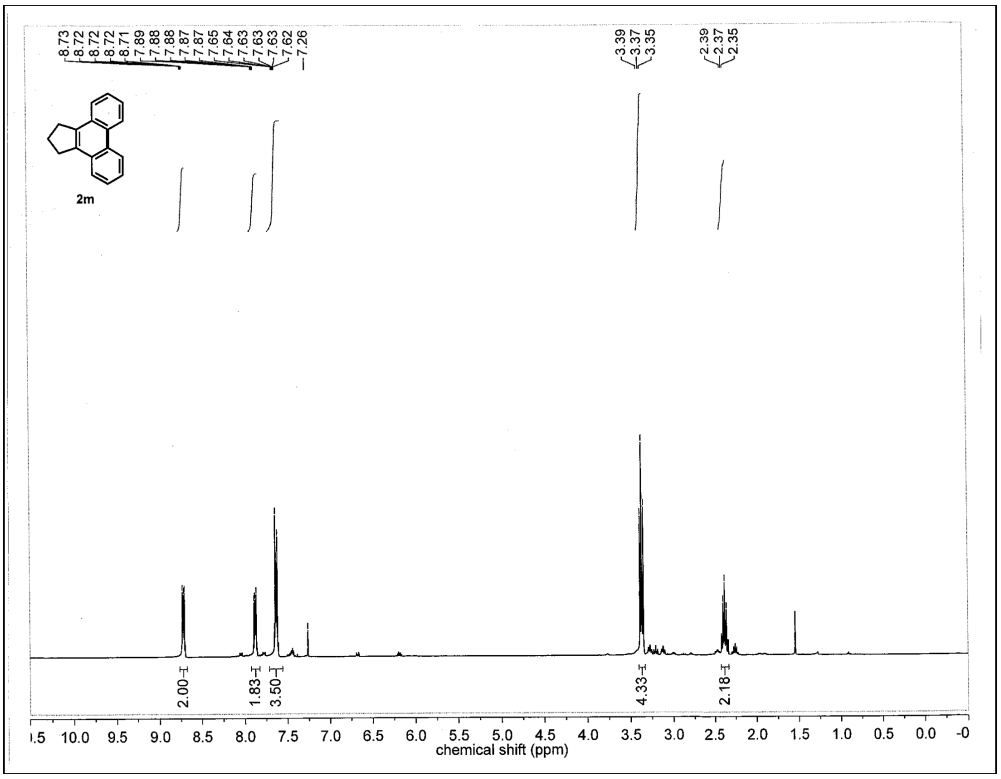
8.73
8.72
8.72
8.72
8.71
7.89
7.88
7.88
7.87
7.87
7.65
7.64
7.63
7.63
7.63
7.62
7.26
3.39
3.37
3.35
2.39
2.37
2.35
2m
2.00
1.83
3.50
4.33
2.18
chemical shift (ppm)

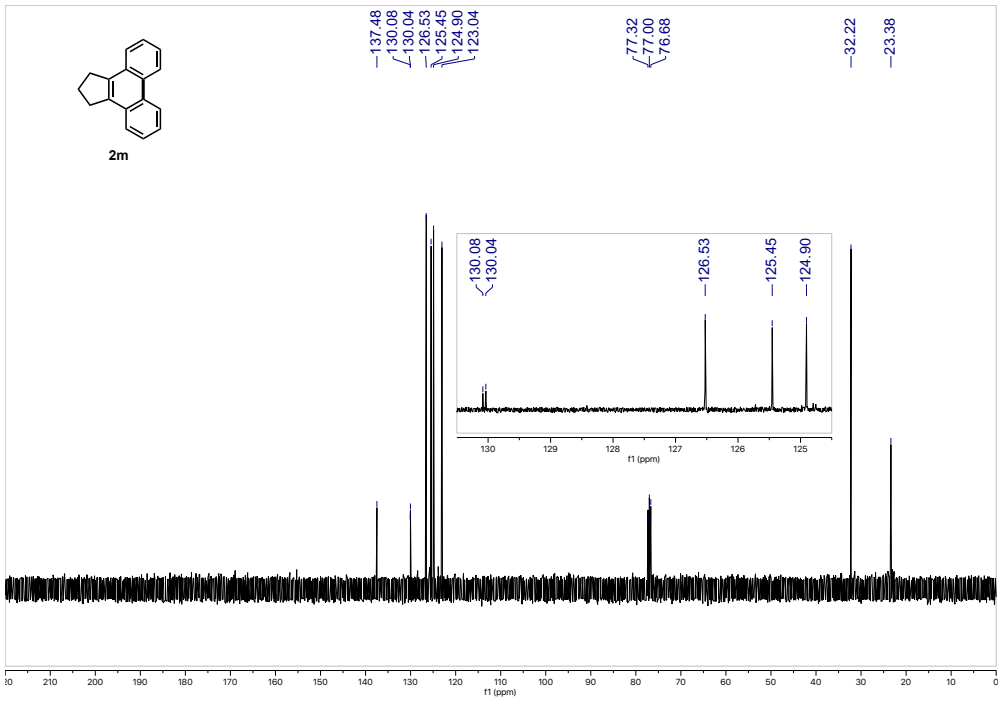
137.48
130.08
130.04
126.53
125.45
124.90
123.04
77.32
77.00
76.68
32.22
23.38
2m
130.08
130.04
126.53
125.45
124.90
f1 (ppm)
f1 (ppm)

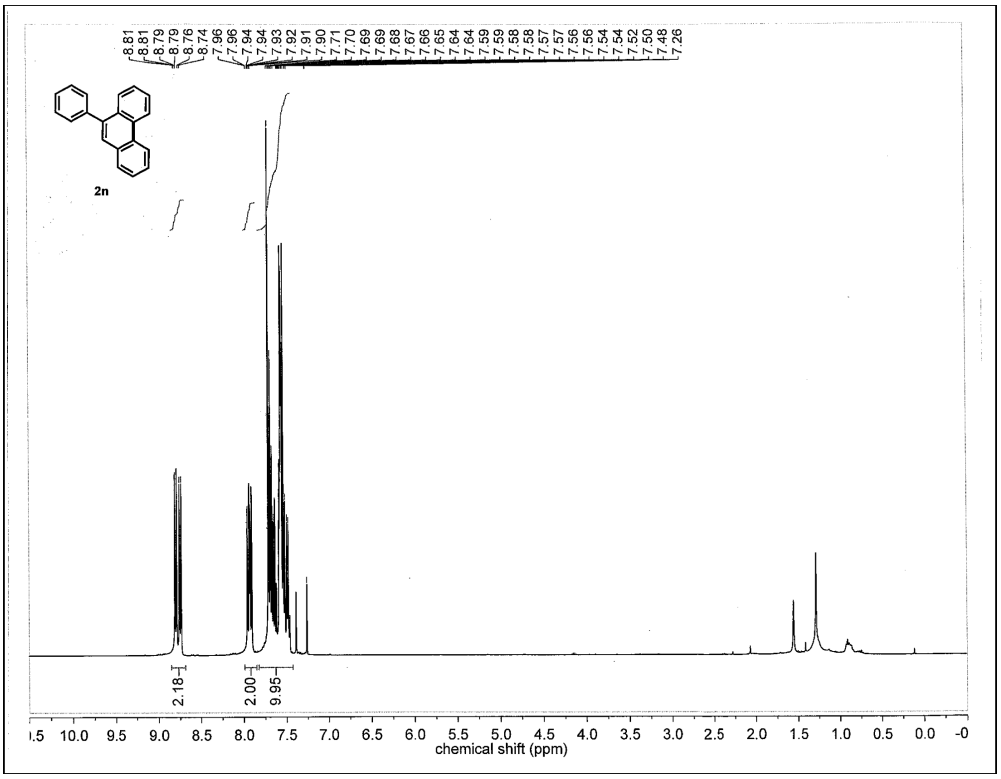
8.81
8.81
8.79
8.79
8.76
8.74
7.96
7.96
7.94
7.94
7.93
7.92
7.91
7.90
7.71
7.70
7.69
7.69
7.68
7.67
7.66
7.65
7.64
7.64
7.59
7.59
7.58
7.58
7.57
7.57
7.56
7.56
7.54
7.54
7.52
7.50
7.48
7.26
2n
2.18
2.00
9.95
chemical shift (ppm)

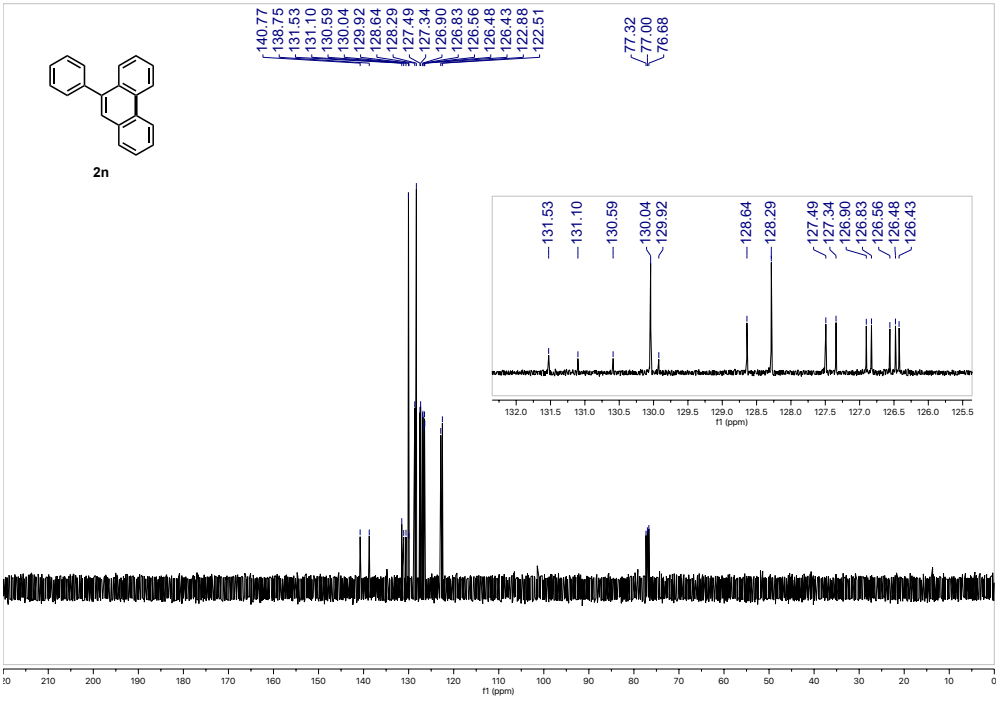
140.77
138.75
131.53
131.10
130.59
130.04
129.92
128.64
128.29
127.49
127.34
126.90
126.83
126.56
126.48
126.43
122.88
122.51
77.32
77.00
76.68
2n
131.53
131.10
130.59
130.04
129.92
128.64
128.29
127.49
127.34
126.90
126.83
126.56
126.48
126.43
f1 (ppm)
f1 (ppm)

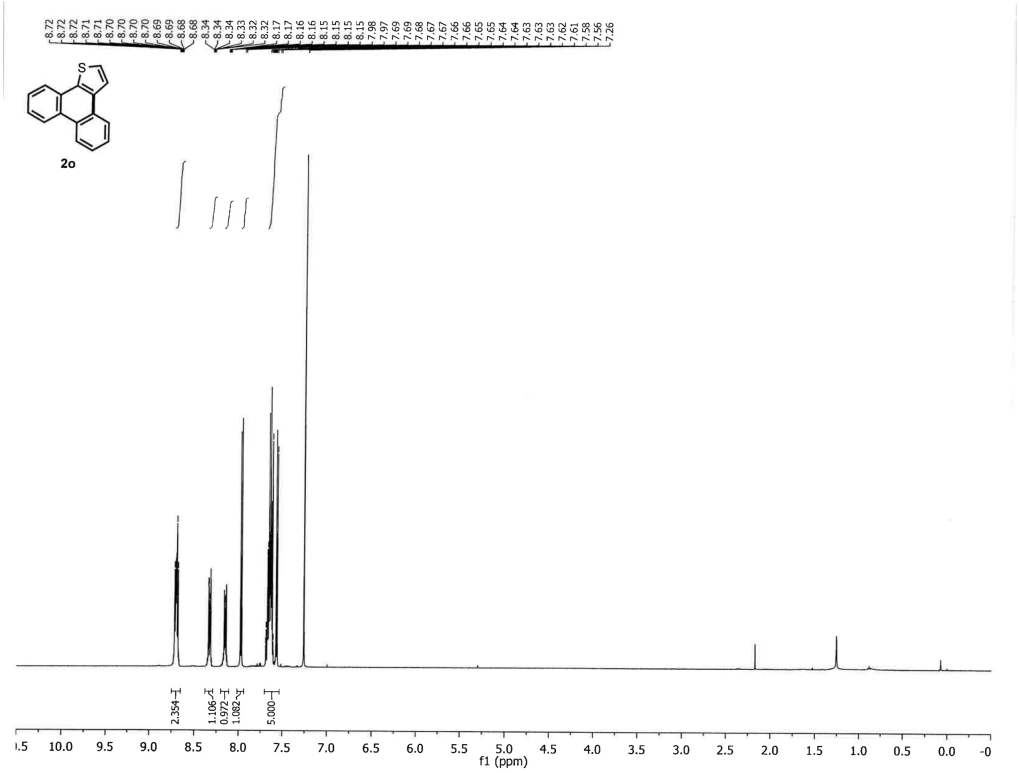
8.72
8.72
8.72
8.71
8.71
8.70
8.70
8.70
8.70
8.69
8.69
8.68
8.68
8.34
8.34
8.34
8.33
8.32
8.32
8.17
8.17
8.16
8.16
8.15
8.15
8.15
8.15
7.98
7.97
7.69
7.69
7.68
7.67
7.67
7.66
7.66
7.65
7.65
7.64
7.64
7.63
7.63
7.63
7.62
7.61
7.58
7.56
7.26
S
2o
2.354
1.106
0.972
1.082
5.000
10.0
9.5
9.0
8.5
8.0
7.5
7.0
6.5
6.0
5.5
5.0
4.5
4.0
3.5
3.0
2.5
2.0
1.5
1.0
0.5
0.0
f1 (ppm)

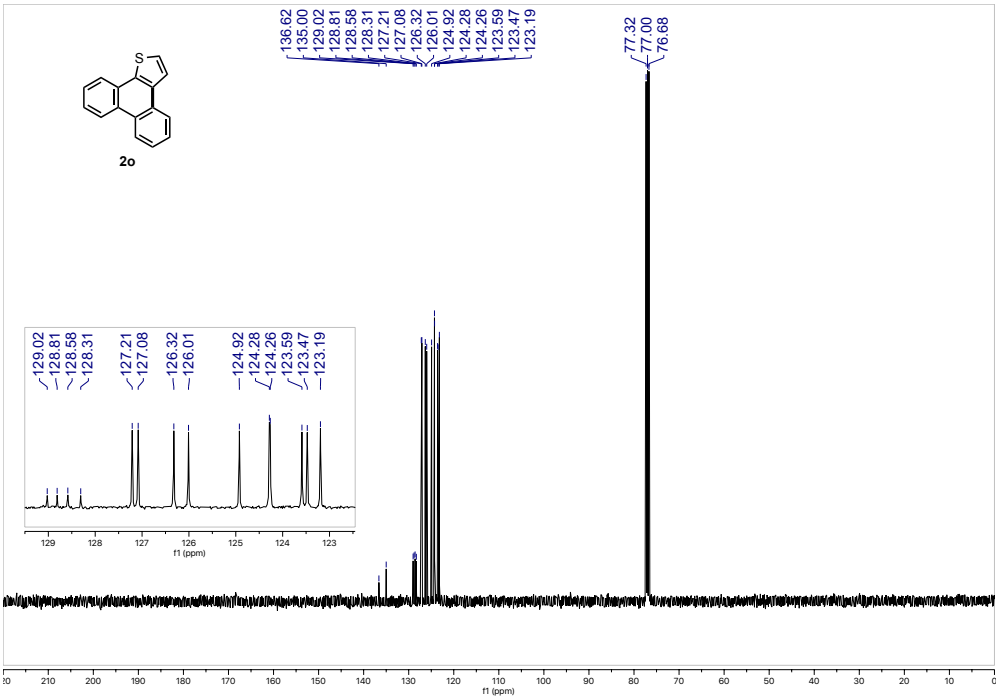
136.62
135.00
129.02
128.81
128.58
128.31
127.21
127.08
126.32
126.01
124.92
124.28
124.26
123.59
123.47
123.19
77.32
77.00
76.68
S
2o
129.02
128.81
128.58
128.31
127.21
127.08
126.32
126.01
124.92
124.28
124.26
123.59
123.47
123.19
129
128
127
126
125
124
123
f1 (ppm)
210
200
190
180
170
160
150
140
130
120
110
100
90
80
70
60
50
40
30
20
10
f1 (ppm)

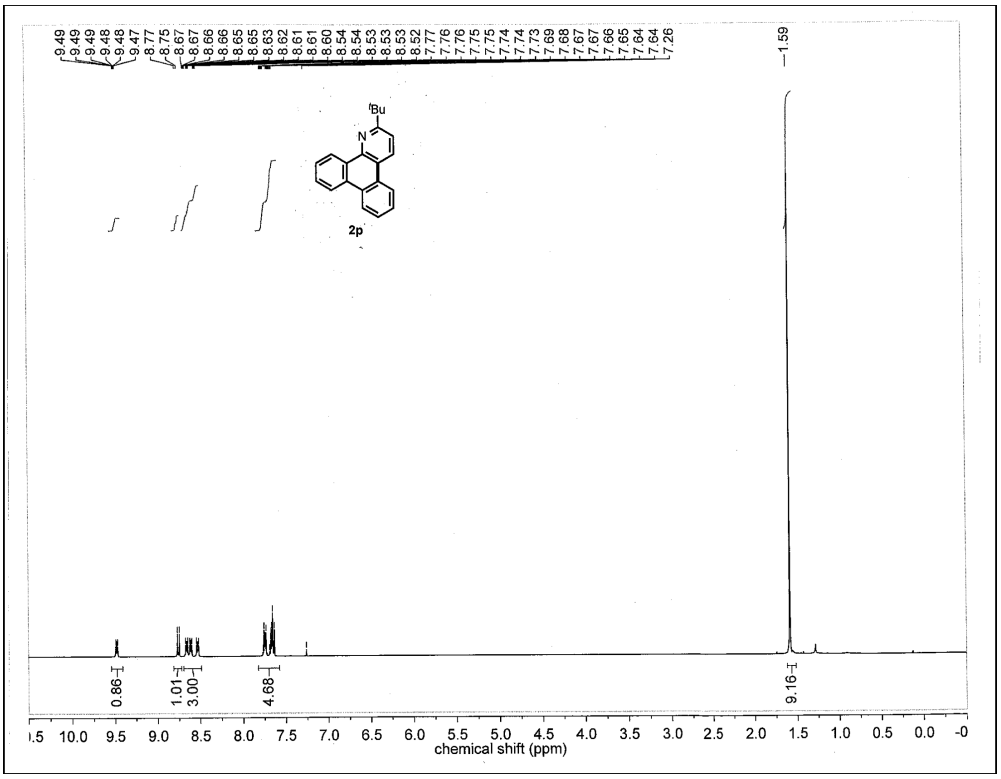
9.49
9.49
9.49
9.48
9.48
9.47
8.77
8.75
8.67
8.66
8.66
8.65
8.65
8.63
8.62
8.61
8.61
8.60
8.54
8.53
8.53
8.52
7.77
7.76
7.76
7.75
7.75
7.74
7.74
7.73
7.69
7.68
7.67
7.67
7.66
7.65
7.64
7.64
7.26
1.59
tBu
N
2p
0.86
1.01
3.00
4.68
9.16
chemical shift (ppm)

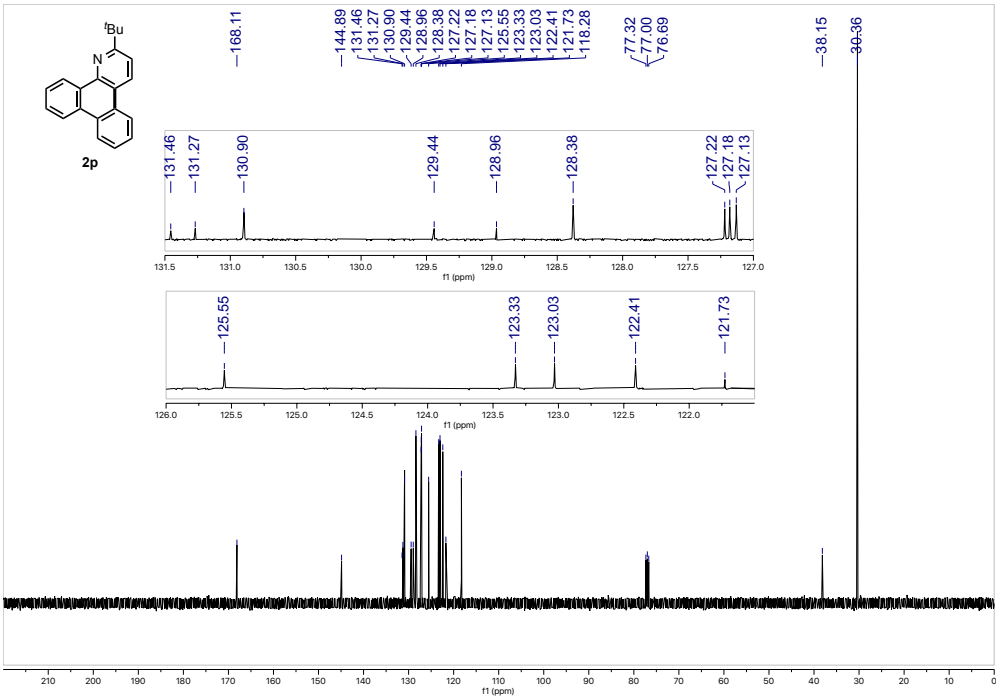
tBu
N
2p
168.11
144.89
131.46
131.27
130.90
129.44
128.96
128.38
127.22
127.18
127.13
125.55
123.33
123.03
122.41
121.73
118.28
77.32
77.00
76.69
38.15
30.36
f1 (ppm)

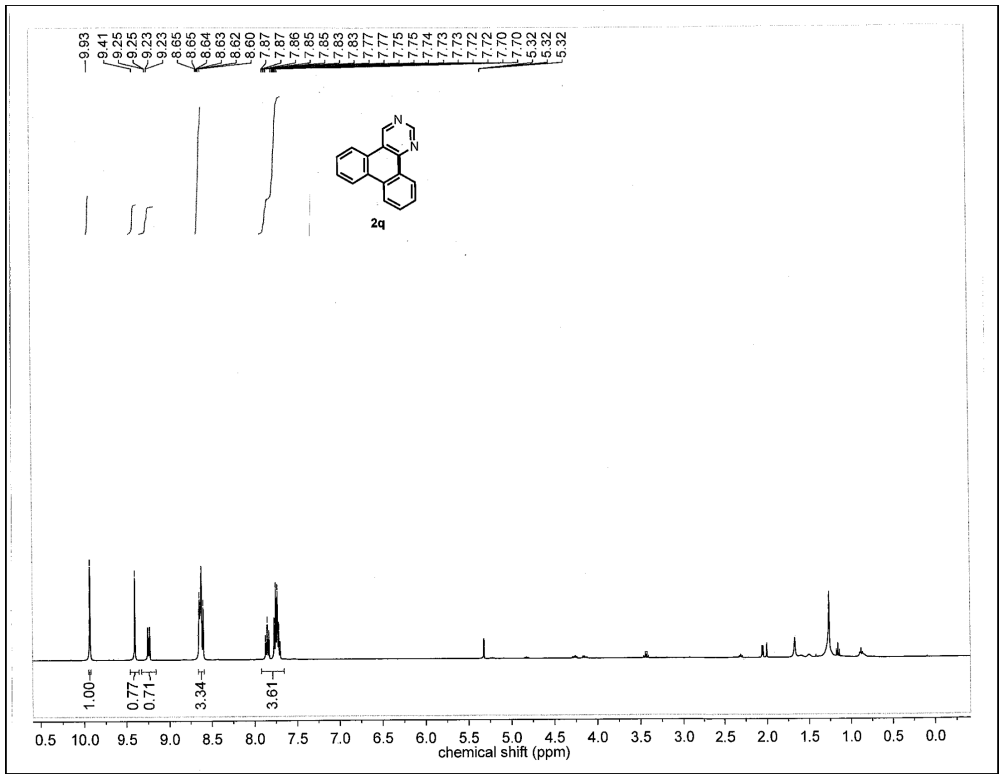
9.93
9.41
9.25
9.25
9.23
9.23
8.65
8.64
8.63
8.62
8.60
7.87
7.87
7.86
7.85
7.85
7.83
7.83
7.77
7.77
7.75
7.75
7.74
7.73
7.73
7.72
7.72
7.70
7.70
5.32
5.32
N
N
2q
1.00
0.77
0.71
3.34
3.61
0.5 10.0 9.5 9.0 8.5 8.0 7.5 7.0 6.5 6.0 5.5 5.0 4.5 4.0 3.5 3.0 2.5 2.0 1.5 1.0 0.5 0.0
chemical shift (ppm)

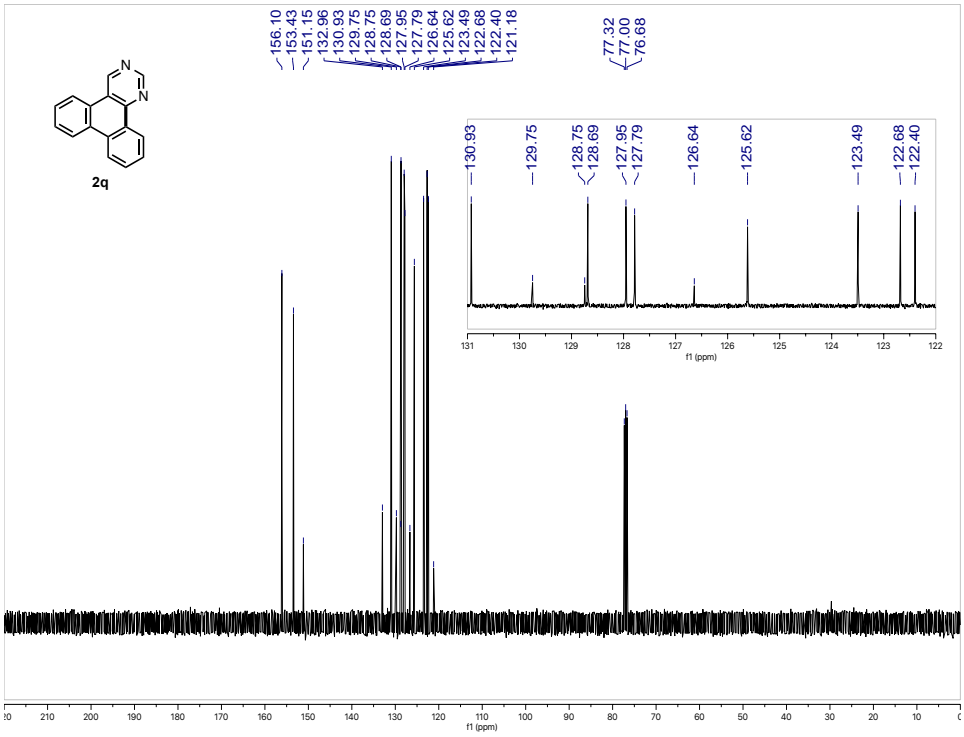
156.10
153.43
151.15
132.96
130.93
129.75
128.75
128.69
127.95
127.79
126.64
125.62
123.49
122.68
122.40
121.18
77.32
77.00
76.68
N
N
2q
130.93
129.75
128.75
128.69
127.95
127.79
126.64
125.62
123.49
122.68
122.40
f1 (ppm)
f1 (ppm)

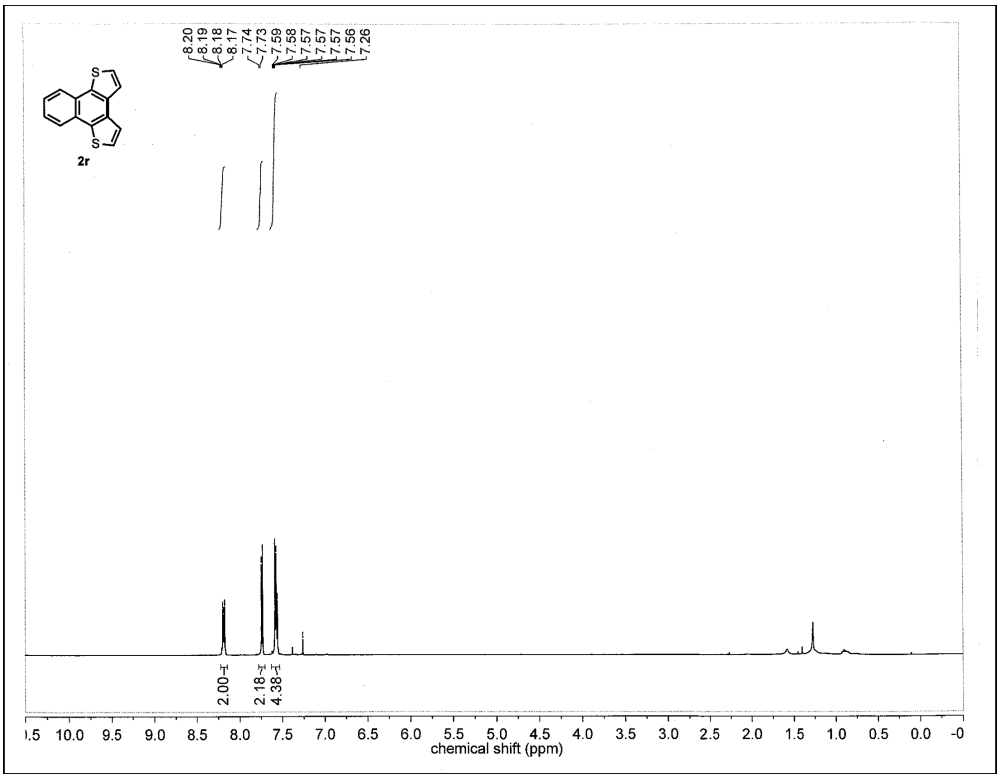
8.20
8.19
8.18
8.17
7.74
7.73
7.59
7.58
7.57
7.57
7.57
7.56
7.26
S
S
2r
2.00
2.18
4.38
chemical shift (ppm)

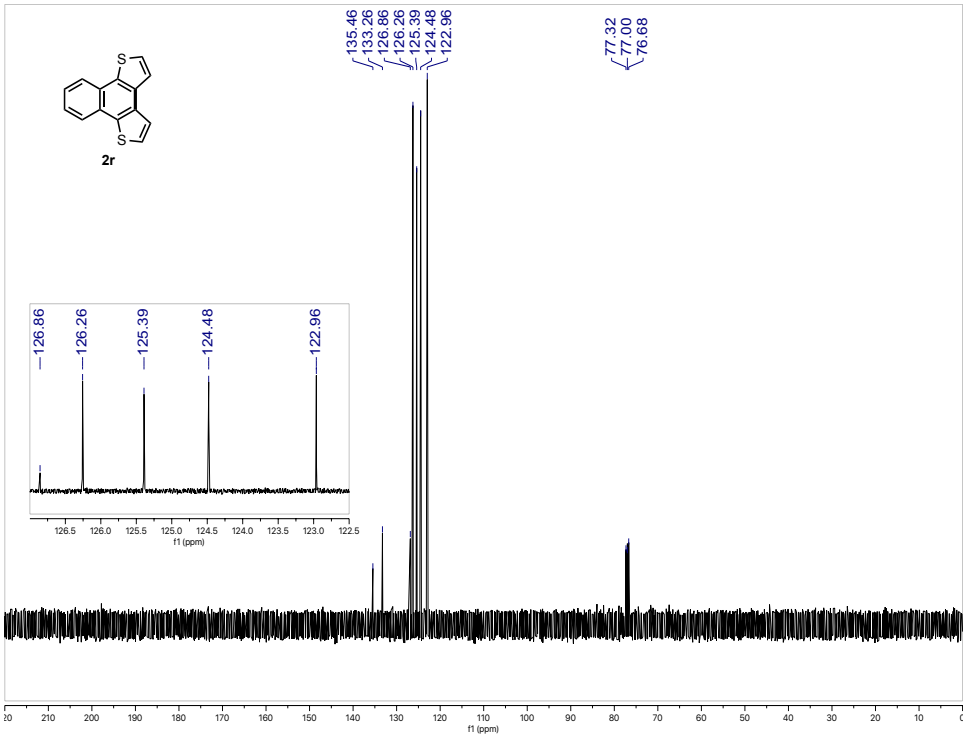
135.46
133.26
126.86
126.26
125.39
124.48
122.96
77.32
77.00
76.68
S
S
2r
126.86
126.26
125.39
124.48
122.96
126.5 126.0 125.5 125.0 124.5 124.0 123.5 123.0 122.5
f1 (ppm)
210 200 190 180 170 160 150 140 130 120 110 100 90 80 70 60 50 40 30 20 10
f1 (ppm)

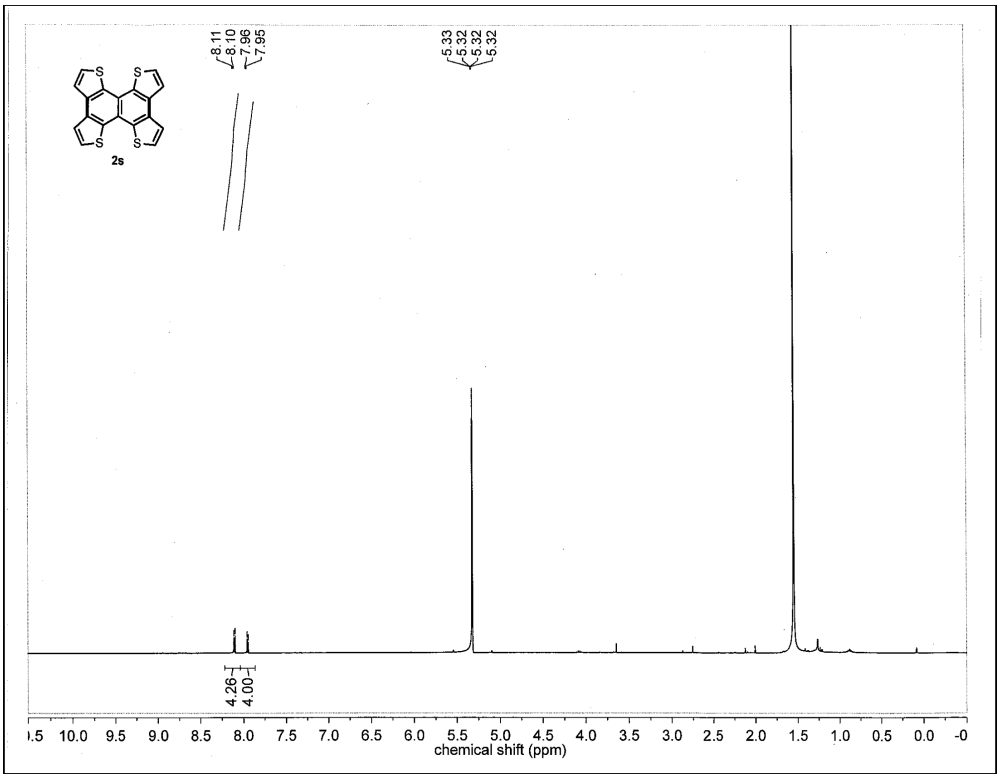
8.11
8.10
7.96
7.95
5.33
5.32
5.32
5.32
2s
4.26
4.00
chemical shift (ppm)

3. Azonia heterocycle synthesis though acceptorless dehydrogenative cyclization of *N*-protonated pyridinium ions

3.1 Introduction

Pyridinium nitrogen centers are isoelectronic to sp^2-hybridized carbons of benzenes. Azonia aromatic heterocycles (AZAHs) are any fully aromatic heterocycles that contain at least one quaternary nitrogen in a bridgehead position. AZAH derivatives have a wide range of potential applications such as bioactive compounds, fluorescent dyes, DNA intercalators, ionic liquids, optical and magnetic materials, and electrode for oxygen reduction reaction (ORR).[1]

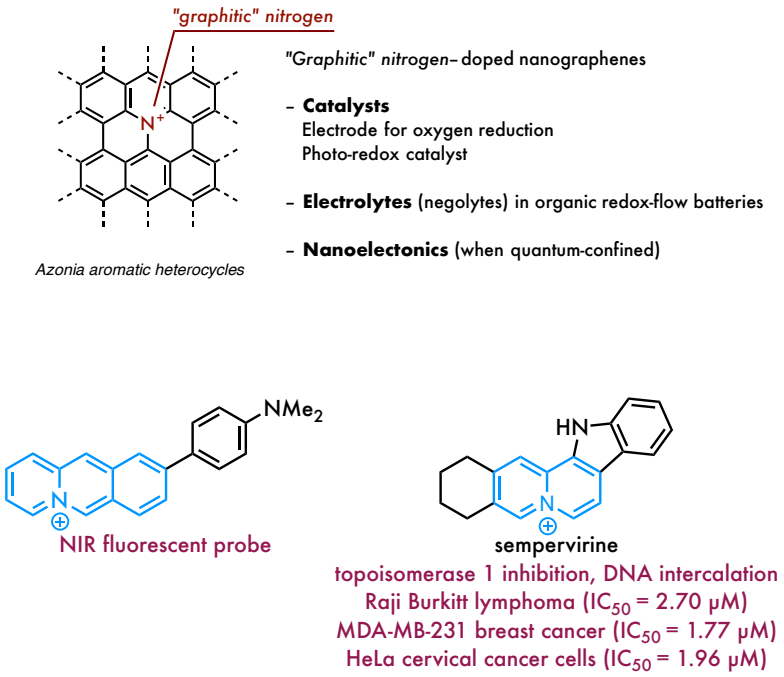

Fig. 3.1. Azonia aromatic heterocycles (AZAHs)

The conventional synthetic methods of AZAHs are categorized depending on the reaction types employed to build up the heterocycle,[2] and they include (1) ring-closing metathesis (RCM) reactions,[3] (2) annulation reactions based on C−H activation,[4,5] and (3) photochemical approaches to AZAH systems,[6] and (4) other miscellaneous methods.[7] However, these methods typically require at least one of the following conditions: long synthetic sequence, expensive catalysts, stoichiometric amount of oxidants, and low-yielding steps, which make synthesis challenging and hamper the derivatization of AZAHs. Despite the extensive synthetic endeavor of azonia nanocarbons, synthesis of the key component of azonia aromatic nanocarbons, pyrido[1,2-*f*]phenanthridin-5-ium core (see Scheme 3.1), has not been accomplished yet. Synthetic reports of diazonia moieties and highly fused polycyclic systems are limited as well.[5b,g] Thus, we envisioned the development of new synthetic methodology to access pyrido[1,2-*f*]phenanthridin-5-ium salts and related new azonia nanographenes, as well as understanding of their physicochemical properties.

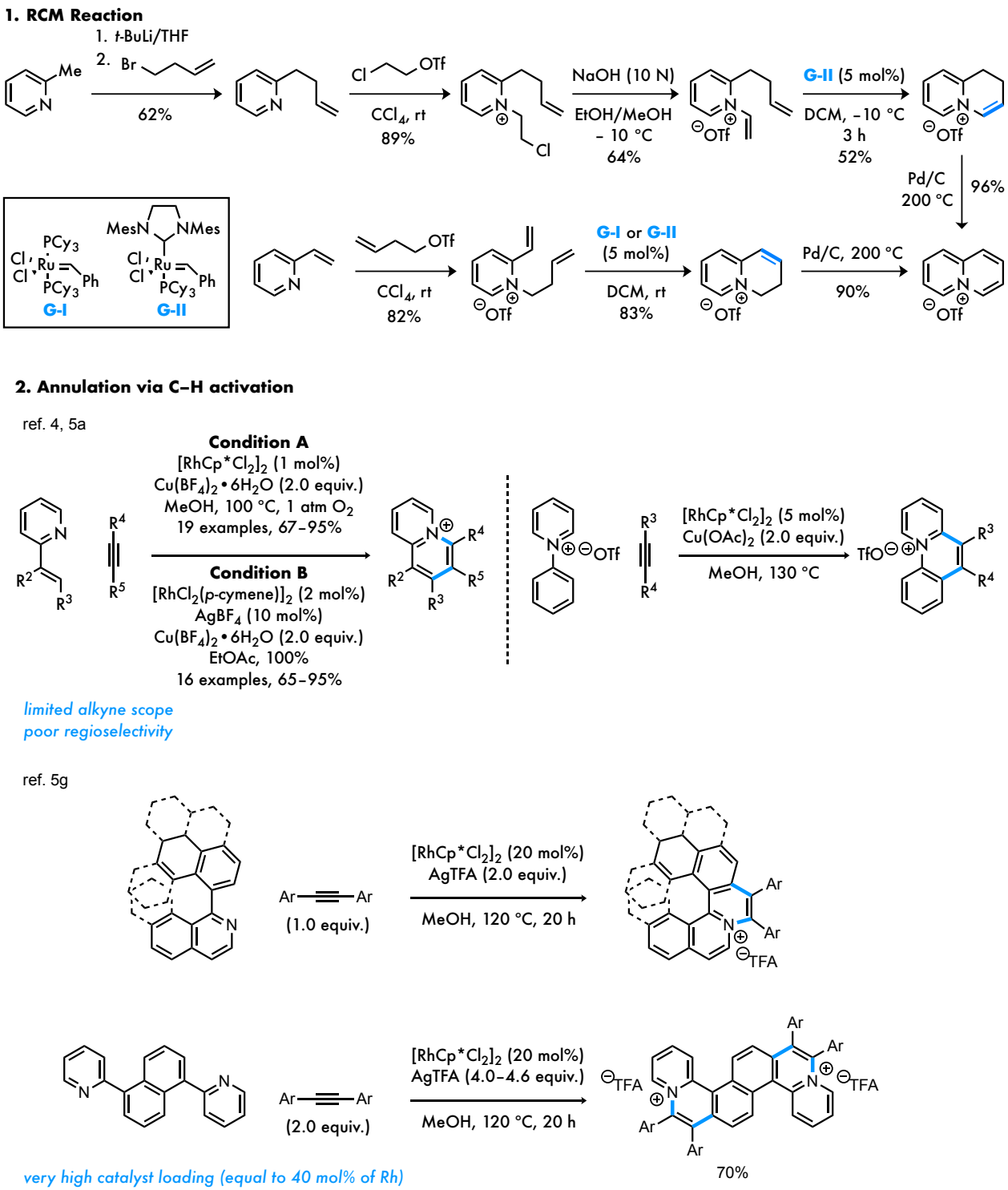

Scheme 3.1 Synthetic approaches to azonia aromatic heterocycles (AZAHs) (continued)

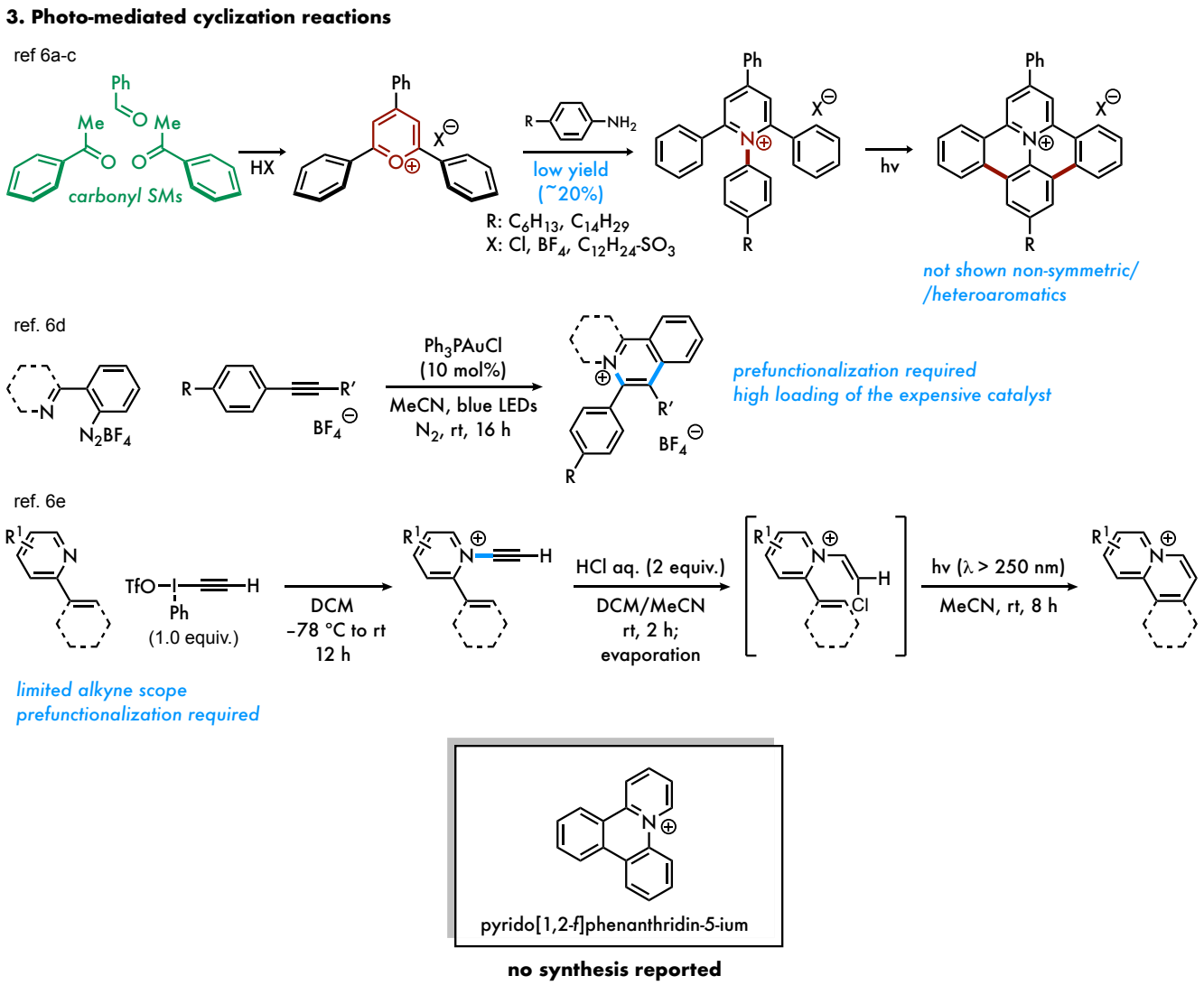

Scheme 3.1 Synthetic approaches to azonia aromatic heterocycles (AZAHs)

In comparison to above-mentioned synthetic approaches, the direct construction of C(sp^2)–N$^+$(sp^2) bond of simple arylpyridines is of high synthetic importance due to the facile access to new types of tetracyclic or further multicyclic AZAH derivatives, which potentially facilitates the AZAH research in optoelectronics and other materials. In this work, based on our previous discoveries on catalytic

dehydrogenative electrocyclization, we aimed at the "isoelectronic" catalytic dehydrogenative electrocyclization: the cobaloxime-catalyzed hydrogen-evolution intramolecular C–N(+) coupling of *N*-protonated pyridinium salt (Scheme 3.2).

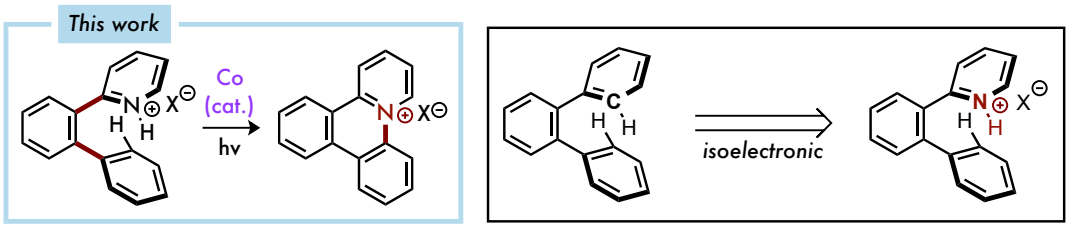

Scheme 3.2 This work

3.2 Results & discussion

3.2.1 Optimization process

In the previous work, we have observed 2-([1,1'-biphenyl]-2-yl)pyridine derivatives afforded the C–C bond formation product under the cobaloxime catalysis. In contrast, our initial study on cobaloxime-catalyzed dehydrogenative cyclization with its protonated analog **1a** gave the C–N bond formation product, not the C–C bond formation product. This result clearly shows that the *C*/*N*-bond formation selectivity was switched by protonation of the pyridine substrate. We hypothesize that protonation of the nitrogen center would lower the LUMO energy of C–N double bond, which

facilitates *N*-selective photochemical 6π electrocyclization. The product structure was unambiguously determined by ^{1}H, ^{13}C-NMR, IR, and HRMS analysis.

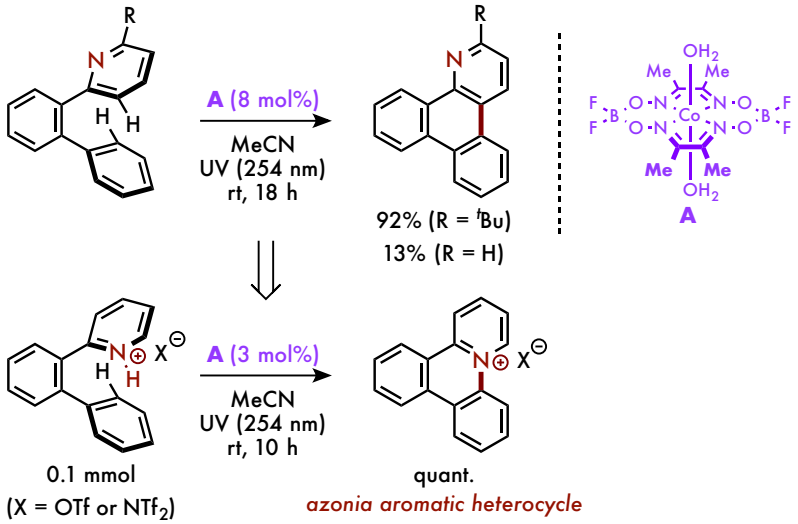

Scheme 3.3. Initial studies

Since the desired AZAH product was obtained in quantitative yield when we applied the optimal condition for the dehydrogenative cyclization of *o*-terphenyl, we examined if we could decrease the catalyst loading. Gratifyingly, the catalyst loading could be decreased to 3 mol% in 0.1 mmol scale (1.2 mg of cobaloxime was used) (Table 3.1, entry 1), and furthermore to 0.5 mol% in 0.5 mmol scale (1.0 mg of cobaloxime was used) without affecting the yield (entry 2). Control experiments were carried out under the catalytic system; first, in the absence of either the cobalt catalyst or light, no desired product was obtained (entries 3 and 4). The wavelength of light was also important, as a longer wavelength

(300 nm) or using the photoredox/cobaloxime dual catalytic system under blue LEDs[10] gave no desired product (entries 5 and 6). The counter anions of the pyridinium substrate have critical effects; Although $^{-}$OTf substrate was slightly less soluble to MeCN than **1a**, it was fully converted to the product, albeit $^{-}$Cl substrate had much lower solubility in MeCN and gave only 18% of the product under the entry 1's condition (entries 7,8). Finally, the solvent effect was studied (entries 9-11). Among all solvent screened, MeCN proved to be the most effective. While less polar solvents, such as MeOH and CH_2Cl_2, gave almost no reactivity, toluene can nevertheless deliver 16% yield of **2a**.

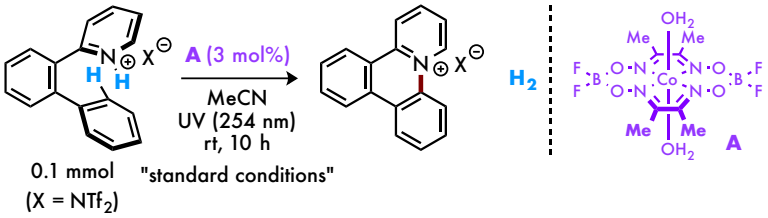

entry	variation(s) from the "standard conditions"	yield(%)[a]
1	none	quant.
2	**A** (0.5 mol%), 0.5 mmol scale	quant.
3	no **A**	< 5
4	no UV	< 5
5	UV (300 nm) instead	< 5
6	Acr-$Mes^+ClO_4^-$ or $Ru(bpy)_3Cl_2$ (3 mol%) **A** (3 mol%), and blue LEDs instead of UV (254 nm)	< 5
7	X = OTf	quant.
8	X = Cl	18
9	PhMe instead of MeCN	16
10	MeOH instead of MeCN	< 5
11	CH_2Cl_2 instead of MeCN	< 5

[a]yields were determined by ^{1}H-NMR using 1,1,2,2-tetrachloroethane as an internal standard.

Table 3.1 Optimization of reaction conditions

3.2.2 Substrate scope

The emergence of new dehydrogenative catalysis in C–N(+) bond formation made me conceive the new synthetic strategy to azonia nanographenes; enabled by transition-metal-catalyzed directed C–H bond activation reactions ("*CONNECT*") and the C–N(+) bond forming C–H functionalization reactions ("*ZIP*"), sequential "C–H zipping" of two commercially- or readily available starting materials will be facile and modular synthetic approach to new azonia nanographenes (Scheme 3.4).

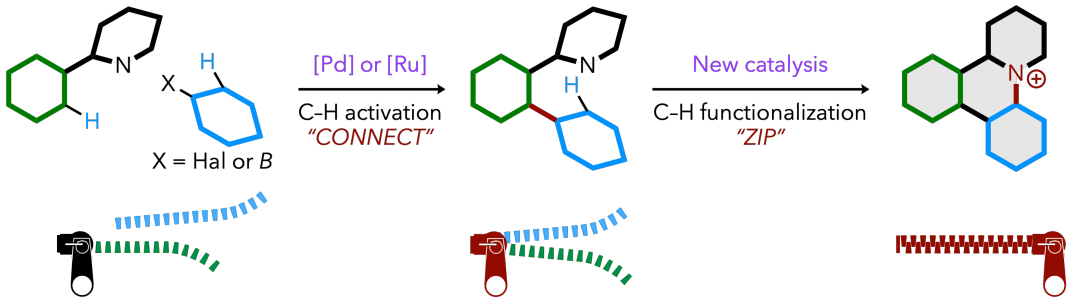

Scheme 3.4 C–H zipping strategy

With the optimal condition and new synthetic approach, I proved the concept and synthesized a series of azonia nanographenes (Scheme 3.5). I employed ruthenium-catalyzed C–H bond arylation of 2-arylpyridines that formed compound **1a'-1c'** and yield was over 90% each case. Treated with $HNTf_2$, resulting pyridinium salts were subjected to the "*ZIP*" reactions which afforded the desired azonia

nanographenes. It is noteworthy that both pentacyclic **2b** and sterically congested **2c** were formed in excellent yield under the new catalysis.

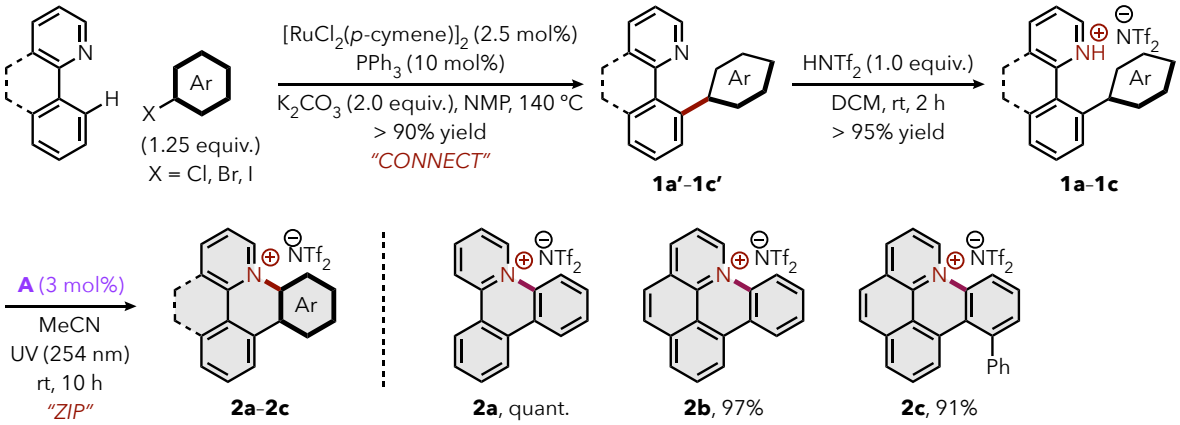

Scheme 3.5 Substrate scope under C–H zipping

I further expanded the scope to double functionalizations, in which the benzo[*h*]quinoline and 4-bromo-4'-iodobiphenyl were coupled smoothly under ruthenium-catalyzed C–H activation reaction ("*CONNECT*") condition. Followed by cobaloxime catalysis, C–H zipping afforded decacyclic diazonia nanographene as a yellow solid (Scheme 3.6).

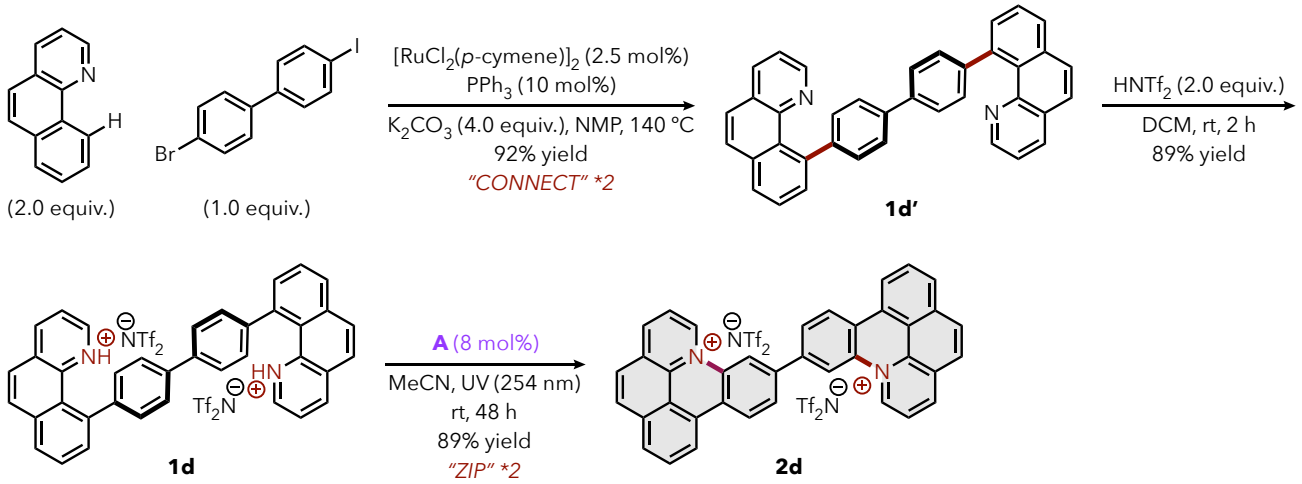

Scheme 3.6 Diazonia synthesis under C–H zipping

With the success on azonia and diazonia nanographene synthesis, I further expanded the substrate scope to more highly fused and complex azonia molecules (Scheme 3.7). Pentacyclic compound **1e'** was prepared from the reported procedure, and subsequent protonation and "*ZIP*" reaction was performed. Gratifyingly, the hexacyclic product **2e**, an isoelectronic chemical entity to benzo[*ghi*]perylene, was obtained in 89% yield as a yellow solid. It has bright yellow color when diluted in acetone.

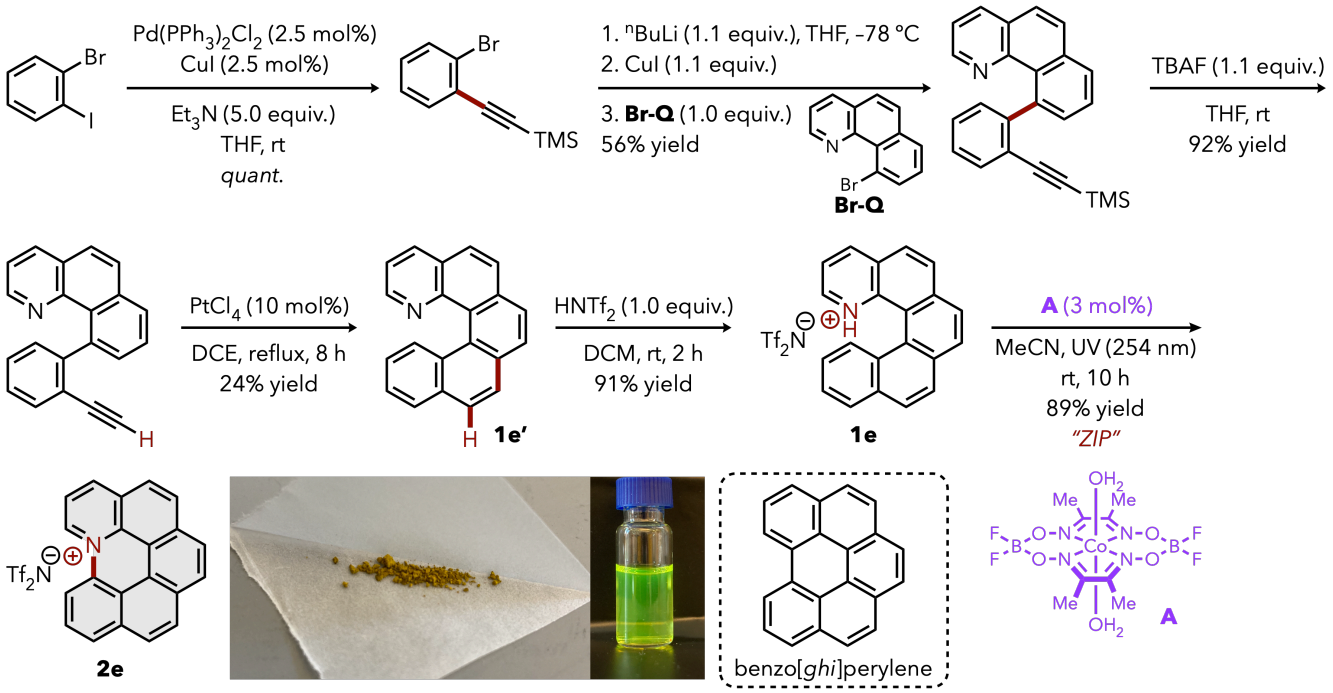

Scheme 3.7 Synthesis of the hexacyclic azonia nanographene

Nevertheless, there are some challenging substrates at this moment (Scheme 3.8). The pyridinium salt with a phenanthrene unit was found to be an unreactive substrate under the cobaloxime catalysis; we reasoned the poor reactivity for the molecular torsions caused by C–H crashes at the cove regions which would make 6π electrocyclization and/or dehydrogenation both kinetically and thermodynamically unfavorable. Another challenging substrate was the pyrazine-type dicationic starting material which was prepared from 9,10-phenanthrene dione and ethylene diamine. The dicationic starting material was subjected to the cobaloxime catalysis, which only gave complex

mixture instead of the desired product. I attribute it to the instability of dicationic aromatic center (e.g. hydrolysis), and installation of aryl or alkyl groups on the dicationic aromatic center could stabilize the intermediate/product and improve the result.

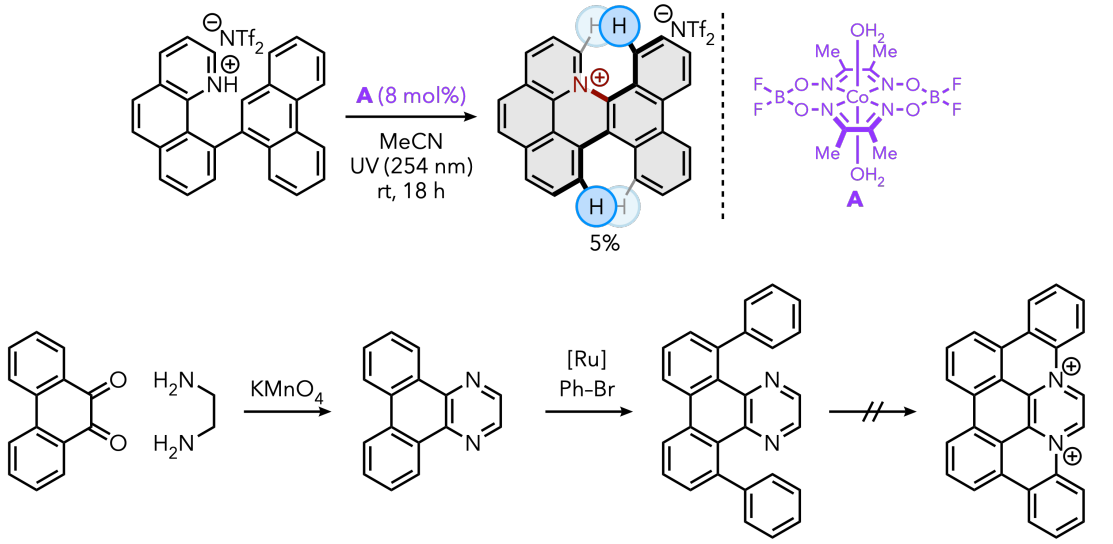

Scheme 3.8 Challenging examples

3.3 Conclusion

In conclusion, dehydrogenative cyclization of *o*-(2-biphenyl)pydirinium salt has been discovered under photochemical cobaloxime catalysis, which enabled the rapid access to new AZAH motifs. The reaction is oxidant-free and operates at near room temperature. Current substrate scope shows that the protocol can afford multicyclic azonia nanographenes. Currently, further substrate scope,

physicochemical studies on the products, and mechanistic studies are ongoing.

3.4 Experimental Sections

General information

All UV-mediated reactions were carried out in 20 mL Quartz test tubes under nitrogen atmosphere. Acetonitrile was purchased from Acros Organics. $Co(dmg(BF_2)_2)(OH_2)_2$ was prepared following the reported procedure[8]. 25W UVC lamps (λ = 254 nm, L x W x H = 8.5 x 2 x 2 inches) were purchased from coospider (https://www.amazon.com/gp/product/B07KYVRVX7/ref=ppx_yo_dt_b_asin_title_o03_s00?ie=UTF8&psc=1), and used as light source. All commercially available substrates were used without further purification. Thin layer chromatography (TLC) analysis was run on silica gel plates purchased from EMD Chemical (silica gel 60, F254). Infrared spectra were recorded on a Nicolet iS5 FT-IR Spectrometer using neat thin film technique. High-resolution mass spectra (HRMS) were obtained on an Agilent 6224 TOF-MS spectrometer and are reported as m/z. Amounts of H_2 generated in the photo-catalytic experiments were determined by gas chromatography (GC) using an SRI 8610C Gas

Chromatograph with the nitrogen carrier gas and a TCD detector. Methane was used as internal standard for the measurement of the yield of H_2. UV–Vis spectra was measured with NanoDrop™ One^C. UV-Vis spectrometer. Nuclear magnetic resonance spectra (^{1}H NMR and ^{13}C NMR) were recorded with a Bruker Model DMX 400 (400 MHz, ^{1}H at 400 MHz, ^{13}C at 101 MHz). For $CDCl_3$ solutions, the chemical shifts were reported as parts per million (ppm) referenced to residual protium or carbon of the solvents: $CHCl_3$ δ H (7.26 ppm) and $CDCl_3$ δ C (77.00 ppm). For CD_2Cl_2 solutions, the chemical shifts were reported as parts per million (ppm) referenced to residual protium or carbon of the solvents: CH_2Cl_2 δ H (5.32 ppm) and CD_2Cl_2 δ C (53.80 ppm). For $CO(CD_3)_2$ solutions, the chemical shifts were reported as parts per million (ppm) referenced to residual protium or carbon of the solvents: $CO(CH_3)_2$ δ H (2.05 ppm) and $CO(\underline{C}H_3)_2$ δ $\underline{C}$ (29.90 ppm). Coupling constants were reported in Hertz (Hz). Data for ^{1}H NMR spectra were reported as following: chemical shift (δ, ppm), multiplicity (br = broad, s = singlet, d = doublet, t = triplet, q = quartet, dd = doublet of doublets, td = triplet of doublets, ddd = doublet of doublet of doublets, m = multiplet), coupling constant (Hz), and integration.

Synthesis and characterization of substrates

Compounds **1a'**, **1b'**, **1c'**, and **1e'** were synthesized according to the literature procedure.[9]

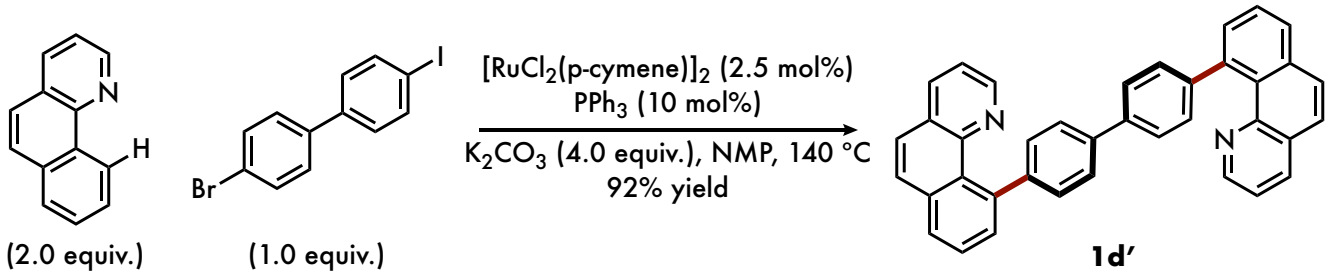

Under nitrogen atmosphere, a mixture of $RuCl_2$(*p*-cymeme)$_2$ (15.3 mg, 0.025 mmol, 2.5 mol%), benzo[h]quinoline (358.4 mg, 2.0 mmol, 2.0 equiv.), 4-bromo-4'-iodo-1,1'-biphenyl (359.0 mg, 1.0 mmol, 1.0 equiv.), PPh_3 (26.2 mg, 0.10 mmol, 10 mol%), and Na_2CO_3 (424.0 mg, 4.0 mmol, 4.0 equiv.) in NMP (4 mL) was stirred at 140 °C for 16 h. After cooled to ambient temperature, Et_2O (30 mL) and H_2O (20 mL) were added. The organic phase was separated and the aqueous layer was extracted with Et_2O (2×20 mL). The combined organic phase was washed with H_2O (20 mL) and brine (20 mL), dried over Na_2SO_4, and then concentrated under reduced pressure. The resultant residue was purified by flash silica gel column chromatography (eluent: hexane/EtOAc=10:1 to 2/1, v/v), affording the target product **1d'** as a pale-green solid (467.9 mg, 92 %).

4,4'-bis(benzo[*h*]quinolin-10-yl)-1,1'-biphenyl (1d'): **^{1}H NMR** (400 MHz, $CDCl_3$) δ 8.57 (dd, *J* = 4.3, 1.8 Hz, 1H), 8.13 (dd, *J* = 8.0, 1.8 Hz, 1H), 7.99 (dd, *J* = 7.9, 1.5 Hz, 1H), 7.90 (dd, *J* = 14.0, 8.3 Hz, 3H), 7.80 – 7.66 (m, 3H), 7.56 (d, *J* = 7.9 Hz, 2H), 7.37 (dd, *J* = 8.0, 4.2 Hz, 1H). **^{13}C NMR** (101 MHz, $CDCl_3$) δ 146.81, 146.74, 145.10, 141.33, 138.40, 135.12, 134.93, 131.46, 129.10, 128.95, 128.19, 127.87, 127.11, 126.98, 125.84, 121.02. **IR** (KBr, cm^{-1}) 3045, 1937, 1566, 1496, 1420, 1324, 1265, 1005, 922, 789. **HRMS** calcd $C_{38}H_{24}N_2$ $[M+H]^+$: 509.2018. Found: 509.2014.

General procedure of pyridine-$HNTf_2$ salt preparation

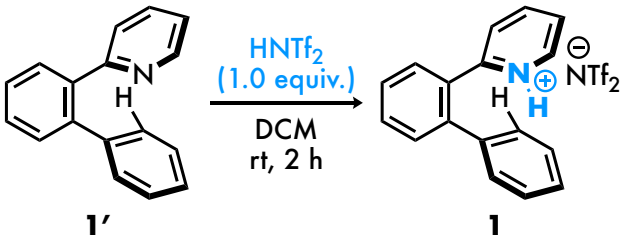

A 20 mL vial was charged with **1'** (1.0 mmol, 1.0 equiv.) and DCM (0.2 mL). The reaction mixture is cooled to 0 ºC, and $HNTf_2$ (281.2 mg, 1.0 equiv.) in DCM (0.2 mL) was added dropwise. The mixture was stirred for 5 min under the same temperature and was warmed to room temperature. The mixture was stirred for 2 hours at room temperature and concentrated in vacuo. The crude product was washed

with hexane/Et_2O (1/1) and supernatant was discarded for three times, then concentrated, which give the product **1**.

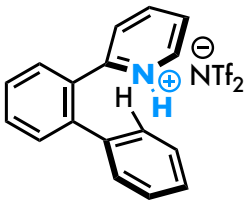

1a

2-([1,1'-biphenyl]-2-yl)pyridin-1-ium bis((trifluoromethyl)sulfonyl)amide (1a): Colorless oil, 99% yield. **^{1}H NMR** (400 MHz, $CO(CD_3)_2$) δ 9.04 – 8.98 (m, 1H), 8.65 (td, *J* = 8.0, 1.6 Hz, 1H), 8.15 (ddd, *J* = 7.6, 5.9, 1.3 Hz, 1H), 7.95 (dt, *J* = 8.1, 1.0 Hz, 1H), 7.88 (dd, *J* = 7.7, 1.4 Hz, 1H), 7.82 (td, *J* = 7.6, 1.4 Hz, 1H), 7.77 – 7.65 (m, 2H), 7.35 (dt, *J* = 4.6, 2.9 Hz, 3H), 7.30 – 7.20 (m, 2H). **^{13}C NMR** (101 MHz, $CO(CD_3)_2$) δ 154.7, 147.5, 143.0, 142.7, 139.5, 133.1, 132.2, 131.7, 131.3, 130.6, 129.7, 129.4, 129.0, 126.8, 121.0 (q, *J* = 323.2 Hz). **IR** (KBr, cm^{-1}) 3109, 1721, 1678, 1613, 1351, 1196, 1136, 1059, 854. **HRMS** calcd $C_{17}H_{14}N$ $[M]^+$: 232.1126. Found: 232.1135.

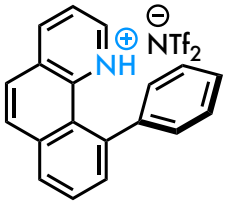

1b

10-phenylbenzo[*h*]quinolin-1-ium bis((trifluoromethyl)sulfonyl)amide (1b): white solid, 98% yield. **^{1}H NMR** (400 MHz, $CO(CD_3)_2$) δ 13.1 (brs, 1H), 9.44 (dd, *J* = 8.2, 1.6 Hz, 1H), 9.04 (dd, *J* = 5.7, 1.6 Hz, 1H), 8.49 (d, *J* = 8.9 Hz, 1H), 8.42 – 8.29 (m, 3H), 8.17 – 8.08 (m, 1H), 7.84 (dd, *J* = 7.3, 1.4 Hz, 1H), 7.78 – 7.66 (m, 5H). **^{13}C NMR** (101 MHz, $CO(CD_3)_2$) δ 147.8, 141.8, 139.5, 138.9, 137.5, 136.8, 133.7, 132.4, 131.5, 130.50, 130.45, 130.0, 129.82, 129.79, 125.3, 125.0, 120.2 (q, *J* = 323.2 Hz), 119.89. **IR** (KBr, cm^{-1}) 2964, 1736, 1691, 1352, 1275, 1260, 1028, 799, 750. **Melting point**: 154-155 ºC. **HRMS** calcd $C_{17}H_{14}N$ $[M]^+$: 256.1126. Found: 256.1117.

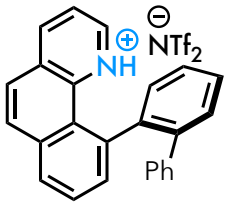

1c

10-phenylbenzo[*h*]quinolin-1-ium bis((trifluoromethyl)sulfonyl)amide (1c): yellow solid, 98% yield. **^{1}H NMR** (400 MHz, $CO(CD_3)_2$) δ 13.2 (brs, 1H), 9.26 (d, *J* = 8.2 Hz, 1H), 9.09 (t, *J* = 6.4 Hz,

1H), 8.30 (dd, *J* = 12.3, 8.3 Hz, 3H), 8.12 – 8.03 (m, 2H), 7.98 – 7.91 (m, 1H), 7.86 (d, *J* = 7.3 Hz, 1H), 7.79 (td, *J* = 6.8, 5.8, 3.9 Hz, 2H), 7.63 (dd, *J* = 6.9, 2.3 Hz, 1H), 6.93 – 6.81 (m, 3H), 6.79 (s, 1H), 6.70 (d, *J* = 7.0 Hz, 2H). **^{13}C NMR** (101 MHz, $CO(CD_3)_2$) δ 147.4, 141.6, 140.9, 139.0, 138.3, 136.7, 136.6, 136.1, 134.4, 132.0, 131.49, 131.46, 131.36, 130.7, 129.9, 129.7, 129.4, 128.4, 127.5, 126.8, 124.6, 123.1, 120.4, 120.1 (q, *J* = 323.2 Hz). **IR** (KBr, cm^{-1}) 3352, 1653, 1559, 1507, 1384, 1195, 1083, 668. **Melting point**: 160-161 ºC. **HRMS** calcd $C_{25}H_{18}N$ $[M]^+$: 332.1439. Found: 332.1435.

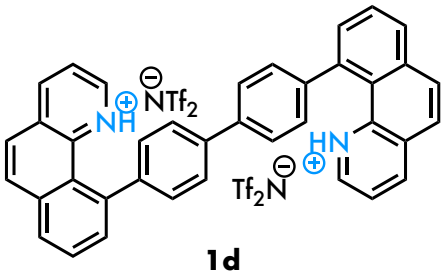

1d

1d: yellow solid, 89% yield**. ^{1}H NMR** (400 MHz, $CO(CD_3)_2$) δ 13.4 (brs, 1H), 9.41 (dd, *J* = 8.2, 1.4 Hz, 1H), 9.02 (dd, *J* = 5.7, 1.6 Hz, 1H), 8.50 (d, *J* = 8.9 Hz, 1H), 8.41 (dd, *J* = 8.0, 1.3 Hz, 1H), 8.38 – 8.27 (m, 2H), 8.22 – 8.11 (m, 3H), 7.95 (dd, *J* = 7.9, 1.5 Hz, 3H).. **^{13}C NMR** (101 MHz, $CO(CD_3)_2$) δ 147.2, 142.0, 140.7, 139.2, 139.0, 138.0, 136.9, 133.7, 132.2, 131.3, 130.6, 130.4, 129.9, 128.6, 125.5, 123.3, 120.5, 120.1 (q, *J* = 323.2 Hz). **IR** (KBr, cm^{-1}) 3697, 1707, 1608, 1349, 1194, 1055, 823, 717. **Melting**

point: 221-222 ºC. **HRMS** calcd $C_{38}H_{26}N_2$ $[M]^{2+}$: 510.2096, m/z: 255.1048. Found m/z: 255.1043.

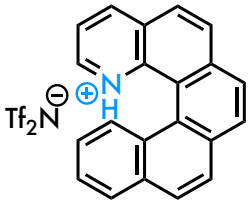

1e

1e: brown oil, 91% yield**.** **^{1}H NMR** (400 MHz, $CO(CD_3)_2$) δ 9.47 (dd, *J* = 8.2, 1.6 Hz, 1H), 9.04 (dd, *J* = 5.5, 1.6 Hz, 1H), 8.52 – 8.39 (m, 2H), 8.34 (dd, *J* = 8.2, 5.1 Hz, 2H), 8.12 – 8.04 (m, 2H), 7.70 (ddd, *J* = 8.1, 6.9, 1.2 Hz, 1H), 7.54 (ddd, *J* = 8.4, 6.9, 1.4 Hz, 1H). **^{13}C NMR** (101 MHz, $CO(CD_3)_2$) δ 147.42, 141.68, 136.40, 136.34, 133.70, 133.39, 132.54, 131.08, 129.77, 129.25, 129.18, 128.12, 127.49, 127.26, 126.53, 126.20, 126.07, 124.47, 123.15, 120.2 (q, *J* = 323.2 Hz), 118.60. **IR** (KBr, cm^{-1}) 3907, 1607, 1553, 1352, 1194, 1134, 1056, 851. **HRMS** calcd $C_{21}H_{14}N$ $[M]^+$: 280.1126. Found: 280.1126.

General procedure of cobaloxime-catalyzed dehydrogenative C–N(+) bond formation reaction

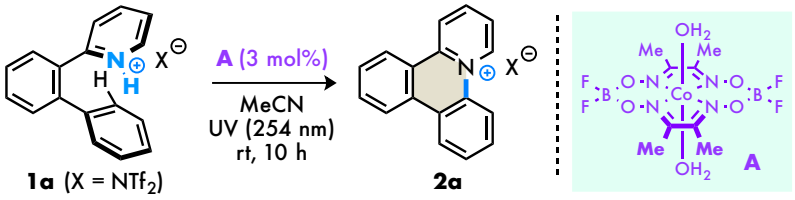

To a flame-dried 20 mL Quartz test tube with a stir bar was added **1a** (51.2 mg, 0.0999 mmol) and $Co(dmg(BF_2))_2(OH_2)_2$ (**A**) (1.3 mg, 0.0031 mmol, 3 mol%). The test tube and the septum were transferred to the glove box. AcroSeal® MeCN (0.16 mL) was added to the test tube, before it was sealed with the septum and transferred out of the glove box. The septum was covered with aluminum foil, and the mixture was irradiated by 25 W UV lamps at room temperature under vigorous stirring for 18 hours (see fig. S1 and S2). After the completion of the reaction, the mixture was recrystallized in $MeCN/Et_2O$ to give desired product.

pyrido[1,2-*f*]phenanthridin-5-ium bis((trifluoromethyl)sulfonyl)amide (2a): white solid (51.0 mg, quantitative yield) in quantitative yield. **^{1}H NMR** (400 MHz, $CO(CD_3)_2$) δ 10.32 (d, J = 6.9 Hz, 1H), 9.50 (dd, J = 8.7, 1.6 Hz, 1H), 9.00 – 8.76 (m, 5H), 8.40 (td, J = 7.1, 1.5 Hz, 1H), 8.13 – 7.91 (m, 4H). **^{13}C NMR** (101 MHz, $CO(CD_3)_2$) δ 145.3, 143.8, 137.1, 135.5, 133.4, 132.4, 132.1, 131.41, 130.3,

127.3, 126.2, 125.8, 125.7, 125.1, 124.2, 123.6, 121.1 (q, J = 322.2 Hz), 119.7. **IR** (KBr, cm^{-1}) 3079, 2926, 1439, 1261, 1148, 1034, 801. **Melting point**: 154-155 ºC. **HRMS** calcd $C_{17}H_{12}N$ $[M]^+$: 230.0969. Found: 230.0978.

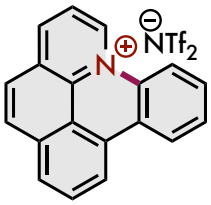

2b

benzo[*mn*]pyrido[3,2,1-*de*]acridin-9-ium bis((trifluoromethyl)sulfonyl)amide (2b): yellow solid (51.8 mg, 97% yield). **^{1}H NMR** (400 MHz, $CO(CD_3)_2$) δ 10.89 (d, J = 6.6 Hz, 1H), 9.60 (d, J = 7.9 Hz, 1H), 9.34 – 9.04 (m, 3H), 8.81 (t, J = 7.3 Hz, 1H), 8.72 – 8.45 (m, 4H), 8.25 – 8.14 (m, 2H). **^{13}C NMR** (101 MHz, $CO(CD_3)_2$) δ 143.2, 135.6, 133.4, 133.1, 132.44, 132.41, 131.8, 131.4, 130.99, 130.97, 129.7, 129.0, 126.6, 126.0, 125.1, 124.7, 123.2, 121.7, 120.2 (q, J = 322.2 Hz), 118.7, 116.6, 116.5. **IR** (KBr, cm^{-1}) 3098, 1731, 1632, 1423, 1357, 1195, 1137, 1055, 839. **Melting point**: 200 ºC (decomp.). **HRMS** calcd $C_{19}H_{12}N$ $[M]^+$: 254.0970. Found: 254.0977.

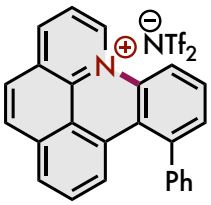

2c

13-phenylbenzo[*mn*]pyrido[3,2,1-*de*]acridin-9-ium bis((trifluoromethyl)sulfonyl)amide (2c): yellow solid (55.5 mg, 91% yield). **^{1}H NMR** (400 MHz, $CO(CD_3)_2$) δ 10.82 (d, *J* = 6.4 Hz, 1H), 9.57 (d, *J* = 7.7 Hz, 1H), 9.19 (d, *J* = 8.7 Hz, 1H), 8.78 (t, *J* = 7.1 Hz, 1H), 8.58 – 8.41 (m, 3H), 8.23 – 8.15 (m, 1H), 8.10 – 7.82 (m, 3H), 7.81 – 7.40 (m, 5H). **^{13}C NMR** (101 MHz, $CO(CD_3)_2$) δ 143.36, 142.69, 142.51, 136.78, 134.91, 134.89, 133.88, 133.69, 131.41, 130.81, 130.63, 129.76, 129.74, 128.88, 128.87, 128.60, 127.23, 125.73, 123.86, 123.24, 120.2 (q, *J* = 322.2 Hz), 118.88, 118.34. **IR** (KBr, cm^{-1}) 3098, 1731, 1632, 1423, 1357, 1195, 1137, 1055, 839. **Melting point**: >295 ºC. **HRMS** calcd $C_{25}H_{16}N$ $[M]^+$: 330.1283. Found: 330.1289.

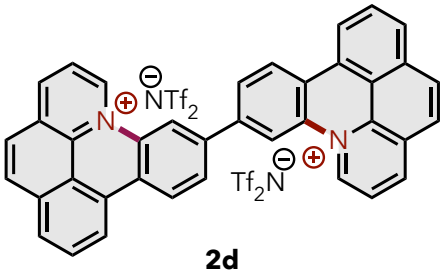

2d

[11,11'-bibenzo[*mn*]pyrido[3,2,1-*de*]acridine]-9,9'-diium bis((trifluoromethyl)sulfonyl)amide **(2d)**: yellow solid (95.0 mg, 89% yield). **^{1}H NMR** (400 MHz, $CO(CD_3)_2$) δ 10.92 (d, *J* = 6.3 Hz, 1H), 9.58 – 9.51 (m, 2H), 9.08 (d, *J* = 8.4 Hz, 1H), 8.91 (d, *J* = 7.8 Hz, 1H), 8.81 – 8.72 (m, 2H), 8.45 (t, *J* = 6.3 Hz, 3H), 8.27 (t, *J* = 7.8 Hz, 1H). **^{13}C NMR** (101 MHz, $CO(CD_3)_2$) δ 143.94, 141.15, 136.07, 133.75, 133.61, 133.18, 132.77, 131.36, 130.68, 129.96, 129.71, 126.34, 126.30, 126.14, 125.26, 123.37, 122.10, 120.2 (q, *J* = 322.2 Hz), 117.67, 116.89. **IR** (KBr, cm^{-1}) 3442, 1637, 1449, 1388, 1347, 1195, 1132, 1055, 833. **Melting point**: >295 ºC. **HRMS** calcd $C_{38}H_{22}N_2$ $[M]^+$: 506.1783, m/z: 253.0891. Found: 253.0800.

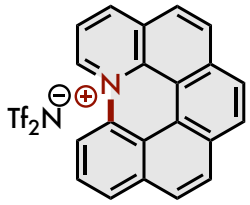

2e

naphtho[2,1,8,7-*klmn*]pyrido[3,2,1-*de*]acridin-6-ium bis((trifluoromethyl)sulfonyl)amide (2e): yellow solid (49.7 mg, 89% yield). **^{1}H NMR** (400 MHz, $CO(CD_3)_2$) δ 10.62 (d, *J* = 6.5 Hz, 1H), 9.47 (d, *J* = 7.8 Hz, 1H), 9.02 (d, *J* = 8.4 Hz, 1H), 8.68 (t, *J* = 7.1 Hz, 1H), 8.47 – 8.29 (m, 3H), 8.20 (t, *J* = 8.1 Hz, 1H), 8.13 – 7.90 (m, 1H). **^{13}C NMR** (101 MHz, $CO(CD_3)_2$) δ 144.1, 136.6, 133.8, 131.94, 131.89, 131.0, 130.9, 130.1, 129.8, 129.0, 128.3, 128.2, 127.7, 127.4, 126.7, 123.3, 120.2 (q, *J* = 322.2 Hz), 119.2, 116.0, 115.8. **IR** (KBr, cm^{-1}) 3076, 1664, 1619, 1407, 1354, 1196, 1136, 1055, 862. **Melting point**: >295 ºC. **HRMS** calcd $C_{21}H_{12}N$ $[M]^+$: 278.0970. Found: 278.0965.

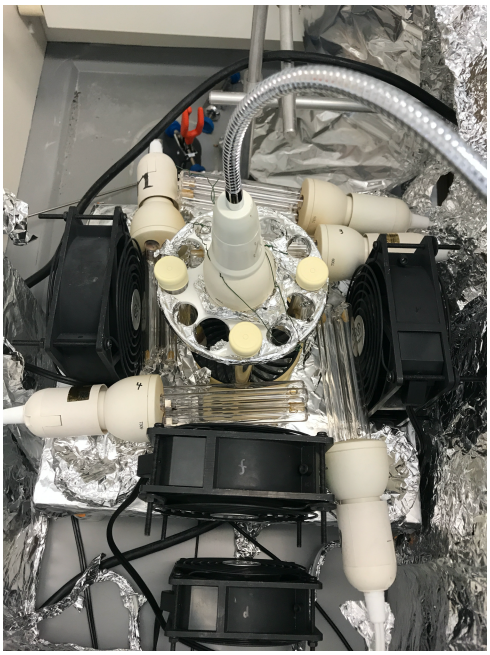

Fig. S1. Top view of the reaction set up for the catalytic dehydrogenative electrocyclization. Six 25 W UV lamps and five fans are used as shown. They are on the cardboard box that has a hole in the center. Side fans on the cardboard box are about 3–4 cm away from the edge of the center fan. CAUTION: cover the reaction setup with cardboard boxes and aluminum foil to avoid exposure to UV.

Fig. S2. Side view of the reaction set up for the catalytic dehydrogenative electrocyclization. Some 20 mL vials are put under the cardboard box to adjust the height and use the fan in the center. CAUTION: cover the reaction setup with cardboard boxes and aluminum foil to avoid exposure to UV.

3.5 ^{1}H, ^{13}C, and ^{19}F NMR spectra

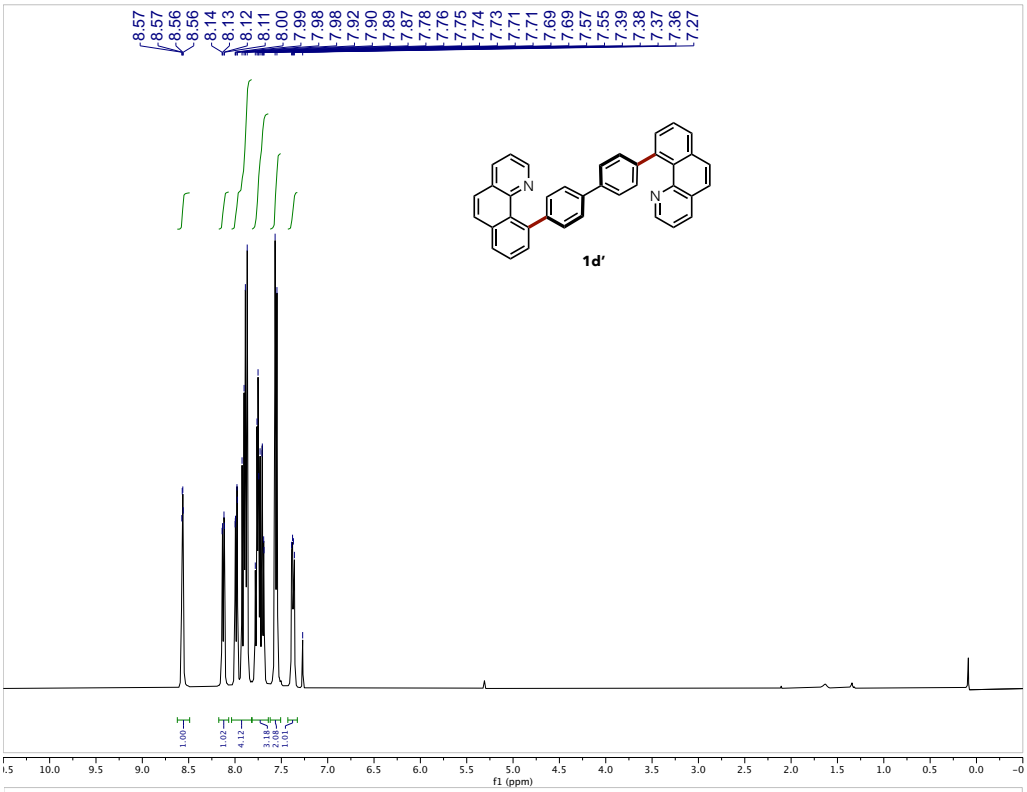

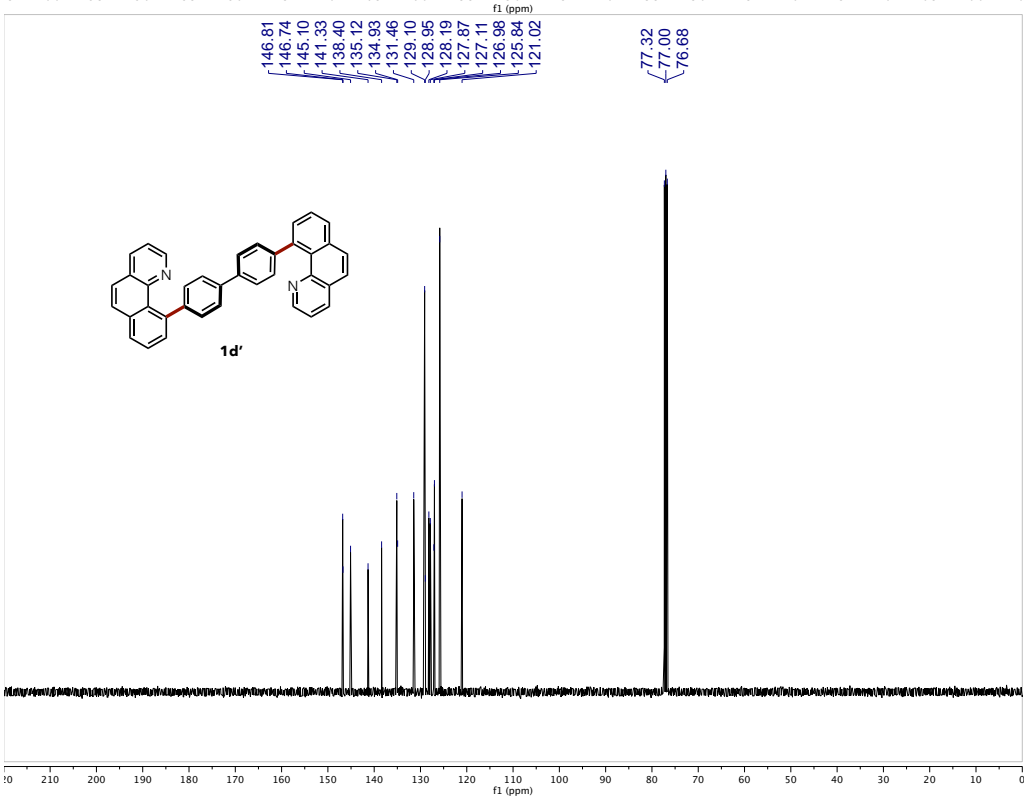

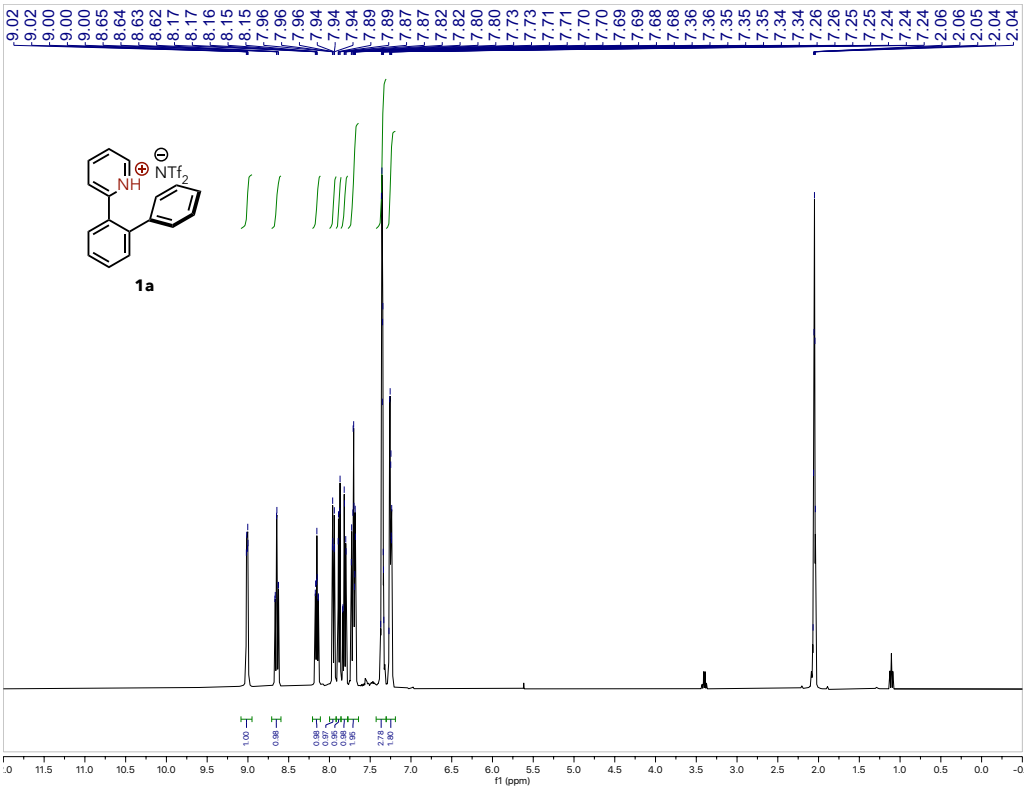
9.02
9.02
9.00
9.00
9.00
8.65
8.64
8.63
8.62
8.17
8.17
8.16
8.15
8.15
7.96
7.96
7.96
7.94
7.94
7.94
7.89
7.89
7.87
7.87
7.82
7.80
7.80
7.73
7.73
7.71
7.71
7.70
7.70
7.69
7.69
7.68
7.68
7.36
7.35
7.35
7.34
7.34
7.26
7.26
7.25
7.25
7.24
7.24
7.24
2.06
2.06
2.05
2.04
2.04
NH
NTf2
1a
1.00
0.98
0.98
0.95
0.98
1.95
2.78
1.80
f1 (ppm)

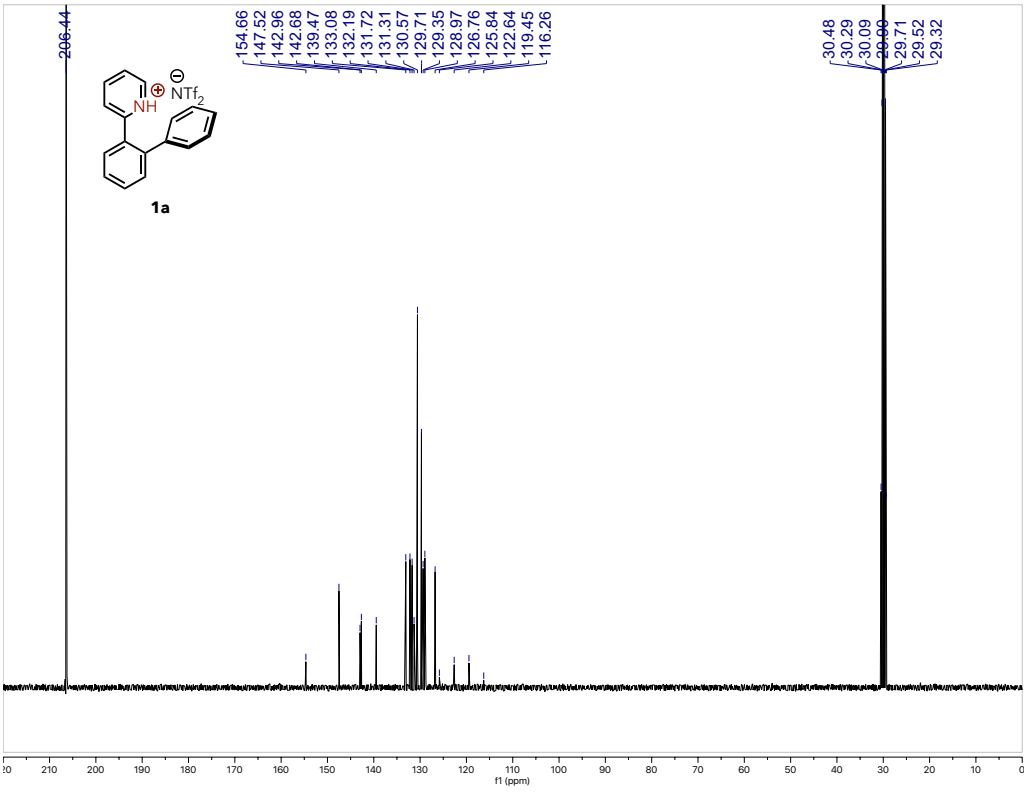
206.44
154.66
147.52
142.96
142.68
139.47
133.08
132.19
131.72
131.31
130.57
129.71
129.35
128.97
126.76
125.84
122.64
119.45
116.26
30.48
30.29
30.09
29.90
29.71
29.52
29.32
NH
NTf2
1a
f1 (ppm)

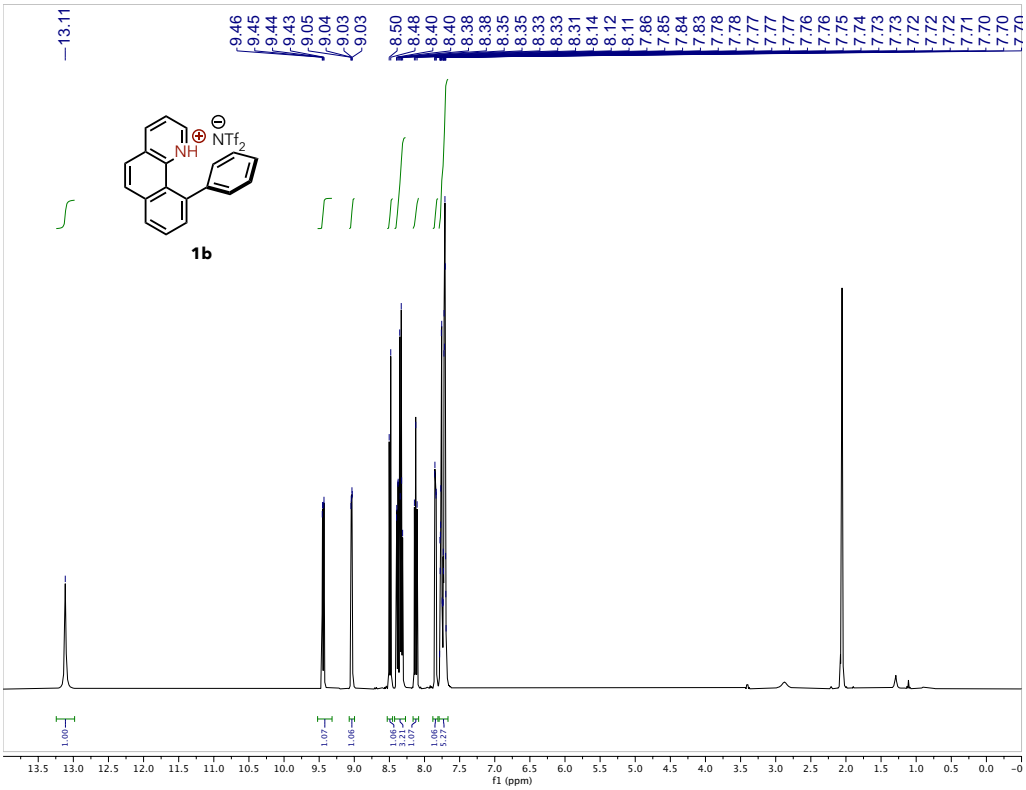
13.11
9.46
9.45
9.44
9.43
9.05
9.04
9.03
9.03
8.50
8.48
8.40
8.40
8.38
8.38
8.35
8.35
8.33
8.33
8.31
8.14
8.12
8.11
7.86
7.85
7.84
7.83
7.78
7.78
7.77
7.77
7.77
7.76
7.76
7.75
7.74
7.73
7.73
7.72
7.72
7.72
7.71
7.70
7.70
7.70
NTf2
NH
1b
1.00
1.07
1.06
1.06
3.21
1.07
1.06
5.27
f1 (ppm)

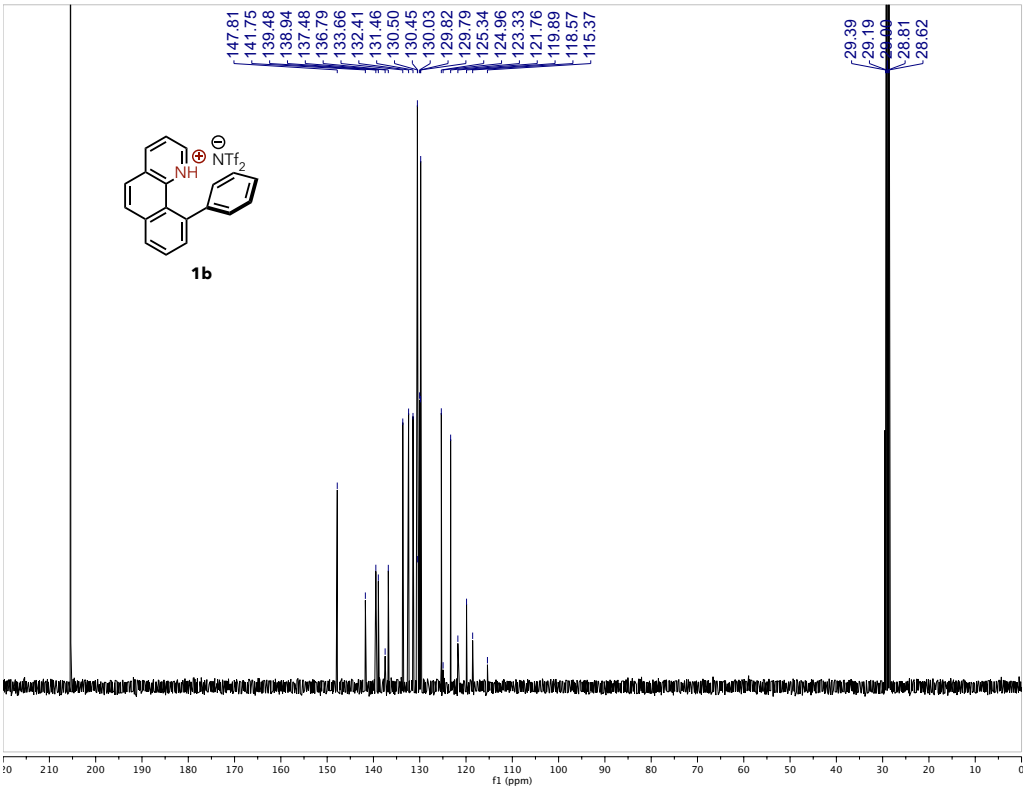
147.81
141.75
139.48
138.94
137.48
136.79
133.66
132.41
131.46
130.50
130.45
130.03
129.82
129.79
125.34
124.96
123.33
121.76
119.89
118.57
115.37
29.39
29.19
28.81
28.62
NTf2
NH
1b
f1 (ppm)

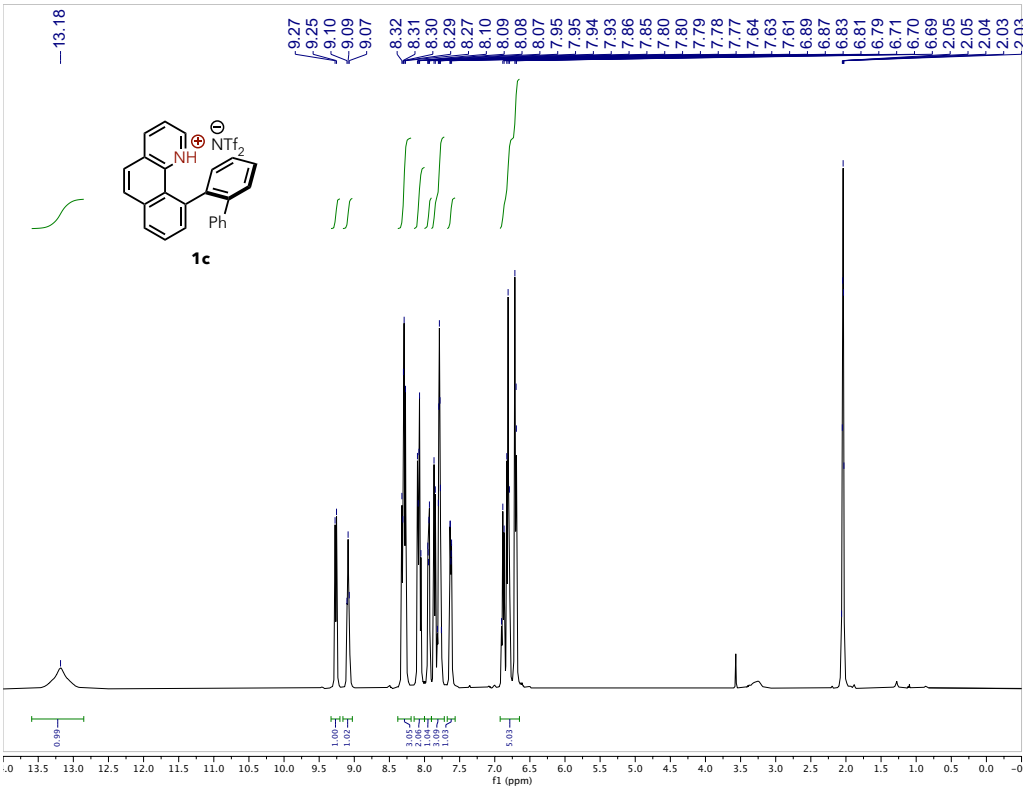
13.18
9.27
9.25
9.10
9.09
9.07
8.32
8.31
8.30
8.29
8.27
8.10
8.09
8.08
8.07
7.95
7.95
7.94
7.93
7.86
7.85
7.80
7.80
7.79
7.78
7.77
7.64
7.63
7.61
6.89
6.87
6.83
6.81
6.79
6.71
6.70
6.69
2.05
2.05
2.04
2.03
NTf2
NH
Ph
1c
0.99
1.00
1.02
3.05
2.06
1.04
1.00
1.03
5.03
f1 (ppm)

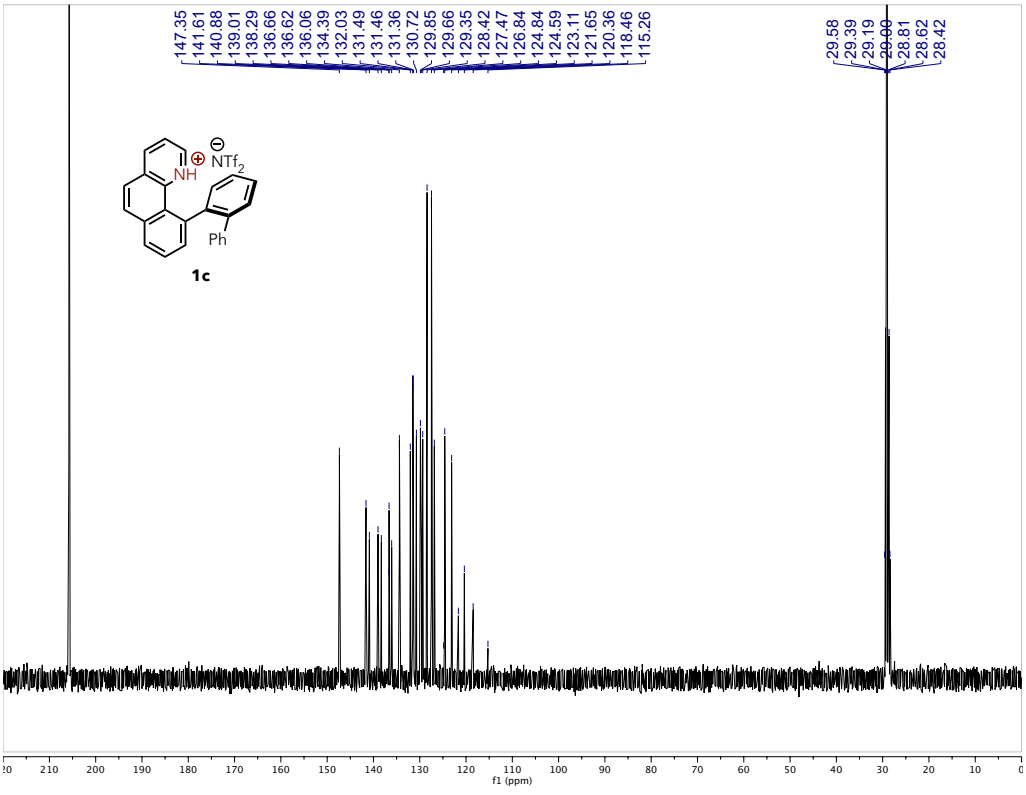
147.35
141.61
140.88
139.01
138.29
136.66
136.62
136.06
134.39
132.03
131.49
131.46
131.36
130.72
129.85
129.66
129.35
128.42
127.47
126.84
124.84
124.59
123.11
121.65
120.36
118.46
115.26
29.58
29.39
29.19
29.00
28.81
28.62
28.42
NTf2
NH
Ph
1c
f1 (ppm)

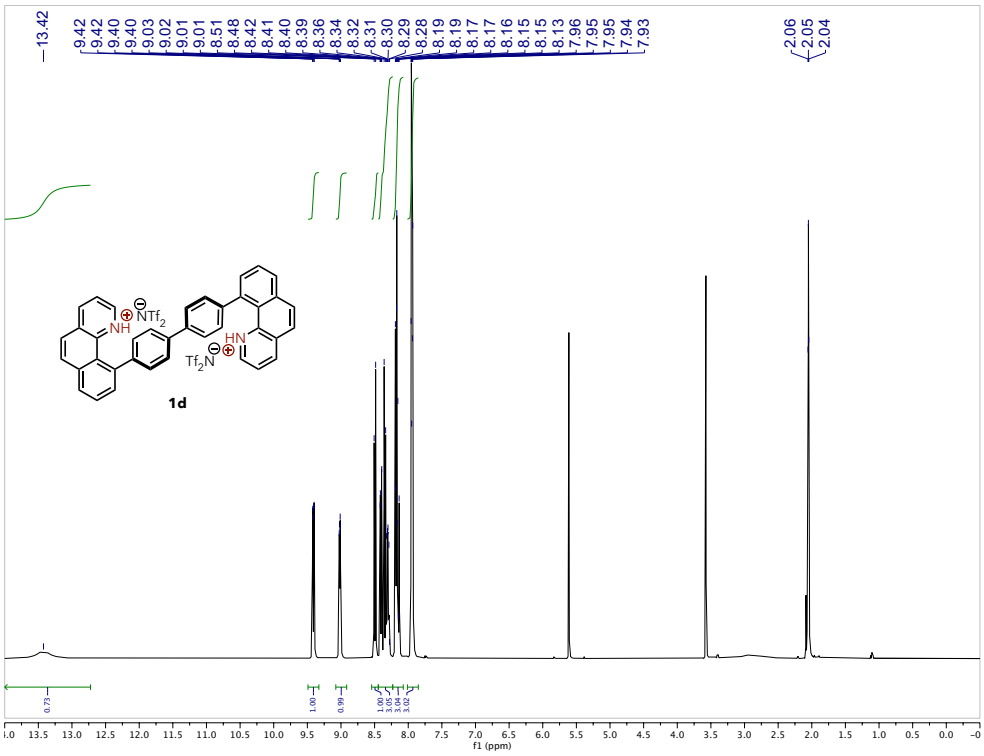
13.42
9.42
9.42
9.40
9.40
9.03
9.02
9.01
9.01
8.51
8.48
8.42
8.41
8.40
8.39
8.36
8.34
8.32
8.31
8.30
8.29
8.28
8.19
8.19
8.17
8.17
8.16
8.15
8.15
8.13
7.96
7.95
7.95
7.94
7.93
2.06
2.05
2.04
NH
NTf2
HN
Tf2N
1d
f1 (ppm)

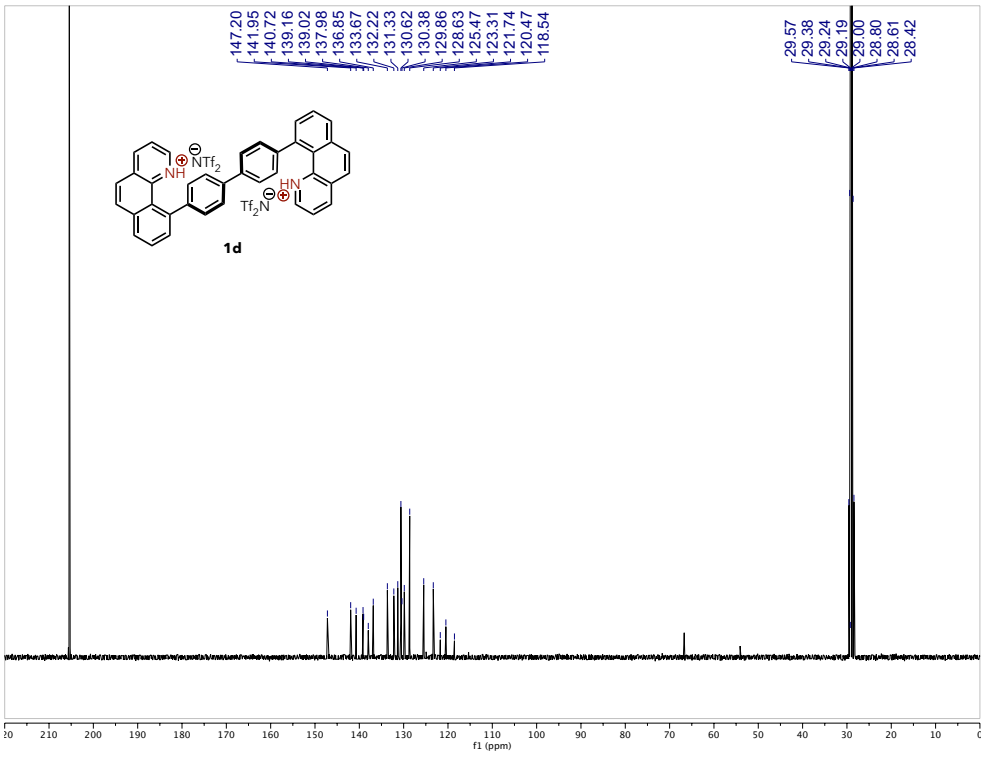
147.20
141.95
140.72
139.16
139.02
137.98
136.85
133.67
132.22
131.33
130.62
130.38
129.86
128.63
125.47
123.31
121.74
120.47
118.54
29.57
29.38
29.24
29.19
29.00
28.80
28.61
28.42
NH
NTf2
HN
Tf2N
1d
f1 (ppm)

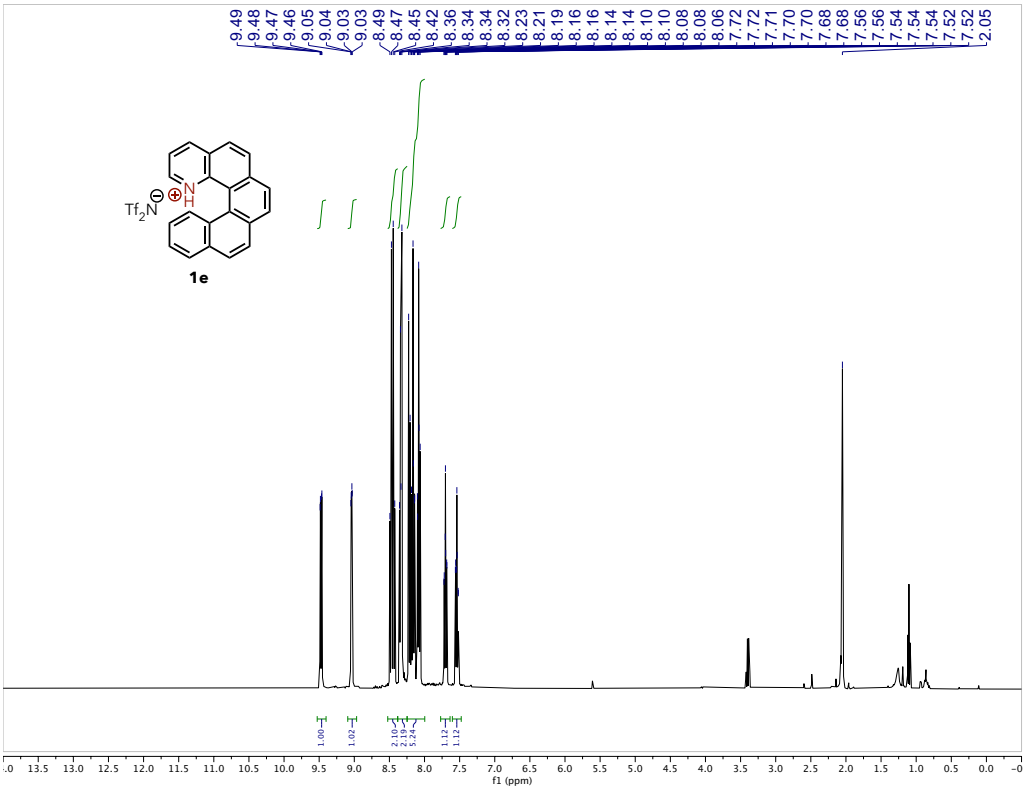
9.49
9.48
9.47
9.46
9.05
9.04
9.03
9.03
8.49
8.47
8.45
8.42
8.36
8.34
8.34
8.32
8.23
8.21
8.19
8.16
8.16
8.14
8.14
8.10
8.10
8.08
8.08
8.06
7.72
7.72
7.71
7.70
7.70
7.68
7.68
7.56
7.56
7.54
7.54
7.54
7.52
7.52
2.05
Tf2N
1e
1.00
1.02
2.10
2.19
5.24
1.12
1.12
f1 (ppm)

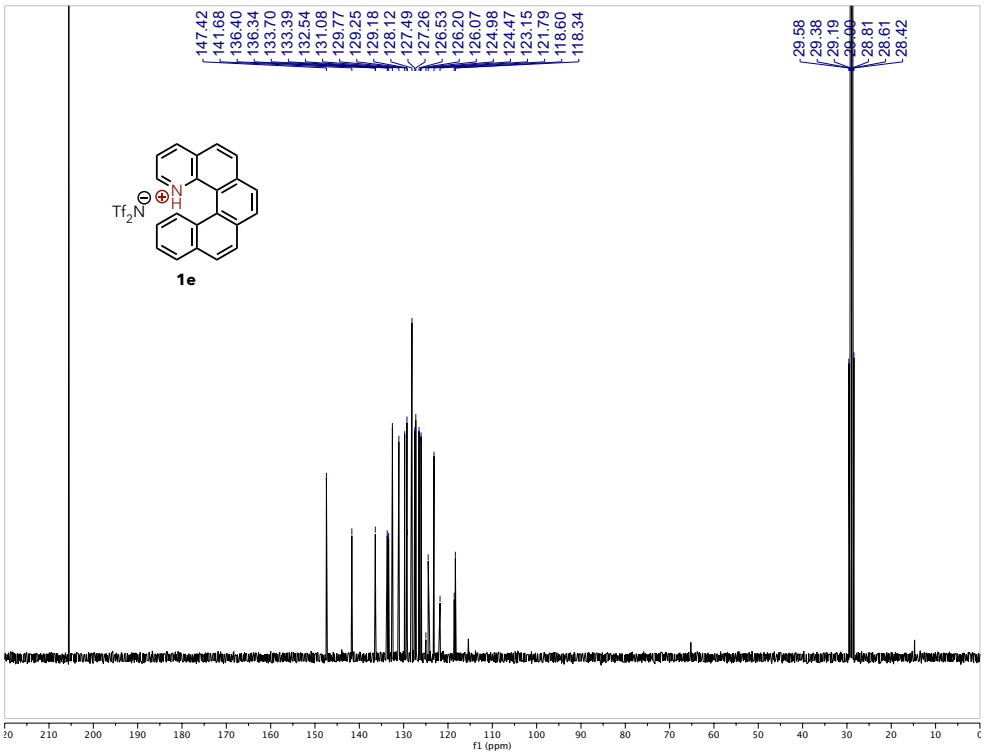
147.42
141.68
136.40
136.34
133.70
133.39
132.54
131.08
129.77
129.25
129.18
128.12
127.49
127.26
126.53
126.20
126.07
124.98
124.47
123.15
121.79
118.60
118.34
29.58
29.38
29.19
29.00
28.81
28.61
28.42
Tf2N
1e
f1 (ppm)

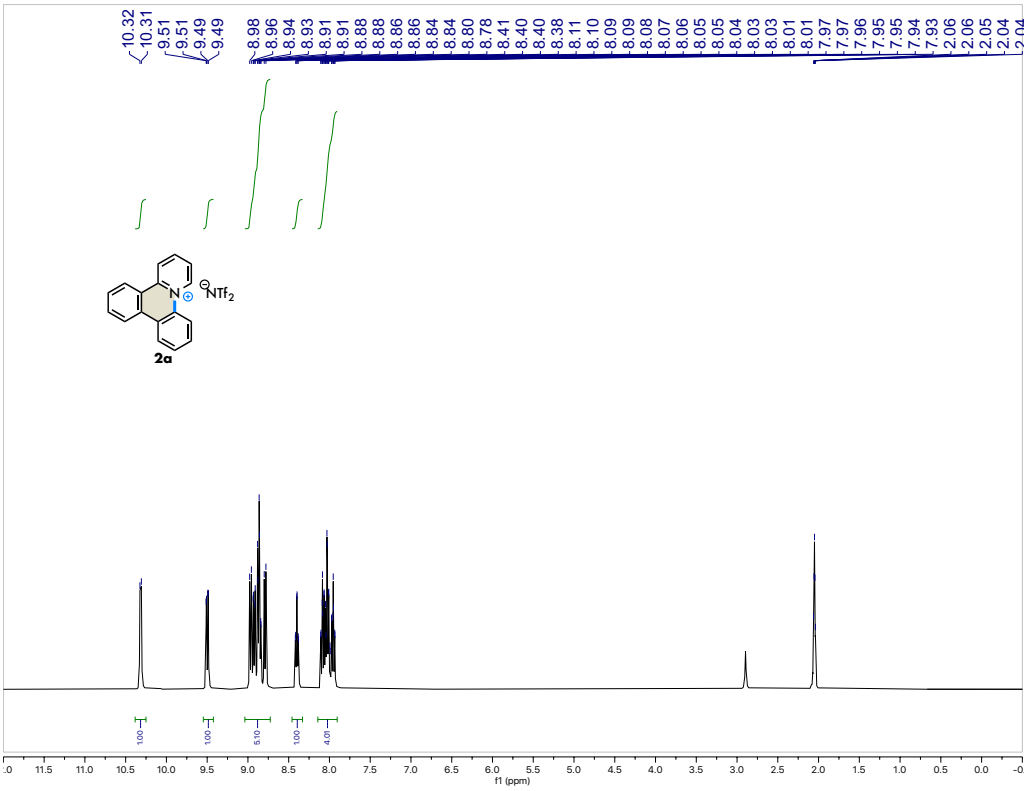
10.32
10.31
9.51
9.51
9.49
9.49
8.98
8.96
8.94
8.93
8.91
8.91
8.88
8.88
8.86
8.86
8.84
8.84
8.80
8.78
8.41
8.40
8.40
8.38
8.11
8.10
8.09
8.09
8.08
8.07
8.06
8.05
8.05
8.04
8.03
8.03
8.01
8.01
7.97
7.97
7.96
7.95
7.95
7.94
7.93
2.06
2.06
2.05
2.04
NTf2
2a
1.00
1.00
5.10
1.00
4.01
f1 (ppm)

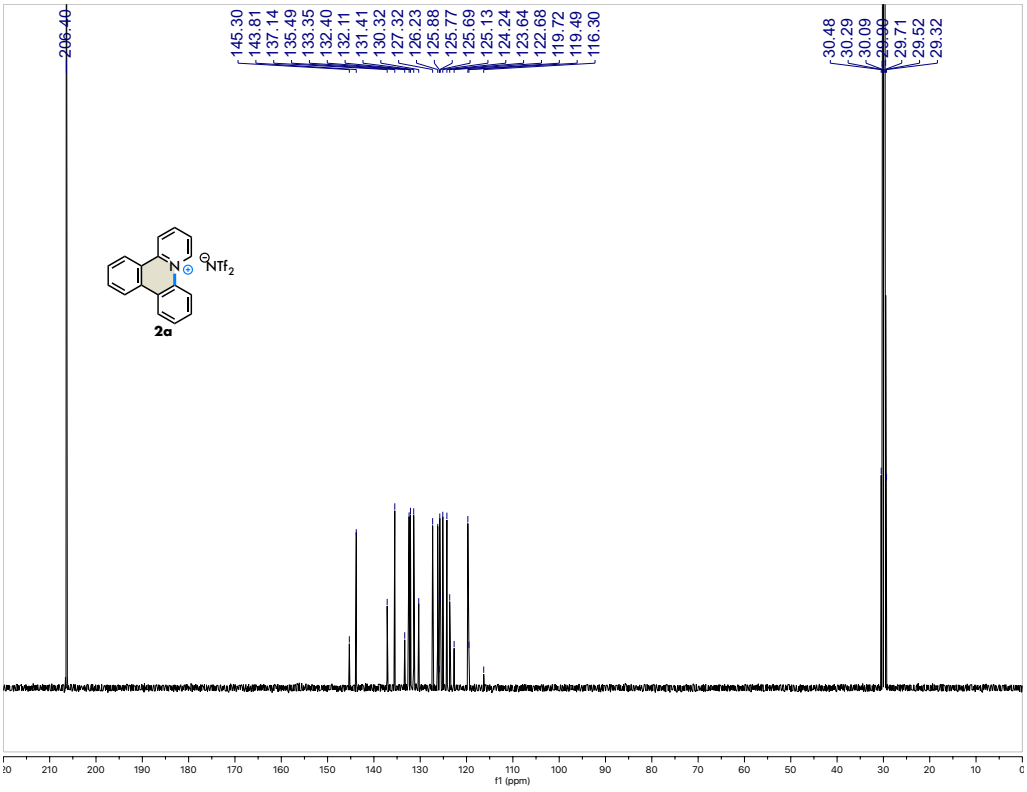
206.40
145.30
143.81
137.14
135.49
133.35
132.40
132.11
131.41
130.32
127.32
126.23
125.88
125.77
125.69
125.13
124.24
123.64
122.68
119.72
119.49
116.30
30.48
30.29
30.09
29.71
29.52
29.32
NTf2
2a
f1 (ppm)

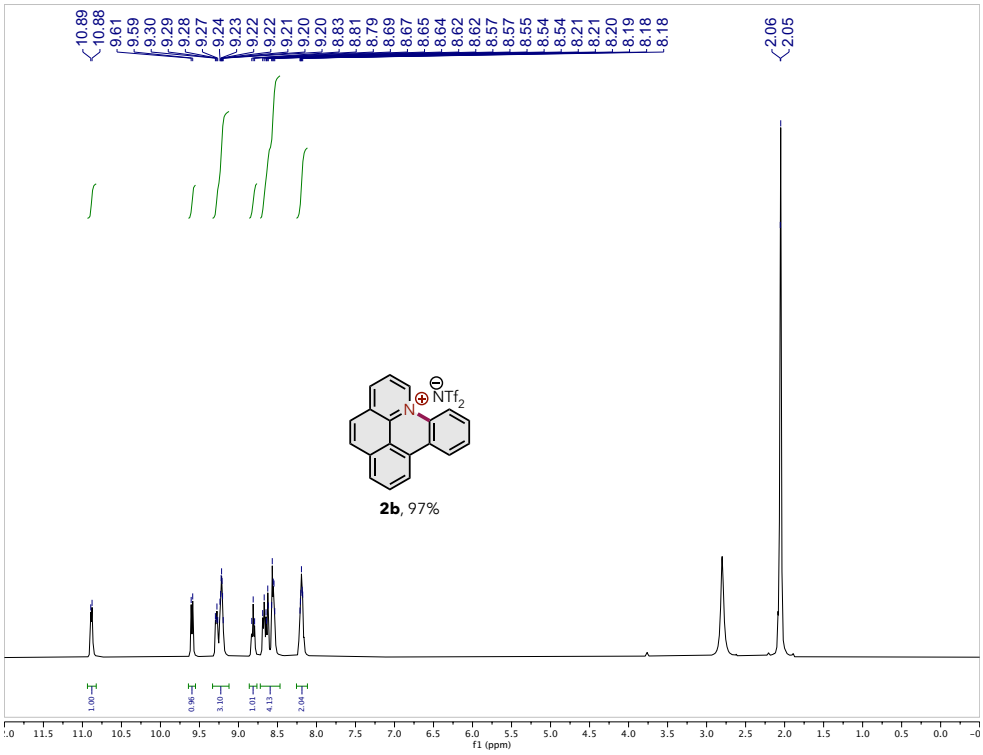
10.89
10.88
9.61
9.59
9.30
9.29
9.28
9.27
9.24
9.23
9.22
9.22
9.21
9.20
9.20
8.83
8.81
8.79
8.69
8.67
8.65
8.64
8.62
8.62
8.57
8.57
8.55
8.54
8.54
8.21
8.21
8.20
8.19
8.18
8.18
2.06
2.05
NTf2
2b, 97%
1.00
0.96
3.10
1.01
4.13
2.04
f1 (ppm)

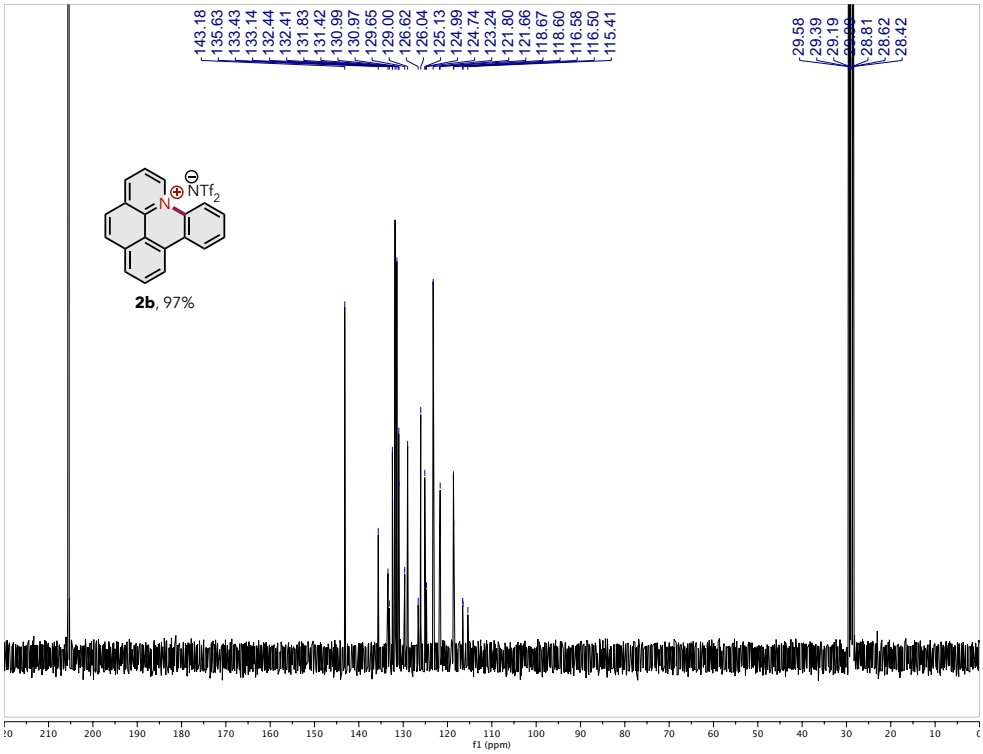
143.18
135.63
133.43
133.14
132.44
132.41
131.83
131.42
130.99
130.97
129.65
129.00
126.62
126.04
125.13
124.99
124.74
123.24
121.80
121.66
118.67
118.60
116.58
116.50
115.41
29.58
29.39
29.19
28.81
28.62
28.42
NTf2
2b, 97%
f1 (ppm)

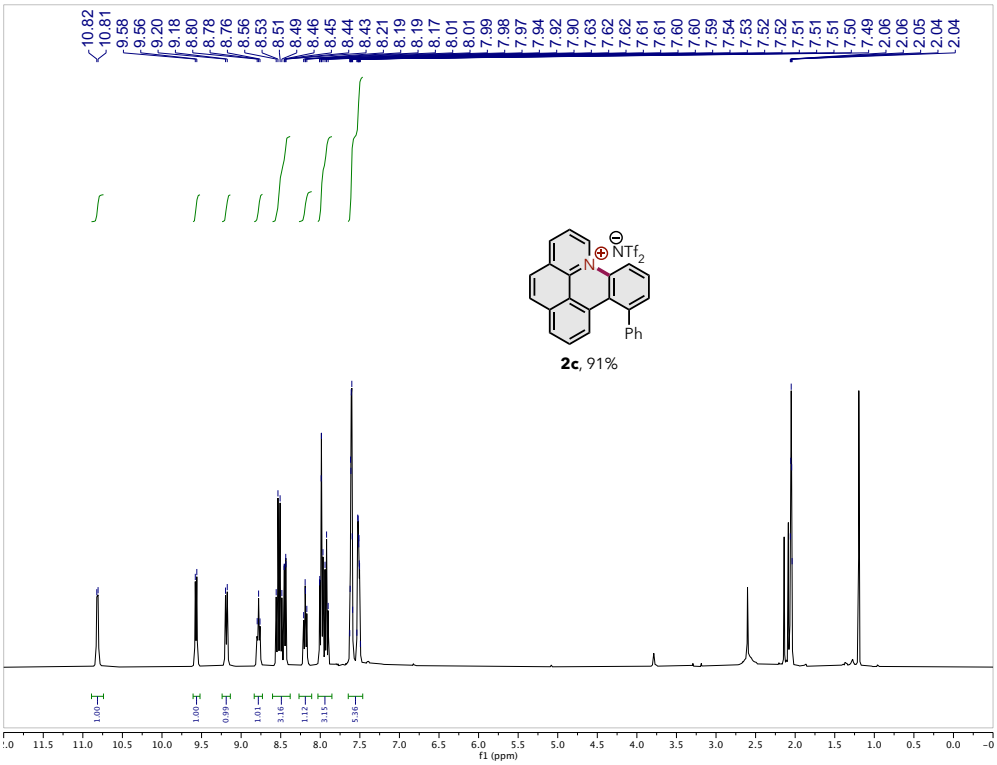
10.82
10.81
9.58
9.56
9.20
9.18
8.80
8.78
8.76
8.56
8.53
8.51
8.49
8.46
8.45
8.44
8.43
8.21
8.19
8.19
8.17
8.01
8.01
7.99
7.98
7.97
7.94
7.92
7.90
7.63
7.62
7.62
7.61
7.61
7.60
7.60
7.59
7.54
7.53
7.52
7.51
7.51
7.51
7.50
7.49
2.06
2.06
2.05
2.04
2.04
NTf2
Ph
2c, 91%
1.00
1.00
0.99
1.01
3.16
1.12
3.15
5.36
f1 (ppm)

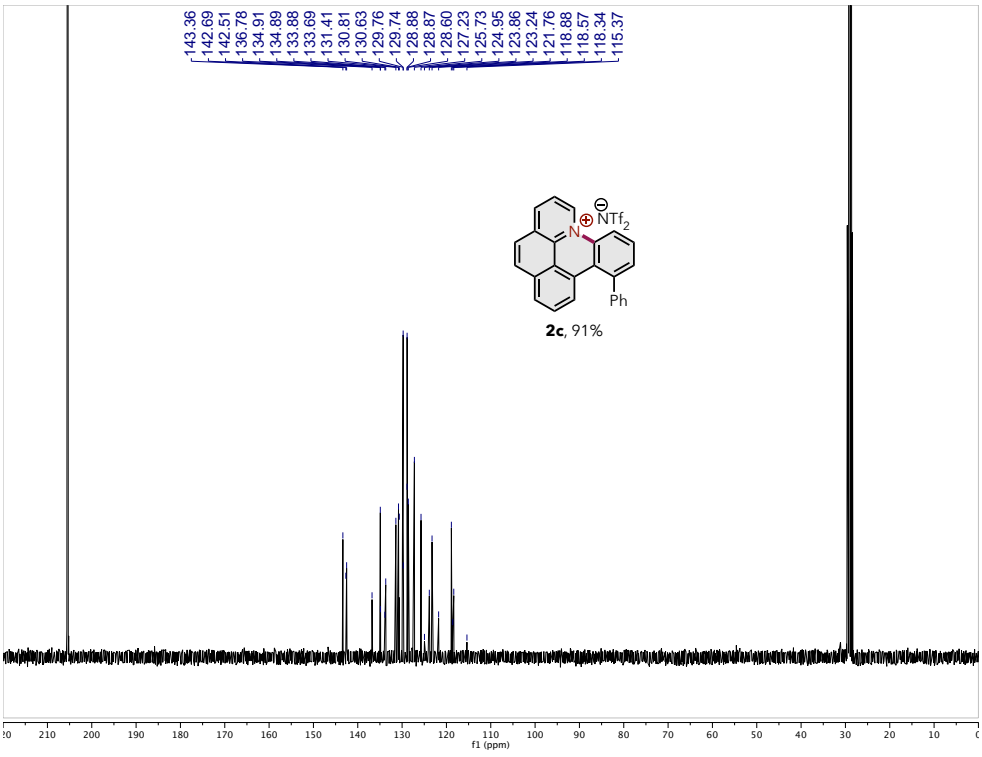
143.36
142.69
142.51
136.78
134.91
134.89
133.88
133.69
131.41
130.81
130.63
129.76
129.74
128.88
128.87
128.60
127.23
125.73
124.95
123.86
123.24
121.76
118.88
118.57
118.34
115.37
NTf2
Ph
2c, 91%
f1 (ppm)

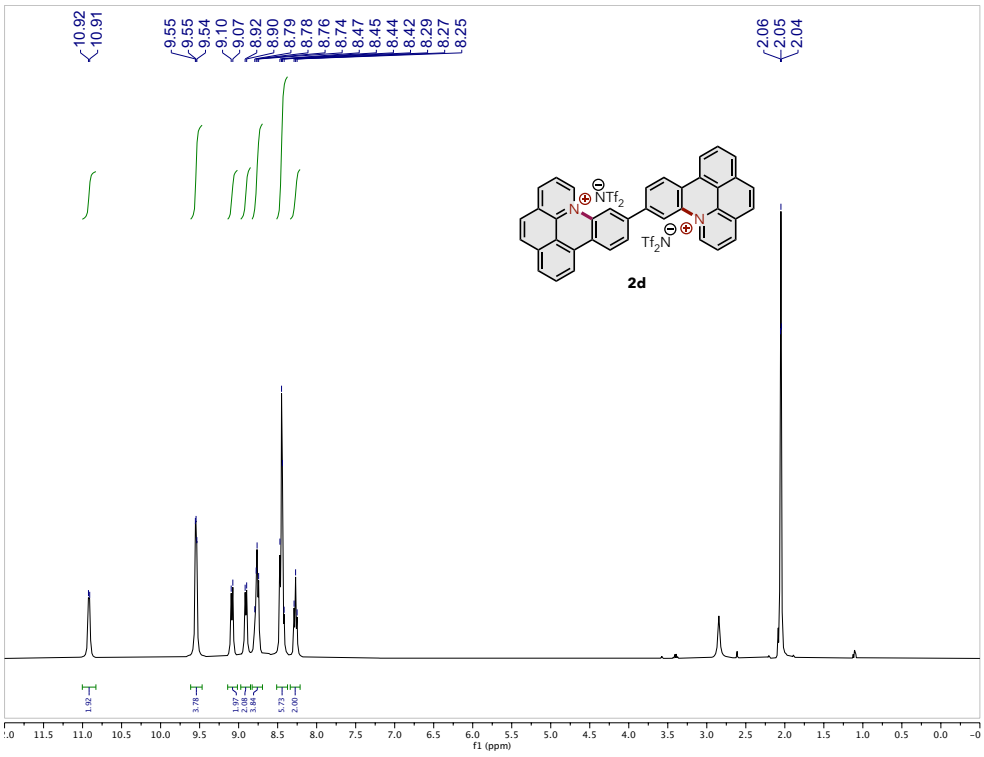
10.92
10.91
9.55
9.55
9.54
9.10
9.07
8.92
8.90
8.79
8.78
8.76
8.74
8.47
8.45
8.44
8.42
8.29
8.27
8.25
2.06
2.05
2.04
2d
f1 (ppm)

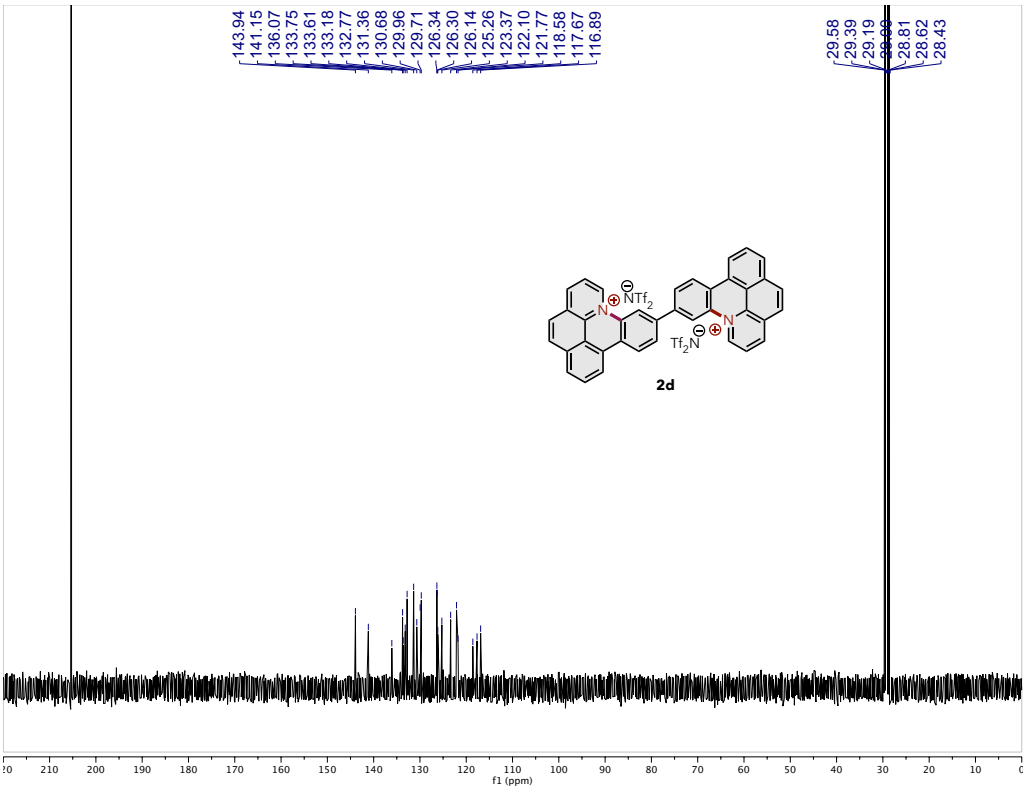
143.94
141.15
136.07
133.75
133.61
133.18
132.77
131.36
130.68
129.96
129.71
126.34
126.30
126.14
125.26
123.37
122.10
121.77
118.58
117.67
116.89
29.58
29.39
29.19
28.81
28.62
28.43
2d
f1 (ppm)

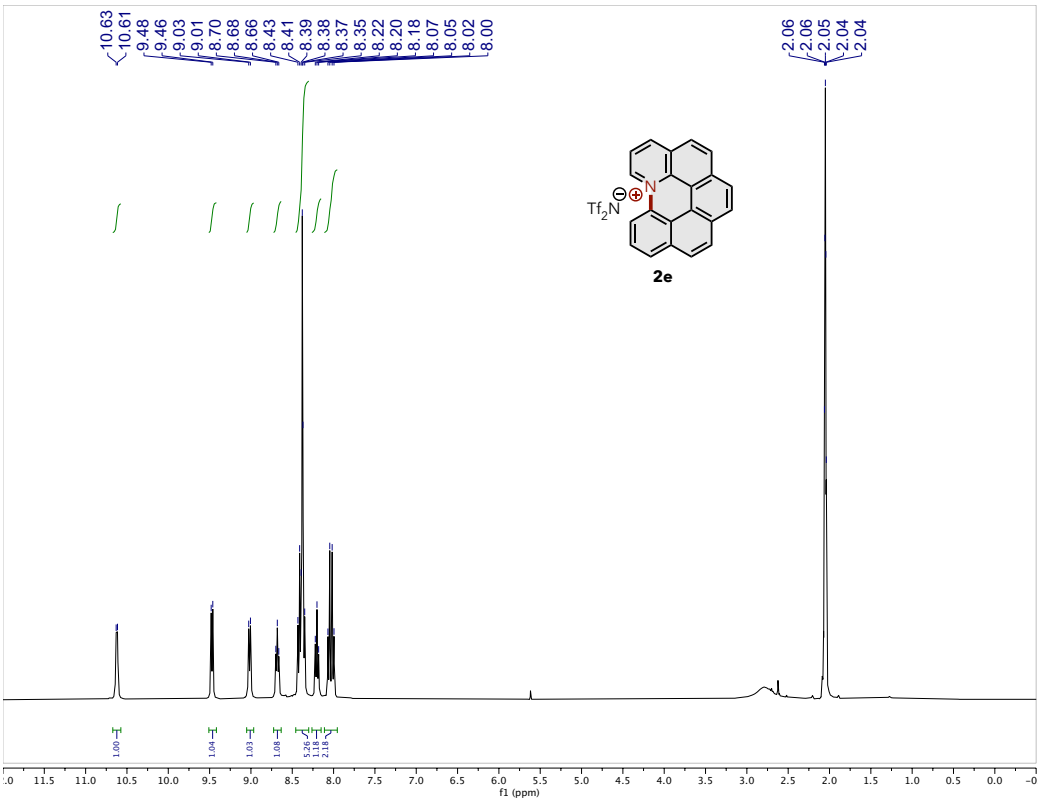
10.63
10.61
9.48
9.46
9.03
9.01
8.70
8.68
8.66
8.43
8.41
8.39
8.38
8.37
8.35
8.22
8.20
8.18
8.07
8.05
8.02
8.00
2.06
2.06
2.05
2.04
2.04
Tf2N
2e
1.00
1.04
1.03
1.08
5.26
1.38
2.18
f1 (ppm)

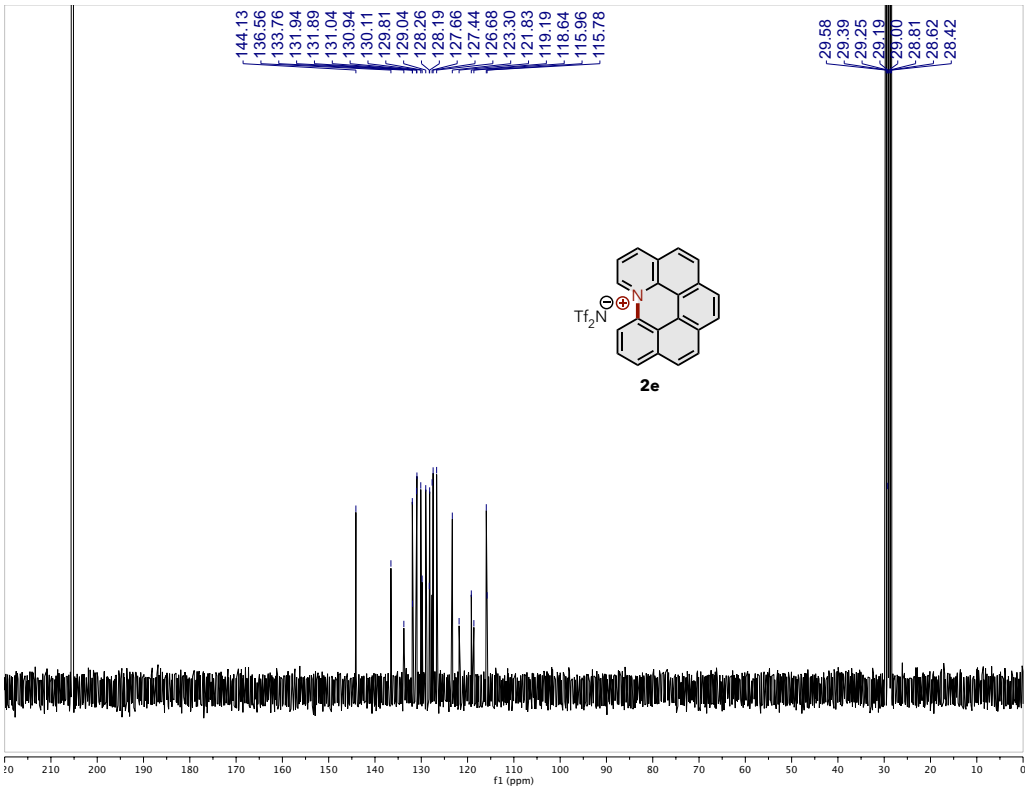
144.13
136.56
133.76
131.94
131.89
131.04
130.94
130.11
129.81
129.04
128.26
128.19
127.66
127.44
126.68
123.30
121.83
119.19
118.64
115.96
115.78
29.58
29.39
29.25
29.19
29.00
28.81
28.62
28.42
Tf2N
2e
f1 (ppm)

3.6 References

[1] For selected examples, see: (a) M. Abe, *Chem. Rev*. **2013**, *113*, 7011. (b) T. Kubo, Chem. Lett. **2015**, *44*, 111. (c) Z. Zeng, X. Shi, C. Chi, J. T. L. Navarrete, J. Casado, J. Wu, *Chem. Soc. Rev.* **2015**, *44*, 6578. (d) Y. Tobe, *Top. Curr. Chem.* **2018**, *376*, 12. (e) G. E. Rudebusch, J. L. Zafra, K. Jorner, K. Fukuda, J. L. Marshall, I. Arrechea-Marcos, G. L. Espejo, R. P. Ortiz, C. J. Glmez-Garc&a, L. N. Zakharov, M. Nakano, H. Ottosson, J. Casado, M. M. Haley, *Nat. Chem.* **2016**, *8*, 753. (f) J. J. Dressler, M. Teraoka, G. L. Espejo, R. Kishi, S. Takamuku, C. J. Glmez-García, L. N. Zakharov, M. Nakano, J. Casado, M. M. Haley, *Nat. Chem.* **2018**, *10*, 1134. (g) Bortolozzi, R.; Ihmels, H.; Thomas, L.; Tian, M.; Viola, G. *Chem. Eur. J.* **2013**, *19*, 8736. (h) Mayer, U. F. J.; Murphy, E.; Haddow, M. F.; Green, M.; Alder, R. W.; Wass, D. F. *Chem Eur. J.* **2013**, *19*, 4287. (i) Cañeque, T.; Cuadro, A. M.; Alvarez-Builla, J.; Perez-Moreno, J.; Clays, K.; Castaño, O.; Andres, J. L.; Vaquero, J. J. *Dyes Pigm.* **2014**, *101*, 116. (j) Bortolozzi, R.; von Gradowski, S.; Ihmels, H.; Schafer, K.; Viola, G. *Chem. Commun.* **2014**, *50*, 8242. (k) Fei, X.; Li, R.; Lin, D.; Gu, Y.; Yu, L. *J. Fluoresc.* **2015**, *25*, 1251. (l) Yue, X.; Armijo, Z.; King, K.; Bondar, M. V.; Morales, A. R.; Frazer, A.; Mikhailov, I. A.; Przhonska, O. V.; Belfield, K. D. *ACS Appl. Mater. Interfaces* **2015**, *7*, 2833. (m) Marcelo, G.; Pinto, S.; Cañeque, T.; Mariz, I. F. A.; Cuadro, A. M.; Vaquero, J. J.; Martinho, J. M. G.; Maçoas, E. M. S. *J. Phys. Chem. A* **2015**, *119*, 2351; (n) T. Cañeque et al. *Dyes and Pigments* **2017**, *144*, 17–31; (o) Y. V. Suseela, N. Narayanaswamy, S. Pratihar, T. Govindaraju. *Chem. Soc. Rev.* **2018**, *47*, 1098–1131.

[2] For the review of synthetic approaches (1)-(3) (Scheme. 1) to AZAHs; D. Sucunza, A. M. Cuadro, J. Alvarez-Builla, J. J. Vaquero. *J. Org. Chem.* **2016**, *81*, 10126–10135.

[3] G. C. Fu, R. H. Grubbs, *J. Am. Chem. Soc.* **1992**, *114*, 5426.

[4] For the review of recent synthetic approaches to AZAHs through transition-metal-catalyzed C–H

activation; J. Jayakumar, C.-H. Cheng. *J. Chin. Chem. Soc.* **2018**, *65*, 11–23.

[5] (a) C.-Z. Luo, P. Gandeepan, C.-H. Cheng, *Chem*. *Commun*. **2013**, *49*, 8528; (b) X. Liu *et al*. *J. Am. Chem. Soc.* **2019**, *141*, 11259−11268; (c) P. Karak, C. Dutta, T. Dutta, A. L. Koner, J. Choudhury. *Chem.Commun.* **2019**, *55*, 6791–6794; (d) J. Yin, F. Zhou, L. Zhu, M. Yang, Y. Lan, J. You, *Chem. Sci*. **2018**, *9*, 5488–5493; (e) V. D. Kadam, B. Feng, X. Chen, W. Liang, F. Zhou, Y. Liu, G. Gao, J. You. *Org. Lett.* **2018**, *20*, 7071−7075; (f) Z. Wang, J. Yin, F. Zhou, Y. Liu, J. You. *Angew. Chem. Int. Ed.* **2019**, *58*, 254–258; (g) K. Xu, Y. Fu, Y. Zhou, F. Hennersdorf, P. Machata, I. Vincon, J. J. Weigand, A. A. Popov, R. Berger, X. Feng. *Angew. Chem. Int. Ed*. **2017**, *56*, 15876–15881.

[6] (a) D. Wu, L. Zhi, G. J. Bodwell, G. Cui, N. Tsao, K. Müllen, *Angew. Chem. Int. Ed.* **2007**, *46*, 5417. (b) J. Fortage, F. Tuyéras, P. Ochsenbein, F. Puntoriero, F. Nastasi, S. Campagna, S. Griveau, F. Bedioui, I. Ciofini, P. P. Lainé. *Chem. Eur. J.* **2010**, *16*, 11047. (c) J. Fortage, C. Peltier, F. Nastasi, F. Puntoriero, F. Tuyéras, S. Griveau, F. Bedioui, C. Adamo, I. Ciofini, S. Campagna, P. P. Lainé. *J. Am. Chem. Soc.* **2010**, *132*, 16700. (d) J. R. Deng *et al. Chem. Sci.* **2017***, 8,* 7537–7544; (e) N. Toriumi, N. Asano, K. Miyamoto, A. Muranaka, M. Uchiyama. *J. Am. Chem. Soc.* **2018**, *140*, 3858.

[7] (a) X. Zhou *et al*. *Chem. Commun.* **2018**, *54*, 4009–4012; (b) M. V. Il'in *et al. New J. Chem.* **2018**, *42*, 9373–9376; (c) R. D. Mule, A. C. Shaikh, A. B. Gade, N T. Patil. *Chem. Commun.* **2018**, *54*, 11909–11912; (d) S. Chae, G. Panomsuwan, M. A. Bratescu, K. Teshima, N. Saito. *ACS Appl. Nano Mater.* **2019**, *2*, 1350−1355.

[8] Bakac, A.; Brynildson, M. E.; Espenson, J. H., *Inorg. Chem.* **1986**, *25*, 4108.

[9] N. Luo, Z. Yu. *Chem. Eur. J.* **2010**, *16*, 787 – 791.

4. Dehydrogenative Alkyne Dicyclization (DAD)

4.1 Introduction

Dibenzo[*g,p*]chrysene (Fig. 4.1) possesses a helically twisted carbon structure,[1] and its derivatives constitute numbers of π-materials such as thin-film transistors[2] and OLEDs[3]; especially, their importance has been demonstrated as potential TNT chemosensors by Swager and his coworkers.[4] Swager group reported the synthesis of dibenzo[*g,p*]chrysene through oxidative cyclization of bis(2-biphenyl)alkyne using stoichiometric amount of $SbCl_5$ (Scheme 4.1). The key process is Sb^V-mediated single-electron oxidation of the alkyne, which ended with poor functional group tolerance. For example, some electron-rich substrate underwent undesired dimerization under their reaction conditions.

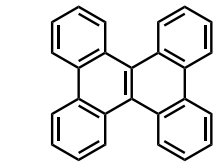

Fig. 4.1 Dibenzo[*g,p*]chrysene

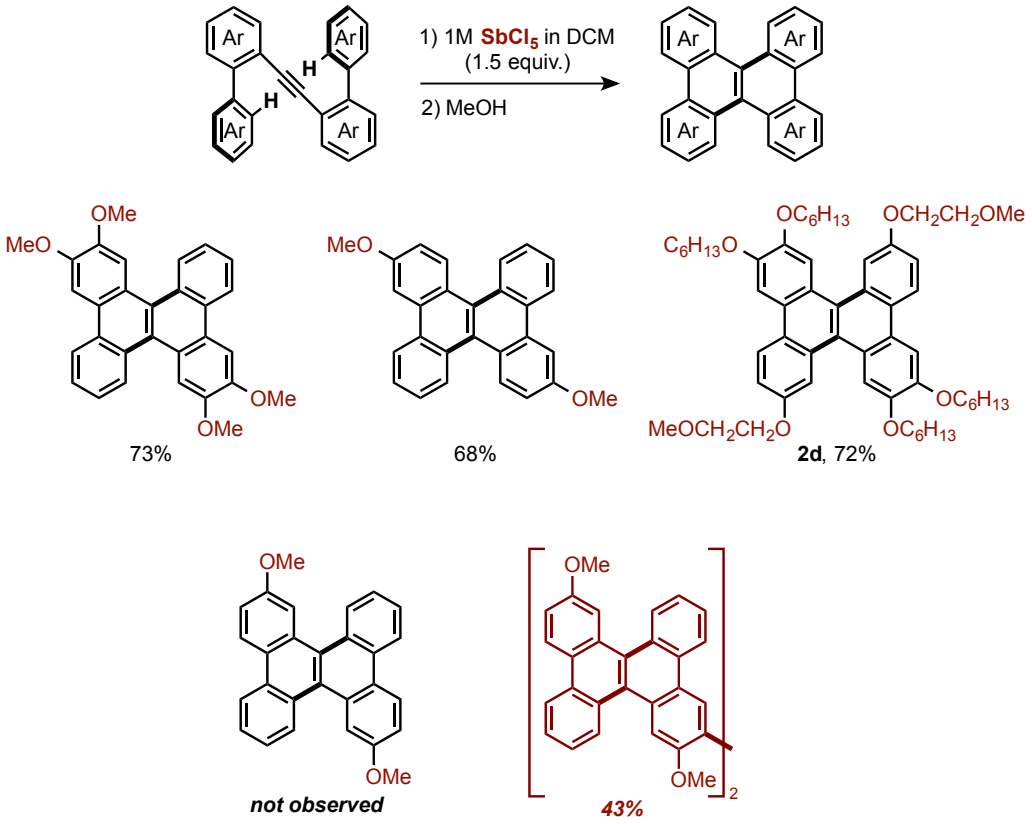

Scheme 4.1. Sb^{V}-mediated oxidative cyclization of bis(2-biphenyl)alkyne

To enable the access to various types of electron-rich and poor dibenzo[*g,p*]chrysenes, we envisioned the mild catalytic protocol, such as CDE catalysis (Scheme 4.2). However, due to the poor solubility of tetraphenylethylene in MeCN, diannulation by CDE catalysis was found to be challenging under the optimal reaction conditions. Thus, we designed another catalysis, dehydrogenative alkyne diannulation

(DAD). DAD will enable the formation of two C–C bonds through releasing one equivarent of hydrogen gas. Potential application to polyarylalkynes would deliver cove-type GNRs as a product (Scheme 4.3).

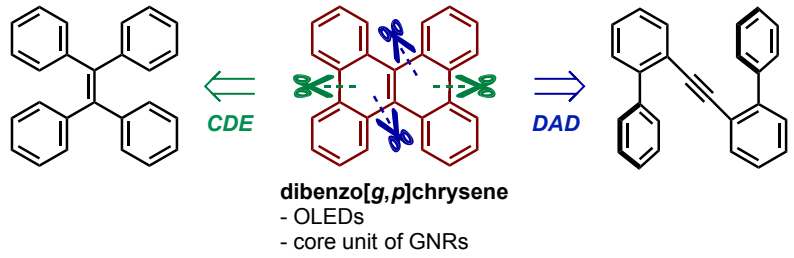

Scheme 4.2. Strategy to dibenzo[*g.p*]chrysene: CDE (left, unsuccessful) and DAD (right, this work)

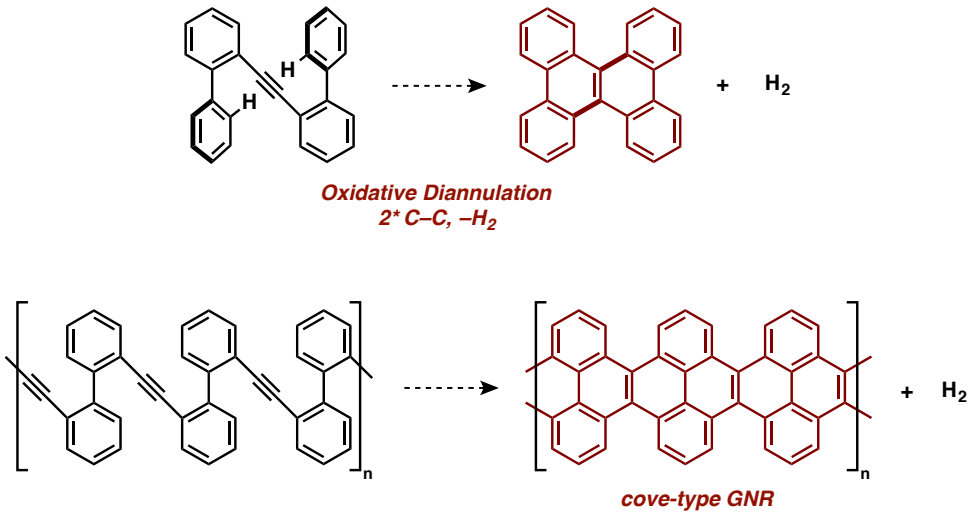

Scheme 4.3. DAD catalysis and its potential application

The design of DAD catalysis is shown (Scheme 4). First, we aimed at 6π electrocylization of ynedienes. Given that its 6π electrocylization intermediate is highly distorted and difficult to form, formation of less distorted intermediate was projected; I envisioned that π-Lewis-acidic metal could activate alkynes (*e.g.*

by forming a three-center-two-electron (3c-2e) complex), [5] which could undergo UV-mediated dehydrogenative 6π electrocylization to form cyclohexadiene intermediate and it is ultimately transformed to aromatic intermediate. This process could be followed by CDE reaction to form dibenzo[*g*,*p*]chrysene as desired product.

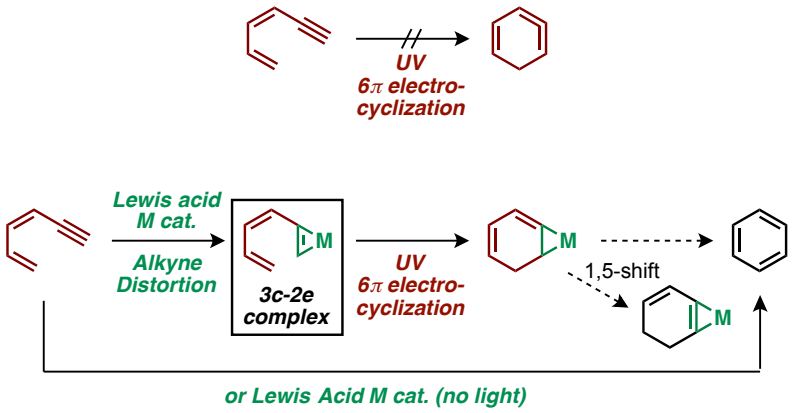

Scheme 4.4. Design of the DAD catalysis

4.2 Results&discussion

In the initial study, we aimed at the formation of the product under UV irradiation of bis(2-biphenyl)alkyne in the presence of catalytic amount of Lewis acid and cobaloxime catalyst **A** (Table 4.1). Among screened Lewis acids, $BiBr_3$ was the most efficient catalyst to give the product, albeit in low yield (entry 14). Furthermore, we have found that the reaction takes place without cobaloxime catalyst

A (entry 23).

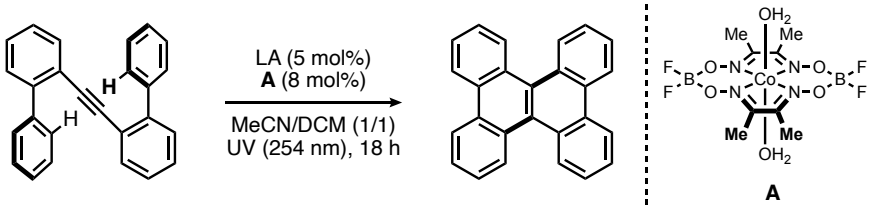

entry	LA	yield(%)
1	none	trace
2	$Cu(OTf)_2$	trace
3	CuOTf•PhH	1
4	CuCl	2
5	$Cu(MeCN)_4BF_4$	2
6	InCl	2
7	InCl (5 mol%) + $AgSbF_6$ (7 mol%)	1
8	$InCl_3$	1
9	$In(OTf)_3$	1
10	Ph_3PAuCl (5 mol%) + $AgSbF_6$ (7 mol%)	trace

entry	LA	yield(%)
11	$PtCl_2$	no rxn
12	$Pr(OTf)_3$	no rxn
13	$BiCl_3$	3
14	**$BiBr_3$**	**4**
15	BiI_3	no rxn
16	$Bi(OTf)_3$	2
17	$SbCl_5$	3
18	$SbBr_3$	3
19	$MoCl_5$	3
20	$W(CO)_6$	no rxn
21	$Ru_3(CO)_{12}$	no rxn
22	$BiBr_3$, > 300 nm UV	no rxn
23	**$BiBr_3$**,w/o **A**	**4**

Table 4.1. Lewis acid screening

With $BiBr_3$ as the optimal catalyst, solvents were screened and it was found that mix solvent system with MeCN/1,4-dioxane afforded both mono- and diannulation product in good yield, whereas DCM, toluene, CCl_4 weren't good solvent (Table 4.2). Further extensive studies on catalyst loading and solvent system revealed that 15 mol% of $BiBr_3$ in EtCN/EtOAc mixed solvent system under irradiation

of 25W UV lamps works as the best condition to deliver diannulation product in 72% NMR yield (58% isolated).

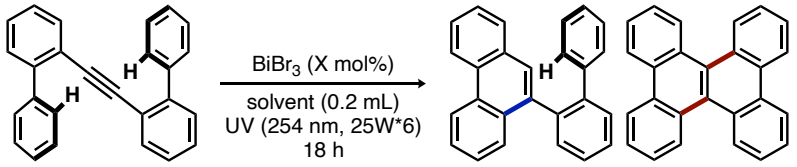

entry	X (mol%)	solvents	*mono*	*di*
1	5	MeCN/1,4-diox. (2/1)	2%	30%
2	5	MeCN/1,4-diox. (3/1)	3%	31%
3	5	MeCN/1,4-diox. (4/1)	2%	31%
4	5	DCM	trace	5%
5	5	toluene	trace	3%
6	5	CCl_4	trace	trace
7	15	EtCN/EtOAc (1/12), 0.4 mL	trace	**72 (58% isolated)**

Table 4.2. Solvent screening

4.3 Conclusion

In this work, we have demonstrated that $BiBr_3$ works as the catalyst for the oxidative transformation of bis(2-biphenyl)alkyne. Further optimization and substrate scope studies are currently ongoing in our laboratory.

4.4 Experimental Sections

General information

All UV-mediated reactions were carried out in 20 mL Quartz test tubes under nitrogen atmosphere. Acetonitrile was purchased from Acros Organics. $Co(dmg(BF_2)_2)(OH_2)_2$ was prepared following the reported procedure. 25W UVC lamps (λ = 254 nm, L x W x H = 8.5 x 2 x 2 inches) were purchased from coospider (https://www.amazon.com/gp/product/B07KYVRVX7/ref=ppx_yo_dt_b_asin_title_o03_s00?ie=UTF8&psc=1), and used as light source. All commercially available substrates were used without further purification. Thin layer chromatography (TLC) analysis was run on silica gel plates purchased from EMD Chemical (silica gel 60, F254). Infrared spectra were recorded on a Nicolet iS5 FT-IR Spectrometer using neat thin film technique. High-resolution mass spectra (HRMS) were obtained on an Agilent 6224 TOF-MS spectrometer and are reported as m/z. Amounts of H_2 generated in the photo-catalytic experiments were determined by gas chromatography (GC) using an SRI 8610C Gas Chromatograph with the nitrogen carrier gas and a TCD detector. Methane was used as internal standard for the measurement of the yield

of H_2. UV–Vis spectra was measured with NanoDrop™ One^C. UV-Vis spectrometer. Nuclear magnetic resonance spectra (^{1}H NMR and ^{13}C NMR) were recorded with a Bruker Model DMX 400 (400 MHz, ^{1}H at 400 MHz, ^{13}C at 101 MHz). For $CDCl_3$ solutions, the chemical shifts were reported as parts per million (ppm) referenced to residual protium or carbon of the solvents: $CHCl_3$ δ H (7.26 ppm) and $CDCl_3$ δ C (77.00 ppm). For CD_2Cl_2 solutions, the chemical shifts were reported as parts per million (ppm) referenced to residual protium or carbon of the solvents: CH_2Cl_2 δ H (5.32 ppm) and CD_2Cl_2 δ C (53.80 ppm). Coupling constants were reported in Hertz (Hz). Data for ^{1}H NMR spectra were reported as following: chemical shift (δ, ppm), multiplicity (br = broad, s = singlet, d = doublet, t = triplet, q = quartet, dd = doublet of doublets, td = triplet of doublets, ddd = doublet of doublet of doublets, m = multiplet), coupling constant (Hz), and integration.

Synthesis and characterization of substrates

Compound **1a** was synthesized following the reported procedure.[6]

General experimental procedure for the catalytic dehydrogenative electrocyclization

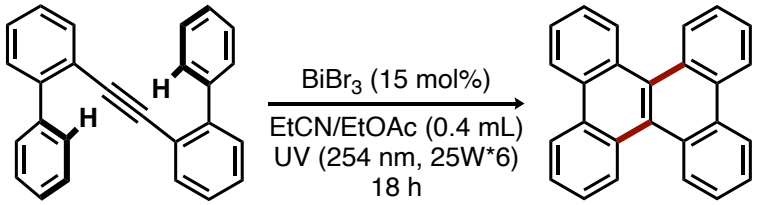

1a **2a**

To a flame-dried 20 mL Quartz test tube with a stir bar was added **1a** (16.5 mg, 0.05 mmol) and $BiBr_3$ (3.4 mg, 0.0075 mmol, 15 mol%). The test tube and the septum were transferred to the glove box. EtCN/EtOAc(v/v = 1/12, 0.4 mL) was added to the test tube, before it was sealed with the septum and transferred out of the glove box. The septum was covered with aluminum foil, and the mixture was irradiated by 25 W UV lamps at room temperature under vigorous stirring for 18 hours (see fig. S1 and S2). After the completion of the reaction, the mixture was diluted with 2 mL of dichloromethane and passed through a plug of silica gel (1 cm). After removing solvents under vacuum, the residue was purified by flush column chromatography (hexane) to give the desired product **2a**.

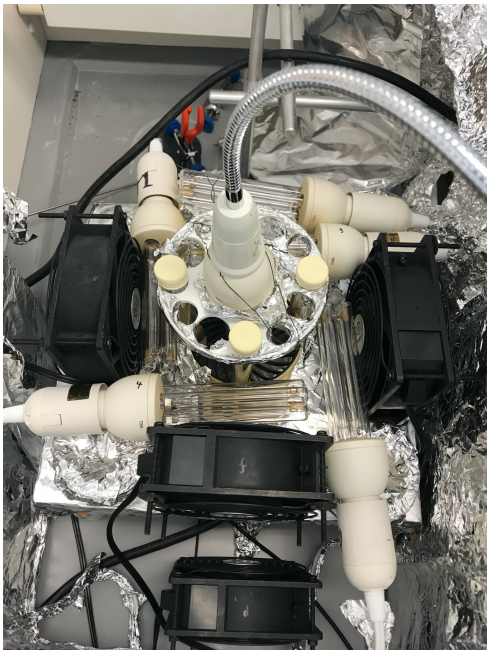

Fig. S1. Top view of the reaction set up for the catalytic dehydrogenative electrocyclization. Six 25 W UV lamps and five fans are used as shown. They are on the cardboard box that has a hole in the center. Side fans on the cardboard box are about 3–4 cm away from the edge of the center fan. CAUTION: cover the reaction setup with cardboard boxes and aluminum foil to avoid exposure to UV.

Fig. S2. Side view of the reaction set up for the catalytic dehydrogenative electrocyclization. Some 20 mL vials are put under the cardboard box to adjust the height and use the fan in the center. CAUTION: cover the reaction setup with cardboard boxes and aluminum foil to avoid exposure to UV.

Characterization of a product

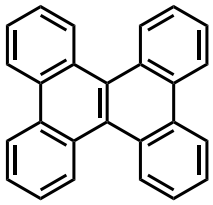

2a

Dibenzo[*g,p*]chrysene (**2a**)[7]: white solid (9.5 mg, 58% yield). R_f = 0.6 (hexane). **^{1}H NMR** (400 MHz, $CDCl_3$) δ 8.74 – 8.71 (m, 8H), 7.72 – 7.63 (m, 8H). **^{13}C NMR** (101 MHz, $CDCl_3$) δ 130.8, 129.2, 128.9, 27.5, 126.6, 123.6.

4.5 ^{1}H, ^{13}C NMR spectra

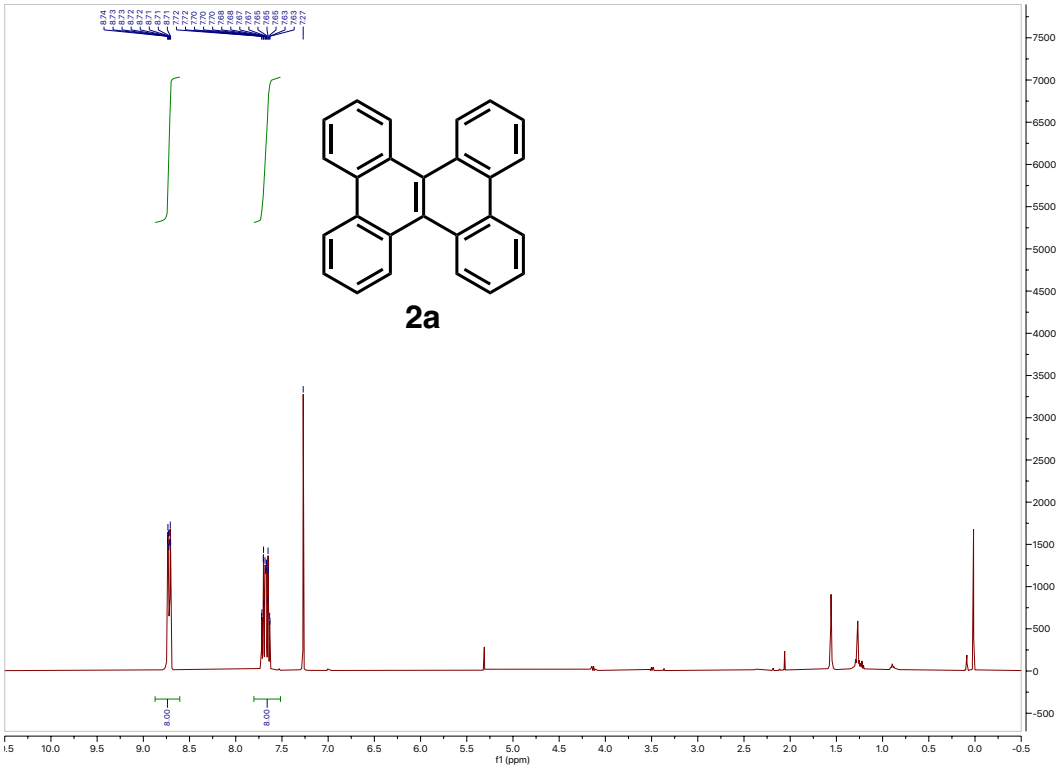

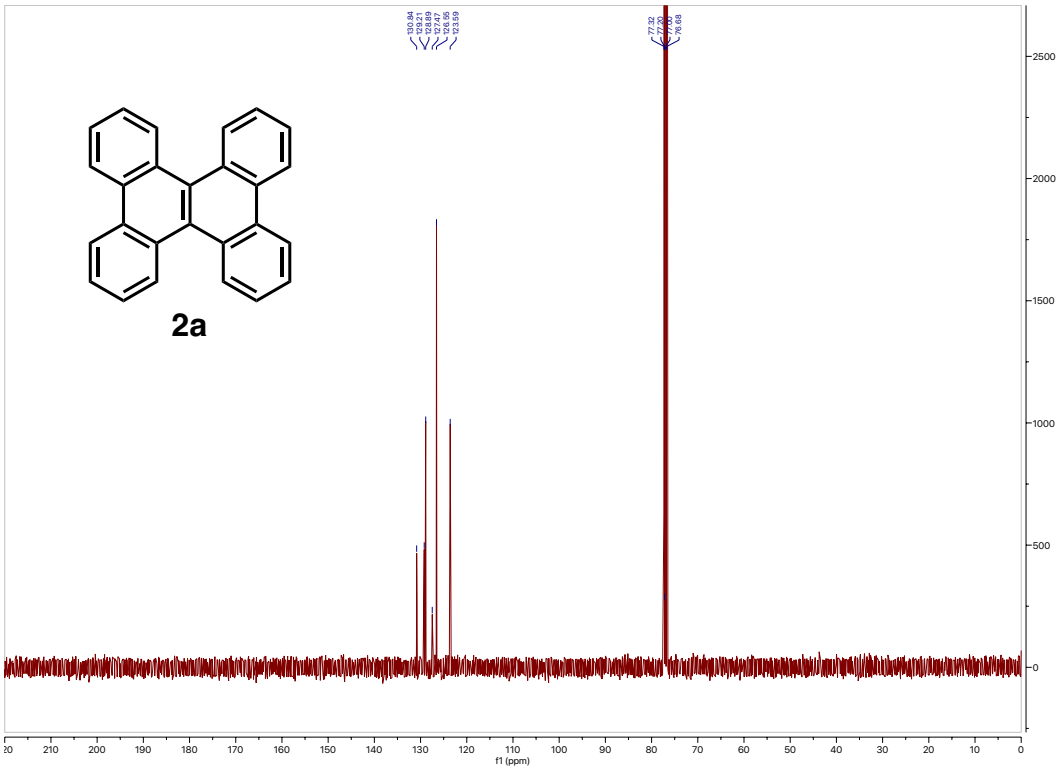
130.84
129.21
128.89
127.47
126.95
123.59
77.32
77.00
76.68
2500
2000
1500
1000
500
0
210
200
190
180
170
160
150
140
130
120
110
100
90
80
70
60
50
40
30
20
10
0
f1 (ppm)

2a

4.6 References

[1] a) F. H. Herbstein, *Acta Crystallogr. B*. **1979**, *35*, 1661; b) H. Tsuji, Y. Ueda, L. Ilies, E. Nakamura, *J. Am. Chem. Soc.* **2010***, 132*, 11853– 11855.

[2] S. Tokito, K. Noda, H. Fujikawa, Y. Taga, M. Kimura, K. Shimada, *App. Phys. Lett*. **2000**, *77*, 160–162.

[3] a) S. Wang, P. Yang, K. Chang, W. Lv, B. Mi, J. Song, X. Zhao, Z. Gao, *Org. Electron.* **2019**, *74*, 269–275; b) T. Mori, K. Fujita, M. Kimura*, J. Photopolym. Sci. Technol.* **2010**, *23*, 317– 322. N. Yoshida *et al*. *Tetrahedron Lett*. **2020**, *61*, 152033. c) R. Chaudhuri, M.-Y. Hsu, C.-W. Li, C.-I. Wang, C.-J. Chen, C.-K. Lai, L.-Y. Chen, S.-H. Liu, C.-C. Wu, R.S. Liu*, Org. Lett*. **2008**, *10*, 3053–3056.

[4] S. Yamaguchi, T. M. Swager, *J. Am. Chem. Soc*. **2001**, *123*, 12087-12088.

[5] (a) W. Debrouwer, T. S. A. Heugebaert, B. I. Roman and C. V. Stevens, *Adv. Synth. Catal.*, **2015**, *357*, 2975; (b) R. Dorel and A. M. Echavarren, *Chem. Rev*. **2015**, *115*, 9028; (c) S. M. A. Sohel and R. Liu, *Chem. Soc. Rev*. **2009**, *38*, 2269.

[6] P. Kyungho et al. *J. Org. Chem.* **2010**, *75*, 6244.

[7] M. Shimizu, I. Nagao, Y. Tomioka, T. Hiyama. *Angew. Chem. Int. Ed*. **2008**, *47*, 8096–8099.